Poly(limonene carbonate): a bio-based & versatile high-performance thermoplastic

Dissertation

zur Erlangung des akademischen Grades
eines Doktors der Naturwissenschaften (Dr. rer. Nat.)
an der Bayreuther Graduiertenschule für Mathematik und
Naturwissenschaften (BayNAT) der Universität Bayreuth

vorgelegt von

Oliver Hauenstein

aus Dortmund

Bayreuth 2016

Die vorliegende Arbeit wurde in der Zeit von November 2012 bis Juni 2016 in Bayreuth am Lehrstuhl Makromolekulare Chemie II unter Betreuung von Herrn Professor Dr. Andreas Greiner angefertigt.

Vollständiger Abdruck der von der Bayreuther Graduiertenschule für Mathematik und Naturwissenschaften (BayNAT) der Universität Bayreuth genehmigten Dissertation zur Erlangung des akademischen Grades eines Doktors der Naturwissenschaften (Dr. rer. nat.).

Dissertation eingereicht am: 13.07.2016

Zulassung durch das Leitungsgremium: 26.07.2016

Wissenschaftliches Kolloquium: 01.02.2017

Amtierender Direktor: Prof. Dr. Stephan Kümmel

Prüfungsausschuss:

Prof. Dr. Andreas Greiner   (Erstgutachter)

Prof. Dr. Hans-Werner Schmidt   (Zweitgutachter)

Prof. Dr. Carlo Unverzagt.   (Vorsitz)

Prof. Dr. Jürgen Senker

Drittgutachter: Prof. Dr. Volker Abetz

Für meine Familie & Hui

Contents

Contents

Abbreviations & symbols

Abbreviations

[PPN]Cl	bis(triphenylphosphine)iminium chloride
APC	aliphatic polycarbonate
ATR	attenuated total reflection
bdi	β-diiminate
BPA	bisphenol A
BPA-PC	bisphenol A polycarbonate
CAc	cellulose acetate
CCS	carbon capture and storage
CCU	carbon capture and utilization
CD	compact disc
CHO	cyclohexene oxide
DCM	dichloromethane
DEA	diethanolamine
DMC	double metal cyanide
DVD	digital versatile disc
EO	ethylene oxide
GC	gas chromatography
GC-MS	gas chromatography-mass spectrometry
GPU	gas permeation unit
HMW	high molecular weight
IEA	international Energy Agency
i-Pr	*iso*-propyl moiety
LO	limonene oxide
LWR	long wave radiation
MAc	mercaptoacetic acid
ME	mercaptoethanol
MEA	monoethanolamine
MeI	iodomethane
MeOH	methanol
MOF	metal-organic framework
mol%	mole percent
OAc	acetate
o-Ps	*ortho*-positronium
PA	polyamide
PALS	positron annihilation lifetime spectroscopy
PC	polycarbonate

PCHC	poly(cyclohexene carbonate)
PEC	poly(ethylene carbonate)
PEG	poly(ethylene glycol)
PEI	poly(ether imide)
PHC	poly(1-hexene carbonate)
PHMG	poly(hexamethylene guanidine) hydrochloride
PI	polyimide
PIM	polymer with intrinsic microporosity
PLimC	poly(limonene carbonate)
PO	propylene oxide
ppb	parts per billion
PPC	poly(propylene carbonate)
ppm	parts per million
PPO	poly(phenylene oxide)
p-Ps	$para$-positronium
Ps	positronium
PSU	polysulfone
ROP	ring-opening polymerization
salan	reduced salen
salen	N,N'-bis(salicylidene)ethylenediamine
scCO$_2$	supercritical carbon dioxide
STP	standard temperature and pressure
SWR	short wave radiation
syngas	synthesis gas
t-Bu	$tert$-butyl moiety
TOX-PIM-1	thermal-oxidatively crosslinked PIM-1
TR-PI	thermally rearranged polyimide
VOC	volatile organic compound
vol%	volume percent
wt%	Weight percent

Physical quantities

symbol		unit
D	diffusion coefficient	m² s^{-1}
$Đ$	dispersity (molecular weight distribution)	-
FFV	fractional free volume	-
J	molecular flux	mol s^{-1}
k_{up}	ROBESON upper bound empirical factor	10^{-10} cm³ cm cm^{-2} s^{-1} cmHg^{-1}
l	thickness	m
M_n	number average molecular weight	g mol^{-1}
M_w	weight average molecular weight	g mol^{-1}
n_{up}	ROBESON upper bound empirical exponent	-
P	permeability (1 barrer)	10^{-10} cm³ cm cm^{-2} s^{-1} cmHg^{-1}
Q	permeance (1 GPU)	10^{-6} cm³ cm^{-2} s^{-1} cmHg^{-1}
r_c	radius of a cavity	nm
S	solubility coefficient	cm³ cm^{-3} cmHg^{-1}
$T_{5\%}$	5% decomposition temperature	°C
T_g	glass transition temperature	°C
T_m	melting temperature	°C
T_{max}	maximum decomposition temperature	°C
TOF	turnover frequency	mol mol$_{cat}$$^{-1}$ h^{-1}
TON	turnover number	g g$_{cat}$$^{-1}$
V_f	free volume	cm³ g^{-1}
V_{sp}	specific volume	cm³ g^{-1}
V_w	VAN DER WAALS volume	cm³ g^{-1}
$\alpha_{A/B}$	separation factor (for gas pair A/B)	-
Δp	(partial) pressure difference	Pa
λ_{po}	rate of pick-off annihilation	s^{-1}
σ_s	tensile strength	MPa
τ	lifetime	s
τ_3	lifetime of a ortho-positronium	s

List of publications

1. Bio-based polycarbonate from limonene oxide and CO_2 with high molecular weight, excellent thermal resistance, hardness and transparency

   Oliver Hauenstein, Marina Reiter, Seema Agarwal, Bernhard Rieger & Andreas Greiner

   Green Chemistry

   2016

   Vol. 18

   pp. 760-770

   high T_g = 130 °C
   high transparency
   superior hardness to BPA-PC

2. Membranes & breathing glass from bio-based polycarbonate

   Oliver Hauenstein, Mushfequr Rahman, Mohamed Elsayed, Reinhard Krause-Rehberg, Volker Abetz & Andreas Greiner

   (to be submitted)

   PLimC – a breathing glass

   sunlight

   heat

   gas exchange

   O_2
   CO_2
   H_2O
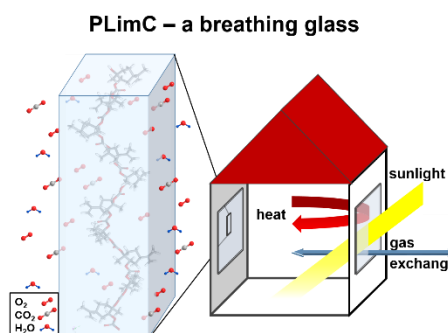
3. Bio-based polycarbonate as synthetic toolbox

   Oliver Hauenstein, Seema Agarwal & Andreas Greiner

   Nature Communications

   2016

   DOI: 10.1038/ncomms11862

   Platform

Abstract

This thesis is comprised of my original contribution to the development of the bio-based material poly(limonene carbonate) (PLimC). There is a huge need for such polymeric materials based on natural resources as the supply of fossil feedstocks is limited and it is going to cease within this century. However, the replacement of those 'old petroleum-base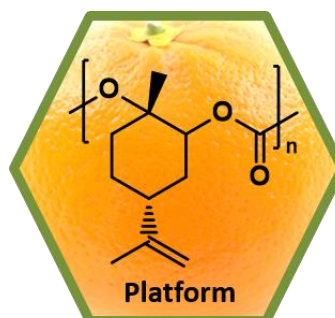d' with 'new bio-based' plastics can only succeed if the performance of the green material can compete with or even excel that of the established polymers. The latter is true for PLimC and thus I have dedicated my entire thesis to this material.

Within the family of such bio-based plastics, PLimC takes a special role as it is the copolymer of (oxidized) limonene (LO) – a by-product of the orange industry – and CO_2. To incorporate this abundant greenhouse gas into a polymeric backbone is a field of research itself but in the case of PLimC this is only a side note. The real excitement to work with this material arises from its properties and the vast diversity of its modifications. The discussions of the development, applications and modifications of PLimC are outlined in dedicated chapters within this thesis (Chapters 3-5).

The discussion starts with the development of the material from a low-molecular-weight polymer into a high-molecular-weight engineering thermoplastic in Chapter 3. The chapter – entitled 'Synthesis and properties of PLimC' – deals with the synthetic strategies towards a controlled and economical production of PLimC and the material's general profile of properties. The control of the molecular weight of PLimC was found to be crucially dependent on the composition of the monomer LO, which is inherently contaminated with hydroxy-carrying molecules. These impurities act as chain transfer agents in the Zn(II)-catalyzed copolymerization and thus keep the molecular weight of PLimC low. The treatment of LO with an *O*-methylating agent was found to quantitatively mask those alcohols as an enabler to yield high molecular weights of PLimC (>100 kDa). These long chains give the material the mechanical integrity to be processed into fibres, films or sheets that can withstand external stress. The economical aspect is covered by a stereo- and regioselective synthesis of the *trans* isomer of LO as the catalyst rejects to incorporate the *cis* isomer into the backbone of PLimC. The epoxidation of limonene would usually yield a 1:1 mixture of *cis*- and *trans*-LO but the detour via the bromohydrin and the subsequent

ring-closure in basic environment gives *trans*-LO (>95%) as the major product. This *trans*-enriched monomer is successfully coupled with CO_2 in high conversions to give PLimC with little residual epoxide. The resulting amorphous thermoplastic exhibits high heat- (T_g of 130 °C) and scratch-resistance with an extraordinary transparency (94%), which render it a potential coating or glazing material.

This application of PLimC as a glazing material is expanded in Chapter 4 'Applications of PLimC' where innovative concepts in terms of breathability and membranes are introduced. The concepts are based on the very high permeability of PLimC for gases like O_2 and CO_2 (12 and 68 barrer, respectively). Together with the exceptional optical and mechanical properties, PLimC constitutes the first polymeric glass with the ability to breathe. Such a breathing glass is still a very good thermal insulator and thus can be utilized as window panes in well-insulated constructions (e.g. in passive houses or closed greenhouses) to supply the interior with fresh air. The advantage of this passive exchange of air is the avoidance of an active ventilation system that has to be accessorily equipped with a heat exchange unit to reduce heat losses due to the introduction of cold fresh air. In case of PLimC as the breathing glass, the transport of fresh air is realized through the polymer matrix while the transport of heat is hindered due to the low thermal conductivity of material (0.15 W K^{-1} m^{-1}). According to our calculations, such a breathing glass made of PLimC cannot replace the entire ventilation system yet but it can already compensate for a part of the ventilation and thus save energy. Further improvements of the material and its processing are envisioned to replace the active ventilation systems eventually. Another application of PLimC arises from the fact, that the material shows not only a high permeability of CO_2 but also a distinct selectivity for the gas over N_2. The development of polymeric membranes for gas separation processes is a rapidly growing field as carbon capture (removal of CO_2 from process gases) is one of the technologies that is anticipated to abate the anthropogenic greenhouse effect. Here, PLimC is a potential candidate to be applied in gas separation units due to its good separation characteristic but moreover due to its above-mentioned mechanical toughness and thermal resistance that should give it the long-term stability and processability most state-of-the-art polymeric membrane materials lack.

To tune the performance of PLimC in respect of the mentioned applications but also to change the nature of the material completely, various manipulations on the double bond of the unsaturated polycarbonate were carried out. These manipulations are discussed in Chapter 5 – entitled 'Modifications of PLimC'. With a variety of polymer analogous reactions it could be shown that PLimC is a real bio-based platform. The spectrum of induced changes and added functionalities spans from rubbery over hydrophilic and smart to antibacterial materials, using simple and cost-effective chemistry. The astonishing transformation of the high-T_g thermoplastic PLimC into a rubber was accomplished by quantitative thiol-ene addition of a short-chained mercaptoester to the double bond. This attachment was accompanied by a drop of T_g and YOUNG's modulus by 120 K and three orders of magnitude (1 MPa), respectively. The hydrophilization, on the other hand, was chosen as a strategy towards an increased rate of biodegradation as we have found PLimC being highly resistant to hydrolysis and microorganism in industrial compost or concentrated enzyme suspensions. Such a hydrophilization was achieved via two synthetic routes: one involves the thiol-ene chemistry with mercaptoethanol, the other being an acid-catalyzed electrophilic addition of an oligomeric poly(ethylene glycol) with one free hydroxy function. The latter can be regarded as greener route, since it avoids the employment of toxic thiols. It is limited to low conversions though, as the residence time of the polycarbonate has to be kept short in such an acidic environment. The contact angle to water and the T_g were depressed successfully in both cases, whereas a biodegradability was still not observed. We would ascribe this high bio-stability to the rigid and bulky backbone of PLimC that readily shields the attack of cleaving agents. The smart behaviour of PLimC is related to its pH-responsiveness when mercaptoacetic acid is attached to the double bond. With this carboxylic acid functionality PLimC becomes soluble in basic media, that is, it readily dissolves in sea-water, whereupon the rate of degradation is accelerated by several orders of magnitude compared to a condensed film. Such a material can significantly reduce waste accumulation in the oceans while keeping structural integrity during the intended use (as long as contact with bases is avoided). The last example of valorising the platform polymer is the addition of antibacterial activity to PLimC in the form of pendant quaternized amine groups in a two-step synthesis. Here, only a partial conversion was performed deliberately to keep the polymer insoluble in water and thus making it a viable choice for application as a coating material with permanent activity

against bacteria. These examples state just a small selection of many possible modifications of PLimC and we anticipate to see many derivatives to be introduced within a short time.

Zusammenfassung

Diese Dissertation beinhaltet meinen originären Beitrag zur Entwicklung des biobasierten Materials Polylimonencarbonat (PLimC). Das Angebot fossiler Rohstoffe ist begrenzt und wird noch innerhalb dieses Jahrhunderts erlöschen. Daher gibt es eine große Notwendigkeit zur Entwicklung solcher polymerer Materialien, die auf natürlichen Ressourcen basieren. **Der Ersatz dieser ‚alten ölbasierten‘ durch ‚neue biobasierte‘** Kunststoffe kann jedoch nur gelingen, wenn die Leistung des grünen Materials mit der etablierter Polymere mithalten oder diese sogar übertreffen kann. Letzteres trifft auf PLimC zu, weshalb ich meine gesamte Doktorarbeit diesem Material gewidmet habe.

Innerhalb der Familie der biobasierten Kunststoffe nimmt PLimC eine besondere Rolle ein, da es das Copolymer des (oxidierten) Limonens (LO) – ein Nebenprodukt der Orangenindustrie – und CO_2 ist. Dabei stellt der Einbau dieses reichlich vorhandenen Treibhausgases ein eigenes Forschungsfeld dar, spielt aber im Falle von PLimC nur eine Nebenrolle. Der wahre Reiz bei der Arbeit mit diesem Material rührt von seinen Eigenschaften und der riesigen Vielfalt seiner Modifikationen her. Den Diskussionen über die Entwicklung, Anwendungen und Modifikationen von PLimC ist in dieser Arbeit je ein Kapitel gewidmet (Kapitel 3 bis 5).

Sie beginnt mit der Entwicklung des Materials von einem niedermolekularen Polymer hin zu einem hochmolekularen technischen Thermoplast in Kapitel 3. Dieses Kapitel mit dem **Titel ‚Synthese und Eigenschaften von PLimC‘ behandelt die Synthesestrategien** hin zu einer kontrollierten und ökonomischen Darstellung von PLimC und das allgemeine Eigenschaftsprofil des Materials. Es wurde schnell ersichtlich, dass die Kontrolle des Molekulargewichts von PLimC sehr eng mit der Zusammensetzung des Monomers LO verknüpft ist, das von Natur aus mit Molekülen verunreinigt ist, die Hydroxygruppen tragen. Diese Verunreinigungen wirken als Kettenübertragungsmittel bei der Zn(II)-katalysierten Copolymerisation und begrenzen folglich das Molekulargewicht. Die Behandlung von LO mit einem *O*-methylierenden Reagens konnte erfolgreich zur Maskierung dieser Alkohole genutzt werden, sodass tatsächlich hohe Molekulargewichte für PLimC (>100 kDa) erreicht werden konnten. Genau diese langen Ketten geben dem Material die mechanische Stabilität, um in Fasern, Filmen oder Platten verarbeitet zu werden, die äußeren Belastungen widerstehen können. Der ökonomische Aspekt wird von

einer stereo- und regioselektiven Synthese des *trans*-Isomers von LO abgedeckt, da der Katalysator den Einbau des *cis*-Isomers ins Rückgrat von PLimC verweigert. Die Epoxidierung von Limonen resultiert normalerweise in einer 1:1 Mischung von *cis*- und *trans*-LO, wohingegen der hier gewählte Umweg über das Bromhydrin mit anschließendem Ringschluss in basischer Umgebung *trans*-LO (>95%) als Hauptprodukt liefert. Dieses *trans*-angereicherte Monomer kann dann erfolgreich mit CO_2 bei hohen Umsätzen und geringem Restgehalt vom Epoxid in PLimC überführt werden. Der erhaltene amorphe Thermoplast zeigt eine hohe Hitzebeständigkeit (T_g bei 130 °C), gute Kratzfestigkeit und zusätzlich außergewöhnliche Transparenz (94%), wodurch er sich zum Beschichtungs- oder Verglasungsmaterial qualifiziert.

Die Anwendung von PLimC als Verglasungsmaterial wird in Kapitel 4 ‚Anwendungen von PLimC' diskutiert. Darin werden innovative Konzepte hinsichtlich Atmungsaktivität und Membranen vorgestellt. Die Konzepte basieren auf der sehr hohen Permeabilität von PLimC für Gase wie O_2 und CO_2 (12 bzw. 68 barrer). Zusammen mit den hervorragenden optischen und mechanischen Eigenschaften stellt PLimC das erste polymere Glas mit der Fähigkeit zu atmen dar. Trotz der Fähigkeit zu atmen ist dieses Glas immer noch ein sehr guter thermischer Isolator und kann deshalb als Scheibe in gut isolierten Gebäuden (z.B. in Passivhäusern oder geschlossenen Treibhäusern) eingesetzt werden, um den Innenraum mit Frischluft zu versorgen. Der Vorteil dieses passiven Luftaustauschs liegt in der Vermeidung einer aktiven Belüftungsanlage, die zusätzlich noch mit einem Wärmetauscher ausgestattet werden muss, um Wärmeverluste, aufgrund von eingebrachter kalter Frischluft, zu reduzieren. Im Falle von PLimC als atmendem Glas wird der Transport von Frischluft durch die Polymermatrix realisiert, wohingegen der Transport von Wärme, aufgrund der geringen Wärmeleitfähigkeit des Materials ($0.15 \, \text{W K}^{-1} \text{m}^{-1}$), stark beeinträchtigt ist. Laut unserer Berechnungen kann ein atmendes Glas aus PLimC die Belüftungsanlage noch nicht komplett ersetzen, aber es kann bereits einen Teil der Belüftung übernehmen und folglich Energie einsparen. Weitere Verbesserungen des Materials und seiner Verarbeitung werden jedoch letztendlich dazu in der Lage sein das Belüftungssystem komplett überflüssig zu machen. Eine andere, ähnliche Anwendung von PLimC rührt daher, dass das Material nicht nur eine hohe Permeabilität für CO_2 aufweist, sondern auch eine ausgeprägte Selektivität für das Gas gegenüber N_2 besitzt. Die Entwicklung von polymeren Membranen zur Gastrennung ist ein schnell wachsendes Feld, da die Kohlenstoffabscheidung (Entfernung von CO_2 aus Prozessgasen) als eine der

Technologien angesehen wird, die den anthropogenen Klimawandel abschwächen kann. In diesem Sinne ist PLimC ein potentieller Kandidat, um in Gastrennungsanlagen aufgrund seiner guten Trenneigenschaften, aber eben auch wegen seiner schon genannten mechanischen und thermischen Robustheit, eingesetzt zu werden. Diese Merkmale geben dem Polymer die Langzeitstabilität und Verarbeitbarkeit, die den meisten hochmodernen Membranmaterialien fehlt.

Um die Leistung von PLimC mit Blick auf die genannten Anwendungen zu verbessern, aber auch um die Natur des Materials komplett zu verändern, wurden verschiedene Manipulationen an der Doppelbindung des ungesättigten Polycarbonats durchgeführt. Die Manipulationen werden in Kapitel 5 ‚Modifikationen von PLimC' diskutiert. Mit einer Reihe von polymeranalogen Reaktionen konnte gezeigt werden, dass PLimC eine echte biobasierte Plattform darstellt. Das Spektrum an herbeigeführten Änderungen und hinzugefügten Funktionalitäten reicht von gummiartigen, über hydrophile und smarte bis hin zu antibakteriellen Materialien, die mit einfacher und kostengünstiger Chemie hergestellt wurden. Die erstaunliche Verwandlung des hoch-T_g Thermoplasten PLimC in einen Gummi konnte durch die quantitative Addition eines kurzkettigen Mercaptoesters – mittels Thiol-ene Chemie – an die Doppelbindung erreicht werden. Diese Anlagerung wurde von einem Absturz des T_g um 120 K und des E-Moduls um drei Größenordnungen (1 MPa) begleitet. Die Hydrophilisierung hingegen wurde als Strategie gewählt, um die Geschwindigkeit der Bioabbaubarkeit zu erhöhen, da wir bei PLimC eine hohe Resistenz gegenüber Hydrolyse und Mikroorganismen in Industriekompost bzw. konzentrierten Enzymsuspensionen festgestellt haben. Diese Hydrophilisierung wurde über zwei synthetische Routen erreicht: die eine greift wieder auf die Thiol-ene Chemie zur Anlagerung von Mercaptoethanol zurück, während sich die andere eine säurekatalysierte elektrophile Addition von oligomerem Polyethylenglykol mit einer freien Hydroxy-funktion zunutze macht. Letztere kann als grünere Route angesehen werden, da die Verwendung von giftigem Thiol vermieden wird. Sie ist jedoch begrenzt auf geringe Umsätze, da die Verweilzeit des Polycarbonats in dieser sauren Umgebung kurz gehalten werden muss. Sowohl der Kontaktwinkel zu Wasser als auch der T_g wurden in beiden Fällen erfolgreich gesenkt, wobei eine Bioabbaubarkeit noch immer nicht beobachtet werden konnte. Wir würden die hohe Biostabilität dem starren und voluminösen Rückgrat von PLimC zuschreiben, das effektiv jegliche Angriffe mit dem Ziel der Kettenspaltung abschirmt. Das smarte Verhalten von PLimC bezieht sich auf seine pH-Empfindlichkeit,

wenn Mercaptoessigsäure an die Doppelbindung addiert wurde. Mit dieser Carbonsäurefunktion wird PLimC löslich in basischen Medien, d.h. es löst sich schnell in Meerwasser auf, woraufhin auch die Zersetzungsgeschwindigkeit um mehrere Größenordnungen gegenüber einem kompakten Film zunimmt. Ein solches Material kann die Ansammlung von Müll in den Ozeanen erheblich senken, wohingegen es während des beabsichtigten Gebrauchs seine strukturelle Integrität beibehält (solange der Kontakt mit Basen vermieden wird). Als ein letztes Beispiel zur Wertsteigerung des Plattformpolymers PLimC sei die Addition von antibakterieller Aktivität in Form von quaternisierten Amingruppen in einer zweistufigen Synthese erwähnt. In diesem Fall wurden die Doppelbindungen absichtlich nur teilweise funktionalisiert, damit das erhaltene Polymer wasserunlöslich bleibt und so als Beschichtungsmaterial mit permanenter Aktivität gegen Bakterien zur Anwendung kommen kann. Die hier genannten Beispiele zeigen nur einen kleinen Ausschnitt von vielen möglichen Modifikationen von PLimC und wir erwarten in naher Zukunft noch viele weitere zu entdecken.

# 1

Introduction

1.1 The versatile molecule CO_2

1.1.1 The greenhouse gas

The natural transformation of annually 200 Gt of CO_2 and water into high-energy substances, known as photosynthesis, is one of the essential processes to make life on earth possible.[1] To date, there exists no equivalent human-created imitation of that process, to exploit sunlight for synthesis, i.e. as a supplier of energy, as efficiently as nature. On the contrary, the anthropogenic emission of CO_2 is an ever growing global menace, mainly caused by incineration of carbon matter, leading to an annual emission of more than 32 Gt.[2,3] CO_2 is a greenhouse gas, which leads to warming of the atmosphere of the earth, eventually increasing the chances of catastrophic weather phenomena and a rising sea level. The contributors to climate change are illustrated in Fig. 1-1. The radiative balance between incoming solar shortwave radiation (SWR) and outgoing longwave radiation (OLR) is influenced by global climate contributors. Solar cycles, leading to fluctuations in the energy output, can cause changes in the energy balance. Human activity changes the emissions of gases and aerosols, which are involved in atmospheric chemical reactions, resulting in modified ozone and aerosol amounts. Ozone and aerosol particles absorb, scatter and reflect SWR, changing the energy balance. Some aerosols act as cloud condensation nuclei modifying the properties of cloud droplets and possibly affecting precipitation. Because interaction of clouds with SWR and LWR is strong, small changes in the properties of clouds have important implications for the radiative budget. Anthropogenic changes in greenhouse gases (CO_2, CH_4, N_2O, ozone, chlorofluorocarbon) and large aerosols (>2.5 µm in size) modify the amount of outgoing LWR by absorbing outgoing LWR and re-emitting less energy at a lower temperature. Surface albedo is altered by changes in the vegetation or land surface properties, snow or ice cover and ocean color. These changes are driven by natural seasonal and diurnal changes (snow cover), as well as human activities (changes in crop type, vegetation in general).[2] From those contributors, CO_2 is identified as the one increasing the most significantly due to anthropogenic emissions.
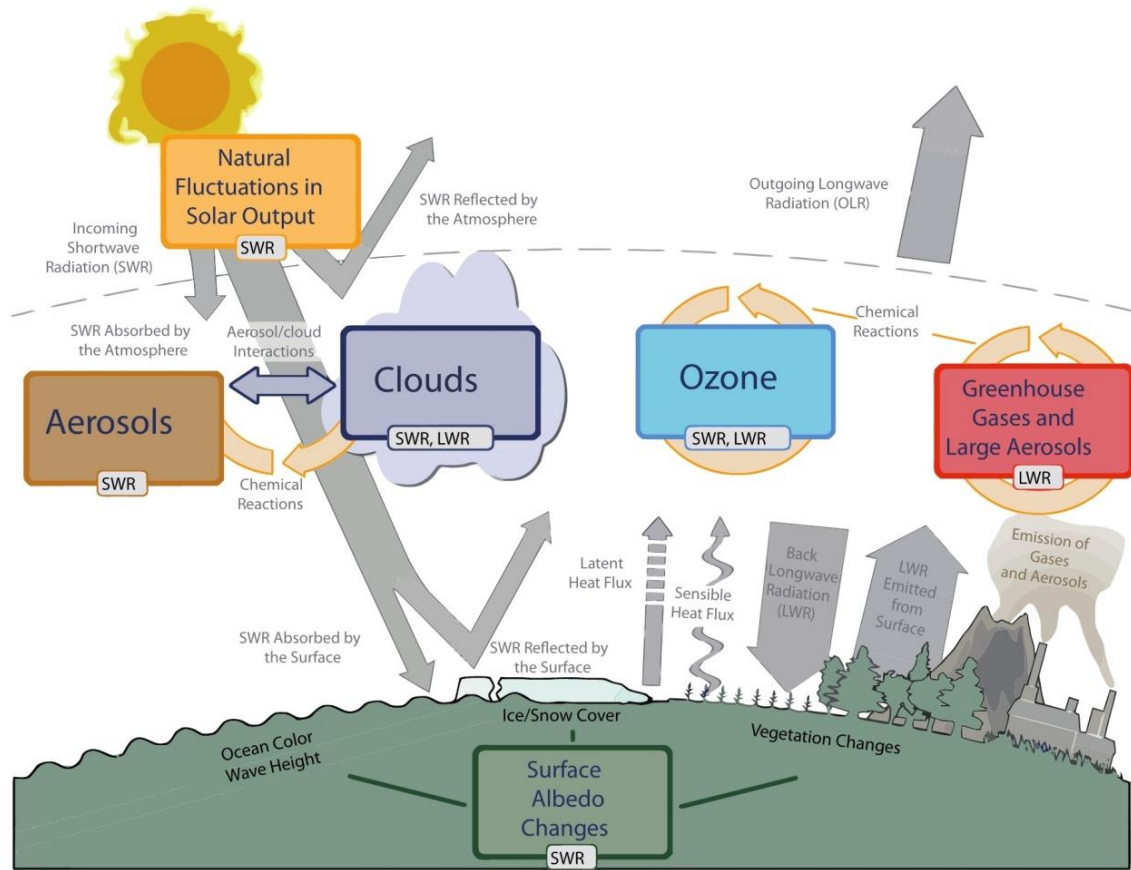
Figure 1-1 | Main contributors to climate change. The input of SWR and output of LWR is influenced by the combination of aerosols, clouds, concentration of ozone and greenhouse gases in the atmosphere. Furthermore, the surface albedo plays an important role, i.e. ocean color, coverage with ice and snow and major changes in the vegetation (reproduced from Forster *et al.*[2]).

This can also be expressed in numbers, by looking at the concentration of the gas in the atmosphere. In the pre-industrial age the concentration would not exceed 280 ppm and even in 1950, i.e. 200 years later, the concentration was below 320 ppm (Fig. 1-2). In the last six decades the accumulation of CO_2 in the atmosphere accelerated dramatically leading to values above 380 ppm in 2010. The predictions (FAR, SAR, TAR and AR4 taken from IPCC reports in 1990, 1996, 2001 and 2007, respectively) draw an even worse scenario of what to expect in the near future. Hence, measures have been taken by people all over the world, to turn this trend around or at least to slow it down. Of course, the reduction of emission is a major strategy to limit global warming. Though, since the need for energy remains high or is more likely even growing, there are technologies evolving which deal with the capture of CO_2 out of the atmosphere, to store or transform it into something useful, just as photosynthesis.[4–6]
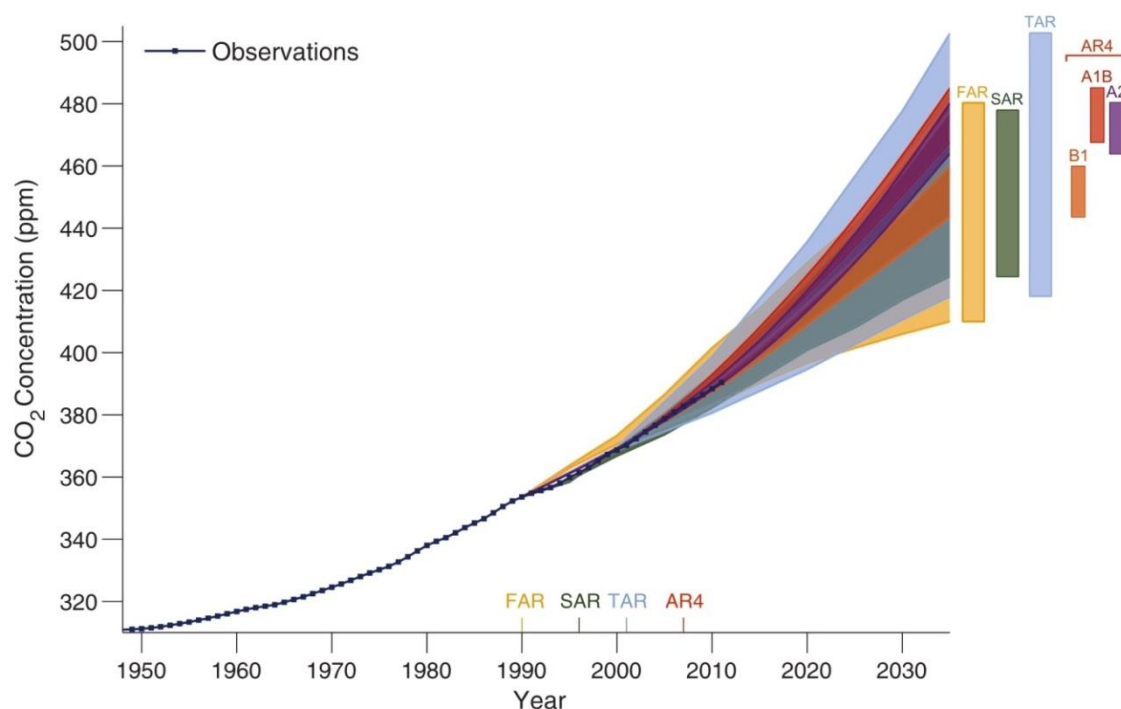
Figure 1-2 | CO₂ in the atmosphere. Projections of the observed increase (dark blue line with dots) of the concentration of CO_2 in the atmosphere from 1950 to 2030. The projections were made in different years (FAR from IPCC report in 1990, SAR from IPCC report in 1996, TAR from IPCC report in 2001 and AR4 from IPCC report in 2007), but all are showing the same trend and confirming the development of concentration (reproduced from Kaspar *et al.*[3]).

1.1.2 The C_1 building block

It seems to be so easy for green plants, to transform CO_2 into biomass but considering the molecular properties of the gas, it becomes obvious that much energy is needed to change its chemical structure. The carbon is in the highest oxidation state (+IV) and the Gibbs free energy is -393 kJ mol⁻¹. The needed energy for a transformation can be supplied externally or by the use of high-energy compounds, supported by a suitable catalyst. Established procedures are the production of urea by reacting CO_2 with ammonia (annual capacity of 150 Mt) or the production of inorganic carbonates like Na_2CO_3 via the Solvay-process (annual capacity of 45 Mt).[7,8] Furthermore, carbon dioxide is transformed into methanol (annual capacity 6 Mt), organic carbonates (annual capacity of 100 kt) or salicylic acid via the Kolbe-Schmitt-process (annual capacity 60 kt).[9–11] The hydrogenation of CO_2 to yield formic acid is still discussed on an academic level but it is gaining significant attention nowadays.[12–16] Apart from the transformation, considerable attention is drawn towards polymeric materials derived from CO_2.[5] Homopolymerization of the gas is currently only a theoretical experiment, as ceiling temperatures are anticipated far below realistic conditions.[17] Actual experiments have been carried out with CO_2 and dienes and with vinyl

ethers[18] or the combination with α,ω-dibromo compounds and potassium salt of diols catalyzed by crown ethers.[19,20] Another example involves formaldehyde as comonomer with bases and Lewis acids as catalysts to give non-alternating adducts.[21,22] More controlled and of growing interest is the reaction of CO_2 with epoxides, which is catalyzed by various organometallic[1,23–26] or organocatalysts[27,28] to give cyclic carbonates and polycarbonates. This topic is discussed in more detail in section 1.3.2.

1.1.3 The supercritical solvent

Carbon dioxide exhibits a phase transition at 31.2 °C and 76.3 bar, where it is entering the supercritical region (see Fig. 1-3).[4] Here, the molecule can act as solvent for many other compounds, which is of advantage compared to other organic solvents, as it is non-toxic, non-flammable and inexpensive. Although quite some energy is needed to maintain these conditions, it might be favorable to use supercritical CO_2 (scCO₂), as it is volatile under atmospheric pressure and as such easy to remove from the reaction mixture.[9,29] By adjustment of the pressure it is possible to tune the solubility of reactants in scCO₂ and thus it is possible to improve turn over frequencies and selectivities of the reaction.[30,31]
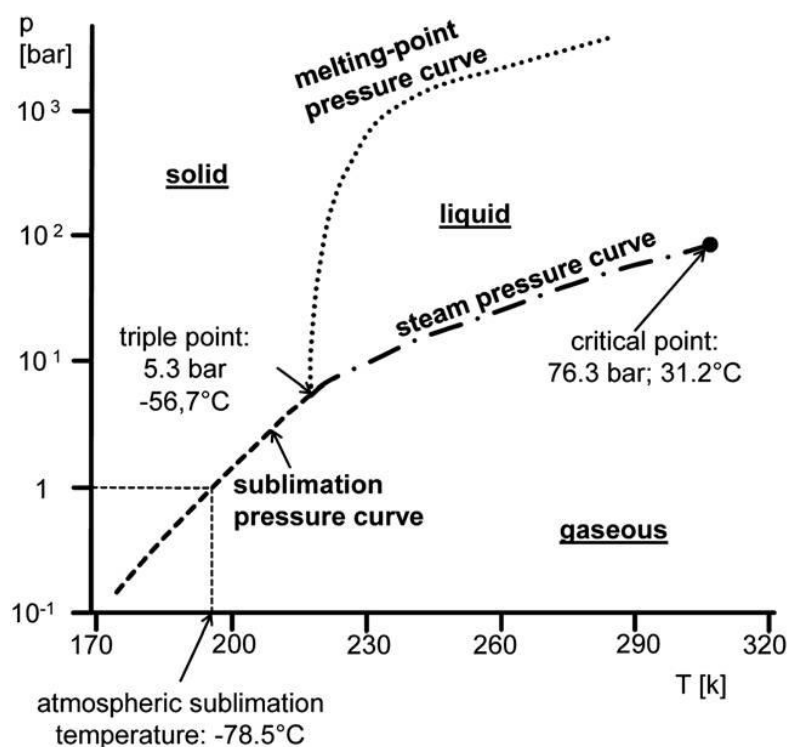
Figure 1-3 | **Phase diagram of CO₂.** In the diagram the triple point at 5.3 bar and -56.7 °C and the critical point at 76.3 bar and 31.2 °C are indicated (reproduced from Markewitz *et al.*[4] with permission from the Royal Society of Chemistry).

A combination of CO_2 as solvent and reactant is also subject of many scientific publications,[32,33] e.g. it was successfully employed for direct synthesis of dimethyl carbonate by Ballivet-Tkatchenko *et al.* which is used as fuel additive.[34] Darensbourg and coworkers used it in copolymerization with epoxides, which eventually could lead to completely green products where not only the monomers are bio-based but also the use of toxic organic solvents is avoided.[35] The supercritical fluid is also extensively employed as solvent and foaming agent in polymer extrusion, showing the great versatility of this molecule in terms of synthesis and processing.[36,37]

1.1.4 Carbon capture and storage technologies

Significance of the technology

The volatility of CO_2 has to be taken into consideration when its utilization as reactant or solvent is desired. It is not technically feasible to separate the gas from the atmosphere, as the concentration is still far too low (<400 ppm) compared to the other constituents like nitrogen and oxygen. Due to this issue two terms have evolved over the past years, one called carbon capture and storage (CCS) and the other carbon capture and utilization (CCU).[4,38,39] The first is mainly focused on storing the greenhouse gas in huge reservoirs that are isolated from atmosphere, whereas the latter addresses the transformation and fixation of CO_2 by turning it into platform and specialty chemicals as discussed in 1.1.2. The projected emission of carbon dioxide in 2050 is reported in the Blue Map Scenario of the International Energy Agency (IEA) to reach nearly 60 Gt a^{-1} as shown in Fig. 1-4.[40]
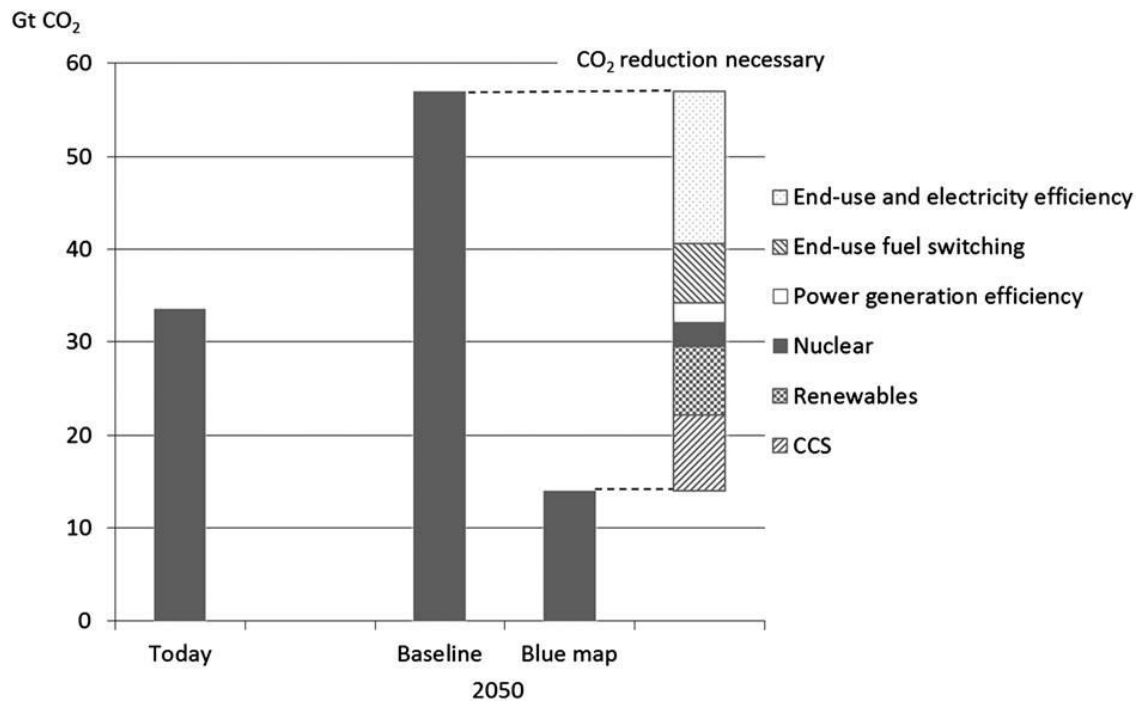
Figure 1-4 | Anthropogenic emission of CO$_2$. The emissions of CO$_2$ (in Gt) today and a projection for 2050 with reduction measures suggested by the IEA Blue Map Scenario published in 2010. According to the IEA the annual emission of CO$_2$ **will rise from today's 33** Gt a^{-1} to 58 Gt a^{-1}, if no counter measures are taken. As such, they identified an improved end-use/electricity and power generation efficiency, a switching of end-user fuels, the expansion of nuclear and renewables power generation and CCS (reproduced from Iglesias *et al.*[40]).

According to this scenario, today's anthropogenic emission of CO$_2$ of 32 Gt a^{-1} will nearly double until 2050. On the other hand, a reduction of 60% would be necessary to fulfill the set climate goals, i.e. to limit the global temperature rise to about 2 °C. This discrepancy is addressed in the report, suggesting various measures to reduce the actual emission of the greenhouse gas by combustion of fossil energy carriers. Besides the improvement of end-use/electricity and power generation efficiency, the authors propose a switching of end-use fuel, the expansion of nuclear and renewables power generation and last but not least the employment of CCS. The latter could contribute to about 8.2 Gt a^{-1}, showing the huge significance of those technologies.

Storage of CO$_2$

CCS and CCU comprise a wide range of technologies that essentially deal with the capture, transport, storage and use of CO$_2$ in various ways. As illustrated in Fig. 1-5, these technologies are in very different stages of development, some having already entered the markets (e.g. urea production or transport in pipelines) while others are tested in pilot plants (e.g. production of aliphatic polycarbonates or postcombustion technologies) or are still investigated in the laboratory (e.g. membranes or photocatalytic and electrocatalytic

activation of CO_2) and a few only exist as ideas and concepts (e.g. artificial photosynthesis).[4] The utilization of CO_2 has already been discussed in detail in the previous chapters and its transport is a simple and established technology as it only involves gas pipelines installed either onshore or offshore. More challenging is the storage of the volatile gas as leaking has to be prevented and large volumes are required. In this sense, geological storage formations are being investigated intensively, whereas the introduction of the gas into the ocean is prohibited due to negative impacts on the flora and fauna living there. A prerequisite for such geological storage options is a gas-tight barrier, trapping the gas inside the reservoir. Usually these barriers consist of a clay stone or salt layer, which is often found above deep-lying porous rock layers, which are filled with brine. When CO_2 is introduced in those so-called saline aquifers, it will be partly absorbed by the ambient rock formation water and in the long term transformed by mineralization.[41,42] Another man-made reservoir is found in depleted petroleum and gas wells, that in some cases can be – if not yet completely depleted – further extracted by injection of CO_2. This advantageous method is called Enhanced Oil Recovery (EOR) or Enhanced Gas Recovery (EGR) and usage of the gas as an extraction agent gives the industry another incentive to inject carbon dioxide in those reservoirs.
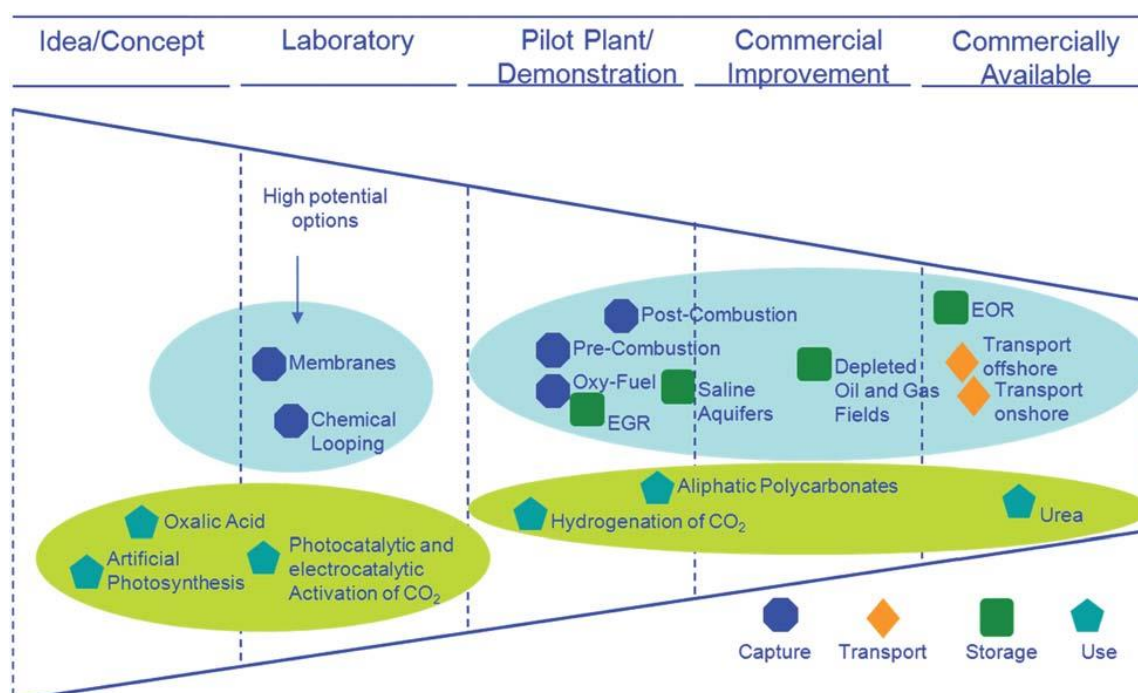
Figure 1-5 | Technologies in carbon capture and utilization. Stages of realization from concept to market entry for various technologies of capturing (blue), transporting (orange), storing (green) and utilizing (turquoise) CO_2 (reproduced from Markewitz *et al.*[4] with permission from the Royal Society of Chemistry).

A similar approach is also taken in non-exploitable coal seams that can be flushed with CO$_2$ to recover the coal seam gas for utilization and to use those seams for storage. The global available storage capacities of these reservoirs can only be estimated but, according to the IEA, saline aquifers might hold 1000 to 10 000 Gt, petroleum/gas fields add up to 600-1200 Gt and coal seams contribute with 3-200 Gt.[43] Until now, about 0.75 Gt CO$_2$ are stored in such reservoirs onshore and offshore all over the world.[4,42]

Capture of CO$_2$

The step so far neglected in the discussion is the actual capture of carbon. Though, this is the step of major importance as it is the least developed of all four (see Fig. 1-5, compare with stages of transport, storage and utilization, which all have at least one technology commercialized). Obviously, only if efficient separation of CO$_2$ can be accomplished, the three other steps can apply. The most important technological concepts for carbon capture involve

- chemical or physical absorption,
- adsorption phenomena and
- organic or inorganic membrane-based

separation techniques.[44,45] Among them, **chemical absorption** is the dominating technology, whereas alkanol amine solutions, e.g. of monoethanolamine (MEA) or diethanolamine (DEA), are the most established 'wet scrubbing' agents.[46] The mechanism relies on the formation of carbamates, which exist in equilibrium with the hydrolytic products hydrogen carbonate and the corresponding ammonium ion. Technically, the reaction is conducted at 40 °C, passing the CO$_2$ enriched gas through the aqueous amine solution in an absorption tower. The gas is subsequently released in a stripping tower at elevated temperatures (100–140 °C), whereas the regeneration of the solvent is connected to a considerable energy penalty, due to the high heat of formation of the carbamates.[47] In this context, new sterically hindered and/or tertiary amines (mechanism for tertiary amines, does not involve formation of carbamate but only hydrogen carbonate and ammonium ion) have been developed, e.g. 2-amino-2-methyl-1-propanol or *N*-methyldiethanolamine, respectively, exhibiting enhanced absorption rates, higher loading capacities, lower binding affinities to CO$_2$ and increased regeneration rates compared to MEA and DEA.[48,49] As an alternative, solutions of inorganics have been investigated, e.g.

aqueous solutions of potassium and sodium carbonate or ammonia, respectively. The latter is implemented in the technical process as the so-called chilled-ammonia process, whereas the underlying chemical reaction between CO_2 and aqueous ammonia is the formation of ammonium bicarbonate at temperatures below 20 °C.[50] The regeneration of the solvent is performed at 80 °C, thus showing an energetic advantage over the MEA and DEA solution process, which are operated at higher temperature in the regeneration stage.

The other absorption-based concept in the scope of carbon capture is the one relying on **physical absorption** at high partial pressure and low temperature. Commercial physical absorbents include mixtures of dialkylethers/poly(ethylene glycol) (Selexol®) or -40 °C cold methanol (Rectisol®), which have already been established industrially for natural gas sweetening. Another class of CO_2-selective physical absorbents constitutes ionic liquids that are promising candidates in the CCS process, as they not only have a very low vapor pressure and dissolve a large quantity of the gas but are also non-flammable, thermally stable and environmentally benign.[51,52] These physical solvents are advantageous over chemical absorbents in the regard of energy consumption during regeneration of the liquid, i.e. removal of the dissolved CO_2, by heat or pressure reduction.[51] Though, they require high pressure streams to absorb a significant amount of gas and thus are only economical if not too much energy has to be expended on compression of the gases involved.

The third class of carbon capture materials relies on **adsorption phenomena** and is usually employed in condensed phase, i.e. packed adsorbent beds in columns. Apart from the engineering challenges involved in the implementation of the process (heat exchange efficiency), adsorbent materials exhibit a superior energy efficiency compared to absorbent liquids, such as MEA, DEA solutions or Selexol®. Among those materials various classes have proven their efficiency in capturing CO_2, e.g. metal oxides, hydrotalcite-like compounds and porous compounds.[53–55] As structural motif, the latter shows either micro- or mesoporous properties, hence, fulfilling the necessity to expose a high surface area for adsorption of CO_2-molecules. Examples are carbonaceous adsorbents like activated carbon or carbon molecular sieves, respectively, zeolites and organic or metal-organic frameworks (MOFs). For all adsorbents, the capacity and selectivity are dependent on operational temperature and pressure, though regarding selectivity there are additional complex parameters to consider, i.e. molecular sieving effects, thermodynamic equilibrium effects and kinetic effects.[56]

The last class discussed here are **membranes**, which are still in a very early stage of development in the field of carbon capture technologies (see Fig. 1-5). Though, they are gaining more and more attention due to their low energy requirements and a high flexibility in terms of configurations and applications in the process.[57] The class can be subdivided into inorganic and organic membranes, the first comprising ceramics, metal oxides, molecular sieves and MOFs, the latter consisting of polymers like cellulose acetate (CAc), polysulfones (PSU), polyamides (PA), polyimides (PI), polycarbonates (PC) etc.[58,59] The performance of membranes is generally evaluated in terms of permeability (transport properties) and selectivity (separation properties). A more comprehensive overview over polymeric membrane materials in gas separation in general is given in section 1.2, while continuing here with a brief look into inorganic membranes and subsequently into technically relevant applications of the presented separation techniques and materials in the context of CCS. Inorganic membranes can be composed of either porous or non-porous materials, which are usually thermally more stable than their organic counterparts. As such, they can be employed for example in hydrogen/carbon dioxide separation at temperatures above 800 °C (conditions in precombustion technology, see next section). They are based on microporous materials, e.g. inorganic perovskite oxides, zeolites or palladium alloy tubes.[44,60] Microporosity was already structural motif for adsorption phenomena discussed previously, and it is not surprising that similar materials can also act as membrane materials. Hence, apart from aluminophosphates, silica and the very expensive palladium alloy tubes, again MOFs, immobilized on a carrier material, play a crucial role.[61,62] They all rely to a high extent on molecular sieving effects, i.e. molecular size and shape selectivity, and consequently, they are limited in view of overall performance. Another challenge to the membrane technology is the scalability of the separation modules, as the volume streams involved in the process are very large.

Large-scale applications of carbon capture technologies

Industrially most pertinent to the concepts of capturing carbon are gas streams in chemical and power plants, due to the large volumes associated with the production of synthesis gas, hydrogen and ammonia or the combustion of fuels, respectively.[7] Furthermore, the sweetening of natural gas, which is typically contaminated with over 40% of CO$_2$ and N$_2$, is a major field in this regard.

Within the scope of power plants, three major routes have evolved (illustrated in Fig. 1-6):[63,64]

- the **postcombustion** technology is implemented within the flue gas stream to capture CO_2 before exhaustion into the atmosphere;
- **precombustion** defines the method of CO_2-separation from synthesis gas (syngas) derived from fuel, prior to energy conversion;
- the **oxyfuel** process involves the recirculation of a concentrated stream of CO_2 into a combustion chamber, where it is injected together with pure oxygen, prepared from an air separation step, and a suitable fuel, e.g. coal, natural gas or syngas.

It has to be stated that all mentioned technologies require additional energy to separate, capture, condition and compress/liquefy the gas. Hence, this extra energy input – ranging between 10 to 14% points – has to be taken into consideration when the real carbon capture value is calculated.
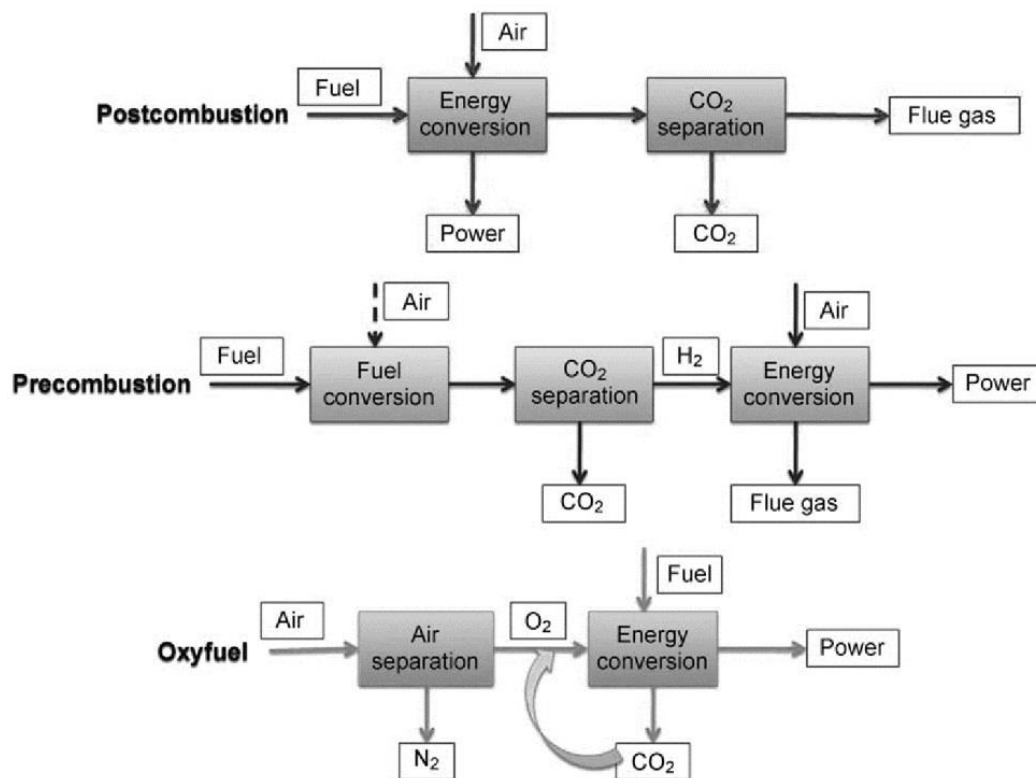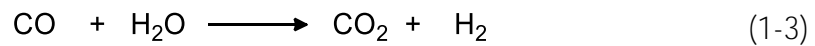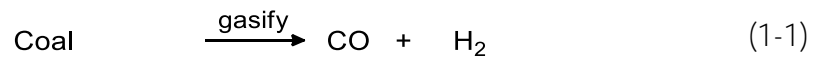

Figure 1-6 | Concepts of carbon capture. An overview of the capturing of CO_2 in the postcombustion, precombustion and oxyfuel processes (reproduced from Feron and Hendriks[65]).

Furthermore, the post-, precombustion and oxyfuel processes implicate different conditions in terms of temperature, pressure, steam content, gas composition and contamination.[4]

The **postcombustion** process is the most developed among those technologies, since retrofitting of existing power plants is most easily realized.[65,66] As the name is suggesting, the process is implemented within the flue gas stream to capture as much CO$_2$ as possible at relatively low temperatures and nearly atmospheric pressure. Before the decarbonized gas is exhausted into the atmosphere a final purification step for the removal of dust, sulfur and nitrogen compounds is installed.[67] The wet scrubbing method with a MEA solution is already implemented in pilot-scale in power plants, leading to a CO$_2$-separation efficiency of 80-95%. Countries like the USA, Denmark and Germany are testing this technology with separation capacities of up to 800 t of CO$_2$ per day.[4,68] A major challenge is the degradation of the solvent due to oxygen and contaminants in the flue gas, such as SO$_x$ and NO$_x$ compounds. The concentration of these contaminants has to be kept below 10 ppm to be negligible, whereas the concentration that is legally allowed for flue gas released into the atmosphere is set to 70 ppm.[69] Consequently, the use of less sensitive washing agents is a measure to increase the lifetime of the solutions used for CO$_2$ separation. Another challenge is the already addressed additional energy demand for solvent regeneration. This is exemplified by the values for energy and steam demand per tonne of CO$_2$ captured, being 4 GJ and about 50% of the low pressure steam in the plant, respectively. Hence, an energy penalty of about 14% for this technology causes an additional output of CO$_2$ and costs of about 30 € per tonne of CO$_2$.[68] The postcombustion technology's high costs of carbon capture compete with its ease of retrofitting it to existing plants.

Thus, alternative routes with improved efficiency are investigated intensively, one of them being the so-called **precombustion** process. Here, the carbon is separated from the fuel gas stream before the combustion. The underlying principle involves the partial oxidation of fossil fuels in an O$_2$-deficient atmosphere (Eq. 1-1 for gasification of coal, Eq. 1-2 for reforming of methane) and the presence of water to produce syngas, i.e. hydrogen and carbon monoxide. The latter is converted to CO$_2$ via the water-gas shift reaction in the presence of water, giving another equivalent of hydrogen (see Eq. 1-3). At this point, decarbonization is achieved by separating CO$_2$ from H$_2$ in the high-pressure, high temperature gas stream. The hydrogen-enriched gas is eventually introduced into gas

turbine combustors to produce energy with high efficiency (see Fig. 1-6 for schematic description of the process).

$$Coal \xrightarrow{gasify} CO + H_2 \qquad (1\text{-}1)$$

$$CH_4 + H_2O \longrightarrow CO + 3H_2 \qquad (1\text{-}2)$$

$$CO + H_2O \longrightarrow CO_2 + H_2 \qquad (1\text{-}3)$$

For power plants using the gasification of coal, the term Integrated Gasification Combined Cycle has evolved with CO_2 separation being an option but not a necessity. The partial oxidation of coal (gasification) or natural gas is carried out in the presence of oxygen and water, whereas nitrogen is separated from air before it is fed into the reactor. This prior air separation step is advantageous, as it leads to higher conversion of the coal/natural gas, facilitates separation of CO_2 from H_2 and leads to an overall decreased volume stream.[70] Integrated Gasification Combined Cycle pilot plants have been built since the 1980s and recently efforts have been made to CCS units before the combustion of the fuel gas.[4] The major advantage of this technology compared to the postcombustion process it the reduced energy capture penalty due to higher concentrations of CO_2 and higher partial pressures. Furthermore, the produced H_2-rich fuel can also be utilized as a feedstock in chemical industry, in fuel cells for direct power generation or as an intermediate for other fuels like methanol.[71] On the other hand, the accompanying higher investment costs and more complex setup, which prohibit retrofitting of existing power plants, have to be assessed against their life cycle environmental impacts.[72]

A different approach is taken for the **oxyfuel** technology, whereas pure oxygen is used for the combustion of fossil fuels. To enrich the stream of CO_2, the gas is recirculated and released only when a sufficient concentration of carbon dioxide for sequestration is reached. For complete exclusion of nitrogen during combustion the introduced air is separated in a preliminary step and only O_2 is introduced into the combustion chamber. The recirculation of the flue gas stream allows enrichment with CO_2 to about 90%, whereas usually the concentration of flue gas from power plants lies below 15%. Due to the high concentration, the gas stream is directly condensed and subsequently demoisturized, cleaned from SO_x and NO_x compounds and compressed for transport and storage. For the separation of O_2 from N_2, state-of-the-art are cryogenic air separation units that are operated at low temperatures (<-182 °C) to condense oxygen and to purify it by high-

pressure distillation. This separation process is of course energy intensive and purities of 99.5 vol% are necessary to maintain high efficiency of the process and alternatives for separation, e.g. oxygen transport membranes are investigated.[68,73–75] The overall energy penalty for the implementation of the oxyfuel process was calculated to range between 8 to 10% points, with 6% points contribution from the air separation, i.e. the efficiency loss is lower compared to post- and precombustion processes.[4] Combined with the low level of CO_2 emission from such power plants the technology is promising, though major challenges are the high investment costs as standard equipment has to be modified and retrofitting existing plants is difficult.

All of the above described technologies, i.e. postcombustion, precombustion and oxyfuel involve at least one gas separation step, be it carbon dioxide from nitrogen in the flue gas, oxygen from nitrogen in an air separation unit or both, respectively. And each of those separation steps requires a significant amount of energy to realize separation. Membranes can provide an alternative in this context, as they avoid extensive energy input for regeneration of absorbents/adsorbents or for cooling air to -182 °C.[57] Among membranes, polymeric materials constitute a major class for separation of gases and the – in this thesis introduced – poly(limonene carbonate) might be a viable choice in one or more of the above described processes, due to its excellent transport and separation properties for CO_2 and other gases.

1.2 Polymeric membranes for gas separation

1.2.1 Significance of membranes in industry

In 1980, the first large scale application of membrane gas separation was launched by Permea (now Air Products). They installed polysulfone (PSU) hollow fiber membrane modules for the separation and recovery of hydrogen from the purge gas stream of ammonia plants with their so-called Prism membranes.[76] Within the next decades, the development of new materials and processes has led to further industrial applications, which is illustrated by the milestones in Fig. 1-7. Apart from PSU, polymers used in commercialized membranes include mainly cellulose acetate (Separex 1982, Cynara 1983, UOP 1995), polyimide (Ube 1989 and Medal 1994), polyphenylene ether (PPE, Delair 1991, also called polyphenylene oxide) and polyethylene oxide (GKSS/MTR 2008).[59]
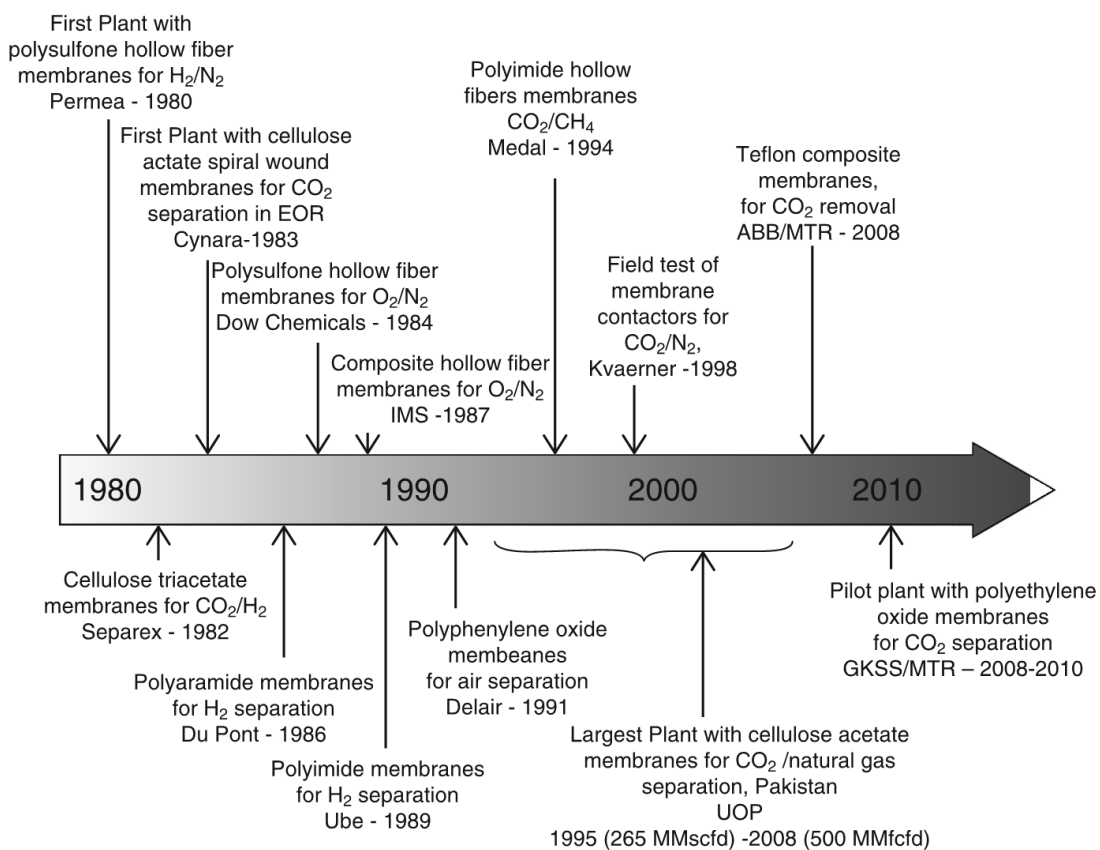
Figure 1-7 | The evolution of membranes for gas separation. Milestones in the evolution of membrane gas separation technology within the first large-scale application in 1980 by Permea until the launch of a pilot plant with PEO membranes in 2010 (reprinted from Ismail *et al.*[59] with permission from Springer International Publishing).

The gas streams in industrial processes are usually large and a high flux of the separated gas (permeate) has to be realized. Hence, a high surface area to module volume ratio of the membrane material is required (> 1000 m² m^{-3}) that is either produced by flat sheet spiral wound or hollow fiber modules.[77] The growing significance of membrane technology can be explained by the advantages of membranes for gas separation:

- Simplicity in concept and operation
- Low energy requirements for complete separation (no regeneration of sorbents etc.)
- Modularity and ease of scale-up
- High efficiency in use of raw materials
- Avoidance of moving parts

These advantages have led to the re-evaluation of technical processes, wherever gas separation plays a crucial role. Except for CO_2 separation in CCS technology in power plants and purification of natural gas, industry is confronted with separation problems among other things in refineries (H_2/hydrocarbons), ammonia plants (H_2/N_2) and polyolefin production (light gases/volatile organic compounds, VOCs). Each of those problems implies a gas mixture of two or more gases. In most cases, the problem can be reduced to the separation of one gas pair, e.g. the separation of hydrogen from nitrogen in the ammonia purge gas.

Table 1-1 | Main industrial applications for gas separation with membrane materials.[59,78,79]

gas pair	industrial process
H_2/CO_2	hydrogen generation in precombustion technology
H_2/N_2	ammonia purge gas
H_2/hydrocarbons	hydrogen recovery in refineries
O_2/N_2	air separation to yield oxygen (oxyfuel, steel industry) and nitrogen
CO_2/CH_4	natural gas sweetening, land fill gas upgrading
CO_2/N_2	flue gas treatment (postcombustion)
H_2O/CH_4	drying of natural gas
H_2S/hydrocarbons	sour gas treatment
hydrocarbons/air	hydrocarbon recovery or pollution control
He/N_2	helium recovery
light gases/VOCs[a]	polyolefin purge gas purification

[a]VOCs like ethylene or propylene

An overview over such fundamental gas pairs and their occurrence in industrial processes is presented in Table 1-1. For the choice of the best membrane material, its selectivity for one molecule of the gas pair is essential. However, membranes for gas separation also imply some practical problems leading to a decreased performance over time. One major effect is fouling of the membrane due to blockage of the surface and/or pores. The fouling can arise from strong physical interaction, i.e. adsorption of sulfur compounds such as H_2S or SO_2 or accumulation of small particles. The latter can be removed by reverse purging with a non-adsorbing gas (or filtered off before contact with the membrane), whereas the first might lead to an irreversible deterioration of the membrane. Another disadvantage of this type of gas separation is the risk of leaks in the membrane that are inherently produced as thin as possible to maintain a high flux of the gas stream. Additionally, polymeric materials are prone to chemical attack by reactive compounds like acids, bases, radicals etc. and might lose mechanical stability or undergo physical or chemical transformations leading to changed separation properties.[78]

## 1.2.2 Fundamentals of membrane transport phenomena

The membrane-based separation of gases is primarily dependent on the transport of the individual molecules through the material. The driving force is, as postulated in FICK's first law, the diffusive flux J along a concentration gradient towards the lower concentration region under the assumption of steady state. The magnitude of this flux is proportional to the concentration difference. The proportionality constant between the flux and the gradient in the concentration for a given system is called diffusivity or diffusion coefficient D as expressed in Eq. 1-4.[80,81]

$$J = -D \frac{\partial c}{\partial x} \qquad (1-4)$$

Another important principle in this context is HENRY's law formulated in 1803, stating that the amount of gas dissolved in the contacting liquid (or here amorphous polymer) is proportional to its partial pressure in the gas phase.[82]

A schematic of the most frequently observed transport mechanisms in membrane separation processes is illustrated in Fig. 1-8. They can be subdivided into porous and non-porous transport phenomena, whereas the KNUDSEN diffusion and molecular sieving belong to the first group and the solution-diffusion mechanism belongs to the latter. For a

given gas pair, the decisive parameter for the KNUDSEN diffusion is the molecular weight of the molecules, as it correlates inversely proportional with the mean free path in a confinement, i.e. a pore. The pores are larger than the gas molecules (2 – 50 nm) but smaller than the mean free path resulting in more collisions with the pore wall than with other gas molecules.[83] Molecular sieving takes advantage of the size difference of molecules, i.e. the kinetic diameter as shown in Table 1-2, and is possible for membranes with very small pores (< 20 Å).[84] For a monodisperse pore diameter distribution a complete separation of gases is theoretically possible if one of the gas molecules is larger than the pore.[85]
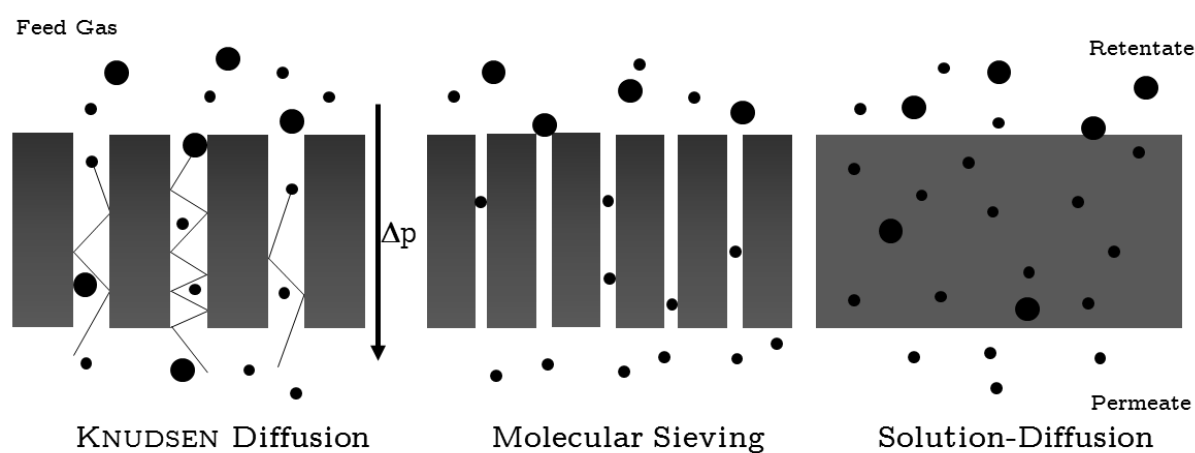
Figure 1-8 | Mechanism of gas transport through membranes. Schematic illustration of the three major mechanisms of transport of gas molecules through porous (KNUDSEN diffusion, molecular sieving) or non-porous (solution-diffusion) membranes. For materials showing KNUDSEN diffusion, the separation is achieved by the difference in molecular weight of the molecules, whereas molecular sieving is based on size exclusion with smaller pores. Solution-diffusion takes place in dense polymeric membranes, which leads to separation if solubility and/or diffusivity of the gas pair differ significantly (adapted from Ismail *et al.*[59]).

For non-porous amorphous polymers solution-diffusion is the dominant transport mechanism. It involves three steps, starting with the adsorption of gas molecules on the surface of the membrane on the feed side.[86,87] After diffusion of the molecules through the polymer matrix, the third step is completed with desorption, i.e. evaporation of the diffusing species. This process was first described in literature by Thomas Graham 150 years ago and it is controlled by two major parameters of the penetrating gas: the diffusion coefficient D and the solubility coefficient S.[88] The rate determining step is the creation of holes with sufficient size in the polymer matrix to allow the penetrant molecules to move along the concentration gradient.

Table 1-2 | Selection of gases relevant to industrial separation processes.

molecule	molecular weight (g mol^{-1})	kinetic diameter (Å)
H_2	2	2.89
CH_4	16	3.80
H_2O	18	2.65
N_2	28	3.64
O_2	32	3.46
CO_2	44	3.30

This thermally stimulated segmental motion of polymer chains is very slow compared to molecular kinetics and can be described with the sorption-diffusion theory.[89] Solubility and diffusivity of the gas may be affected by the chain packing density, orientation of the chains, crystallinity, polarity, nature of functional group, plasticizers, fillers and humidity. The performance of a non-porous polymeric membrane with respect to a single gas is expressed by the permeability P, which is defined as the product of diffusivity and solubility (see Eq. 1-5).

$$P = D \times S \tag{1-5}$$

Alternatively, the permeability can also be expressed by J and the partial pressure difference Δp normalized by the thickness l of the membrane as shown in Eq. 1-6:

$$P = \frac{J \cdot l}{\Delta p} \tag{1-6}$$

Typically for membrane materials, i.e. high flux materials, the unit for permeability is given in barrer, with:

$$1 \; barrer = 10^{-10} \frac{cm^3 \; (STP) cm}{cm^2 \; s \; cmHg}$$

The membrane thickness-normalized permeability is sometimes replaced by the thickness dependent permeance Q to give a more practical value for the performance of a membrane (see Eq. 1-7) that is only a few micrometers (or even 100 nm) thick:

$$Q = \frac{J}{\Delta p} \tag{1-7}$$

The unit often used in the context of permeance of polymeric membranes is gas permeation unit (GPU) and is by definition:

$$1 \ GPU = 10^{-6} \frac{cm^3 \ (STP)}{cm^2 \ s \ cmHg}$$

The other decisive parameter for gas separation membranes is the selectivity α (A/B) for gas A in a mixture of the two gases A and B, i.e. the ratio of permeabilities for a given gas pair A/B. When the permeabilities – obtained from single gas measurements – are used for the calculation, the ideal separation factor, the so-called permselectivity is defined by Eq. 1-8.

$$\alpha(A/B) = \frac{P_A}{P_B} \tag{1-8}$$

Selectivities in non-porous membranes are usually high, while the effective transport of gas molecules through the materials is rather slow compared to porous membranes. The size of the permeating species in non-porous membranes is of minor importance and rather the solubility in the medium governs the performance of the material in regard of gas separation. From a technical point of view, both the permeability and the selectivity of a membrane material should be as high as possible, thus leading to a fast separation of high purity gases. However, there is an inherent trade-off, i.e. reciprocal relationship between both parameters that is empirically described by Eq. 1-9.

$$P_A = k_{up}\alpha(A/B)^{n_{up}} \tag{1-9}$$

with k_{up} and n_{up} being empirically determined parameters for a given gas pair. This relationship can be visualized in an upper bound when selectivity is plotted against permeability. Lloyd M. Robeson established this upper bound in systematic studies and published this line in the above-mentioned special type of plot for the first time in 1991.[90,91] In Fig. 1-9 such a ROBESON plot for the gas pair CO_2/CH_4 is shown for a vast variety of glassy and rubbery polymers. The dashed line represents the empirically found upper bound that was not yet surpassed 25 years ago. However, 17 years later, Robeson updated and revised his database of glassy and polymeric membrane materials and shifted the upper bound to higher values, which was recently again outperformed by new materials and shall be discussed further in the 'state-of-the-art' section 1.2.3.[79,91]
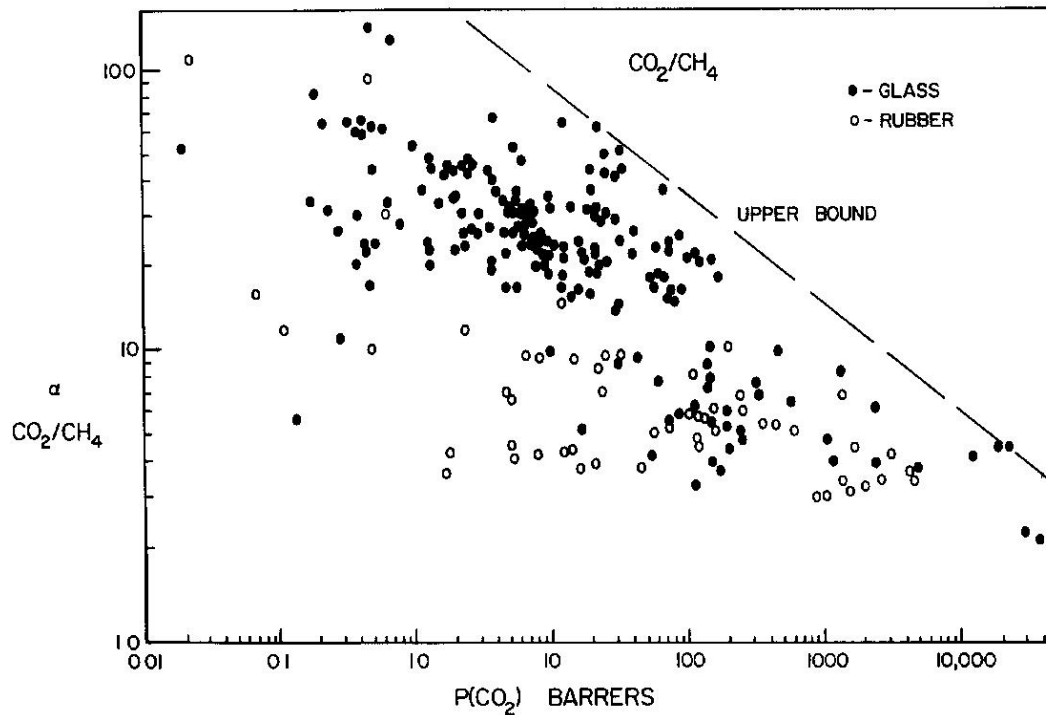
Figure 1-9 | Original ROBESON plot from 1991. The plot for the separation factor of $\alpha_{CO2/CH4}$ versus the permeability of CO_2 for glassy and rubbery polymeric membranes. The dashed line indicates the upper bound as an empirical border, representing the trade-off between selectivity and permeability (reprinted from Robeson[90] with permission from Elsevier).

Another important property related to membrane materials and their performance is the distribution of free volume elements in the polymer matrix, as transport is facilitated in an interconnected microporous environment. The free volume V_f is the space not occupied by molecular chains in the glassy polymer, due to limited packing density of amorphous domains. V_f can be expressed mathematically as the difference of the specific volume V_{sp} and the specific VAN DER WAALS volume $V_{W,s}$ multiplied by 1.3 (see Eq. 1-10). The VAN DER WAALS volume is calculated using the group contribution method of BONDI and the factor is introduced to compensate for the steric demand of any molecule that is, even at 0 K, higher than its $V_{W,s}$.[92–94]

$$V_f = V_{sp} - 1.3V_{W,s} \tag{1-10}$$

A quantity often reported in literature is the fractional free volume (FFV) that is obtained by division of the free volume by the specific volume of the polymer:

$$FFV = \frac{V_f}{V_{sp}} \tag{1-11}$$

Typically, values of the FFV range from 0.11 for barrier materials to 0.29 for membrane materials.[95,96]

The theoretical approach using VAN DER WAALS radii of molecules to deduce free volume can be supported by experimental values, obtained from positron annihilation lifetime spectroscopy (PALS). Rather than the fraction of free volume, here, the mean pore size (even on the sub-nanometer scale) is measured that is usually proportional to the *FFV*.[97–99] To interpret the data recorded in a PALS experiment the TAO-ELDRUP model is applied.[100–102] The non-destructive technique involves the generation of positrons from a radioactive source, which are injected into the condensed matter under investigation. The positrons interact primarily with the electrons in the matrix to produce a metastable positron/electron state called positronium (Ps). The latter usually annihilates rapidly – accompanied by the emission of a photon – by interaction with other (free) electrons in the matrix. However, if voids, e.g. cavities in a polymer membrane, are present the electron-density-free space has a prolonging influence on the lifetime τ of a positronium. From this difference in lifetime of positroniums the cavity radius r_c can be deduced. To explain the theoretical background of the spectroscopic technique it has to be mentioned that positroniums exist in two spin states. For opposite spin of the electron and the positron the term *para*-positronium (*p*-Ps) is used with a self-annihilation lifetime in vacuum of 125 ps. The lifetime of an *ortho*-positronium (*o*-Ps, parallel spin of electron and positron), on the other hand, is three orders of magnitude higher (142 ns) in vacuum, while pick-off of an electron of opposite spin leads to a reduction of lifetime to < 4 ns. This reduction is dependent on the size of the void the *o*-Ps is trapped in and thus the rate of pick-off annihilation λ_{po} is inversely proportional to r_c of the hole. In the semi-empirical TAO-ELDRUP model the potential well of finite height associated with the hole is replaced by an infinitely high potential with the radius $r_c + \delta r$ (the penetration depth δr of a Ps wave function into the cavity walls was empirically found to be 1.66 Å). The mathematical expression for the relation of pick-off rate, the lifetime of the *o*-Ps τ_3 and the cavity radius is shown in Eq. 1-12.[98]

$$\lambda_3 = \frac{1}{\tau_3} = 2\,ns^{-1}\left[1 - \frac{r_c}{r_c + \delta r} + \frac{1}{2\pi}sin\left(\frac{2\pi r_h}{r_c + \delta r}\right)\right] \qquad (1\text{-}12)$$

The spectroscopically obtained lifetime distribution can be transformed by numerical Laplace inversion into a r_c probability function and subsequently into a hole volume distribution that is a major interest in terms of membrane science.[103,104]

1.2.3 State-of-the-art polymers for gas separation

Many classes of polymers have been evaluated in terms of applicability in membrane technology, e.g. polyamides,[105] polyimides,[106,107] polycarbonates,[108,109] polyarylates,[110] poly(phenylene ether)s,[111] poly(ethylene oxide)s,[112] polyanilines,[113,114] polysulfones,[115,116] polyacetylenes,[117,118] acetylated cellulose[119] etc. For the purpose of CO_2 separation, those polymers with a high permeability (> 100 barrer) and selectivity (> 30) for the gas are limited in number. Polymers that are commercially available in membrane modules are illustrated in Fig. 1-10 with a selection of membrane-related properties shown in Table 1-3. Except for the acetylated cellulose, a common motif are aromatic units like bisphenol A (BPA) that give rise to rather rigid backbones, which is reflected in the high glass transition temperatures (> 150 °C) and fair CO_2 permeabilities ranging from 2.6 barrer for the poly(ether imide) (PEI) to 48 barrer for PPE.[120,121] The selectivities of these established materials are mediocre with regard to the upper bound in a ROBESON plot. The highly permeable polymer PPE exhibits the lowest selectivity of only 17, while PI shows the highest α (CO_2/CH_4) with 41 and a fair P (CO_2) of 12.[122]
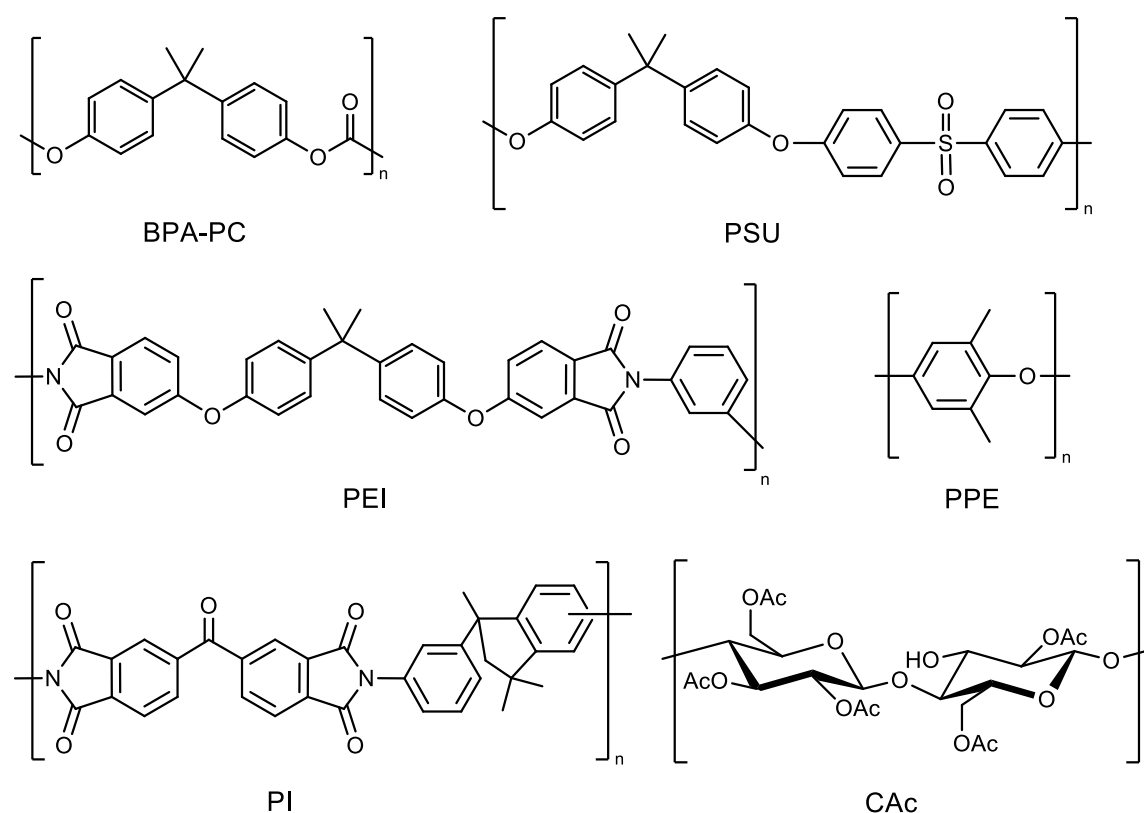
Figure 1-10 | Commercial polymers for the gas separation. Examples of commercial polymers employed in membrane modules are bisphenol-A polycarbonate (BPA-PC), polysulfones (PSU), poly(ether imide) (PEI), poly(phenylene ether) (PPE), polyimide (PI) and cellulose acetate (CAc, with triplicate substitution of hydroxy groups).

Efforts have been made to improve the performance of these established membrane materials. Successful techniques involve the halogenation or introduction of sterically demanding groups to increase free volume.[121,123–125] The addition of functional groups for facilitated transport (solute interacts chemically with matrix material, thus greatly improving solubility of the permeate) is another promising route to increase the performance of a membrane.[126] However, state-of-the-art materials have been developed from new monomers to give permeabilities for small molecules like CO_2 beyond 100 barrer, as shown in Fig. 1-11 and Table 1-3.

Table 1-3 | Properties of commercially available and state-of-the-art membrane materials.

polymer	T_g (°C)	FFV	Δp (kPa)	P (CO_2) (barrer)	α (CO_2/CH_4)	ref.
State-of-the-art						
PTMSP	>300	0.29	100	47000	1.6	[117,127]
PIM-1	-	0.26	400	5100	9.6	[128]
TR-PI	-	0.27	100	1620	46	[129]
TOX-PIM-1	-	-	400	1100	60	[128]
DATRI-PI[a]	430	0.23	100	189	31	[122]
commercial						
PPE	215		70	48	17	[123]
PI[b]	300	0.17	100	12	41	[96]
CAc	188	0.21	100	6.9	37	[78,119,130]
BPA-PC	150	0.16	100	6.8	25	[131]
PSU	186	0.15	100	5.6	22	[96,116]
PEI	216	0.14	300	2.6	39	[120]

[a]permeability tested at 35 °C, [b]permeability tested at 30 °C

For the design of new membrane materials there are some considerations to be made. Properties that promise high performance as membrane materials include a high fraction of free volume and selective solubility for one gas. For glassy polymers, important structural motifs are very rigid and twisted backbones or a high chain mobility, as they are found in polymers with intrinsic microporosity (PIMs) like PIM-1 or poly(1-trimethylsilyl-1-propyne) (PTMSP), respectively.[118,132–134]
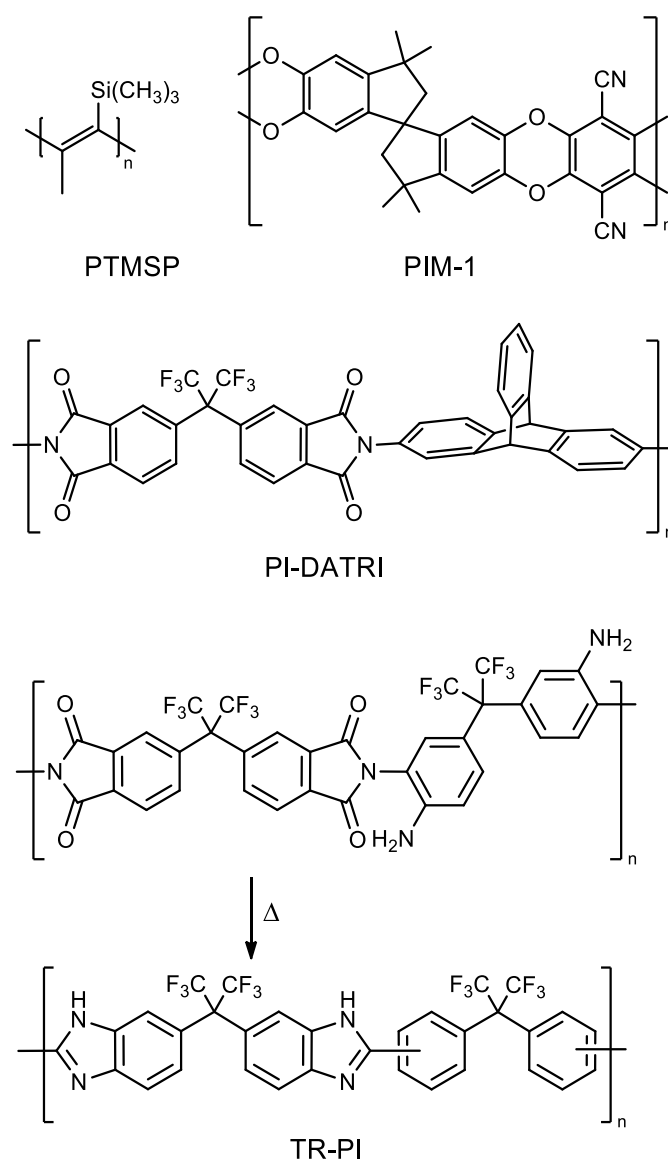
Figure 1-11 | State-of-the-art polymeric membrane materials. Structures of polymers with very high permeabilities and selectivities for state-of-the-art membrane applications: poly(1-trimethylsilyl-1-propyne) (PTMSP), polymer with intrinsic microporosity 1 (PIM-1), poly(4,4'-hexafluoroisopropylidene-2,6-triptycene imide) (PI-DATRI), thermally rearranged polyimide (TR-PI).

The first is based on a spirobisindane ladder structure and yields permeation rates for CO_2 of over 5000 barrer combined with – for this permeation – excellent selectivity of nearly 10. Even one order of magnitude higher is $P(CO_2)$ (47 000 barrer) of the latter, which is based on a substituted acetylene species (the repeating units are shown in Fig. 1-11). However, the intrinsic trade-off demands a low selectivity of 1.6 over CH_4. The other two polymers shown in Fig. 1-11 contain imide linkages possessing enhanced rigidity in the backbone compared to traditional PIs. The copolymerization of the sterically very demanding triptycene-based monomer 2,6-diaminotriptycene (DATRI) with the fluorinated diphthalic anhydride derivative yield a polymer (DATRI-PI) with an extremely high T_g of

430 °C and a P(CO_2) of nearly 200 barrer accompanied by a very high CO_2/CH_4 selectivity of over 30.[122] The permeation performance is further improved for the thermally rearranged PI (TR-PI) yielding either polybenzimidazole, polybenzoxazole or polybenzothiazole membranes (depending on the initial PI carrying amine, alcohol or thiol functions in *ortho*-linkage position, respectively)[129,135] For the here presented polybenzimidazole an exceptional combination of very high CO_2 permeability (P(CO_2) = 1620 barrer) and strong selectivity over methane (α (CO_2/CH_4) = 46) was achieved. This high free volume polymer is an example for a material actually surpassing the upper bound proposed by Robeson in 2008 as illustrated in Fig. 1-12.[91]
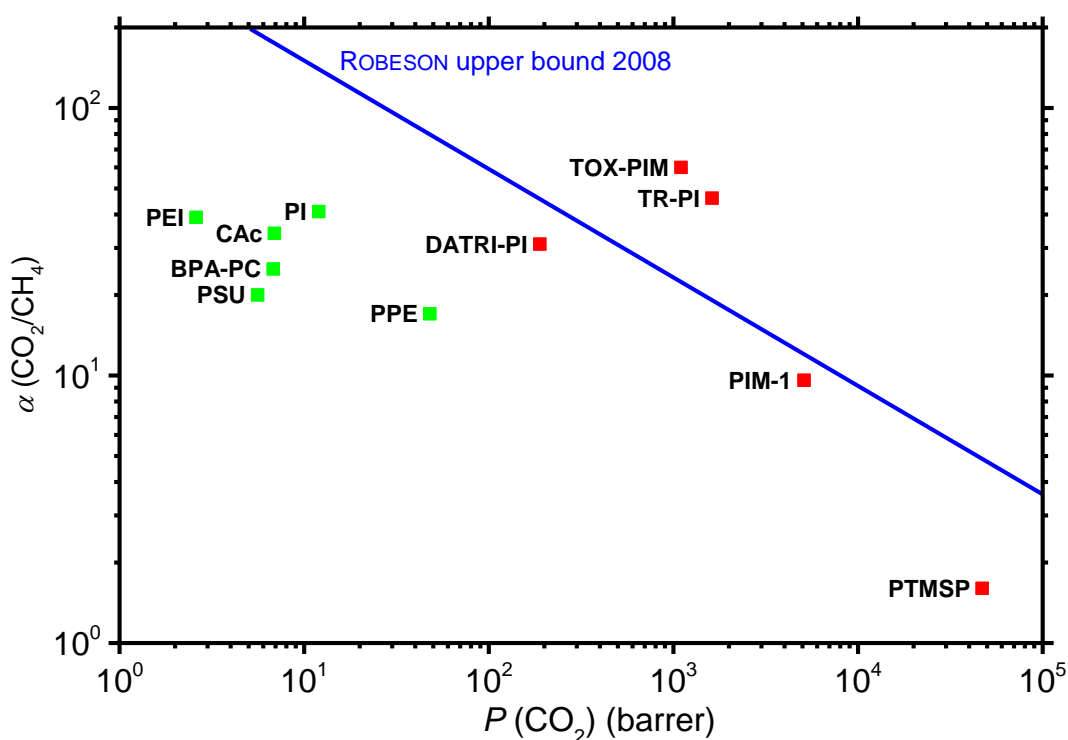
Figure 1-12 | ROBESON plot with state-of-the-art polymers. The plot for the gas pair CO_2/CH_4 with the commercial and state-of-the-art polymeric membrane materials shows that some of the latter can actually surpass the ROBESON upper bound from 2008.

Thermal rearrangement seems to be the method of choice to produce materials surpassing the upper bound of 2008, as it is also the case for PIM-1 that was annealed at high temperatures (> 300 °C) in the presence of oxygen to yield thermal-oxidatively crosslinked PIM-1 (TOX-PIM-1) with a permeability of 1100 barrer and a selectivity of about 60 versus methane.[128] The new generation of membrane polymers suffers mainly from aging and fouling effects that lead to deterioration of the performance in a relatively short time. The aging can be ascribed mainly to the relaxation of the polymer backbone into a

thermodynamically favorable state.[97,117,136] Also, the used monomers are rather expensive thus leading to high investment costs when applied on larger scale. Consequently, there is a need for materials that can combine high performance as a gas separating membrane with long-term stability and affordability.
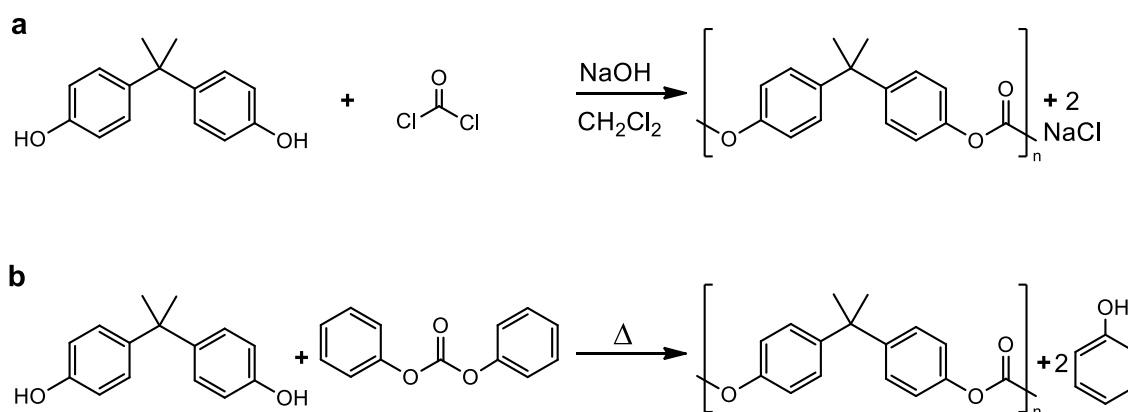
1.3 Polycarbonates

First discoveries in the field of PCs date back to 1898, when Einhorn reported the successful transformation of hydroquinone- and resorcinol-derivatives into polymers.[137] He copolymerized the aromatic diols with phosgene in pyridine solution to produce linear polycarbonates. The reaction with hydroquinone yielded an insoluble crystalline solid, melting above 280 °C. The resorcinol derivative, on the other hand, gave an amorphous material, that would decompose already at 200 °C. Four years later, an alternative route towards the same PCs was reported by Bischoff and Hedenstroem, who employed a transesterification with diphenyl carbonate as a substitute for phosgene.[138] It took another three decades until attention was drawn towards this class of materials again, which is likely explained by the poor solubility and processability of those resins. Two pioneers in the field of macromolecular chemistry, Carothers and van Natta, demonstrated two pathways for the production of aliphatic, low molecular weight, low melting polycarbonates by either transesterification of diols with diethyl carbonate or ring opening polymerization (ROP) of cyclic carbonates.[139] The latter route was taken up by a coworker of the DuPont company, who filed a patent on the transesterification of 1,6-hexandiol and dibutyl carbonate to yield a high molecular weight polymer with low melting point.[140] These materials with low softening temperatures were not really commercially successful, because applications in everyday life were very limited. In 1954, Schnell and coworkers from Bayer AG took up the initial concept of aromatic PC, to produce high melting, high molecular weight polymers.[141] At the time, 4,4'-dihydroxydiphenyl alkanes were investigated in the context of PC, which is the family of compounds bisphenol A also belongs to.

1.3.1 Aromatic polycarbonates

This can be seen as the breakthrough in the field of thermoplastic PCs, as the materials – especially those derived from BPA – were not only stable at elevated temperature but also soluble in organic solvents, transparent (i.e. amorphous) and mechanically superior to other commercially available plastics.[142,143] Because of this excellent property profile, many companies initiated research and development of bisphenol A polycarbonate (BPA-PC). After some legal disputes involving General Electric and Mobay Chemical, the Bayer AG received the rights for the – at the time commercially most relevant – production of BPA-PC via an interfacial reaction of BPA and phosgene (Fig. 1-13a).[144–146] To date this method

still dominates the market with only minor alterations of the process. The transesterification of BPA (also covered in the patent of Schnell *et al.*) with diphenyl carbonate is not as popular, but it has gained more attention in the 1980s, when several plants in China, Japan and Spain have been built in this regard (Fig. 1-13b).[147–150]

Figure 1-13 | The production of BPA-PC. Industrially employed processes for the production of BPA-PC via (**a**) interfacial copolymerization of BPA and phosgene or (**b**) melt polycondensation of BPA with diphenyl carbonate.

Technically, the interfacial process involves in the first step the dissolution of BPA in dichloromethane (DCM) together with phenol as end-capper to maintain control over the molecular weight. The next step consists of the addition of phosgene and aqueous sodium hydroxide to the reactor, which will result in a two-phase liquid-liquid system, with the base NaOH intercepting hydrogen chloride and leading to hydrolysis of BPA phosgene condensates and deprotonation of BPA. After completion, the organic phase is separated from the aqueous phase and washed several times with acidified and pure water to remove residual salts and base. In the last step, the PC is isolated either by solvent exchange and subsequent evaporation of the solvent, steam precipitation or addition of a non-solvent and subsequent filtration and drying. The low reaction temperature (40 °C) leads to a kinetically driven distribution of molecular weights and makes a quantitative end-capping necessary. Otherwise the material is going to redistribute into its thermodynamic product, which is accompanied by a decrease of molecular weight.

The transesterification process, on the other hand, comprises the base-catalyzed condensation of the phosgene-synthon diphenyl carbonate and BPA. The reaction temperature has to be kept high in order to keep both starting materials and products molten. The applied temperatures span from 150 to 350 °C, starting with pressures of 200 mbar and a stepwise reduction to 1 or even 0.1 mbar for an efficient removal of phenol.

The quality of the resulting product is directly related to the starting materials (no solvents, no workup and no phosgene are needed) and thus if the latter are contaminant-free so is the product. The catalyst loading level lies in the parts per billion (ppb) region and is negligible with regard to the final product.[150] Another advantage of the transesterification process is thermodynamically controlled molecular weight distribution of the final product. Hence, a processing-induced redistribution of the polymer chains is avoided, which improves the processability of the material. Since the use of phosgene is also avoided, this route is environmentally and processing-related favorable over the interfacial route.[151] However, from an economic and product quality viewpoint, the latter is still more feasible from an industrial point of view.

The production of the thermoplastic resin BPA-PC is an ever growing market, which is reflected in the annual growth rates of approximately 8%.[152] A total consumption of 3.7 Mt was reported for 2012, with Asia having a share of 60% followed by Europe, the Middle East and Africa with 23%, North America with 15% and lastly South America with 2%.[153] Typical applications of PC are electronic, household, optical, automotive, construction and medical devices. The key properties of the thermoplastic to give it such a broad range of applications are its outstanding impact strength, transparency, toughness, high elongation, good heat resistance, light weight and dimensional stability. Especially the use of PC in data storage technology, i.e. compact discs (CD), digital versatile discs (DVD) or – more recently – Blu-ray discs are famous examples, where the key properties impact strength and clarity of the material are mandatory. Another example is the use as medical devices, which need to be biocompatible and sterilizable. PC is both, biocompatible and exposable to all important sterilizing techniques, e.g. ethylene oxide (EO), gamma rays, electron beams or steam and hence a suitable choice to produce connectors, valves, controls, catheters etc.[147]
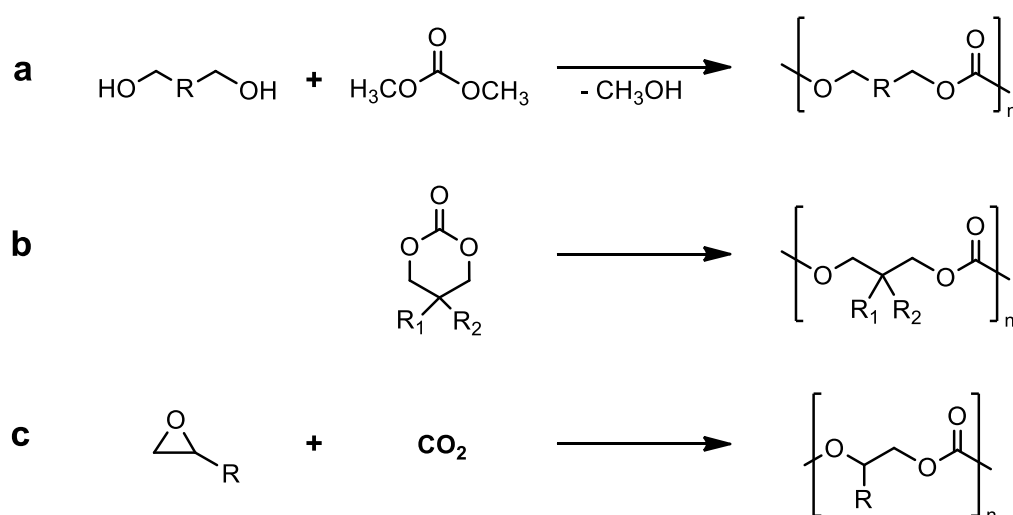
1.3.2 Aliphatic polycarbonates

Historic evolution

As mentioned briefly in paragraph 1.3, the first aliphatic polycarbonates (APC) were reported by Carothers and van Natta in 1930, when DuPont evaluated market potential of this new kind of polymers.[139] The low T_g materials were prone to hydrolysis and as such considered inferior to other engineering thermoplastics. With the discovery of BPA-PC in the 1950s an ongoing success story of aromatic PC distracted attention from APCs even

further. A landmark in the field was established by Inoue *et al.,* who published pioneering work in 1969 on the synthesis of aliphatic polycarbonates by zinc-catalyzed copolymerization of CO_2 and epoxides.[154,155] But APCs were hardly recognized until the 1990s, when academic and commercial interest rose due to emerging markets in the field of biomedical and biodegradable applications.[26,44,156–158] Current industrial applications are limited to low molecular weight polyols used for the production of polyurethanes and segments in copolymers, respectively, as the poor thermal and mechanical properties have hindered expansion into the area of thermoplastic resins.[159,160] However, in regard of biomedical applications, the low glass transition temperatures, superior biocompatibility and degradability of APCs are advantageous properties that are recently exploited in the field.[161,162]

Synthetic routes towards aliphatic PCs

Synthetic strategies towards aliphatic PCs are versatile, as the polycondensation (transesterification) and ROP have already been presented by Carothers and van Natta in 1930 and 1932, respectively, and the copolymerization of CO_2 with epoxides was shown by Inoue *et al.* in 1969 (see Fig. 1-14).[139,154] Based on these fundamental routes various modifications of the synthesis[163–168] and introduction of new functional monomers[169–178] have revived academic research in the field.


Figure 1-14 | The production of APCs. Synthetic routes towards aliphatic polycarbonates either by (**a**) polycondensation/transesterification of diols (or polyols) with dimethyl carbonate, (**b**) ROP of cyclic carbonates or (**c**) copolymerization of epoxides and CO_2.

In the early days, **polycondensation** of APCs was accomplished by the employment of phosgene and its derivatives to yield polymers with broad molecular weight distribution.[139] The control over the outcome of polymerization was improved when knowledge from the BPA-PC production was transferred to the synthesis of APCs. The use of dialkyl carbonates enabled higher degrees of polymerization by running a two-step process.[179–181] In the first step, oligocondensates of aliphatic diols and alkyl carbonates are produced in the melt. Subsequently, transesterification of the end-groups using a suitable transesterification catalyst would lead to high-molecular-weight (HMW) polycarbonates. A TiO_2/SiO_2-based catalyst was reported to produce polycarbonates of diols of butane, pentane and hexane, respectively, having weight average molecular weights (M_w) of $> 166\,kg\,mol^{-1}$ and low dispersity ($Đ < 1.9$).[165] Others have reported the successful preparation of APCs by polycondensation using enzymes as catalyst, which enables milder reaction conditions and a higher tolerance with respect to functional groups on the monomers.[182] However, drawbacks of the enzymatic polycondensation are high catalyst loadings, long reaction times, low molecular weights and a high $Đ$.

The obvious advantage of polycondensation for the preparation of APCs compared to ROP and CO_2/epoxide coupling is the flexibility of carbon number between two carbonate groups. Consequently, linkages with ten and more carbon atoms have been realized in the PC backbone, which is a unique way of tuning the properties of the APC.[183]

ROP of six-membered cyclic carbonates (five-membered rings are thermodynamically stable and do not undergo ROP)[1], on the other hand, is more effective for the production of high molecular weight APCs with low dispersity. The technique was applied to trimethylene carbonate **1** (Fig. 1-15) by Carothers *et al.* just two years after their discovery of polycarbonates, though the products suffered from low purity and low molecular weight.[184] Due to similarities of cyclic carbonates to lactones, most catalysts used in ROP of lactones have also been tested for their carbonate counterparts. As such, the reaction can be conducted in melt or in solution, while the mechanism range from anionic, cationic over coordination-insertion and monomer activation to enzymatically promoted polymerization.[185] Apart from metal-based catalysts, recently, organocatalytic ROP has received much attention to lower the level of toxic residues in the polymer. Basic catalysts[167,186,187] like tertiary amines, guanidines, amidines etc. and acidic catalysts like diphenyl phosphate[188] and triflic acid[189–191] have been used successfully for the conversion

of cyclic carbonates into polymers. Furthermore, enzymes have shown activity in ROP of these compounds, though they lack in efficiency and control of molecular weight compared to metal- and organo-based catalysts.[164,168,192–194] The great variety of catalysts for ROP is matched by the variety of monomers available for the ring-opening reaction. Besides trimethylene carbonate, the most widely used structures shown in Fig. 1-15: carbonates of 2,2-bis(hydroxymethyl)propionic acid,[195] pentaerythritol[196] and trimethyolalkane[197] giving **2, 3a/b** and **4**, respectively. The resulting structures are ideal candidates for biomedical application as they show tunable degradation rates by adjustment of hydrophilicity and T_g. Furthermore, the ROP of carbonates tolerates a broad range of functionalities to produce APCs under mild conditions. Hence, much effort has been spent on engineering of tissue scaffolds by electrospinning of fiber mats[198,199] or the synthesis of biodegradable elastomers,[200–203] hydrogels[204–208] and drug-delivery carriers.[209–211]
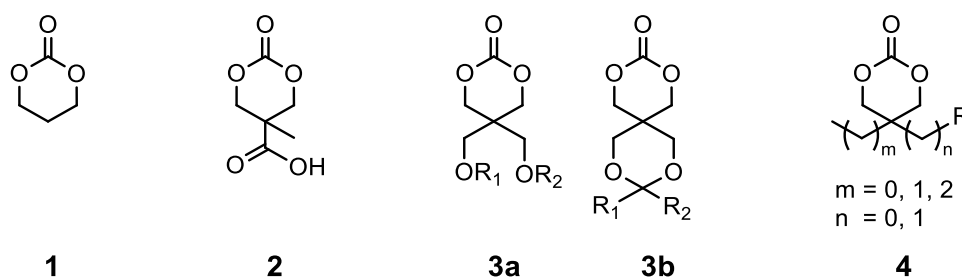

Figure 1-15 | Cyclic carbonates for the production of APCs. Most widely used cyclic carbonates for the ROP to produce APCs: trimethylene carbonate **1** and carbonates of 2,2-bis(hydroxymethyl)propionic acid **2**, carbonate of pentaerythritol **3a/b** and carbonate of trimethyolalkane **4**.

The third major route towards APCs is the **coupling** of highly reactive **epoxides** with the nearly inert molecule CO_2 (energetic considerations were discussed in 1.1.2). In respect of CCU, it turned out to be a very economic and sustainable pathway to produce thermoplastics, binders, coating resins or foams using this copolymerization technique.[1,212–219] It is one of the most recent examples of utilization of CO_2 on a large scale and thus a vast number of epoxides and catalysts have been screened to expand the spectrum of this chemical route.[154,220,221] Recently, it was reported that some catalysts are resistant to co-contaminants (water, N_2, CO, thiols and amines) present in the CO_2 exhausted from power stations and show high activity in the coupling of the gas with epoxides. This is an important step in the field of carbon capture and utilization.[222]

Mechanistically, the metal-catalyzed copolymerization follows a coordination-insertion process with the initial insertion of a ring-opened epoxide into the metal-oxygen bond and subsequent insertion of CO_2 to give the carbonate group as shown in Fig. 1-16 (example

with propylene oxide (PO)). For a strictly alternating insertion of epoxide and CO_2 a defect-free polycarbonate is obtained. However, this ideal case is often flawed by the consecutive addition of epoxides or backbiting reactions leading to undesired ether linkages in the backbone. The latter also produces cyclic carbonates that will compromise yield of the APC and might act as a plasticizer in the final product.[1,223]
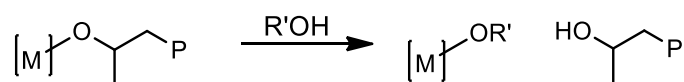
initiation
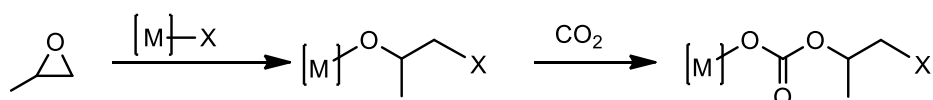

chain growth
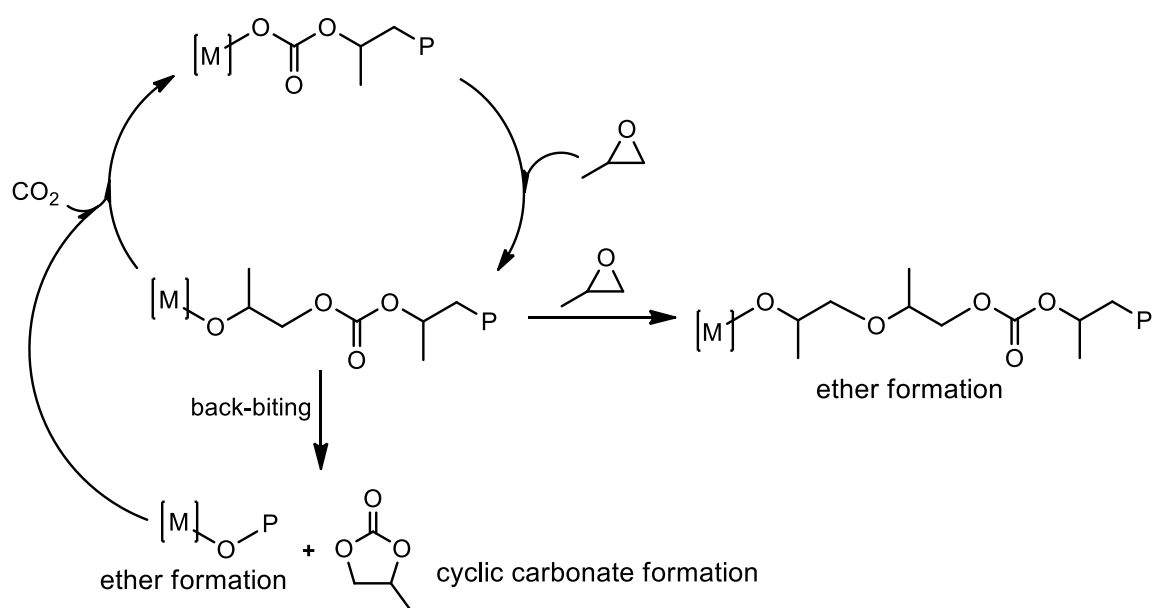
chain transfer

R' = H or alkyl chain

Figure 1-16 | Catalytic cycle of the production of PPC. The catalytic cycle of metal-catalyzed polymerization of propylene oxide with CO_2. The reaction is initiated by the insertion of the epoxide into the metal-oxygen bond and subsequent insertion of CO_2. In the ideal case, this sequence is repeated as a strictly alternating insertion of epoxide and CO_2 to yield a defect-free polycarbonate. However, the consecutive addition of epoxide and backbiting leads to undesired ether formation, whereas the latter produces cyclic carbonate as a side-product.

The presence of hydroxy-containing compounds in the reaction mixture might lead to chain transfer reactions that result in low molecular weight polymers.[224–227] The regioselectivity of the copolymerization depends on the epoxide and the catalytic system in use. State-of-the-art catalysts are able to produce poly(propylene carbonate) (PPC) with a very high ratio of head-to-tail linkages, i.e. a regioregular copolymer, as can be verified by an analysis of the carbonyl region in ^{13}C NMR spectra (> 150 ppm).[228] The stereoselectivity is another important parameter determining the microstructure of the produced APC. For PO syndio-enriched PPC and for cyclohexene oxide (CHO) completely syndiotactic poly(cyclohexene carbonate) (PCHC) were obtained by careful design of the catalytic system.[229,230]

Epoxides and catalysts used for the coupling with CO_2

Besides CHO and PO (shown in Fig. 1-17 as **7** and **12**, respectively), many other **epoxides** have been successfully transformed into polycarbonates by copolymerization with CO_2 as shown in Fig. 1-17.[231–236] Among them, the polymers of ethylene oxide **6** and hexene oxide **8c** poly(ethylene carbonate) (PEC) and poly(hexene carbonate) (PHC) were tested together with PPC, PCHC and BPA-PC in regard of their thermal and mechanical properties with the data collected in Table 1-4. The glass transition temperature is rather low for open chain APCs as it is -10 °C for PHC and only rises to 40 °C for PPC.

6   **7**   **8a-e**   **9**   **10**

11   **12**   **13**   **14**   **15**
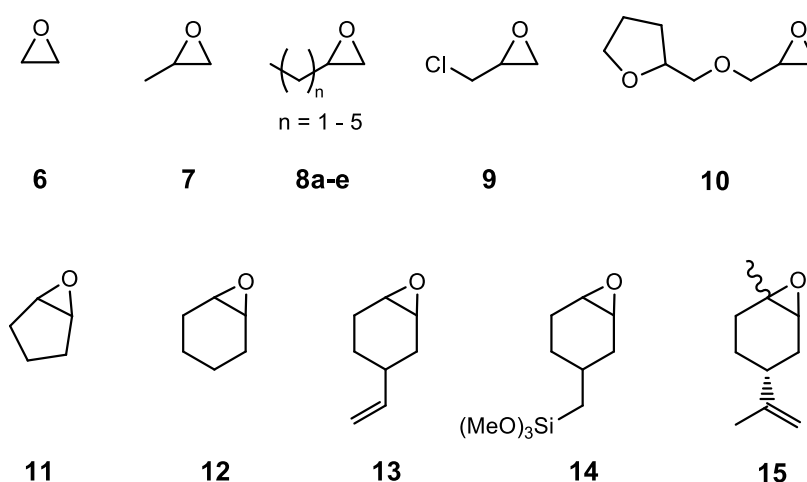
Figure 1-17 | Epoxides for the production of APCs. A selection of epoxides successfully copolymerized with CO_2 to produce APCs using a variety of organometallic catalysts.

For alicyclic polycarbonates like PCHC a glass transition (118 °C) closer to BPA-PC (149 °C) was reported, though the mechanical properties of the latter are not reached by any of the aliphatic counterparts. PCHC might have a similar tensile strength σ_s and elastic

modulus though elongation is limited to about 1% until it breaks, which already hints at the brittleness of the polymer in contrast to the very tough BPA-PC.[237] The open chain APCs cannot compare to the aromatic counterpart as their softening temperature is at least one order of magnitude lower and they do not aim for applications as engineering thermoplastics but rather soft blocks in copolymers or synthetic elastomers. Of all the other epoxides shown in Fig. 1-17, the alicyclic bio-based *(R)*-limonene oxide (LO) **15** shall be highlighted as it is the "backbone" of this thesis. The discovery of its copolymerization with CO_2 and microstructural composition of the resulting APC are introduced here while the results and discussion of this thesis are dedicated to the valorization, processing and applications of poly(limonene carbonate) (PLimC).

Table 1-4 | Thermal and mechanical data of APCs and BPA-PC.

polymer	epoxide	T_g [a] (°C)	T_{max} [b] (°C)	σ_s (MPa)	Young's modulus (MPa)	strain at break (%)	ref.
PEC	**6**	10	230		3-8	>600	[238]
PPC	**7**	40	252	7-30	700-1400	600-1200	[239,240]
PHC	**8c**	-10	290				[238]
PCHC	**12**	118	308	40-44	3500	1.1-2.3	[237,241]
BPA-PC	-	149	500	47	2400	30-50	[237,242]

[a]measured at 10 K min^{-1} in differential scanning calorimetry experiment, [b]measured at 10 K min^{-1} heating rate under N_2 in thermogravimetric analysis experiment.

However, most research has been directed towards the synthesis of PPC, which is a low-T_g amorphous thermoplastic that is produced on an industrial scale.[243,244] The epoxide PO is a readily available commodity chemical and the production capacity of 10 000 t a^{-1} has been surpassed by established companies (Covestro AG and Empower Materials) and newcomers (Novomer Inc.).[245] The 'clean' decomposition above 200 °C have made it applicable as temporary binder while its biodegradability have made it eligible for blending with natural polymers like starch.[246]

Both, PCHC and PPC have been subjected to countless organometallic **heterogeneous and homogeneous catalysts**, respectively.[1,218,220,245,247] Most common metals are Zn(II), Co(III) and Cr(III) coordinated by more or less sterically demanding, symmetric or asymmetric ligands.

Prominent **heterogeneous** catalysts are zinc glutarate **16** (or other carboxylates) and double metal cyanides (DMCs) **17** (see Fig. 1-18a). Typical features are Lewis acidity and

low redox reactivity of the metals and ligands like alkoxides, carboxylates, halides and other anionic groups.[231,248–251] In contrast to their homogeneous counterparts, these solid catalysts require much more forcing conditions, that is, high pressures of CO_2 (> 5 MPa) and elevated temperature (60-130 °C) to produce APCs characterized by numerous defects, i.e. an ether-enriched backbone of the polycarbonate. The productivity, or turn-over number (*TON*, grams of polymer produced per gram of catalyst) of the most widely used heterogeneous catalyst zinc glutarate for the production of PPC is typically in the range of 70 g PPC/g Zn. Furthermore, the activity, that is, turn-over frequency (*TOF*, moles of polymer produced per mole of catalyst per hour) is limited to < 10 h^{-1}.[252,253] Despite of the low performance of zinc glutarate, it is industrially relevant because of the inexpensive reagents and its simple synthesis, both mandatory for large-scale applications.[26] DMCs, on the other hand, show high catalytic performance in the conversion of epoxides and CO_2 into polymers. For the Co-Zn species **17**, turnover numbers of up to 1000 have been reported,[254,255] while a Co-Ni DMC has an *TOF* of 1860 h^{-1}.[256] However, DMCs are also active in the homopolymerization of epoxides and thus the percentage of ether linkages in the polymer is very high.

Characterization of the catalysts' active sites is an inherent challenge that is – together with the production of high ether contents – not compensated by the very high activity of the species. Hence, academic focus has been shifted towards the development of efficient homogeneous catalysts. A selection of **homogeneous bicomponent catalyst** systems is given in Fig. 1-18b. They consist of metal(III) centers in combination with co-catalysts, such as bis(triphenylphosphine)iminium chloride ([PPN]Cl) or LEWIS bases like 4-dimethylaminopyridine. As ligand porphyrins **18**,[257–260] *N,N*'-bis(salicylidene)ethylene-diamine (salen) **19**[221,223,241,261] and salans (reduced salen) [228,262,263] are most commonly attached to the metal. Newer generations of bicomponent salens have the co-catalyst covalently attached to the ligand **20**, which results in even higher *TOFs* than for the detached systems.[264] Generally, porphyrin-based catalysts exhibit rather low activity with *TOFs* of 3-21 h^{-1} and produce low molecular weight copolymers of PO/CHO and CO_2.[258,265] Salen-Co complexes **19** with the co-catalyst [PPN]Cl and *tert*-butyl (R = *t*-Bu) moieties give rise to a *TOF* of 1400 h^{-1}, i.e. two orders of magnitude higher than that of porphyrin complexes. Higher selectivities and activities at low temperature are realizable when the co-catalyst is covalently attached to the salen ligand, as it is the case for salen **20** that is tethered to a piperidinium moiety. At room temperature and 1.4 MPa pressure of CO_2 a *TOF* of

250 h^{-1} and a selectivity towards the carbonate of >99% was accomplished.[264] For a similar Co-salen complex that is tethered with four quaternary ammonium moieties, an unrivaled *TOF* of 26 000 h^{-1} was reported by Sujith *et al.* for the copolymerization of PO and CO_2 at 2 MPa and 80 °C, which is more than 200 000 times higher than the first experiments carried out by Inoue in 1969 (*TOF* = 0.12 h^{-1}).[155,266]

a

X = H₂O, Cl, Br, ROH

16 **17**

b

M = Al, Co, Cr, Mn
X = Cl, F, OAc

M = Al, Co, Cr, Mn
X = Cl, N₃, NO₃
R'= Ar, alicyl, CH₃, H, Ph

18 **19** **20**

c

R₁, R₃ = H, Me, Et, *i*Pr
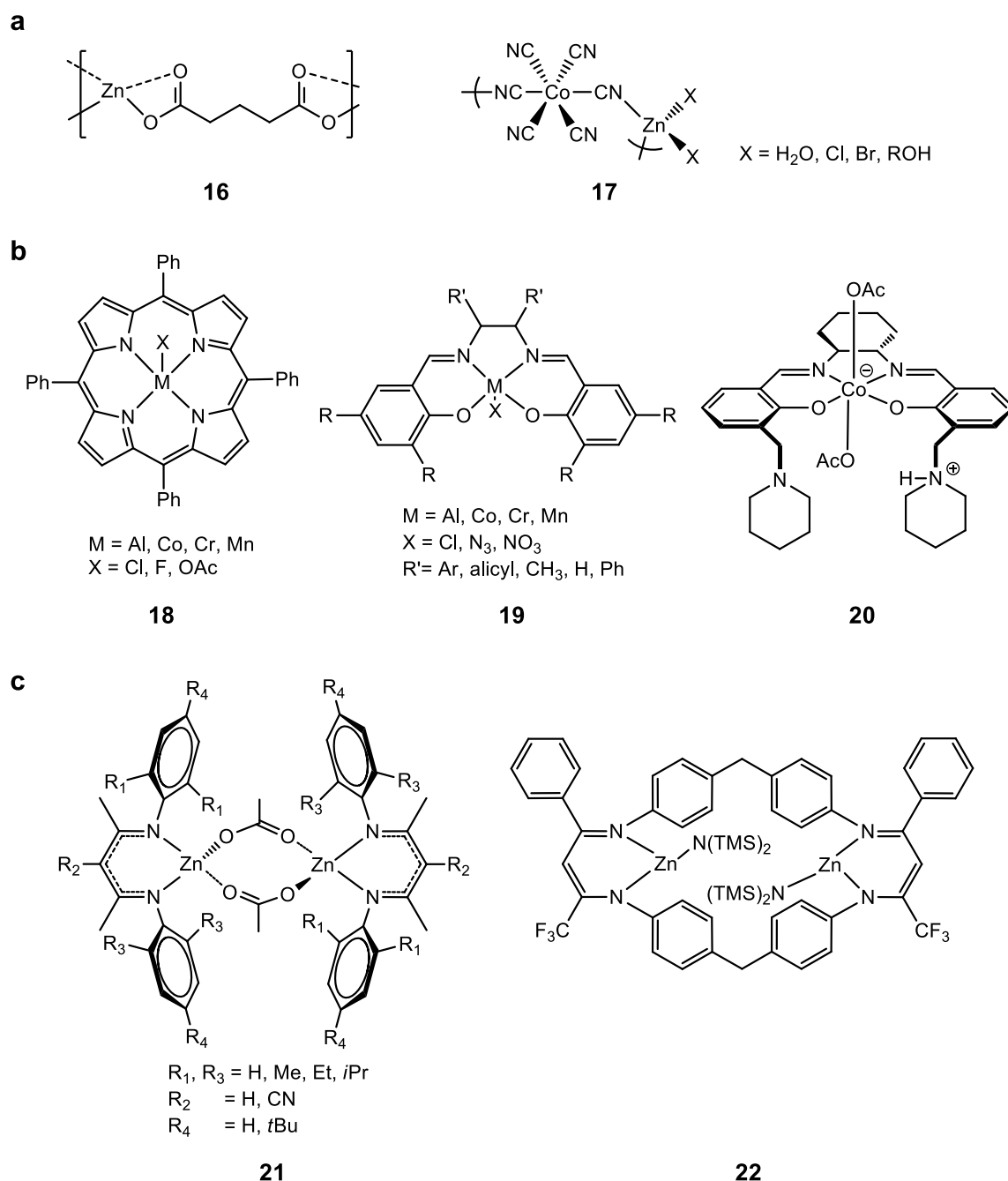R₂   = H, CN
R₄   = H, *t*Bu

21 **22**

Figure 1-18 | Catalysts employed for the coupling of epoxides and CO₂. A selection of (a) heterogeneous catalysts such as zinc glutarate **16** or double metal cyanide **17** complexes and (b) homogeneous bicomponent catalyst systems such as porphyrins **18**, salen **19** and bifunctional salen complexes tethered to piperidinium moieties **20** and (c) dinuclear, i.e. bimetallic catalysts such as β-diiminate **21** and tethered bdi **22** complexes used in the copolymerization of epoxides and CO₂ to give APCs.

Examples of homogeneous **dinuclear catalysts** are shown in Fig. 1-18c. Metals with oxidation state +2 and +3 are employed in combination with either mononucleating or dinucleating ligands, e.g. Zn(II)-based β-diiminates (bdi) **21** [267–271] or tethered Zinc bdi complexes **22** [272,273] and Mg(II)/Zn(II)/Co(II/III)-based salans, respectively.[274] Coates and coworkers were the first to develop highly active bdi-based catalysts.[271] The secret of their high activity was identified to be the existence of dimeric species that are only loosely associated. This observation was confirmed by kinetic studies, which revealed reaction orders of zinc between 1.0 and 1.8, i.e. implicating dimers bridged by either small ligands like acetate (OAc) or the growing polymer chains.[269] The activity of the **21** is very susceptible to the choice of the *N*-aryl moieties on the bdi ligands (R_1 and R_3 of **21**), which is reflected by the unproductive complex for the copolymerization of CHO and CO_2 with R_1/R_3 being methyl moieties. However, exchange of the methyl moieties by ethyl or *iso*-propyl (*i*-Pr) groups raises *TOFs* to 431 h^{-1} and 360 h^{-1}, respectively,[269] while the asymmetric catalyst (R_1 = ethyl, R_3 = *i*-Pr) would even increase *TOF* to 729 h^{-1}. To further improve activity, the electronic of the complex can be tuned by replacing the R_2 proton by an electron-withdrawing cyano substituent, as the resulting asymmetric catalyst yields PCHC with a *TOF* of 2290 h^{-1}.[275] Based on these findings, much effort has been directed towards the tethering of two metal centers to bring them into vicinity. Most successful in regard of activity was the group of Rieger in Munich, who connected two asymmetric fluorinated bdi ligands with aryl bridges to give the dinuclear catalyst **22**. Its performance towards the CHO/CO_2 copolymerization was found to be the highest at 100 °C and 3 MPa, showing an unprecedented *TOF* of 155 000 h^{-1}.[273]

1.3.3 The versatile molecule limonene

The epoxide *(R)*-LO is derived from *(R)*-limonene (**23a**), which is an doubly unsaturated alicyclic terpene. It is found in the peel of citrus fruits (orange, lemon, lime, mandarin, grapefruit), while its stereoisomer *(S)*-limonene (**23b**) is found in the essential oils of oaks and pines (see Fig. 1-19).[276] The latter has a turpentine smell, whereas the *(R)*-isomer is responsible for the typical orange odour in many cosmetics and food. *(R)*-limonene has a share of roughly 95% in orange oil,[277] which corresponds to 3.8 wt% of the entire peel.[278] Considering an annual production of oranges of about 52 million tonnes, this results in a capacity of more than 500 kt a^{-1} (estimated from 70 Mt a^{-1} oranges produced) of which 70 kt are extracted by centrifugation or steam distillation each year.[279,280] Hence, the terpene

shows an abundance that makes it a viable choice as feedstock for industrial processes. Furthermore, as it is derived from the waste, that is, the peel of the oranges, there is no competing interest with the production of food. This is a clear advantage of limonene over starch-based materials, such as poly(lactic acid), since the latter are derived from corn, which, in turn, is an integral part of the nutrition in many regions of the world.[281]

23a   **23b**
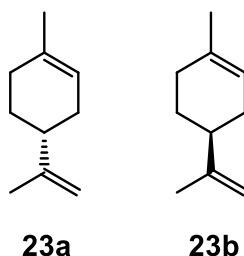
Figure 1-19 | The stereoisomers of limonene. Limonene is a bio-based alicyclic terpene that is found in several plants and fruits. The *(R)*-isomer **23a** is the major component in citrus fruits, such as oranges and lemons, whereas *(S)*-limonene (**23b**) is emitted by oaks and pines.

Limonene has a growing number of applications, due to its availability and non-toxicity. One of the earliest uses as a cleaning agent is based on the good solvent properties of limonene (it can hold up to 2.5 times of its own weight).[282] The environmentally benign biosolvent can replace toxic solvents, such as toluene, n-hexane and halogenated organic solvents. For instance, it was used in a formulation with a surfactant in large quantities for degreasing of equipment after the Deepwater Horizon oil spill in 2011.[280] The employment as solvent of limonene can also be expanded chemical processes, where it is readily used in chromatography and extraction of natural products.[283,284] Besides the application as a solvent, the unmodified terpene is also added to natural pesticides in order to repel insects without harming mammals, birds or fish.[285] Furthermore, *(R)*-limonene exhibits activity in the treatment of cancerous cells and the prevention of asthma.[286,287]

However, the true potential of the doubly unsaturated terpene lies in the chemical modifications on the reactive double bonds. A comprehensive review on the possible manipulations was presented by Thomas and Bessière in 1989,[277] Apart from the attachment of small molecules, the terpene was successfully homopolymerized cationically by FRIEDEL-CRAFTS or radically by ZIEGLER-NATTA catalysts.[288,289] The use of those low-molecular-weight polymers and the control of the resulting structures was limited, though, and it was only in the last two decades that a number of new polymeric materials have emerged based on limonene. One approach involves the dehydrogenation of limonene to give the aromatic *p*-cymene that is subsequently oxidized to terephthalic acid for the

production of polyesters such as PET.[290,291] Another chemical route exploits the double bonds of limonene for the thiol-ene 'click' reaction. The addition of various thiols has led to materials that are suitable as sealants and adhesives.[292–294] Yet another approach – utilized within this thesis – is based on the partial (LO) or complete epoxidation of the double bonds of limonene. These highly active epoxy groups can be coupled catalytically with the nearly inert CO_2 to give polycarbonates or dicarbonates for the isocyanate-free production of polyurethanes, respectively.[160,295] Besides the copolymerization with CO_2, LO was employed as monomer for direct cationic polymerization[296] and as comonomer for the production of polyesters.[297]

1.3.4 Poly(limonene carbonate)

Catalyst **21** was successfully employed in the copolymerization of the bio-based and sterically very demanding epoxide *(R)*-limonene oxide **15** with CO_2 to yield PLimC.[295] Only few other bio-based oxiranes have been subjected to the copolymerization with CO_2, amongst them epoxidized fatty acids[298] and 1,4-cyclohexdiene.[299,300] Upon partial oxidation, a mixture of *cis*-LO (**15a**) and *trans*-LO (**15b**) is obtained, differing in the orientation of the methyl and the *iso*-propylene moieties. This rather subtle difference in stereochemistry has a dramatic effect on the reactivity of the epoxides, as the *cis*-isomer is nearly completely omitted in the copolymerization and **15b** is enriched in the backbone of PLimC.
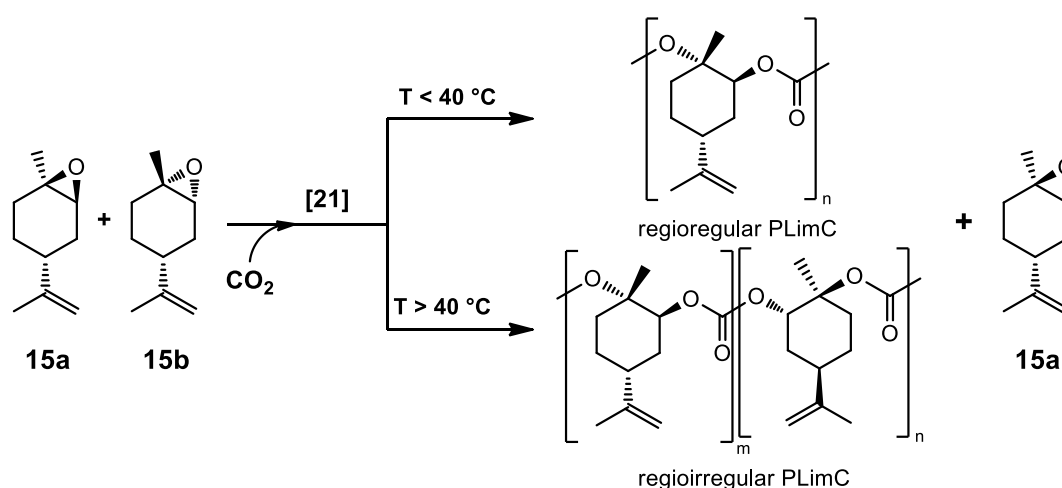
Figure 1-20 | The production of PLimC. The copolymerization of *(R)*-limonene oxide and CO_2 catalyzed by the zinc complex **21**, giving regioregular PLimC below 40 °C and regioirregular PLimC above 40 °C, respectively, while the *cis*-isomer does not take part in the reaction.

The schematic of the reaction is shown in Fig. 1-20 also illustrating the importance of reaction temperature. Byrne *et al.* reported that samples produced below 40 °C resulted exclusively in head-to-tail connected (regioregular) PLimC, while above 40 °C the regiocontrol was compromised and regioirregular PLimC was obtained. The catalytic activity of various derivatives of **21** was also evaluated, whereas one of the best bdi catalysts was that with ethyl moieties (R_1, R_3 = ethyl, R_2, R_4 = H) giving a moderate *TOF* of 32 h^{-1} at 25 °C, 0.7 MPa pressure of CO_2 and a catalyst loading of 0.4 mol% (Đ > 1.13). The molecular weights of the amorphous copolymers were limited to 10.8 kg mol^{-1} and 25.0 kg mol^{-1} for *(R)*-LO and *(S)*-LO, respectively. Even with those low molecular weights, a promising glass transition temperature of 110 °C (close to the T_g of high molecular weight PCHC with 118 °C)[241] was achieved, indicating a high rigidity of the backbone. On the one hand, this rigidity was expected to result in a T_g similar to that of BPA-PC for higher degrees of polymerization. On the other hand, the rigidity should also result in a low packing density of the polymer chains and thus a high free volume, which is a prerequisite for high performance in respect to transport phenomena. The latter can be related to optics or membrane technology and the facilitated movement of photons or small molecules, respectively, eventually giving highly transparent and permeable materials. Based on these assumptions, the research was material scientifically-driven: firstly, improving general polymeric properties by increasing molecular weight of PLimC, secondly creating a portfolio of properties for the bio-based APC and, last but not least, identifying applications of the new material.

Recently, reports have been published on stereocomplexed PLimC (regioregular enantiopure *(S)*- and *(R)*-PLimC blended after polymerization),[301] evaluation of an α,ω-diol of PLimC as coating material[216] and the activity of an Al-based amino-tris(phenolate) catalyst towards the incorporation of both *cis*/*trans*-LO, respectively.[302] However, in all cases only low molecular weight PLimC was obtained, thus not interfering with this thesis' claim.

1.4 References

1.   Kember, M. R., Buchard, A. & Williams, C. K. Catalysts for CO_2/epoxide copolymerisation. *Chem. Commun.* **47,** 141–163 (2011).

2.   Forster, P., Ramaswamy, V. & Artaxo, P. *Fourth assessment report of the intergovernmental panel on climate change; Chapter 2: changes in atmospheric constituents and in radiative forcing.* (2007).

3.   Kaspar, F., Meinshausen, M. & Schulz, M. *Fifth assessment report of the intergovernmental panel on climate change; Chapter I: the physical science basis.* (2013).

4.   Markewitz, P. *et al.* Worldwide innovations in the development of carbon capture technologies and the utilization of CO2. *Energy Environ. Sci.* **5,** 7281–7305 (2012).

5.   Mascia, L. & Acierno, D. Polymers in industry: from guncotton to CO_2 glass. *Adv. Polym. Technol.* **31,** 179–192 (2012).

6.   Beckman, E. J. Making Polymers from Carbon Dioxide. *Science* **283 ,** 946–947 (1999).

7.   Peters, M. *et al.* Chemical technologies for exploiting and recycling carbon dioxide into the value chain. *ChemSusChem* **4,** 1216–1240 (2011).

8.   Quadrelli, E. A., Centi, G., Duplan, J.-L. & Perathoner, S. Carbon dioxide recycling: emerging large-scale technologies with industrial potential. *ChemSusChem* **4,** 1194–1215 (2011).

9.   Song, C. Global challenges and strategies for control, conversion and utilization of CO_2 for sustainable development involving energy, catalysis, adsorption and chemical processing. *Catal. Today* **115,** 2–32 (2006).

10.   Haas, G. R. Green and sustainable polymers: high-value aliphatic polycarbonates from CO_2 and epoxides, Thesis University of Ulm. (2009).

11.   Ausfelder, F. & Bazzanella, A. *Verwertung und Speicherung von CO₂ , DECHEMA Working paper.* (2008).

12.   Jessop, P. G., Ikariya, T. & Noyori, R. Homogeneous Hydrogenation of Carbon Dioxide. *Chem. Rev.* **95,** 259–272 (1995).

13.   Jessop, P. G., Joó, F. & Tai, C.-C. Recent advances in the homogeneous hydrogenation of carbon dioxide. *Coord. Chem. Rev.* **248,** 2425–2442 (2004).

14.   Leitner, W. Carbon dioxide as a raw material: the synthesis of formic acid and its derivatives from CO_2. *Angew. Chemie Int. Ed. English* **34,** 2207–2221 (1995).

15.   Boddien, A. *et al.* Towards the development of a hydrogen battery. *Energy Environ. Sci.* **5,** 8907–8911 (2012).

16.   Dietrich, J. & Schindler, S. Kinetische Untersuchungen zur Hydrierung von Kohlendioxid zu Ameisensäure mit einem Rhodiumkomplex als Katalysator. *Zeitschrift für Anorg. und Allg. Chemie* **634,** 2487–2494 (2008).

17.   Baughman, R. H., Iqbal, Z., Eckhardt, H. & Okamoto, Y. Structure, properties, and thermodynamics of poly(carbon dichalcogenides). *Macromolecules* **21,** 1832–1838 (1988).

18.   Ikeda, S. *et al.* New polycarbonates from dienes and vinyl ethers. *Asahi Garusu Kogyo Gijuutsu Shoreikai Kenkyu Hokoku* **31,** 87–91 (1997).

19.   Soga, K., Hosoda, S. & Ikeda, S. A new synthetic route to polycarbonate. *J. Polym. Sci. Polym. Lett. Ed.* **15,** 611–614 (1977).

20.   Soga, K., Hosoda, S. & Ikeda, S. A new synthetic route to polycarbonate. *J. Polym. Sci. Polym. Chem. Ed.* **17,** 517–529 (1979).

21.   Sharma, R. K. & Olson, E. S. Copolymerization reactions of carbon dioxide. *EERC* 676–680 (1999).

22.   Müller, T. E., Gürtler, C., Vogt, H., Krautschick, M. & Leitner, W. Method for producing formaldehyde/CO_2 copolymers. WO 20150337070 (2015).

23.   Darensbourg, D. J. & Yeung, A. D. Thermodynamics of the carbon dioxide–epoxide

copolymerization and kinetics of the metal-free degradation: a computational study. *Macromolecules* **46,** 83–95 (2013).

24. Allen, S. D., Moore, D. R., Lobkovsky, E. B. & Coates, G. W. High-activity, single-site catalysts for the alternating copolymerization of CO_2 and propylene oxide. *J. Am. Chem. Soc.* **124,** 14284–14285 (2002).

25. Darensbourg, D. J. & Zimmer, M. S. Copolymerization and terpolymerization of CO_2 and epoxides using a soluble zinc crotonate catalyst precursor. *Macromolecules* **32,** 2137–2140 (1999).

26. Luinstra, G. A. Poly(propylene carbonate), old copolymers of propylene oxide and carbon dioxide with new interests: catalysis and material properties. *Polym. Rev.* **48,** 192–219 (2008).

27. Bhanage, B. M. & Arai, M. *Transformation and utilization of carbon dioxide.* (Springer Berlin Heidelberg, 2014). doi:10.1007/978-3-642-44988-8

28. Mikami, K. *et al.* Polycarbonates derived from glucose via an organocatalytic approach. *J. Am. Chem. Soc.* **135,** 6826–6829 (2013).

29. Kemmere, M. & Meyer, T. *Supercritical carbon dioxide in polymer reaction engineering.* (Wiley-Vch Verlag, 2005).

30. Burk, M. J., Feng, S., Gross, M. F. & Tumas, W. Asymmetric catalytic hydrogenation reactions in supercritical carbon dioxide. *J. Am. Chem. Soc.* **117,** 8277–8278 (1995).

31. Wood, C. D., Cooper, A. I. & DeSimone, J. M. Green synthesis of polymers using supercritical carbon dioxide. *Curr. Opin. Solid State Mater. Sci.* **8,** 325–331 (2004).

32. Super, M., Berluche, E., Costello, C. & Beckman, E. Copolymerization of 1,2-epoxycyclohexane and carbon dioxide using carbon dioxide as both reactant and solvent. *Macromolecules* **30,** 368–372 (1997).

33. Tian, J.-S. *et al.* One-pot synthesis of dimethyl carbonate catalyzed by n-Bu₄NBr/n-Bu₃N from methanol, epoxides, and supercritical CO_2. *Appl. Catal. A Gen.* **301,** 215–221 (2006).

34. Ballivet-Tkatchenko, D. *et al.* Direct synthesis of dimethyl carbonate with supercritical carbon dioxide: Characterization of a key organotin oxide intermediate. *Catal. Today* **115,** 80–87 (2006).

35. Darensbourg, D. J., Stafford, N. W. & Katsurao, T. Supercritical carbon dioxide as solvent for the copolymerization of carbon dioxide and propylene oxide using a heterogeneous zinc carboxylate catalyst. *J. Mol. Catal. A Chem.* **104,** 1–4 (1995).

36. Nalawade, S. P., Picchioni, F. & Janssen, L. P. B. M. Supercritical carbon dioxide as a green solvent for processing polymer melts: Processing aspects and applications. *Prog. Polym. Sci.* **31,** 19–43 (2006).

37. Sauceau, M., Fages, J., Common, A., Nikitine, C. & Rodier, E. New challenges in polymer foaming: A review of extrusion processes assisted by supercritical carbon dioxide. *Prog. Polym. Sci.* **36,** 749–766 (2011).

38. von der Assen, N., Jung, J. & Bardow, A. Life-cycle assessment of carbon dioxide capture and utilization: avoiding the pitfalls. *Energy Environ. Sci.* **6,** 2721–2734 (2013).

39. Zhao, M., Minett, A. I. & Harris, A. T. A review of techno-economic models for the retrofitting of conventional pulverised-coal power plants for post-combustion capture (PCC) of CO_2. *Energy Environ. Sci.* **6,** 25–40 (2013).

40. Iglesias, A. & Quiroga, S. *Energy Technology Perspectives – Scenarios & Strategies to 2050 - ISBN: 978-92-64-08597-8.* (2010).

41. Zevenhoven, R. & Fagerlund, J. *Developments and innovation in carbon dioxide (CO₂) capture and storage technology.* (Woodhead Publishing Series in Energy Vol. 2, 2010).

42. May, F. CO_2 storage in geological rock formations. *VGB PowerTech* **85,** 32–37 (2005).

43. Tanaka, N. *CO₂ capture and storage (ISBN 978-92-64-04140-0).* (2008).

44. D'Alessandro, D. M., Smit, B. & Long, J. R. Carbon dioxide capture: prospects for new materials. *Angew. Chemie Int. Ed.* **49,** 6058–6082 (2010).

45. Li, J.-R. *et al.* Carbon dioxide capture-related gas adsorption and separation in metal-organic frameworks. *Coord. Chem. Rev.* **255,** 1791–1823 (2011).

46. Rochelle, G. T. Amine Scrubbing for CO_2 Capture. *Science* **325,** 1652–1654 (2009).

47. Vaidya, P. D. & Kenig, E. Y. CO_2-alkanolamine reaction kinetics: a review of recent studies. *Chem. Eng. Technol.* **30,** 1467–1474 (2007).

48. Mimura, T., Suda, T., Iwaki, I., Honda, A. & Kumazawa, H. Kinetic of the reaction between carbon dioxide and sterically hindered amines for carbon dioxide recovery from power plant flue gases. *Chem. Eng. Commun.* **170,** 245–260 (1998).

49. Dibenedetto, A., Aresta, M., Fragale, C. & Narracci, M. Reaction of silylalkylmono- and silylalkyldi-amines with carbon dioxide: evidence of formation of inter- and intra-molecular ammonium carbamates and their conversion into organic carbamates of industrial interest under carbon dioxide catalysis. *Green Chem.* **4,** 439–443 (2002).

50. Darde, V., Thomsen, K., van Well, W. J. M. & Stenby, E. H. Chilled ammonia process for CO_2 capture. *Energy Procedia* **1,** 1035–1042 (2009).

51. Smiglak, M., Metlen, A. & Rogers, R. D. The second evolution of ionic liquids: from solvents and separations to advanced materials - energetic examples from the ionic liquid cookbook. *Acc. Chem. Res.* **40,** 1182–1192 (2007).

52. Cadena, C. *et al.* Why is CO_2 so soluble in imidazolium-based ionic liquids? *J. Am. Chem. Soc.* **126,** 5300–5308 (2004).

53. Choi, S., Drese, J. H. & Jones, C. W. Adsorbent materials for carbon dioxide capture from large anthropogenic point sources. *ChemSusChem* **2,** 796–854 (2009).

54. Harlick, P. J. E. & Sayari, A. Applications of pore-expanded mesoporous silicas. 3. Triamine silane grafting for enhanced CO_2 adsorption. *Ind. Eng. Chem. Res.* **45,** 3248–3255 (2006).

55. Lee, K. B., Beaver, M. G., Caram, H. S. & Sircar, S. Reversible chemisorbents for carbon dioxide and their potential applications. *Ind. Eng. Chem. Res.* **47,** 8048–8062 (2008).

56. Li, J.-R., Kuppler, R. J. & Zhou, H.-C. Selective gas adsorption and separation in metal–organic frameworks. *Chem. Soc. Rev.* **38,** 1477–1504 (2009).

57. Ebner, A. D. & Ritter, J. A. State-of-the-art adsorption and membrane separation processes for carbon dioxide production from carbon dioxide emitting industries. *Sep. Sci. Technol.* **44,** 1273–1421 (2009).

58. Yampolskii, Y. Polymeric gas separation membranes. *Macromolecules* **45,** 3298–3311 (2012).

59. Ismail, A. F., Chandra Khulbe, K. & Matsuura, T. *Gas Separation Membranes.* (Springer International Publishing, 2015). doi:10.1007/978-3-319-01095-3

60. Carreon, M. A., Li, S., Falconer, J. L. & Noble, R. D. Alumina-supported SAPO-34 membranes for CO_2/CH_4 aeparation. *J. Am. Chem. Soc.* **130,** 5412–5413 (2008).

61. Guo, H., Zhu, G., Hewitt, I. J. & Qiu, S. 'Twin copper source' growth of metal–organic framework membrane: $Cu_3(BTC)_2$ with high permeability and selectivity for recycling H_2. *J. Am. Chem. Soc.* **131,** 1646–1647 (2009).

62. Liu, Y. *et al.* Synthesis of continuous MOF-5 membranes on porous α-alumina substrates. *Microporous Mesoporous Mater.* **118,** 296–301 (2009).

63. Boot-Handford, M. E. *et al.* Carbon capture and storage update. *Energy Environ. Sci.* **7,** 130–189 (2014).

64. Haszeldine, R. S. Carbon capture and storage: how green can black be? *Science* **325,** 1647–1652 (2009).

65. Feron, P. H. M. & Hendriks, C. A. CO_2 capture process principles and costs. *Oil Gas Sci. Technol.* **60,** 451–459 (2005).

66. Figueroa, J. D., Fout, T., Plasynski, S., McIlvried, H. & Srivastava, R. D. Advances in CO_2 capture technology—The U.S. Department of Energy's Carbon Sequestration Program. *Int. J. Greenh. Gas*

Control **2,** 9–20 (2008).

67. Wang, M., Lawal, A., Stephenson, P., Sidders, J. & Ramshaw, C. Post-combustion CO_2 capture with chemical absorption: a state-of-the-art review. *Chem. Eng. Res. Des.* **89,** 1609–1624 (2011).

68. Stolten, D. & Scherer, V. *Efficient Carbon Capture for Coal Power Plants.* (Wiley VCH, 2011).

69. Rao, A. B. & Rubin, E. S. A technical, economic, and environmental assessment of amine-based CO_2 capture technology for power plant greenhouse gas control. *Environ. Sci. Technol.* **36,** 4467–4475 (2002).

70. Fischedick, M. *et al.* CO_2-Abtrennung im Kraftwerk : ist eine Nachrüstung für bestehende Anlagen sinnvoll? *VGB PowerTech* **86,** 108–117 (2006).

71. Eide, L. I. & Bailey, D. W. Precombustion Decarbonisation Processes. *Oil Gas Sci. Technol.* **60,** 475–484 (2005).

72. Cuéllar-Franca, R. M. & Azapagic, A. Carbon capture, storage and utilisation technologies: A critical analysis and comparison of their life cycle environmental impacts. *J. CO2 Util.* **9,** 82–102 (2014).

73. Engels, S., Beggel, F., Modigell, M. & Stadler, H. Simulation of a membrane unit for oxyfuel power plants under consideration of realistic BSCF membrane properties. *J. Memb. Sci.* **359,** 93–101 (2010).

74. Stadler, H. *et al.* Oxyfuel coal combustion by efficient integration of oxygen transport membranes. *Int. J. Greenh. Gas Control* **5,** 7–15 (2011).

75. Kneer, R. *et al.* OXYCOAL-AC: Towards an integrated coal-fired power plant process with ion transport membrane-based oxygen supply. *Energy Environ. Sci.* **3,** 198–207 (2010).

76. Baker, R. W. Future directions of membrane gas separation technology. *Ind. Eng. Chem. Res.* **41,** 1393–1411 (2002).

77. Strathmann, H. Membrane separation processes: Current relevance and future opportunities. *AIChE J.* **47,** 1077–1087 (2001).

78. Bernardo, P., Drioli, E. & Golemme, G. Membrane gas separation: a review/state-of-the-art. *Ind. Eng. Chem. Res.* **48,** 4638–4663 (2009).

79. Du, N., Park, H. B., Dal-Cin, M. M. & Guiver, M. D. Advances in high permeability polymeric membrane materials for CO_2 separations. *Energy Environ. Sci.* **5,** 7306–7322 (2012).

80. Fick, A. Über Diffusion. *Poggendorff's Ann. der Phys. und Chemie* **94,** 59–86 (1855).

81. Fick, A. On liquid diffusion. *J. Memb. Sci.* **100,** 33–38 (1995).

82. Henry, W. Experiments on the quantity of gases absorbed by water, at different temperatures, and under different pressures. *Philos. Trans. R. Soc. London* **93,** 29–274 (1803).

83. Javaid, A. Membranes for solubility-based gas separation applications. *Chem. Eng. J.* **112,** 219–226 (2005).

84. Koros, W. J., Fleming, G. K., Jordan, S. M., Kim, T. H. & Hoehn, H. H. Polymeric membrane materials for solution-diffusion based permeation separations. *Prog. Polym. Sci.* **13,** 339–401 (1988).

85. Rouquerol, J. *et al.* Recommendations for the characterization of porous solids (Technical Report). *Pure Appl. Chem.* **66,** (1994).

86. **Paul, D. & Yampol'skii, Y.** *Polymeric Gas Separation Membranes.* (CRC Press, 1994).

87. Spillman, R. W. Chemical Engineering Progress. *Chem. Eng. Prog.* **85,** 41–62 (1989).

88. Graham, T. On the absorption and dialytic separation of gases by colloid septa. *Philos. Trans. R. Soc. London* **156,** 399–439 (1866).

89. Efremov, S. N. & Zolotarev, P. P. Theory of diffusion through, and sorption in, a biporous sorbent membrane with a constant difference in concentration at the membrane faces and linear sorption isotherm 3. Sorption in the transport pore system. *Bull. Acad. Sci. USSR Div. Chem. Sci.* **31,** 215–220 (1982).

90.   Robeson, L. M. Correlation of separation factor versus permeability for polymeric membranes. *J. Memb. Sci.* **62,** 165–185 (1991).

91.   Robeson, L. M. The upper bound revisited. *J. Memb. Sci.* **320,** 390–400 (2008).

92.   Bondi, A. VAN DER WAALS volumes and radii. *J. Phys. Chem.* **68,** 441–451 (1964).

93.   Van Krevelen, D. W. & Te Nijenhuis, K. in *Prop. Polym.* 71–108 (Elsevier, 2009). doi:10.1016/B978-0-08-054819-7.00004-2

94.   Lee, W. M. Selection of barrier materials from molecular structure. *Polym. Eng. Sci.* **20,** 65–69 (1980).

95.   Thran, A., Kroll, G. & Faupel, F. Correlation between fractional free volume and diffusivity of gas molecules in glassy polymers. *J. Polym. Sci. Part B Polym. Phys.* **37,** 3344–3358 (1999).

96.   Recio, R. *et al.* Effect of fractional free volume and Tg on gas separation through membranes made with different glassy polymers. *J. Appl. Polym. Sci.* **107,** 1039–1046 (2008).

97.   Staiger, C. L., Pas, S. J., Hill, A. J. & Cornelius, C. J. Gas separation, free volume distribution, and physical aging of a highly microporous spirobisindane polymer. *Chem. Mater.* **20,** 2606–2608 (2008).

98.   Dlubek, G. *et al.* The free volume in two untreated, pressure-densified, and CO_2 gas exposed polymers from positron lifetime and pressure-volume-temperature experiments. *e-Polymers* **108,** 1–20 (2007).

99.   Pethrick, R. A. Positron annihilation—A probe for nanoscale voids and free volume? *Prog. Polym. Sci.* **22,** 1–47 (1997).

100. Brandt, W., Berko, S. & Walker, W. W. Positronium decay in molecular substances. *Phys. Rev.* **120,** 1289–1295 (1960).

101. Tao, S. J. Positronium annihilation in molecular substances. *J. Chem. Phys.* **74,** 4754–4760 (1981).

102. Eldrup, M., Lightbody, D. & Sherwood, J. N. The temperature dependence of positron lifetimes in solid pivalic acid. *Chem. Phys.* **63,** 51–58 (1981).

103. Liu, J., Deng, Q. & Jean, Y. C. Free-volume distributions of polystyrene probed by positron annihilation: comparison with free-volume theories. *Macromolecules* **26,** 7149–7155 (1993).

104. Gregory, R. B. Free-volume and pore size distributions determined by numerical Laplace inversion of positron annihilation lifetime data. *J. Appl. Phys.* **70,** 4665–4670 (1991).

105. Flaconneche, B., Martin, J. & Klopffer, M. H. Permeability, diffusion and solubility of gases in polyethylene, polyamide 11 and poly(vinylidene fluoride). *Oil Gas Sci. Technol.* **56,** 261–278 (2001).

106. Pinnau, I. & Koros, W. J. Gas-permeation properties of asymmetric polycarbonate, polyestercarbonate, and fluorinated polyimide membranes prepared by the generalized dry–wet phase inversion process. *J. Appl. Polym. Sci.* **46,** 1195–1204 (1992).

107. Chatzidaki, E. K., Favvas, E. P., Papageorgiou, S. K., Kanellopoulos, N. K. & Theophilou, N. V. New polyimide-polyaniline hollow fibers: synthesis, characterization and behavior in gas separation. *Eur. Polym. J.* **43,** 5010–5016 (2007).

108. Koros, W. J. W. J., Paul, D. R. & Rocha, A. A. Carbon dioxide sorption and transport in polycarbonate. *J. Polym. Sci. Polym. Phys. Ed.* **14,** 687–702 (1976).

109. Sridhar, S., Aminabhavi, T. M. & Ramakrishna, M. Separation of binary mixtures of carbon dioxide and methane through sulfonated polycarbonate membranes. *J. Appl. Polym. Sci.* **105,** 1749–1756 (2007).

110. Villegas-Coss, I., Ruiz-Treviño, F. A. & Hernández-López, S. Syntheses and gas transport properties of polyarylates based on isophthalic and terephthalic acids and mixtures of bisphenol A and 1, 1 bi-2-naphthol. *J. Polym. Sci. Part B Polym. Phys.* **44,** 256–263 (2006).

111. Ilinitch, O. M. *et al.* Intrinsic microporosity and gas transport in polyphenylene oxide polymers. *Microporous Mesoporous Mater.* **31,** 97–110 (1999).

112. Lin, H. & Freeman, B. D. Gas solubility, diffusivity and permeability in poly(ethylene oxide). *J.*

Memb. Sci. **239,** 105–117 (2004).

113. Anderson, M. R., Mattes, B. R., Reiss, H. & Kaner, R. B. Conjugated polymer films for gas separations. *Science* **252,** 1412–1415 (1991).

114. Liang, W. & Martin, C. R. Gas transport in electronically conductive polymers. *Chem. Mater.* **3,** 390–391 (1991).

115. Ismail, A. F., Dunkin, I. R., Gallivan, S. L. & Shilton, S. J. Production of super selective polysulfone hollow fiber membranes for gas separation. *Polymer* **40,** 6499–6506 (1999).

116. Julian, H. & Wenten, I. G. Polysulfone membranes for CO_2/CH_4 separation: state of the art. *IOSR J. Eng.* **02,** 484–495 (2012).

117. Wang, X.-Y. *et al.* Molecular simulation and experimental study of substituted polyacetylenes: fractional free volume, cavity size distributions and diffusion coefficients. *J. Phys. Chem. B* **110,** 12666–12672 (2006).

118. Morisato, A. *et al.* Polymer characterization and gas permeability of poly(1-trimethylsilyl-1-propyne) [PTMSP], poly(1-phenyl-1-propyne) [PPP], and PTMSP/PPP blends. *J. Polym. Sci. Part B Polym. Phys.* **34,** 2209–2222 (1996).

119. Akai, Y. N., Oshimizu, H. Y. & Sujita, Y. T. Enhancement of gas permeability in HPC , CTA and PMMA under microwave irradiation. *Polym. J.* **38,** 376–380 (2006).

120. Chã, M. S. V *et al.* Synthesis and characterization of sulfonated poly(ether imide) with higher thermal stability and effect on CO_2, N_2, and O_2 permeabilities. *Mater. Res.* **17,** 714–719 (2014).

121. Yu, B., Cong, H. & Zhao, X. Hybrid brominated sulfonated poly(2,6-diphenyl-1,4-phenylene oxide) and SiO_2 nanocomposite membranes for CO_2/N_2 separation. *Prog. Nat. Sci. Mater. Int.* **22,** 661–667 (2012).

122. Cho, Y. J. & Park, H. B. High performance polyimide with high internal free volume elements. *Macromol. Rapid Commun.* **32,** 579–586 (2011).

123. Hamad, F. & Matsuura, T. Performance of gas separation membranes made from sulfonated brominated high molecular weight poly(2,4-dimethyl-I,6-phenylene oxide). *J. Memb. Sci.* **253,** 183–189 (2005).

124. Pessan, L. A., Koros, W. J., Schmidhauser, J. C. & Richards, W. D. Gas transport properties of polymers based on spirobiindane bisphenol. *J. Polym. Sci. Part B Polym. Phys.* **33,** 487–494 (1995).

125. Grayson, S. M. *et al.* Synthesis and characterization of norbornanediol isomers and their fluorinated analogues. *J. Org. Chem.* **71,** 341–4 (2006).

126. Figoli, A., Sager, W. F. C. & Mulder, M. H. V. Facilitated oxygen transport in liquid membranes: review and new concepts. *J. Memb. Sci.* **181,** 97–110 (2001).

127. Hu, Y., Shiotsuki, M., Sanda, F., Freeman, B. D. & Masuda, T. Synthesis and properties of indan-based polyacetylenes that feature the highest gas permeability among all the existing polymers. *Macromolecules* **41,** 8525–8532 (2008).

128. Song, Q. *et al.* Controlled thermal oxidative crosslinking of polymers of intrinsic microporosity towards tunable molecular sieve membranes. *Nat. Commun.* **5,** 4813 (2014).

129. Han, S. H., Lee, J. E., Lee, K.-J., Park, H. B. & Lee, Y. M. Highly gas permeable and microporous polybenzimidazole membrane by thermal rearrangement. *J. Memb. Sci.* **357,** 143–151 (2010).

130. Puleo, A. C., Paul, D. R. & Kelley, S. S. The effect of degree of acetylation on gas sorption and transport behavior in cellulose acetate. *J. Memb. Sci.* **47,** 301–332 (1989).

131. Hellums, M. W., Koros, W. J. & Schmidhauser, J. C. Gas separation properties of spirobiindane polycarbonate. *J. Memb. Sci.* **67,** 75–81 (1992).

132. Thomas, S., Pinnau, I., Du, N. & Guiver, M. D. Pure- and mixed-gas permeation properties of a microporous spirobisindane-based ladder polymer (PIM-1). *J. Memb. Sci.* **333,** 125–131 (2009).

133. Li, F. Y., Xiao, Y., Chung, T.-S. & Kawi, S. High-performance thermally self-cross-linked polymer of intrinsic microporosity (PIM-1) membranes for energy development. *Macromolecules* **45,** 1427–

1437 (2012).

134.   Scholes, C. A., Jin, J., Stevens, G. W. & Kentish, S. E. Competitive permeation of gas and water vapour in high free volume polymeric membranes. *J. Polym. Sci. Part B Polym. Phys.* **53,** 719–728 (2015).

135.   Park, H. B., Han, S. H., Jung, C. H., Lee, Y. M. & Hill, A. J. Thermally rearranged (TR) polymer membranes for CO_2 separation. *J. Memb. Sci.* **359,** 11–24 (2010).

136.   Cui, L., Qiu, W., Paul, D. R. & Koros, W. J. Physical aging of 6FDA-based polyimide membranes monitored by gas permeability. *Polymer* **52,** 3374–3380 (2011).

137.   Einhorn, A. Ueber die Carbonate der Dioxybenzole. *Justus Liebig's Ann. der Chemie* **300,** 135–155 (1898).

138.   Bischoff, C. A. & von Hedenström, A. Ueber aromatische Ester der Kohlensäure und Oxalsäure. *Berichte der Dtsch. Chem. Gesellschaft* **35,** 3431–3437 (1902).

139.   Carothers, W. H. & van Natta, F. J. Studies on polymerization and ring formation. III. Glycol esters of carbonic acid. *J. Am. Chem. Soc.* **52,** 314–326 (1930).

140.   Petersen, W. R. Superpolycarbonate. US 2210817 (1940).

141.   Schnell, H., Bottenbruch, L. & Krimm, H. Procede de preparation de matières artificielles thermoplastiques. 1–7 (1954).

142.   Schnell, H. Polycarbonate, eine Gruppe neuartiger thermoplastischer Kunststoffe. Herstellung und Eigenschaften aromatischer Polyester der Kohlensäure. *Angew. Chemie* **68,** 633–640 (1956).

143.   Schnell, H. *Chemistry and Physics of Polycarbonates.* (Wiley-Interscience, 1964).

144.   Schnell, H., Bottenbruch, L. & Krimm, H. Thermoplastic aromatic polycarbonates and their manufacture. US 3028365 (1962).

145.   Fox, D. W. Production of aryl ethers. (1959).

146.   Fox, D. W. Polycarbonates of dihydroxyaryl ethers. (1964).

147.   LeGrand, D. G. & Bendler, J. T. *Handbook of Polycarbonate Science and Technology.* (Marcel Dekker, Inc., 2000).

148.   Sakashita, T. & Shimoda, T. Melt preparation of copolycarbonate with alkaline compound catalyst and boric acid compound catalyst. EU A3511168 (1988).

149.   Sakashita, T. & Shimoda, T. Polycarbonate, polyestercarbonate resin compounds and preparing methods thereof. US 3148172 (1991).

150.   Sakashita, T. & Shimoda, T. Catalytic melt preparation of polycarbonate with subsequent addition of sulfonic acid compound. US 5306801 (1994).

151.   Grigo, U., Kircher, K. & Müller, H.-H. in *Kunstst. Handb.* (Hanser, 1992).

152.   Franz, U. *et al.* Polycarbonat (PC) und seine Blends. *Kunststoffe (10)* 100–110 (2007). at <www.kunststoffe.de>

153.   Horn, K., Schnieders, F., Pophusen, D. & Yesildag, C. Marktentwicklung Polycarbonat (PC). *Kunststoffe (10)* 90–95 (2013). at <https://www.kunststoffe.de>

154.   Inoue, S., Koinuma, H. & Tsuruta, T. Copolymerization of carbon dioxide and epoxide with organometallic compounds. *Die Makromol. Chemie* **130,** 210–220 (1969).

155.   Inoue, S., Koinuma, H. & Tsuruta, T. Copolymerization of carbon dioxide and epoxide. *Polym. Lett.* **7,** 287–292 (1969).

156.   Fukuoka, S. *et al.* A novel non-phosgene polycarbonate production process using by-product CO_2 as starting material. *Green Chem.* **5,** 497 (2003).

157.   Tempelaar, S., Mespouille, L., Coulembier, O., Dubois, P. & Dove, A. P. Synthesis and post-polymerisation modifications of aliphatic poly(carbonate)s prepared by ring-opening polymerisation. *Chem. Soc. Rev.* **42,** 1312–1336 (2013).

158.   Feng, J., Zhuo, R.-X. & Zhang, X.-Z. Construction of functional aliphatic polycarbonates for biomedical applications. *Prog. Polym. Sci.* **37,** 211–236 (2012).

159. Kim, I., Ahn, J.-T., Ha, C. S., Yang, C. S. & Park, I. Polymerization of propylene oxide by using double metal cyanide catalysts and the application to polyurethane elastomer. *Polymer* **44,** 3417–3428 (2003).

160. Bähr, M., Bitto, A. & Mülhaupt, R. Cyclic limonene dicarbonate as a new monomer for non-isocyanate oligo- and polyurethanes (NIPU) based upon terpenes. *Green Chem.* **14,** 1447–1454 (2012).

161. Xia, H., Suo, Z. Y., Qiang, G. J. & Chang, C. J. Synthesis, characterization, and degradation of a novel L-tyrosine-derived polycarbonate for potential biomaterial applications. *J. Appl. Polym. Sci.* **110,** 2168–2178 (2008).

162. Kim, G. *et al.* Biological affinity and biodegradability of poly(propylene carbonate) prepared from copolymerization of carbon dioxide with propylene oxide. *Macromol. Res.* **16,** 473–480 (2008).

163. Bisht, K. S. *et al.* Lipase-catalyzed ring-opening polymerization of trimethylene carbonate. *Macromolecules* **30,** 7735–7742 (1997).

164. Al-Azemi, T. F. & Bisht, K. S. Novel functional polycarbonate by lipase-catalyzed ring-opening polymerization of 5-methyl-5-benzyloxycarbonyl-1,3-dioxan-2-one. *Macromolecules* **32,** 6536–6540 (1999).

165. Park, J. H. *et al.* Preparation of high-molecular-weight aliphatic polycarbonates by condensation polymerization of diols and dimethyl carbonate. *Macromolecules* **46,** 3301–3308 (2013).

166. Darensbourg, D. J., Ganguly, P. & Choi, W. Metal salen derivatives as catalysts for the alternating copolymerization of oxetanes and carbon dioxide to afford polycarbonates. *Inorg. Chem.* **45,** 3831–3833 (2006).

167. Nederberg, F. *et al.* Organocatalytic ring-opening polymerization of trimethylene carbonate. *Biomacromolecules* **8,** 153–160 (2007).

168. Yamamoto, Y., Kaihara, S., Toshima, K. & Matsumura, S. High-molecular-weight polycarbonates synthesized by enzymatic ROP of a cyclic carbonate as a green process. *Macromol. Biosci.* **9,** 968–978 (2009).

169. Zhou, Q. *et al.* Biodegradable CO₂-based polycarbonates with rapid and reversible thermal response at body temperature. *J. Polym. Sci. Part A Polym. Chem.* **51,** 1893–1898 (2013).

170. Wu, D.-Q. *et al.* Biodegradable and pH-sensitive hydrogels for cell encapsulation and controlled drug release. *Biomacromolecules* **9,** 1155–1162 (2008).

171. Chen, W. *et al.* Versatile synthesis of functional biodegradable polymers by combining ring-opening polymerization and postpolymerization modification via michael-type addition reaction. *Macromolecules* **43,** 201–207 (2010).

172. Wang, R. *et al.* Unprecedented access to functional biodegradable polymers and coatings. *Macromolecules* **44,** 6009–6016 (2011).

173. Mei, H., Zhong, Z., Long, F. & Zhuo, R. Synthesis and characterization of novel glycerol-derived polycarbonates with pendant hydroxyl groups. *Macromol. Rapid Commun.* **27,** 1894–1899 (2006).

174. Sanders, D. P. *et al.* A simple and efficient synthesis of functionalized cyclic carbonate monomers using a versatile pentafluorophenyl ester intermediate. *J. Am. Chem. Soc.* **132,** 14724–14726 (2010).

175. Tempelaar, S., Mespouille, L., Dubois, P. & Dove, A. P. Organocatalytic synthesis and postpolymerization functionalization of allyl-functional poly(carbonate)s. *Macromolecules* **44,** 2084–2091 (2011).

176. Engler, A. C. *et al.* Accessing new materials through polymerization and modification of a polycarbonate with a pendant activated ester. *Macromolecules* **46,** 1283–1290 (2013).

177. Wang, L.-S., Cheng, S.-X. & Zhuo, R.-X. Novel biodegradable aliphatic polycarbonate based on ketal protected dihydroxyacetone. *Macromol. Rapid Commun.* **25,** 959–963 (2004).

178. Venkataraman, S., Veronica, N., Voo, Z. X., Hedrick, J. L. & Yang, Y. Y. 2-Amino-1,3-propane diols: a versatile platform for the synthesis of aliphatic cyclic carbonate monomers. *Polym. Chem.* **4,**

2945–2948 (2013).

179. Ono, Y. Dimethyl carbonate for environmentally benign reactions. *Catal. Today* **35,** 15–25 (1997).

180. Pacheco, M. a. & Marshall, C. L. Review of dimethyl carbonate (DMC) manufacture and its characteristics as a fuel additive. *Energy & Fuels* **11,** 2–29 (1997).

181. Zhu, W. *et al.* High-molecular-weight aliphatic polycarbonates by melt polycondensation of dimethyl carbonate and aliphatic diols: synthesis and characterization. *Polym. Int.* **60,** 1060–1067 (2011).

182. Jiang, Z., Liu, C., Xie, W. & Gross, R. A. Controlled lipase-catalyzed synthesis of poly(hexamethylene carbonate). *Macromolecules* **40,** 7934–7943 (2007).

183. Gunatillake, P. A., Meijs, G. F., McCarthy, S. J., Adhikari, R. & Sherriff, N. Synthesis and characterization of a series of poly(alkylene carbonate) macrodiols and the effect of their structure on the properties of polyurethanes. *J. Appl. Polym. Sci.* **69,** 1621–1633 (1998).

184. Carothers, W. H., Dorough, G. L. & Natta, F. J. van. Studies of polymerization and ring formation X. The reversible polymerization of six-membered cyclic esters. *J. Am. Chem. Soc.* **54,** 761–772 (1932).

185. Xu, J., Feng, E. & Song, J. Renaissance of aliphatic polycarbonates: new techniques and biomedical applications. *J. Appl. Polym. Sci.* **131,** 1–16 (2014).

186. Nederberg, F., Connor, E. F., Möller, M., Glauser, T. & Hedrick, J. L. New paradigms for organic catalysts: the first organocatalytic living polymerization. *Angew. Chemie Int. Ed.* **40,** 2712–2715 (2001).

187. Helou, M., Miserque, O., Brusson, J.-M., Carpentier, J.-F. & Guillaume, S. M. Organocatalysts for the controlled 'immortal' ring-opening polymerization of six-membered-ring cyclic carbonates: a metal-free, green process. *Chem. - A Eur. J.* **16,** 13805–13813 (2010).

188. Makiguchi, K., Ogasawara, Y., Kikuchi, S., Satoh, T. & Kakuchi, T. Diphenyl phosphate as an efficient acidic organocatalyst for controlled/living ring-opening polymerization of trimethylene carbonates leading to block, end-functionalized, and macrocyclic polycarbonates. *Macromolecules* **46,** 1772–1782 (2013).

189. Delcroix, D., Martín-Vaca, B., Bourissou, D. & Navarro, C. Ring-opening polymerization of trimethylene carbonate catalyzed by methanesulfonic acid: activated monomer versus active chain end mechanisms. *Macromolecules* **43,** 8828–8835 (2010).

190. Nemoto, N., Sanda, F. & Endo, T. Cationic ring-opening polymerization of six-membered cyclic carbonates with ester groups. *J. Polym. Sci. Part A Polym. Chem.* **39,** 1305–1317 (2001).

191. Campos, J. M., Ribeiro, M. R., Ribeiro, M. F., Deffieux, A. & Peruch, F. A new insight into the mechanism of the ring-opening polymerization of trimethylene carbonate catalyzed by methanesulfonic acid. *Macromol. Chem. Phys.* **214,** 85–93 (2013).

192. Al-Azemi, T. F., Harmon, J. P. & Bisht, K. S. Enzyme-catalyzed ring-opening copolymerization of 5-methyl-5-benzyloxycarbonyl-1,3-dioxan-2-one (MBC) with trimethylene carbonate (TMC): synthesis and characterization. *Biomacromolecules* **1,** 493–500 (2000).

193. Feng, J., Zhuo, R., He, F. & Wang, X. Synthesis of functional polycarbonates by lipase-catalyzed ring-opening polymerization. *Macromol. Symp.* **195,** 237–240 (2003).

194. Gross, R. A., Kalra, B. & Kumar, A. Polyester and polycarbonate synthesis by in vitro enzyme catalysis. *Appl. Microbiol. Biotechnol.* **55,** 655–660 (2001).

195. Pratt, R. C., Nederberg, F., Waymouth, R. M. & Hedrick, J. L. Tagging alcohols with cyclic carbonate: a versatile equivalent of (meth)acrylate for ring-opening polymerization. *Chem. Commun.* **1,** 114–116 (2008).

196. Tryznowski, M. *et al.* Aliphatic hyperbranched polycarbonates: synthesis, characterization, and solubility in supercritical carbon dioxide. *Macromolecules* **45,** 6819–6829 (2012).

197. He, F. *et al.* Synthesis, characterization and ring-opening polymerization of a novel six-membered

cyclic carbonate bearing pendent allyl ether group. *Polymer* **49,** 1185–1190 (2008).

198. Wu, R. *et al.* Reactive electrospinning and biodegradation of cross-linked methacrylated polycarbonate nanofibers. *Biomed. Mater.* **6,** 035004 (2011).

199. Welle, A. *et al.* Electrospun aliphatic polycarbonates as tailored tissue scaffold materials. *Biomaterials* **28,** 2211–2219 (2007).

200. Hou, Q., Grijpma, D. W. & Feijen, J. Creep-resistant elastomeric networks prepared by photocrosslinking fumaric acid monoethyl ester-functionalized poly(trimethylene carbonate) oligomers. *Acta Biomater.* **5,** 1543–1551 (2009).

201. Bat, E., Feijen, J. & Grijpma, D. W. Biodegradable elastomeric networks: highly efficient cross-linking of poly(trimethylene carbonate) by gamma irradiation in the presence of pentaerythritol triacrylate. *Biomacromolecules* **11,** 2692–2699 (2010).

202. Bat, E. *et al.* Ultraviolet light crosslinking of poly(trimethylene carbonate) for elastomeric tissue engineering scaffolds. *Biomaterials* **31,** 8696–8705 (2010).

203. Dargaville, B. L. *et al.* Cross-linked poly(trimethylene carbonate-*co*-L-lactide) as a biodegradable, elastomeric scaffold for vascular engineering applications. *Biomacromolecules* **12,** 3856–3869 (2011).

204. Kim, S. Y., Lee, K. E., Han, S. S. & Jeong, B. Vesicle-to-spherical micelle-to-tubular nanostructure transition of monomethoxy-poly(ethylene glycol)−poly(trimethylene carbonate) diblock copolymer. *J. Phys. Chem. B* **112,** 7420–7423 (2008).

205. Zhang, C., Aung, A., Liao, L. & Varghese, S. A novel single precursor-based biodegradable hydrogel with enhanced mechanical properties. *Soft Matter* **5,** 3831 (2009).

206. Bat, E., Grijpma, D. W. & Feijen, J. Thermoreversible gelation behaviour of PTMC-PEG-PTMC triblock copolymers. *J. Control. Release* **132,** e37–e39 (2008).

207. Fan, C., Zhang, C., Jing, Y., Liao, L. & Liu, L. Preparation and characterization of a biodegradable hydrogel containing oligo(2,2-dimethyltrimethylene carbonate) moieties with tunable properties. *RSC Adv.* **3,** 157–165 (2013).

208. Li, Y. *et al.* Nanostructured PEG-based hydrogels with tunable physical properties for gene delivery to human mesenchymal stem cells. *Biomaterials* **33,** 6533–6541 (2012).

209. Chen, W., Meng, F., Cheng, R. & Zhong, Z. pH-Sensitive degradable polymersomes for triggered release of anticancer drugs: A comparative study with micelles. *J. Control. Release* **142,** 40–46 (2010).

210. Cooley, C. B. *et al.* Oligocarbonate molecular transporters: oligomerization-based syntheses and cell-penetrating studies. *J. Am. Chem. Soc.* **131,** 16401–16403 (2009).

211. Peng, T., SU, J., Cheng, S.-X. & Zhuo, R.-X. Poly-α,β-(*N*-(2-hydroxyethyl)-L-aspartamide)-g-poly(1,3-trimethylene carbonate) amphiphilic graft co-polymer as a potential drug carrier. *J. Biomater. Sci. Polym. Ed.* **17,** 941–951 (2006).

212. Allen, S. D. *et al.* Polycarbonate polyol compositions and methods. US 2013/0066044 (2013).

213. Fritz, N., Dao, H., Allen, S. A. B. & Kohl, P. A. Polycarbonates as temporary adhesives. *Int. J. Adhes. Adhes.* **38,** 45–49 (2012).

214. Füßl, A. *et al.* Foams comprising polypropylene carbonate. US 20130059141 (2013).

215. Ku, S. Y. *et al.* Solution-processed nanostructured benzoporphyrin with polycarbonate binder for photovoltaics. *Adv. Mater.* **23,** 2289–2293 (2011).

216. Li, C., Sablong, R. J. & Koning, C. E. Synthesis and characterization of fully bio-based α,ω-dihydroxyl poly(limonene carbonate)s and their initial evaluation in coating applications. *Eur. Polym. J.* **67,** 449–458 (2015).

217. Noel, A., Borguet, Y. P., Raymond, J. E. & Wooley, K. L. Poly(carbonate-amide)s derived from bio-based resources: poly(ferulic acid-co-tyrosine). *Macromolecules* **47,** 2974–2983 (2014).

218. Lu, X.-B. & Darensbourg, D. J. Cobalt catalysts for the coupling of CO_2 and epoxides to provide

polycarbonates and cyclic carbonates. *Chem. Soc. Rev.* **41,** 1462–1484 (2012).

219. Langanke, J. *et al.* Carbon dioxide (CO_2) as sustainable feedstock for polyurethane production. *Green Chem.* **16,** 1865–1870 (2014).

220. Coates, G. W. & Moore, D. R. Discrete metal-based catalysts for the copolymerization of CO_2 and epoxides: discovery, reactivity, optimization, and mechanism. *Angew. Chemie Int. Ed.* **43,** 6618–6639 (2004).

221. Darensbourg, D. J. Making plastics from carbon dioxide: salen metal complexes as catalysts for the production of polycarbonates from epoxides and CO_2. *Chem. Rev.* **107,** 2388–2410 (2007).

222. Chapman, A. M., Keyworth, C., Kember, M. R., Lennox, A. J. J. & Williams, C. K. Adding value to power station captured CO_2 : tolerant Zn and Mg homogeneous catalysts for polycarbonate polyol production. *ACS Catal.* **5,** 1581–1588 (2015).

223. Darensbourg, D. J. Salen metal complexes as catalysts for the synthesis of polycarbonates from cyclic ethers and carbon dioxide. *Adv. Polym. Sci.* 1–27 (2011). doi:10.1007/12_2011_135

224. van Meerendonk, W. J., Duchateau, R., Koning, C. E. & Gruter, G. M. Unexpected side reactions and chain transfer for zinc-catalyzed copolymerization of cyclohexene oxide and carbon dioxide. *Macromolecules* **38,** 7306–7313 (2005).

225. Jutz, F., Buchard, A., Kember, M. R., Fredriksen, S. B. & Williams, C. K. Mechanistic investigation and reaction kinetics of the low-pressure copolymerization of cyclohexene oxide and carbon dioxide catalyzed by a dizinc complex. *J. Am. Chem. Soc.* **133,** 17395–17405 (2011).

226. Duchateau, R. *et al.* Ester-functionalized polycarbonates obtained by copolymerization of ester-substituted oxiranes and carbon dioxide: a MALDI-ToF-MS analysis study. *Macromolecules* **39,** 7900–7908 (2006).

227. Helou, M., Miserque, O., Brusson, J.-M., Carpentier, J.-F. & Guillaume, S. M. Ultraproductive, zinc-mediated, immortal ring-opening polymerization of trimethylene carbonate. *Chem. - A Eur. J.* **14,** 8772–8775 (2008).

228. Darensbourg, D. J., Poland, R. R. & Strickland, A. L. (Salan)CrCl, an effective catalyst for the copolymerization and terpolymerization of epoxides and carbon dioxide. *J. Polym. Sci. Part A Polym. Chem.* **50,** 127–133 (2012).

229. Cohen, C. T., Thomas, C. M., Peretti, K. L., Lobkovsky, E. B. & Coates, G. W. Copolymerization of cyclohexene oxide and carbon dioxide using (salen)Co complexes: synthesis and characterization of syndiotactic poly(cyclohexene carbonate). *Dalt. Trans.* **1,** 237–249 (2006).

230. Cohen, C. T., Chu, T. & Coates, G. W. Cobalt catalysts for the alternating copolymerization of propylene oxide and carbon dioxide: combining high activity and selectivity. *J. Am. Chem. Soc.* **127,** 10869–10878 (2005).

231. Kim, I. *et al.* Biodegradable polycarbonate synthesis by copolymerization of carbon dioxide with epoxides using a heterogeneous zinc complex. *Macromol. Symp.* **224,** 181–192 (2005).

232. Geschwind, J. & Frey, H. Poly(1,2-glycerol carbonate): a fundamental polymer structure synthesized from CO_2 and glycidyl ethers. *Macromolecules* **46,** 3280–3287 (2013).

233. Kim, I. *et al.* Aliphatic polycarbonate synthesis by copolymerization of carbon dioxide with epoxides over double metal cyanide catalysts prepared by using ZnX2 (X=F, Cl, Br, I). *Catal. Today* **111,** 292–296 (2006).

234. Inoue, S. Copolymerization of carbon dioxide and epoxide: functionality of the copolymer. *J. Macromol. Sci. Part A - Chem.* **13,** 651–664 (1979).

235. Tan, C.-S., Juan, C.-C. & Kuo, T.-W. Polyethercarbonate–silica nanocomposites synthesized by copolymerization of allyl glycidyl ether with CO_2 followed by sol–gel process. *Polymer* **45,** 1805–1814 (2004).

236. Hu, Y. *et al.* Synthesis and stabilization of novel aliphatic polycarbonate from renewable resource. *Macromolecules* **42,** 9251–9254 (2009).

237. Koning, C. *et al.* Synthesis and physical characterization of poly(cyclohexane carbonate), synthesized from CO_2 and cyclohexene oxide. *Polymer* **42,** 3995–4004 (2001).

238. Thorat, S. D., Phillips, P. J., Semenov, V. & Gakh, A. Physical properties of aliphatic polycarbonates made from CO_2 and epoxides. *J. Appl. Polym. Sci.* **89,** 1163–1176 (2003).

239. Peng, S. *et al.* Thermal degradation kinetics of uncapped and end-capped poly(propylene carbonate). *Polym. Degrad. Stab.* **80,** 141–147 (2003).

240. Luinstra, G. A. & Borchardt, E. in *Synth. Biodegrad. Polym.* 29–48 (Springer Berlin / Heidelberg, 2012). doi:10.1007/12_2011_126

241. Ren, W.-M. *et al.* Highly active, bifunctional Co(III)-salen catalyst for alternating copolymerization of CO_2 with cyclohexene oxide and terpolymerization with aliphatic epoxides. *Macromolecules* **43,** 1396–1402 (2010).

242. Puglisi, C., Sturiale, L. & Montaudo, G. Thermal decomposition processes in aromatic polycarbonates investigated by mass spectrometry. *Macromolecules* **32,** 2194–2203 (1999).

243. Takeda, N. & Inoue, S. Polymerization of 1,2-epoxypropane and copolymerization with carbon dioxide catalyzed by metalloporphyrins. *Die Makromol. Chemie* **179,** 1377–1381 (1978).

244. Wang, S. J., Du, L. C., Zhao, X. S., Meng, Y. Z. & Tjong, S. C. Synthesis and characterization of alternating copolymer from carbon dioxide and propylene oxide. *J. Appl. Polym. Sci.* **85,** 2327–2334 (2002).

245. Trott, G., Saini, P. K. & Williams, C. K. Catalysts for CO_2/epoxide ring-opening copolymerization. *Philos. Trans. R. Soc. A* **374,** 1–19 (2016).

246. Luinstra, G. A. & Borchardt, E. in *Adv. Polym. Sci.* 29–48 (2011). doi:10.1007/12_2011_126

247. Motika, S. A., Pickering, T. L., Rokicki, A. & Stein, B. K. Catalyst for the copolymerization of epoxides with CO_2. US 5026676 (1991).

248. Klaus, S., Lehenmeier, M. W., Anderson, C. E. & Rieger, B. Recent advances in CO_2/epoxide copolymerization—New strategies and cooperative mechanisms. *Coord. Chem. Rev.* **255,** 1460–1479 (2011).

249. Lu, X.-B., Ren, W.-M. & Wu, G.-P. CO_2 copolymers from epoxides: catalyst activity, product selectivity, and stereochemistry control. *Acc. Chem. Res.* **45,** 1721–1735 (2012).

250. Nozaki, K. Asymmetric catalytic synthesis of polyketones and polycarbonates. *Pure Appl. Chem.* **76,** 541–546 (2004).

251. Romain, C., Thevenon, A., Saini, P. K. & Williams, C. K. *Dinuclear metal complex-mediated formation of CO_2-based polycarbonates*. (Springer International Publishing, 2015). doi:10.1007/3418_2015_95

252. Ree, M., Bae, J. Y., Jung, J. H. & Shin, T. J. A new copolymerization process leading to poly(propylene carbonate) with a highly enhanced yield from carbon dioxide and propylene oxide. *J. Polym. Sci. Part A Polym. Chem.* **37,** 1863–1876 (1999).

253. Ree, M. *et al.* New findings in the catalytic activity of zinc glutarate and its application in the chemical fixation of CO_2 into polycarbonates and their derivatives. *Catal. Today* **115,** 134–145 (2006).

254. Chen, S., Hua, Z., Fang, Z. & Qi, G. Copolymerization of carbon dioxide and propylene oxide with highly effective zinc hexacyanocobaltate(III)-based coordination catalyst. *Polymer* **45,** 6519–6524 (2004).

255. Chen, S., Qi, G.-R., Hua, Z.-J. & Yan, H.-Q. Double metal cyanide complex based on Zn3[Co(CN)6]2 as highly active catalyst for copolymerization of carbon dioxide and cyclohexene oxide. *J. Polym. Sci. Part A Polym. Chem.* **42,** 5284–5291 (2004).

256. Robertson, N. J. *et al.* Two-dimensional double metal cyanide complexes: highly active catalysts for the homopolymerization of propylene oxide and copolymerization of propylene oxide and carbon dioxide. *Dalt. Trans.* **45,** 5390–5395 (2006).

257. Mang, S., Cooper, A. I., Colclough, M. E., Chauhan, N. & Holmes, A. B. Copolymerization of CO_2 and 1,2-cyclohexene oxide using a CO_2-soluble chromium porphyrin catalyst. *Macromolecules* **33**, 303–308 (2000).

258. Sugimoto, H., Ohshima, H. & Inoue, S. Alternating copolymerization of carbon dioxide and epoxide by manganese porphyrin: The first example of polycarbonate synthesis from 1-atm carbon dioxide. *J. Polym. Sci. Part A Polym. Chem.* **41**, 3549–3555 (2003).

259. Chatterjee, C. & Chisholm, M. H. Influence of the metal (Al, Cr, and Co) and the substituents of the porphyrin in controlling the reactions involved in the copolymerization of propylene oxide and carbon dioxide by porphyrin metal(III) complexes. 2. Chromium chemistry. *Inorg. Chem.* **51**, 12041–12052 (2012).

260. Aida, T. & Inoue, S. Activation of carbon dioxide with aluminum porphyrin and reaction with epoxide. Studies on (tetraphenylporphinato)aluminum alkoxide having a long oxyalkylene chain as the alkoxide group. *J. Am. Chem. Soc.* **105**, 1304–1309 (1983).

261. Qin, Z., Thomas, C. M., Lee, S. & Coates, G. W. Cobalt-based complexes for the copolymerization of propylene oxide and CO_2: active and selective catalysts for polycarbonate synthesis. *Angew. Chemie Int. Ed.* **42**, 5484–5487 (2003).

262. Rao, D.-Y., Li, B., Zhang, R., Wang, H. & Lu, X.-B. Binding of 4-(N,N- dimethylamino)pyridine to salen- and salan-Cr(III) cations: a mechanistic understanding on the difference in their catalytic activity for CO_2/epoxide Copolymerization. *Inorg. Chem.* **48**, 2830–2836 (2009).

263. Li, B. *et al.* Asymmetric, regio- and stereo-selective alternating copolymerization of CO_2 and propylene oxide catalyzed by chiral chromium Salan complexes. *J. Polym. Sci. Part A Polym. Chem.* **46**, 6102–6113 (2008).

264. Nakano, K., Kamada, T. & Nozaki, K. Selective formation of polycarbonate over cyclic carbonate: copolymerization of epoxides with carbon dioxide catalyzed by a cobalt(III) complex with a piperidinium end-capping arm. *Angew. Chemie Int. Ed.* **45**, 7274–7277 (2006).

265. **Sugimoto, H. & Kuroda, K. The cobalt porphyrin–lewis base system: a highly selective catalyst for** alternating copolymerization of CO_2 and epoxide under mild conditions. *Macromolecules* **41**, 312–317 (2008).

266. Sujith, S., Min, J. K., Seong, J. E., Na, S. J. & Lee, B. Y. A highly active and recyclable catalytic system for CO2/propylene oxide copolymerization. *Angew. Chemie Int. Ed.* **47**, 7306–7309 (2008).

267. Cheng, M. *et al.* Single-site beta-diiminate zinc catalysts for the alternating copolymerization of CO_2 and epoxides: catalyst synthesis and unprecedented polymerization activity. *J. Am. Chem. Soc.* **123**, 8738–8749 (2001).

268. Rieth, L. R., Moore, D. R., Lobkovsky, E. B. & Coates, G. W. Single-site beta-diiminate zinc catalysts for the ring-opening polymerization of beta-butyrolactone and beta-valerolactone to poly(3-hydroxyalkanoates). *J. Am. Chem. Soc.* **124**, 15239–48 (2002).

269. Moore, D. R., Cheng, M., Lobkovsky, E. B. & Coates, G. W. Mechanism of the alternating copolymerization of epoxides and CO_2 using beta-diiminate zinc catalysts: evidence for a bimetallic epoxide enchainment. *J. Am. Chem. Soc.* **125**, 11911–11924 (2003).

270. Ellis, W. C. *et al.* Copolymerization of CO_2 **and meso epoxides using enantioselective β**-diiminate catalysts: a route to highly isotactic polycarbonates. *Chem. Sci.* **5**, 4004–4011 (2014).

271. Cheng, M., Lobkovsky, E. B. & Coates, G. W. Catalytic reactions involving C_1 feedstocks: new high-activity Zn(II)-based catalysts for the alternating copolymerization of carbon dioxide and epoxides. *J. Am. Chem. Soc.* **120**, 11018–11019 (1998).

272. Lehenmeier, M. W. *et al.* Flexibly tethered dinuclear zinc complexes: a solution to the entropy problem in CO_2/epoxide copolymerization catalysis? *Angew. Chemie - Int. Ed.* **52**, 9821–9826 (2013).

273. Kissling, S. *et al.* Dinuclear zinc catalysts with unprecedented activities for the copolymerization of cyclohexene oxide and CO_2. *Chem. Commun.* **51**, 4579–4582 (2015).

274. Kember, M. R., White, A. J. P. & Williams, C. K. Highly active di- and trimetallic cobalt catalysts for the copolymerization of CHO and CO_2 at atmospheric pressure. *Macromolecules* **43,** 2291–2298 (2010).

275. Moore, D. R., Cheng, M., Lobkovsky, E. B. & Coates, G. W. Electronic and steric effects on catalysts for CO_2/epoxide polymerization: subtle modifications resulting in superior activities. *Angew. Chem. Int. Ed. Engl.* **41,** 2599–602 (2002).

276. Schween, J. H., Dlugi, R., Hewitt, C. N. & Foster, P. Determination and accuracy of VOC-fluxes above the pine/oak forest at Castelporziano. *Atmos. Environ.* **31,** 199–215 (1997).

277. Thomas, A. F. & Bessière, Y. Limonene. *Nat. Prod. Rep.* **6,** 291 (1989).

278. Pourbafrani, M., Forgács, G., Horváth, I. S., Niklasson, C. & Taherzadeh, M. J. Production of biofuels, limonene and pectin from citrus wastes. *Bioresour. Technol.* **101,** 4246–4250 (2010).

279. *Citrus Fruit Fresh and Processed, Food and Agriculture Organization of the United Nations.* (2012).

280. Ciriminna, R., Lomeli-Rodriguez, M., Demma Carà, P., Lopez-Sanchez, J. A. & Pagliaro, M. Limonene: a versatile chemical of the bioeconomy. *Chem. Commun.* **50,** 15288–15296 (2014).

281. Mecking, S. Nature or petrochemistry?—Biologically degradable materials. *Angew. Chemie Int. Ed.* **43,** 1078–1085 (2004).

282. Dejoye Tanzi, C., Abert Vian, M., Ginies, C., Elmaataoui, M. & Chemat, F. Terpenes as green solvents for extraction of oil from microalgae. *Molecules* **17,** 8196–8205 (2012).

283. Faure, K., Bouju, E., Suchet, P. & Berthod, A. Use of limonene in countercurrent chromatography: a green alkane substitute. *Anal. Chem.* **85,** 4644–4650 (2013).

284. Chemat, F., Vian, M. A. & Cravotto, G. Green extraction of natural products: concept and principles. *Int. J. Mol. Sci.* **13,** 8615–8627 (2012).

285. Hollingsworth, R. G. Limonene, a citrus extract, for control of mealybugs and scale insects. *J. Econ. Entomol.* **98,** 772–779 (2005).

286. Russin, W. A., Hoesly, J. D., Elson, C. E., Tanner, M. A. & Gould, M. N. Inhibition of rat mammary carcinogenesis by monoterpenoids. *Carcinogenesis* **10,** 2161–2164 (1989).

287. Keinan, E. *et al.* Natural ozone scavenger prevents asthma in sensitized rats. *Bioorg. Med. Chem.* **13,** 557–562 (2005).

288. Roberts, W. J. & Day, A. R. A study of the polymerization of α- and β-pinene with Friedel—Crafts type catalysts. *J. Am. Chem. Soc.* **72,** 1226–1230 (1950).

289. Modena, M., Bates, R. B. & Marvel, C. S. Some low molecular weight polymers of d-limonene and related terpenes obtained by Ziegler-type catalysts. *J. Polym. Sci. Part A Gen. Pap.* **3,** 949–960 (1965).

290. Martin-Luengo, M. A. *et al.* Sustainable *p*-cymene and hydrogen from limonene. *Appl. Catal. A Gen.* **387,** 141–146 (2010).

291. Colonna, M. *et al.* Synthesis and radiocarbon evidence of terephthalate polyesters completely prepared from renewable resources. *Green Chem.* **13,** 2543 (2011).

292. Firdaus, M., Montero De Espinosa, L. & Meier, M. A. R. Terpene-based renewable monomers and polymers via thiol-ene additions. *Macromolecules* **44,** 7253–7262 (2011).

293. Firdaus, M. & Meier, M. A. R. Renewable polyamides and polyurethanes derived from limonene. *Green Chem.* **15,** 370 (2013).

294. Claudino, M., Mathevet, J.-M., Jonsson, M. & Johansson, M. Bringing d-limonene to the scene of bio-based thermoset coatings via free-radical thiol–ene chemistry: macromonomer synthesis, UV-curing and thermo-mechanical characterization. *Polym. Chem.* **5,** 3245–3260 (2014).

295. Byrne, C. M., Allen, S. D., Lobkovsky, E. B. & Coates, G. W. Alternating copolymerization of limonene oxide and carbon dioxide. *J. Am. Chem. Soc.* **126,** 11404–11405 (2004).

296. Park, H. J., Ryu, C. Y. & Crivello, J. V. Photoinitiated cationic polymerization of limonene 1,2-oxide and α-pinene oxide. *J. Polym. Sci. Part A Polym. Chem.* **51,** 109–117 (2013).

297.   Nejad, E. H., Paoniasari, A., van Melis, C. G. W., Koning, C. E. & Duchateau, R. Catalytic ring-opening copolymerization of limonene oxide and phthalic anhydride: toward partially renewable polyesters. *Macromolecules* **46,** 631–637 (2013).

298.   Zhang, Y. *et al.* Synthesis of fully alternating polycarbonate with low T_g from carbon dioxide and bio-based fatty acid. *RSC Adv.* **4,** 36183–36188 (2014).

299.   Darensbourg, D. J., Chung, W., Arp, C. J., Tsai, F. & Kyran, S. J. Copolymerization and cycloaddition products derived from coupling reactions of 1,2-epoxy-4-cyclohexene and carbon dioxide. Postpolymerization functionalization via thiol–ene click reactions. *Macromolecules* **47,** 7347–7353 (2014).

300.   Winkler, M., Romain, C., Meier, M. A. R. & Williams, C. K. Renewable polycarbonates and polyesters from 1,4-cyclohexadiene. *Green Chem.* **17,** 300–306 (2015).

301.   Auriemma, F. *et al.* Stereocomplexed poly(limonene carbonate): a unique example of the cocrystallization of amorphous enantiomeric polymers. *Angew. Chemie Int. Ed.* **54,** 1215–1218 (2015).

302.   Peña Carrodeguas, L., González-Fabra, J., Castro-Gómez, F., Bo, C. & Kleij, A. W. Al III-catalysed formation of poly(limonene)carbonate: DFT analysis of the origin of stereoregularity. *Chem. - A Eur. J.* **21,** 6115–6122 (2015).

303.   Nof, S. Y. *Springer Handbook of Automation.* (Springer, 2009).

2

Overview of the thesis

2.1 Outline

The central element of this thesis is the bio-based amorphous material PLimC. The polymer was already introduced in 2004 by Coates and coworkers, but only after our findings regarding the synthesis of high molecular weight PLimC, the polymer would transition into a thermoplastic material that is comparable to established engineering thermoplastics like BPA-PC (Chapter 3). The original PLimC possesses a unique profile of properties that implies not only good mechanics and optics but also a high permeability of gases. This unique combination of properties suggests applications as a breathable glazing material in well-insulated constructions or as a membrane for gas separation in CCU processes (Chapter 4).
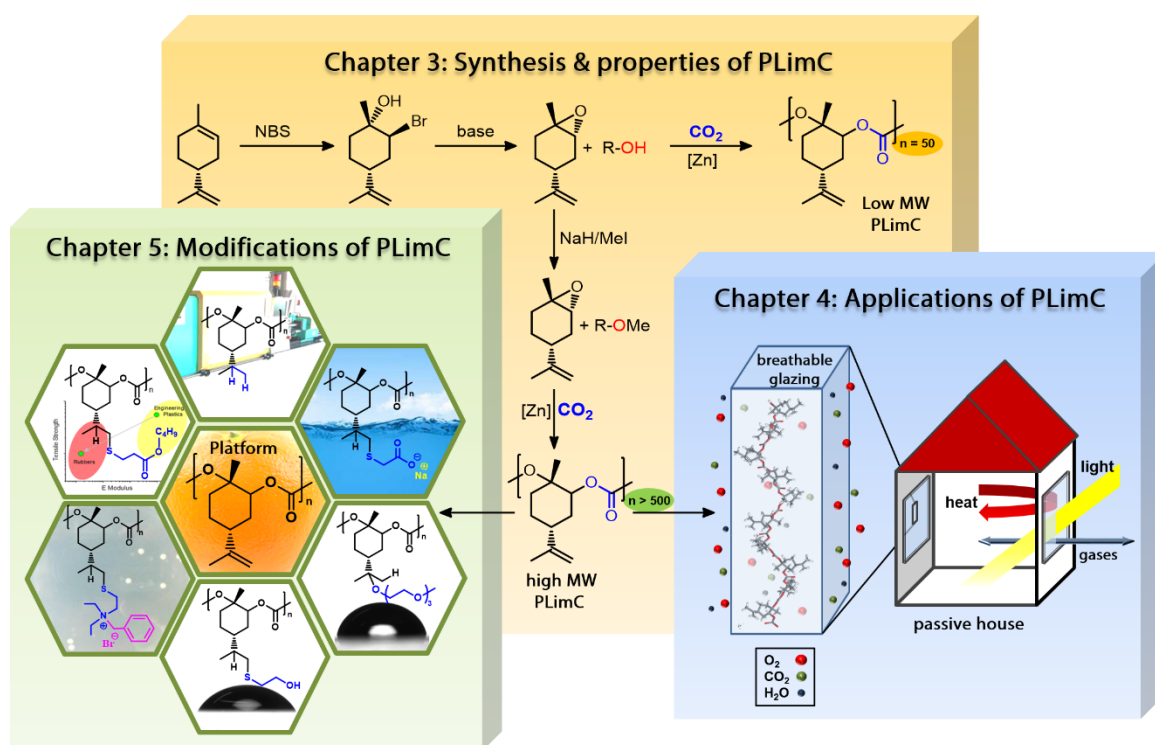
Figure 2-1 | The evolution of PLimC. This thesis is dedicated to the development of a high-performance thermoplastic material with a vast number of possible modifications and innovative applications. The syntheses involved in the economical production of high-MW PLimC and its macroscopic properties are discussed in Chapter 3. These syntheses include the stereoselective production of *trans*-LO, the subsequent masking of hydroxy impurities by methylation and eventually the zinc-catalyzed copolymerization of LO with CO_2 to give high-MW PLimC in high yields on the kg-scale. Potential applications of PLimC are discussed in Chapter 4. The concepts include the application of PLimC as a breathing glass for a passive gas exchange in well-insulated buildings and as gas separation membrane. Chemical modifications of PLimC by addition of various compounds to the double bond are discussed in Chapter 5. The new materials are characterized by dramatic changes in mechanical (rubbery), functional (antibacterial, hydrophilic or pH-responsive) and processability (saturated) properties.

We have identified the great versatility of PLimC being a platform polymer due to the unsaturated backbone. The double bonds were exploited for simple addition reactions to induce dramatic changes in terms of mechanical (transition from a high-T_g thermoplastic to rubber), functional (addition of antibacterial activity, hydrophilicity and pH-responsiveness, respectively) or processability (melt stability) properties (Chapter 5). The complete evolution of PLimC from a low-MW polymer to a versatile high-performance thermoplastic is illustrated in Figure 2-1 and as such summarizes the contents of this dissertation.

2.2 Synthesis & properties of PLimC

(published in: *Green Chemistry* **2016**, 18, 760)

The Zn(II) catalyst (used throughout this thesis) shown in Figure 2-2 is capable of coupling LO and CO_2 to give PLimC. However, the catalyst – carrying a bulky β-diiminate (bdi) ligand and an acetate moiety as initiator – incorporates only the *trans* isomer of LO due to steric effects.
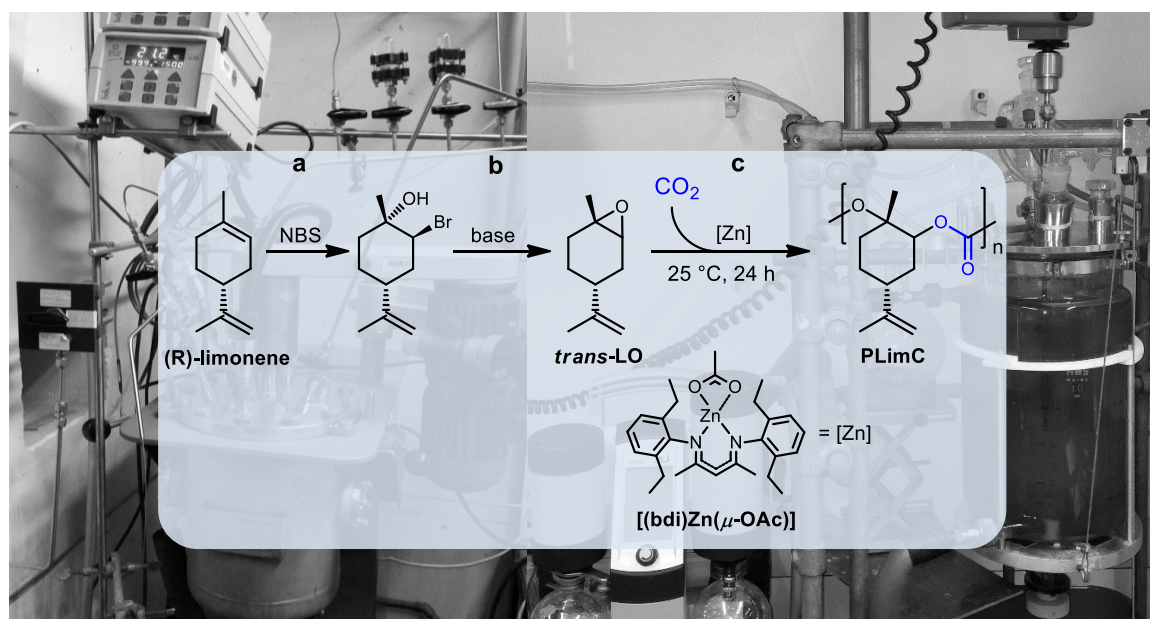
Figure 2-2 | Catalytic coupling of LO and CO₂. Schematic of the (**a**) stereo- and regioselective conversion of (*R*)-limonene into the bromohydrin and (**b**) the subsequent ring-closure in the presence of a base to give the *trans* isomer of LO. (**c**) The schematic shows the zinc-catalyzed copolymerization of *trans*-LO and CO_2 to give PLimC. The catalyst employed throughout this thesis is a β-diiminate Zn(II) complex with an acetate moiety [(bdi)Zn(μ-OAc)] as initiator for the copolymerization. In the background of the schemes the 10 L reactors of polymer and monomer syntheses are shown that were employed for the kg-batch-production.

Thus, starting from the orange-peel-based *(R)*-limonene, a stereo- and regioselective route was employed to produce *trans*-LO as major product. The selective conversion of limonene first into its bromohydrin using *N*-bromosuccinimide (NBS), and subsequently into the reactive monomer in the presence of a base, is an important step towards a sustainable synthesis of PLimC, as the polymer yield is close to 100% and no valuable bio-based LO (a commercial mixture consists of 50% *cis*-LO) is wasted. The high conversion of LO was also mandatory for the kg-batches produced of PLimC (10 L reactor of both monomer and polymer production shown as background of Figure 2-2), since a high amount of unreacted *cis*-LO would be very solvent-intensive and tedious and therefore un-economical.

Another key towards the economical production of PLimC is an efficient and fast catalysis of the process. In cooperation with a group of the TU Munich we have investigated the kinetic parameters of the copolymerization of CO_2 and LO catalyzed by [(bdi)Zn(μ-OAc)]. To our surprise, the coupling of both monomers is dependent of the square of the concentration of LO, as shown in Eq. 2-1 (k is the apparent rate constant).

$$\frac{d[PLimC]}{dt} = k \times [CO_2]^0 \times [LO]^2 \times [Zn]^1 \qquad (2\text{-}1)$$

It is widely recognized that the incorporation of the epoxide into the polymer chain is the rate-determining step. However, usually the rate of polymerization is only singly dependent on the concentration of the epoxide and thus we have proposed a different mechanism for the production of PLimC.
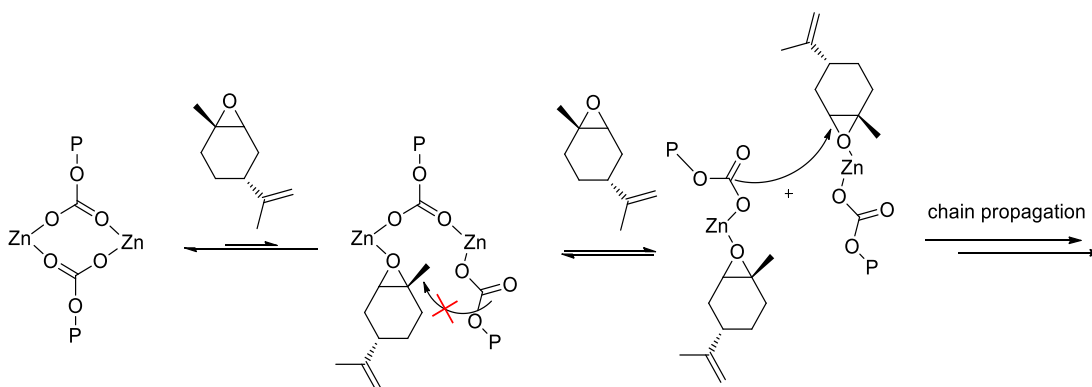
Figure 2-3 | Steric effects during chain propagation of PLimC. In kinetic investigations of the polymerization of PLimC, the Zn-based catalyst was found to be active only if two consecutive insertions of LO occur. Since the insertion of LO is the rate-determining step, the rate of polymerization is dependent on the square of the concentration of LO.

The key step, as shown in Figure 2-3 – is the consecutive insertion of two LO monomers into the dimeric species of the catalytic centre, whereas the pathway of chain propagation, with only one LO attached, is blocked, due to sterical hindrance of the bulky epoxide. Thus, the development of new catalysts, which are less dependent on the concentration/stereochemistry (catalyst for incorporation of *trans*- and *cis*-LO presented in 2015) of LO and show higher TOFs, is highly desirable.

The crucial step in the development of PLimC as a material with substantial mechanical strength was the production of high-MWs of the polymer. Since the first trials of the copolymerization of LO and CO_2 yielded only oligomers even with high *trans*-LO/catalyst ratios (catalyst incorporates only *trans* isomer in polymer backbone), we had a closer look at the catalytic system (see red circles in Figure 2-4c). The zinc-based catalyst was identified as the crucial component of the copolymerization, as it is very sensitive to chain transfer agents, that is, compounds carrying hydroxy functions. In gas chromatography-mass spectrometry (GC-MS) experiments a number of such impurities were found in quite substantial amounts as illustrated in Figure 2-4a.
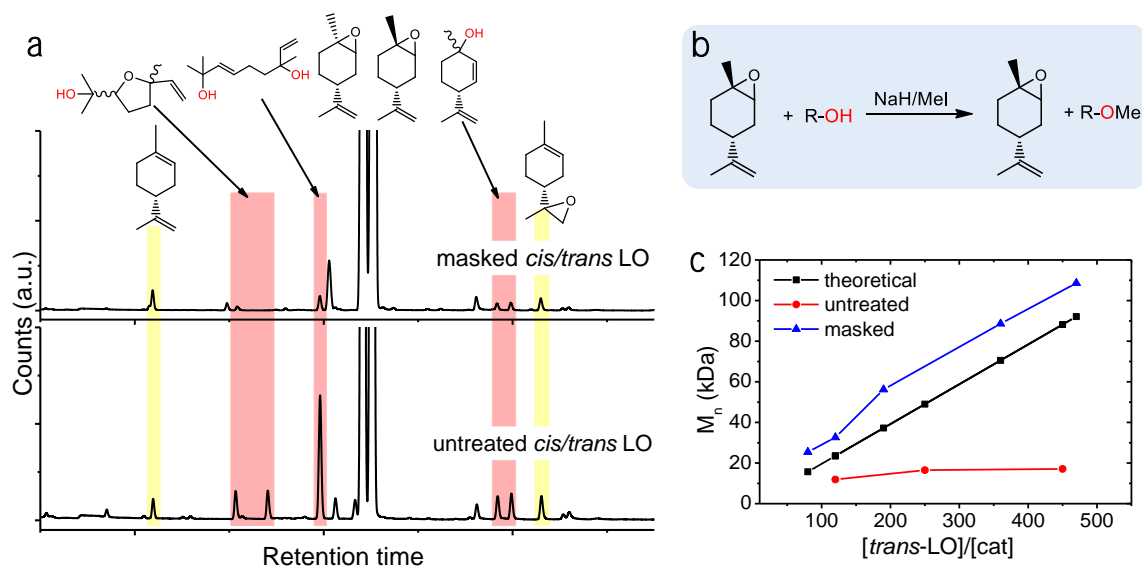
Figure 2-4 | The production of high-MW PLimC. (a) The gas chromatograms of a commercial mixture of *cis*- and *trans*-LO before and after a treatment with the masking agents NaH and MeI. Among the molecular structures – identified by GC-MS – in the LO mixture, a number of compounds was found carrying hydroxy groups, which act as CTAs in the zinc-catalyzed copolymerization of LO and CO_2. (b) A scheme of the masking reaction with NaH and MeI indicates the quantitative masking of hydroxy impurities in the LO monomer. The use of the strong base NaH and the small methylating agent MeI are necessary to account for the weak acidity of the protons and the sterical demand of the tertiary alcohols, respectively. (c) The copolymerization of LO and CO_2 is crucially dependent on the masking of any potential CTAs that would limit the number of repeating units of PLimC, resulting in MWs well below 20 kDa. Only with the masking reaction there is a linear dependency of MW on the *trans*-LO/catalyst ratio that was otherwise not observed.

These tertiary alcohols are typical side-products of the bio-based LO and due to very similar boiling points their thermal separation is virtually impossible. Alternatively, a chemical deactivation of the protic compounds was sought of that could suppress any chain transfer reactions without compromising the stability of the reactive epoxide LO. Such a deactivation was accomplished with a treatment of the monomer with sodium hydride (NaH) and iodomethane (MeI) (see Figure 2-4b). The strong base NaH and the small methylating agent MeI are required **to compensate for the tertiary alcohols' low acidity and** the sterical demand, respectively. Such a treatment leads to quantitative masking of the impurities and the copolymerization proceeds without chain transfer reagents that would limit the MW of the polymer. Hence, the theoretically expected linear dependency of M_h of PLimC on the *trans*-LO/catalyst ratio was eventually found (see blue triangles in Figure 2-4c). Only after the discovery of this masking reaction, the production of PLimC with MWs well above 100 kDa (Đ of 1.12) was readily accessible and with it the desired mechanical robustness.

The major drawback of PLimC – as of all aliphatic PCs – is the thermal lability of the melt. Due to its high T_g of 130 °C a temperature above 200 °C is required to reduce the viscosity of the melt to a value that is compatible to extrusion or injection molding processes. A crude sample of PLimC decomposes well below 200 °C, exhibiting a 5% mass loss at 205 °C ($T_{5\%}$) (see Figure 2-5a). This thermal instability is primarily influenced by residual catalyst, that is, Zn(II) species and hydroxy groups on the polymer chain ends. The removal of metal traces was achieved by the addition of the chelating agent ethylenediaminetetraacetic acid (EDTA) immobilized on silica particles (EDTA-Si, see Figure 2-5b) to a concentrated solution of crude PLimC. The heterogeneous EDTA-Si particles are simply filtered off from the polymer solution after the successful complexation of Zn(II) (complete removal of EDTA is compulsory, since carboxylic acid groups also destabilize the melt of PLimC). The chain ends, on the other hand, are readily capped with anhydrides, such as acetic anhydride (see Figure 2-5c), which esterify the hydroxy groups in moisture-free environment (anhydride most conveniently added as a quenching agent to the solution of polymerization with the metal catalyst still attached to the chain end). Both, the residual catalyst and the terminal hydroxy groups in the polymer enable hydrolytic cleavage of the backbone at elevated temperature. The concerted treatment with EDTA-Si and an anhydride after polymerization yield a pure PLimC with a $T_{5\%}$ of 240 °C. The by 35 °C improved thermal stability of the melt contributes significantly to a facilitated processing of the thermoplastic.

To date, no further stabilization was achieved, since many pathways exist that involve abstraction of more or less acidic protons from the backbone of PLimC. This abstraction is accompanied by the eventual release of CO_2 as a major driving force.
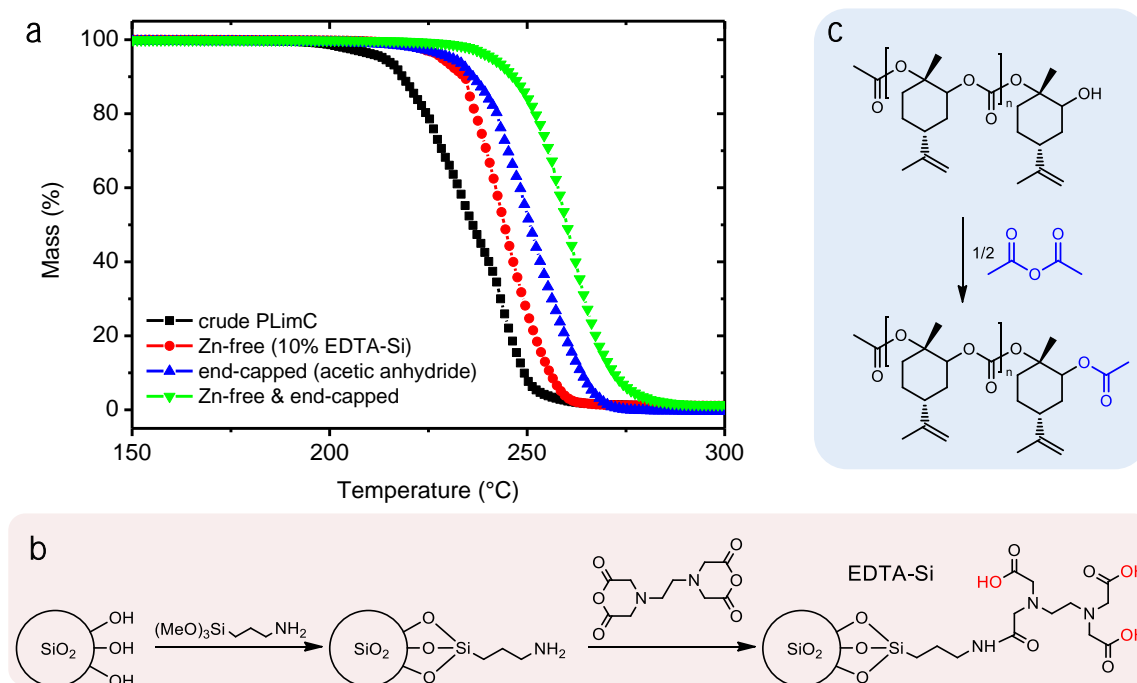
Figure 2-5 | Thermal stabilization of PLimC. (a) Thermogravimetric analysis of PLimC measured at 10 K min^{-1} in N_2 atmosphere. Crude PLimC decomposes quickly at temperatures well below 200 °C due to residual catalyst (Zn(II)) traces and hydroxy groups at the chain ends of the polymer, whereas Zn removal and end-capping can significantly improve stability of the melt of PLimC. (b) The scheme illustrates the synthesis of EDTA-Si that is employed as heterogeneous Zn(II) removal agent in the purification of PLimC. EDTA-Si is added to a concentrated solution of PLimC and removed by simple filtration after chelating of any residual metal catalyst. This route allows a significant reduction of organic solvents involved in the purification of PLimC, since no repetitive precipitation from diluted polymer solutions is necessary (extremely important on large-scale production of polymer). (c) The second detrimental effect concerning thermal stability arises from terminal hydroxy groups at the chain ends of PLimC that increase hydrolytic activity of the melt at elevated temperatures. The scheme shows the exemplary end-capping of PLimC chains with acetic anhydride that is readily accomplished in a moisture free environment.

An initial aim of the synthesis of PLimC was to provide a bio-based alternative to the bisphenol A and phosgene derived BPA-PC. To substitute these toxic monomers with the main component of orange peel, that is, a by-product of the orange industry, and the greenhouse gas CO_2 is an engrossing motivation in its own right. But to provide a viable alternative to the engineering thermoplastic BPA-PC was the real challenge. In terms of mechanical, thermal and optical properties, PLimC is a surprisingly strong competitor, as it has a lower density (light weight construction), similar tensile performance and a glass transition (130 °C) only 18 °C below that of its aromatic counterpart (see Table 2-1). Additionally, the optical characteristics of PLimC are superior to those of BPA-PC,

exhibiting higher overall transmission of visible light, a similar haze and higher clarity. This profile of properties suggests the utilization of PLimC in optical applications where mechanical robustness is necessary.

Table 2-1 | Comparison of bulk properties of PLimC and BPA-PC.

property	PLimC	BPA-PC
general		
density (g/cm^3)	1.08	1.22
carbonate content (%)	99+	100
contact angle to water (°)	93	82
M_n (kDa)	53.4	28.5
$Đ$	1.10	1.77
mechanical		
Young's modulus (GPa)[a]	0.95	2.35
tensile strength (MPa)[a]	55	65
elongation at break (%)[a]	15	50
pencil hardness[b]	B	8B
thermal[c]		
T_g (°C)	130	148
T_m (°C)	-	-
$T_{5\%}$ (°C)	240	490
optical[d]		
transmission (%)	94	89
haze (%)	0.75	0.8
clarity (%)	99.8	99.5

[a] measured at 5 mm min^{-1} strain rate, [b] test conducted according to ISO 15184 with BYK Pencil Hardness Tester and Derwent Graphic pencils, [c] measured at 10 K min^{-1} in N_2 atmosphere, [d] thickness of sample 0.24 mm.

2.3 Applications of PLimC

(to be submitted)

It was very exciting when we found that PLimC is not only permeable to light but also very permeable to gases like CO_2 (68 barrer) and O_2 (12 barrer). As a matter of fact, it is one order of magnitude more permeable to those small molecules than BPA-PC. As PLimC also exhibits a distinct selectivity for CO_2 over N_2 the material is applicable to the separation of CO_2 in carbon capture processes. Furthermore, with its unique combination mechanical, optical and permeation properties, PLimC actually constitutes a new class of polymers that

we have termed 'breathing glass'. Both applications of PLimC as breathing glass and as membrane are discussed in this chapter, starting here with the former.

The high transport of CO_2 through the dense matrix of PLimC is accompanied by a high selectivity for the gas over N_2 (selectivity of 22). This selectivity gives the polymer the characteristics to function as a membrane for the separation of fuel and flue gases (the relevant gas pair is CO_2/N_2). Such a membrane is illustrated in Figure 2-6a, where the feed side is a mixture of both gases, while the permeate side is CO_2-enriched. The temperature-dependent permeabilities of PLimC for the gases H_2, CO_2, N_2 and CH_4 are shown in Figure 2-6b and the fast transport of the gases is ascribed to the large interconnected cavities in PLimC (see blue 'CONNOLLY' surface in the simulation of an amorphous cell of PLimC in Figure 2-6c). We used PALS measurement to determine the cavity size experimentally and found a mean cavity radius of 3.3 Å (Figure 2-6d). These pores are significantly larger than those of BPA-PC or PMMA with 2.9 Å and 2.4 Å, respectively, and thus explain the higher diffusion through the matrix of PLimC.
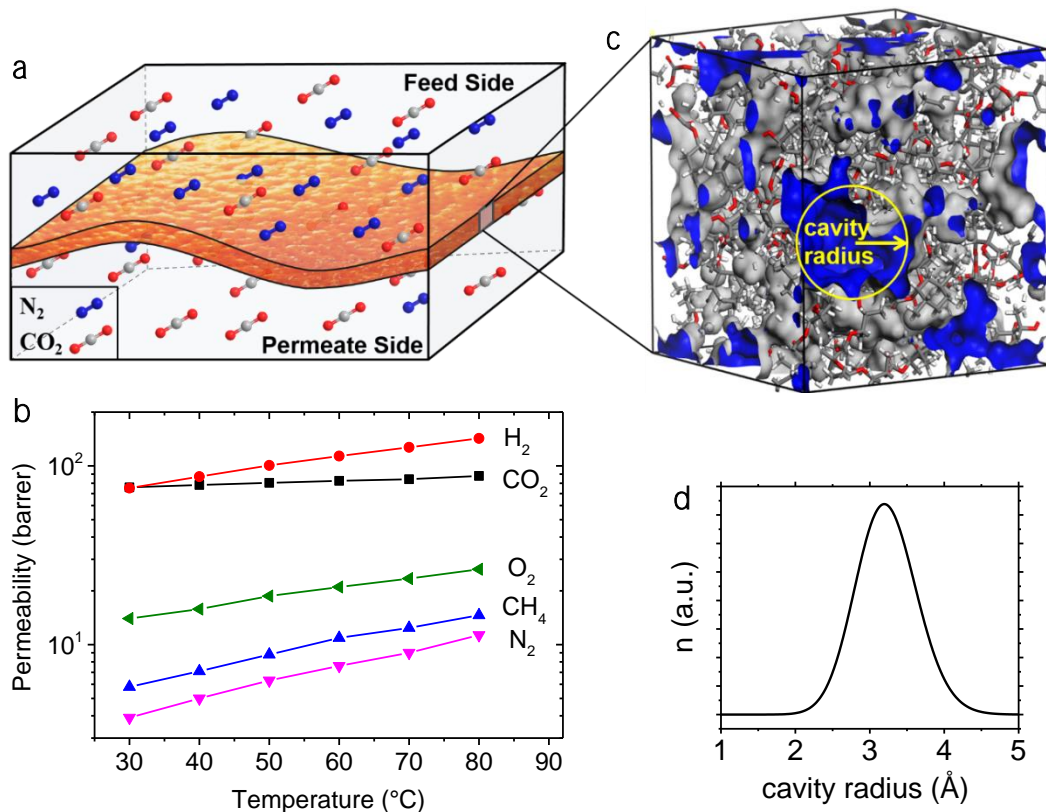
Figure 2-6 | PLimC as membrane for gas separation. (a) Illustration of PLimC as membrane for the separation of CO_2/N_2. (b) Molecular dynamics simulation of the amorphous unit cell of PLimC and the CONNOLLY surface (blue) to illustrate the loose packing of polymer chains, resulting in cavities that are responsible for the high permeability for small molecules. (c) Temperature-dependent permeabilities of PLimC for H_2, CO_2, O_2, CH_4 and N_2. (d) The cavity size distribution of an as-cast film of PLimC determined by PALS measurements.

We compared the commercialized polymers for gas separation applications, such as BPA-PC, CAc, PI, PEI, PSU and PPE with PLimC in a ROBESON plot for the gas pair CO_2/N_2 (Figure 2-7) and found the aliphatic polycarbonate to be superior in terms of permeability and selectivity. Although state-of-the-art polymeric membrane materials like PIM-1 and PTMSP (for chemical structures see Figure 2-7a) are even more permeable than PLimC by two or even three order of magnitude, respectively, they lack in mechanical robustness, long-term stability and processability. Furthermore, the building blocks of PLimC, that is limonene and CO_2, are far less expensive than those of most state-of-the-art materials, which give PLimC a competitive edge over them. Another key to success might be the great susceptibility of the aliphatic PC to chemical modifications on the double bond.
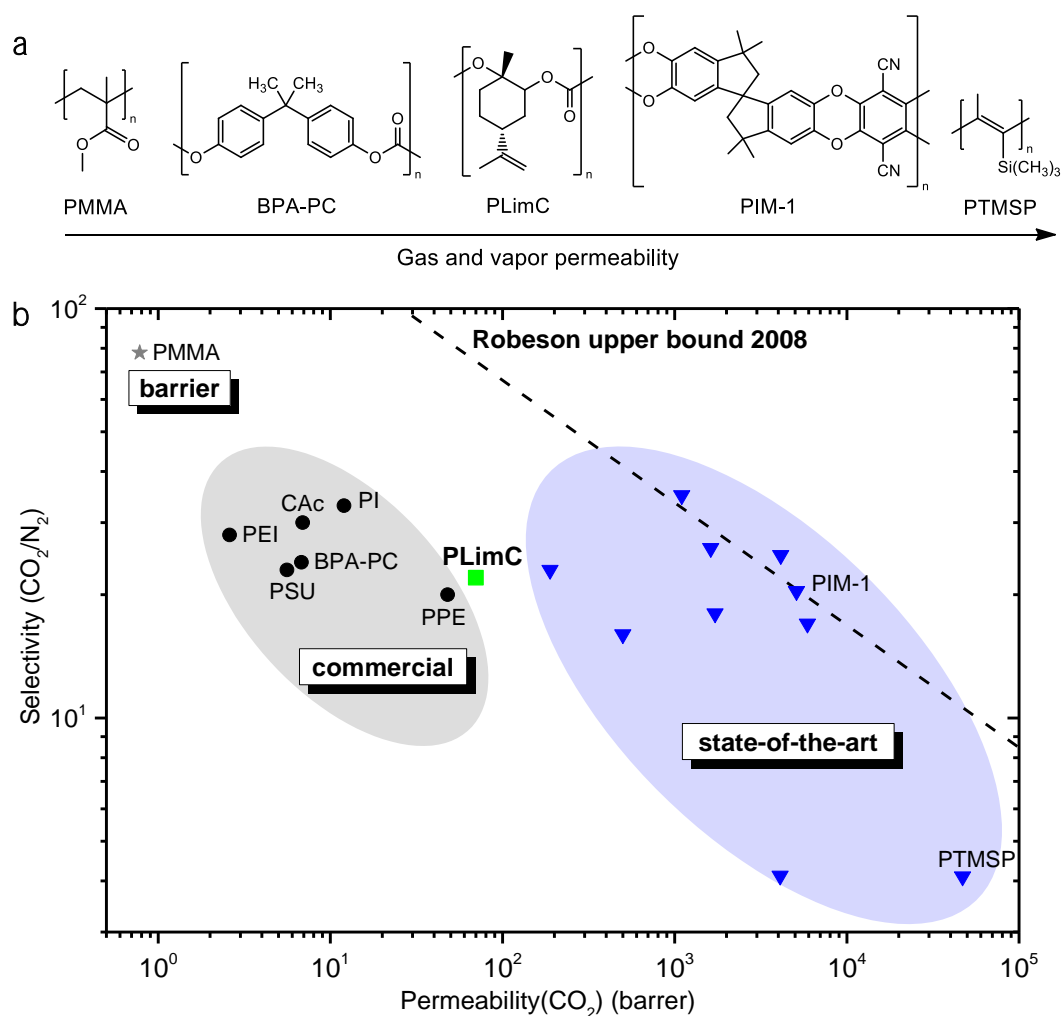
Figure 2-7 | Membrane properties of PLimC. (a) The molecular structures of PMMA, BPA-PC, PLimC, PIM-1 and PTMSP in order of increasing permeability. (b) ROBESON plot for the gas pair CO_2/N_2 with PLimC compared to commercial and state-of-the-art polymeric membrane materials. The commercial polymers include cellulose acetate (CAc), polyimide (PI), polyetherimide (PEI), polysulfone (PSU) and poly(phenylene ether) (PPE).

In contrast to the application as a membrane, an illustration of the use of PLimC as breathing glass in closed greenhouses and passive houses is given in Figure 2-8. The sheets made of PLimC readily transmit sunlight and the small molecules O_2, CO_2 and H_2O, whereas the transport of heat is very limited due to the insulating characteristics of the polymer (PLimC exhibits a low thermal conductivity, which is seven times lower than that of soda-lime glass).
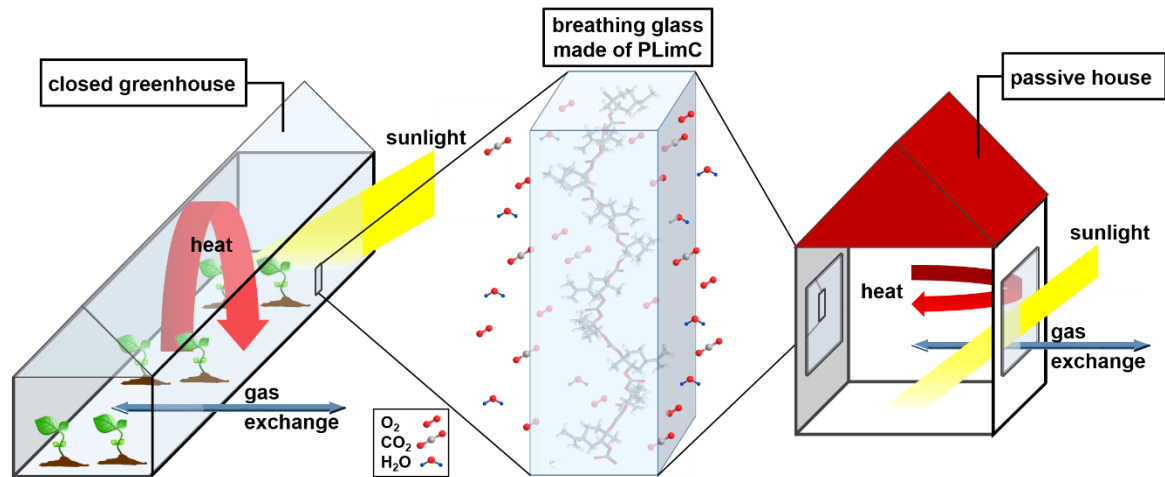
Figure 2-8 | PLimC as breathable glazing material. The glass-like PLimC can be processed into window panes with high permeability of gases like O_2 and CO_2. The breathing window panes are installed in passive houses and greenhouses to supply the interior with fresh air without the need of active ventilation. Due to the thermal insulation properties of the glazing only gas but no heat is exchanged between in- and exterior and thus no energy is lost in the ventilation process.

The concepts of both, the passive house and the greenhouse, are based on extensive insulation to minimize heat losses through the cladding. As the constructions are more or less gas-tight, the interior has continuously to be supplied with fresh air (in most cases colder than the exchanged stale air) from ventilations systems that additionally have to be equipped with heat-exchange units to reduce the heat losses due to ventilation. Here, the breathing glass can act as a passive ventilation system while being a good thermal insulator and thus reducing energy consumption due to heat losses and the installation and operation of sophisticated ventilation systems. For the assessment of feasibility of such a breathing glass, we focused on the exchange of CO_2 between the in- and exterior of the buildings as it is the limiting factor in both constructions. In the case of the passive house the exhaled air from the resident leads to an accumulation of CO_2 in a toxic concentration that is reached sooner than the depletion of O_2 is going to affect the well-being of the resident. On the other hand, the plants in the greenhouse need a lot of CO_2 for the photosynthesis and as the concentration of CO_2 in the atmosphere is only 400 ppm (or 0.04%) the driving force to

transport the gas through the breathing glass is very limited (the transport, that is, the permeance of a gas through a membrane is dependent on the difference of partial pressure on both sides and the partial pressure is directly dependent on the concentration of a gas; for CO_2 the partial pressure in the atmosphere is only 0.04 kPa and thus the difference of pressure can only be smaller than this value when the gas is consumed).

An estimation of the counterbalancing of the CO_2 level in both cases is presented in Table 2-2. Taking the area and thickness of the glazing and the pressure difference into consideration, the values of respiration rate (resident or plants, respectively) and the permeance of the glazing are to be matched as far as possible to compensate the levels of CO_2. For the greenhouse gas the calculated counterbalancing is only achieved to 0.1% of the necessary value (partial pressure is too low), but for the passive house a compensation of 2.5% is achieved with PLimC as breathing glass. Of course, this value has to be improved in order to replace the conventional ventilation system but the concept of breathing glasses has proven successful by this value, as a partial compensation of stale air can already save substantial amounts of energy. Further improvements of the material's breathability and engineering are expected to drive the value of counterbalancing of CO_2-levels to 100% or even beyond.

Table 2-2 | Estimation of CO_2 counterbalancing in PLimC glazed greenhouses and passive houses.

	passive house	closed greenhouse
area of glazing (m^2)	20	500
thickness of glazing (mm)	1.0	0.1
partial pressure difference CO_2 (kPa)	5.0[a]	0.02
respiration type	exhalation of resident	uptake by plants (200 m^2)
respiration rate[b] ($g_{[CO2]}$ h^{-1})	41	400
permeance of PLimC glass[c] ($g_{[CO2]}$ h^{-1})	1.0	0.4
ratio of counterbalancing CO_2 levels (%)	2.5	0.1

[a]the partial pressure of 5.0 kPa corresponds to 5% CO_2 in the atmosphere, which is already a value where a headache can occur when exposed to for a longer time [b]values taken from reference [303], [c]calculated from P(CO_2) of PLimC of 68 barrer.

Their breathability is the new and exciting aspect of glazing materials, but to qualify as such, also the conventional requirements of this class of materials have to be met in order to be regarded as a true competitor. In Figure 2-9 the performance in typical mechanical, optical, thermal and the innovative breathing properties of the predominant organic (BPA-PC and PMMA) and inorganic (soda-lime glass, the standard material for window panes, bottles, etc.) glazing materials are compared with PLimC. The radar chart illustrates very well that

the profile of PLimC is very balanced and that it can keep up or – in some instances – can even outperform the other materials. Besides the unmatched permeability (BPA-PC is one, PMMA is two orders of magnitude less permeable and soda-lime glass a real barrier to gases) of PLimC, the polymer can also convince with outstanding mechanical strength, as it is almost as impact resistant as – the number one among the commercial plastics – BPA-PC and nearly as scratch-resistant as the hard PMMA. Among the four, PLimC exhibits the best insulating efficiency (thermal conductivity) and it is the lightest material (specific gravity), which is of importance wherever weight is a relevant criterion. Such a relevance is given for the construction of windows, which are in turn relying on a high optical clarity that is equally high for PMMA and PLimC. In conclusion, PLimC is a viable choice as glazing material in the construction sector but in combination with its high gas-permeability it is the first breathing glass with a huge potential to reduce energy consumption in well-insulated buildings. A further chemical modification could eventually yield a breathing glass that can replace ventilation systems completely and thus save a substantial amount of energy.
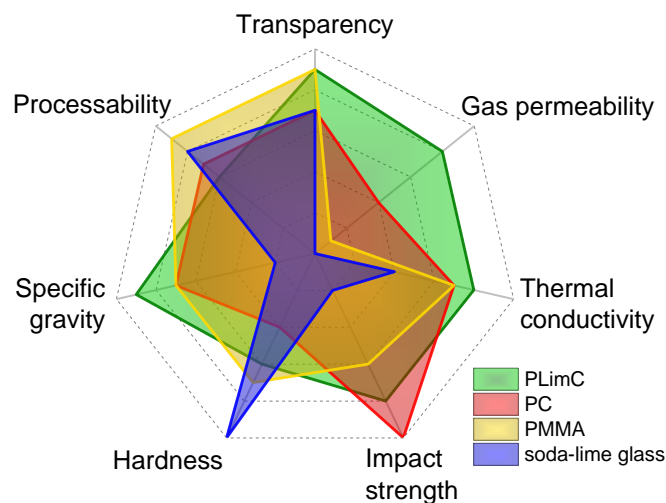
Figure 2-9 | **Performance of typical glazing materials.** The relative performance of PLimC compared with the popular glazing materials BPA-PC, PMMA and soda-lime glass in various properties that are relevant for the application as glazing material.

The right choice of attachment can enable an even higher permeation through PLimC, giving it the decisive advantage over other materials with respect to both the membrane and the breathing glass applications. Although the molecules to improve the permeation properties are yet to be found, we have successfully exploited the versatility of PLimC in many other instances and discuss the possibilities in the following chapter.

2.4 Modifications of PLimC

As exciting as the pure PLimC is, due to its inherent unsaturation, the aliphatic PC is susceptible to chemical addition reactions that can induce dramatic changes to the properties of the original PLimC. We attached a number of molecules to the backbone, by exploiting various chemical routes. The versatility of PLimC as a platform for new materials is illustrated in Figure 2-10. The alteration of mechanical and thermal properties of PLimC by chemical modifications is illustrated in Figure 2-11. The mechanics of the high-T_g (130 °C) thermoplastic PLimC – being similar to common engineering thermoplastics like BPA-PC and PET – can be changed on the order of magnitudes by quantitative attachment of the bio-based thiol-functionalized ester butyl-3-mercaptopropionate (B3MP) to the double bond of PLimC (Figure 2-11a). The produced material PLimC-B3MP is actually soft at room temperature, as a result of the by 120 °C depressed T_g. The very different behavior of polymeric chains above T_g lead to mechanical behavior of PLimC-B3MP that is typical for rubbers.
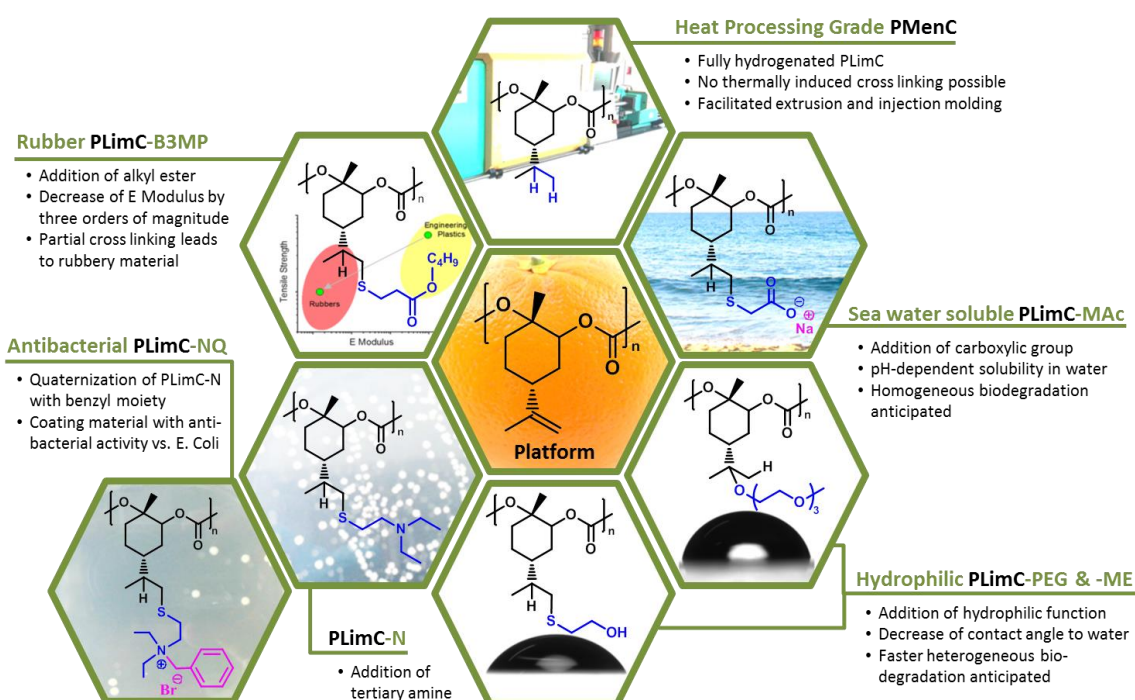
Figure 2-10 | Modifications of PLimC. The high-T_g thermoplastic PLimC is readily transformed into rubbery (PLimC-B3MP), antibacterial (PLimC-NQ), hydrophilic (PLimC-N, PLimC-ME, PLimC-PEG), pH-responsive/sea water-soluble (PLimC-MAc) or heat-processable (PMenC) materials by simple chemical manipulations on the double bond. The chemical routes imply thiol-ene click-chemistry, acid-catalyzed electrophilic addition (both polymer-analogous) or metal-catalyzed hydrogenation of the precursor limonene, respectively.

Hence, we have investigated the tensile properties of PLimC rubber (see ASHBY plot with tensile strength vs. YOUNG's moduli for various engineering thermoplastic and rubbers in Figure 2-11b). We found a YOUNG's modulus similar to natural rubber or, in numbers, a modulus of 1 MPa and thus a decrease by three orders of magnitude compared to the original PLimC. The softness compromised tensile strength only by a factor of 5 (10 MPa for PLimC-B3MP), while the ductility was increased from 15% for unmodified PLimC to 420% of its rubber. Such a tremendous change in mechanics suggests applications of the rubber PLimC-B3MP in completely new areas where PLimC would not be viable. Not a mechanical but rather a processability (thermal) upgrade was achieved by complete saturation of PLimC (Figure 2-11c).
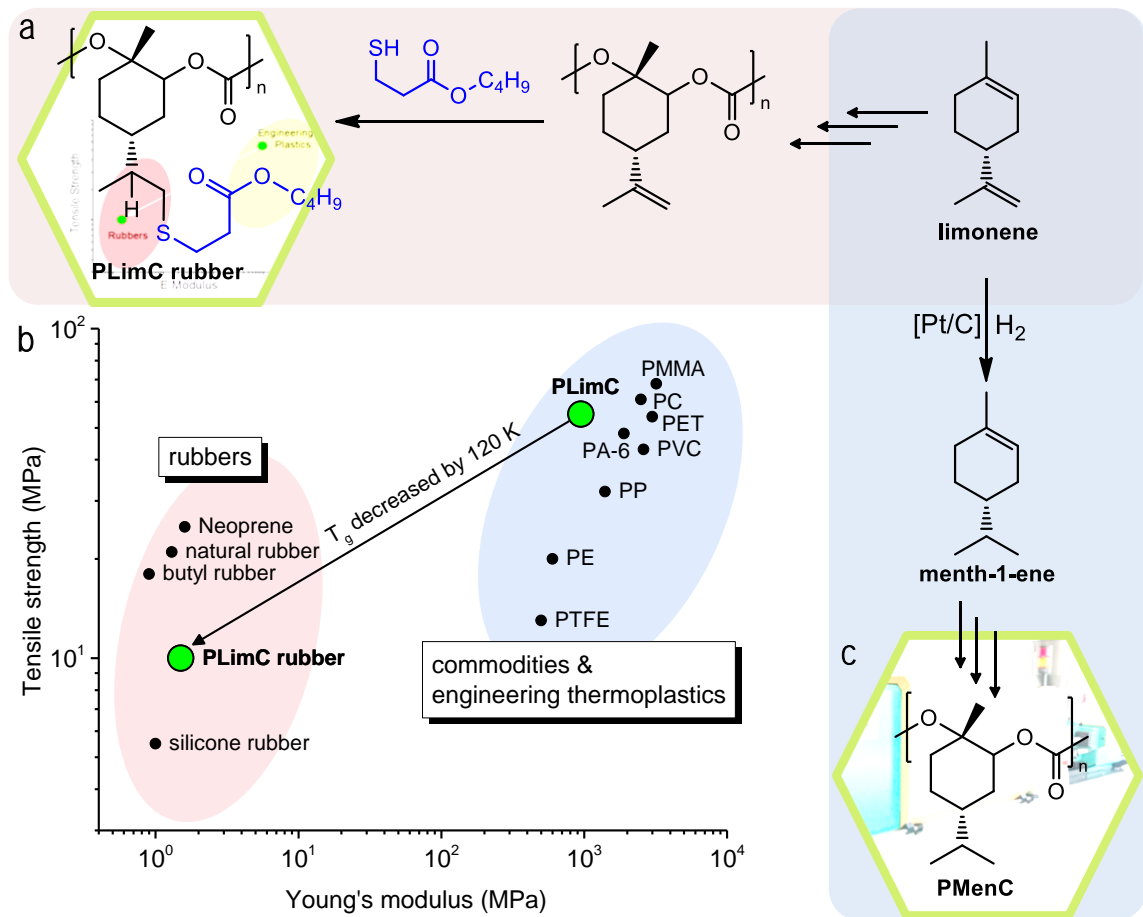
Figure 2-11 | Modification of mechanical and thermal properties of PLimC. (a) Attachment of a short-chain mercapto-ester (B3MP) via polymer-analogous thiol-ene reaction. (b) The added ester induces a dramatic change in mechanical properties, turning the high-T_g PLimC into a rubber (PLimC-B3MP) with a decrease of T_g of 120 K. (c) The saturation of PLimC is achieved by regioselective hydrogenation of the precursor (R)-limonene with molecular hydrogen in the presence of Pt. The partially hydrogenated pre-monomer menth-1-ene is stereoselectively epoxidized to give the *trans* isomer (same route as in Figure 2-2 involving the bromohydrin as transition state) that is subsequently copolymerized with CO_2 to give PMenC.

The hydrogenation of the double bond of every repeating unit renders the resulting poly(menthene carbonate) (PMenC) unreactive, that is, not cross-linkable, when it is heat-processed in extrusion or injection molding processes. In contrast to the production of the PLimC rubber, the manipulation is performed on the precursor *(R)*-limonene by regioselective hydrogenation of the *exo* iso-propylene moiety with H_2 in the presence the heterogeneous catalyst Pt on charcoal. The singly unsaturated menth-1-ene is epoxidized with NBS (compare with *trans*-LO production shown in Figure 2-2) to give the *trans* isomer of menthene oxide as major product. The detour via the bromohydrin is necessary as the catalyst [(bdi)Zn(μ-OAc)] is again selective for the coupling of the *trans* isomer of the saturated monomer with CO_2. The properties of the amorphous PMenC are very similar to PLimC, both exhibiting a glass transition at 130 °C. But in contrast to PLimC, the saturated PMenC cannot crosslink or react with radicals like O_2 at elevated temperatures. Thus, for the latter a better processability, i.e. extrusion and injection molding, and a prolonged UV stability are achieved.

A variety of functional groups was attached to the platform PLimC to give the material a completely new set of active and passive properties (Figure 2-12). One common aim of the functionalizations of the unsaturated PC with mercaptoacetic acid (MAc), mercaptoethanol (ME) and poly(ethylene glycol) (PEG) (Figure 2-12a-c) is the hydrophilization and a decrease of T_g with an increasing degree of functionalization (DF). For carrying oxygen and not just carbon in the backbone, PLimC was expected to degrade in biological environments, that is, in the presence of enzymes like lipase or esterase or in highly active industrial compost. The rather hydrophobic (contact angle to water of 93°) and rigid polymer was not attacked by any of the species it was exposed to though. In order to facilitate enzymatic attack and cleavage of the backbone into smaller chains and eventually small molecules, the interaction between the polymer and the aqueous phase has to be increased by adding polar groups and eased segmental motion. This aim was achieved with the acid (MAc), alcohol (ME) and ether (PEG) functions and the dependences of the contact angle to water and the T_g on the degree of functionalization (DF) are shown in Figure 2-12d. For the addition of PEG to the double bond of PLimC a different chemical route, involving the acid-catalyzed electrophilic addition of the free hydroxyl group of the PEG-derivative, was utilized. The advantage of this synthetic route is the evasion of – often toxic – thiol groups on the functional molecule. However, the necessary acid in the reaction mixture degrades the PC-backbone rather quickly and thus only low DFs were

accomplished with PEG (< 20%) within the limited time of reaction. The acid MAc, on the other hand, can be attached quantitatively to PLimC using the radical pathway and this function renders the resulting material not only hydrophilic but also pH-responsive. This solubility in basic media (pH > 7) adds a very interesting characteristic to PLimC, as it is in this case sea water-soluble and thus much more prone to degradation of the backbone once it reaches the ocean.
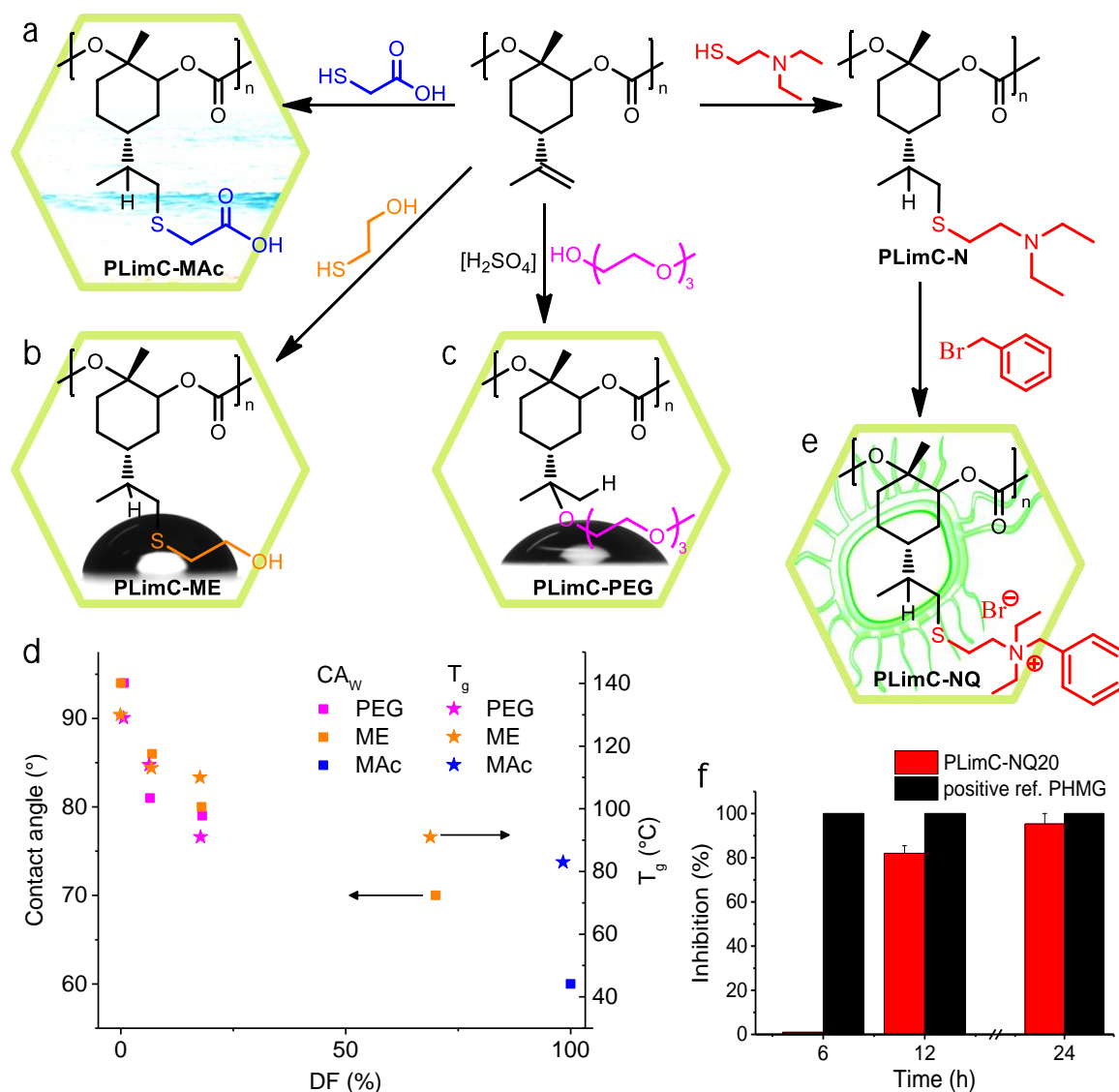
Figure 2-12 | Functionalization of PLimC. (a) The addition of mercaptoacetic acid (MAc) to PLimC yields a pH-responsive PLimC-MAc that is soluble in basic media such as sea water. (b) The thiol-ene reaction with mercaptoethanol (ME) or (c) the acid-catalyzed electrophilic addition of poly(ethylene glycol) (PEG) give hydrophilic PLimC-ME and PLimC-PEG, respectively, both exhibiting decreased T_gs. (d) The dependency of the contact angle to water and the T_g of PLimC-MAc/ME/PEG on the DF. (e) The click reaction with a thiol-carrying tertiary amine and the subsequent quaternization with an aryl moiety add antibacterial activity to PLimC-NQ. (f) The time-dependent bacterial inhibition performances of PLimC-NQ20 (20% quaternized amine) and highly active PHMG as positive reference material relative to pure PLimC in a shaking flask test.

This property could help to reduce the waste accumulation but still guarantee reasonable stability during use wherever basic media are avoided. Such an active function is also added by the introduction of a quaternized amine into the backbone of PLimC (Figure 2-12e). In this case the function is an antibacterial activity that has been successfully proven against the gram-negative bacteria *Escherichia coli* (*E. coli*). The two-step synthetic route starts again with a click-reaction to attach a tertiary amine to the double bond (PLimC-N) that is subsequently quaternized with an aryl moiety (PLimC-NQ). The DF was held below 50% to keep the material insoluble in water, since an application as antibacterial transparent coating is targeted for PLimC-NQ. The activity for a sample with 20% quaternized amine in the backbone was tested in a shaking flask test where the film is contacted to a bacteria suspension. PLimC-NQ20 shows inhibition of growth of bacteria after 12 h while the positive reference poly(hexamethylene guanidine) (PHMG) is already active after 6 h and PLimC shows no inhibition at all (Figure 2-12f). It is not surprising that the condensed PLimC-NQ (film does not disintegrate in contact with bacteria suspension) is less active than the dissolved PHMG but is actually a great property that PLimC-NQ20 exhibits antibacterial activity *despite* of the condensed state. Further improvement by the variation of DF, type of amine and type of quaternization moiety is still anticipated.

The six new materials derived from the platform PLimC are only a small excerpt of the possibilities of modifications and still illustrate the versatility of the bio-based polymer. I would expect the PLimC family to grow rapidly in the forthcoming years.

2.5 Individual contribution to joint publications

The results and manuscripts of this thesis are the collaborative outcome of the efforts of several scientists. In this section the individual contributions of all authors are specified

Chapter 3 – Synthesis & properties of PLimC

The manuscript of this chapter was published in *Green Chemistry* **2016**, 18, 760 under the title:

Bio-based polycarbonate from limonene oxide and CO_2 with high molecular weight, excellent thermal resistance, hardness and transparency

by <u>Oliver Hauenstein</u>, Marina Reiter, Seema Agarwal, Bernhard Rieger and Andreas Greiner

I designed and conducted the experiments, characterized the materials and wrote the manuscript except for the part of the kinetic investigations of the copolymerization.

Marina Reiter planned and carried out the kinetic investigations of the copolymerization of LO and CO_2 and wrote that part of the manuscript.

Seema Agarwal co-supervised the project and corrected the manuscript.

Bernhard Rieger supervised the kinetic investigations of the copolymerization and corrected the manuscript.

Andreas Greiner supervised the project and corrected the manuscript.

Chapter 4 – Applications of PLimC

The manuscript of this chapter is intended to be submitted under the title:

Membranes & breathing glass from bio-based polycarbonate

by <u>Oliver Hauenstein</u>, Mushfequr Rahman, Mohamed Elsayed, Reinhard Krause-Rehberg, Volker Abetz and Andreas Greiner

I designed and coordinated the experiments, characterized the materials and wrote the manuscript.

Mushfequr Rahman planned and carried out the measurements of the permeabilities of the materials and discussed the results.

Mohamed Elsayed carried out the PALS experiments and discussed the results.

Reinhard Krause-Rehberg supervised the PALS experiments and discussed the results.

Volker Abetz supervised the permeation measurements and discussed the results.

Andreas Greiner supervised the project and corrected the manuscript.

Chapter 5 – Modifications of PLimC

The manuscript of this chapter was published as full paper in *Nature Communications* **2016** (DOI: 10.1038/ncomms11862) under the title

Bio-based polycarbonate as synthetic toolbox

by <u>Oliver Hauenstein</u>, Seema Agarwal and Andreas Greiner

I designed and conducted the experiments, characterized the materials and wrote the manuscript except for the part of the kinetic investigations of the copolymerization.

Seema Agarwal co-supervised the project and corrected the manuscript.

Andreas Greiner supervised the project and corrected the manuscript.

3

Synthesis & properties of PLimC

Published under the title:

Bio-based polycarbonate from limonene oxide and CO₂ with high molecular weight, excellent thermal resistance, hardness and transparency

Oliver Hauenstein,[a] Marina Reiter,[b] Seema Agarwal,[a] Bernhard Rieger[b] and Andreas Greiner[a]

[a] Macromolecular Chemistry II, University of Bayreuth, Universitätsstr. 30, 95440 Bayreuth, Germany.

[b] WACKER Chair for Macromolecular Chemistry, TU Munich, Lichtenbergstr 4, 85747 Garching bei München.
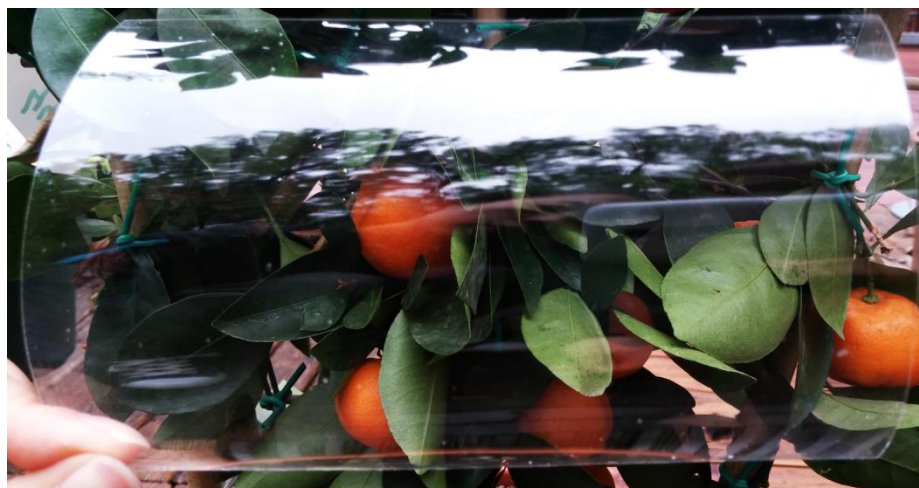
Abstract

Completely bio-based, high molecular weight (>100 kDa) poly(limonene carbonate) (PLimC) with attractive thermal (glass transition temperature, T_g = 130 °C) and optical properties (transmission 94%, haze 0.75%) was prepared by coupling bio-based limonene oxide (LO) and carbon dioxide (CO_2) using a β-diiminate zinc catalyst [(bdi)Zn(OAc)]. The molar mass of the polymer could be controlled by changing the ratio of catalyst and monomer, keeping molar mass dispersities low. The synthesis of the LO with very high content (>85%) of *trans*-isomer and absence of impurities with hydroxyl functionality was also established, which was necessary to obtain a high molar mass of polymer and almost quantitative conversion of epoxide during polymerisation. The upscaled syntheses of both the monomer and the polymer (> 1 kg/batch) were readily realised, suggesting an easy transfer to pilot plant scale. The polymerisation kinetics were studied suggesting a second order dependence on LO concentration, wherefrom a mechanism is proposed with an alternating insertion of LO and CO_2. The effect of chain-ends on the thermal stability of PLimC was studied with a thermal desorption unit coupled with gas chromatography–mass spectrometry (GC–MS) experiments. PLimC with thermal stability as high as 240 °C could be achieved using appropriate end-capping agents. PLimC is characterized by excellent transparency and hardness.

3.1 Introduction

The conventional polycarbonate (PC) made by the condensation of bisphenol-A (BPA) and phosgene is an amorphous polymer with high impact strength, toughness, heat resistance and transparency, which finds applications as medical, automotive, optical and electronic devices.[1] The drawback of BPA-PC is found in the choice of monomers, with phosgene being a highly toxic volatile compound and BPA raising concerns regarding negative health effects due to leaching out of the polymer when in contact with food.[2] Additionally, both monomers are petro-based compounds and, recently, efforts have been made to replace them, at least partially, with bio-based diols, e.g. isosorbide derived from carbohydrate,[3,4] L-tyrosyine[5] or terpene derivatives.[6] An alternative route to the synthesis of PCs is the reaction of epoxides with CO_2.[7] This route avoids the use of poisonous phosgene by replacement with CO_2, which is the most abundant greenhouse gas, far less hazardous and inherently bio-based.[8] Inoue *et al.* published pioneering work in 1969 on the synthesis of aliphatic polycarbonates by coupling CO_2 and epoxides with a zinc catalyst.[9,10] Since then, a lot of research has been directed towards the copolymerization of CO_2 and the commodity chemical propylene oxide (PO) to yield poly(propylene carbonate), which is a low T_g (~40 °C) amorphous thermoplastic that is produced on an industrial scale.[11–13] The softening temperature of this material obviously limits the range of applications, thus, the use of bulkier epoxides resulting in higher dimensional stability at elevated temperature is desirable. Cyclohexene oxide is such an example for the coupling with CO_2 that gives a PC with a T_g at around 120 °C, but, similar to PO, it is a petro-based monomer and its brittle nature results in poor mechanical properties.[14] The PC produced in this way is always partially bio-based and can become fully bio-based depending upon the source of epoxide. In order to produce 100% sustainable PC, the choice of epoxide is crucial and, to the best of our knowledge, only epoxidized fatty acids,[15] 1,4-cyclohexadiene[16,17] and limonene have been investigated.[18] Limonene is an abundant alicyclic terpene, found in the peel of many citrus fruits and is the main component of orange oil, resulting in a capacity of more than 520 000 tons/a (estimated from 70 Mt/a oranges produced) of which 70 kt are extracted each year.[19,20] This available renewable non-food resource is a great choice for sustainable chemistry and the oxidation product LO is used as a monomer for direct cationic polymerisation,[21] as a dioxide for isocyanate-free synthesis of polyurethanes[22] or for copolymerisation with CO_2.[18,23,24] Coates *et al.* discovered an efficient single-site β-diiminate

(bdi) zinc catalyst for copolymerisation of CO_2 and LO to produce poly(limonene carbonate) with promising T_g (110 °C).[18] The molar mass reported for the polymer was limited to 25 kDa and less material characterisation was reported. The polymerisation is stereoselective, incorporating only *trans*-LO in the polymer. Therefore, the commercial mixture of LO with an approximate content of at least 45% of the *cis* stereoisomer is rather uneconomical for this reaction because there is a huge amount of unreacted high boiling epoxide in the reaction mixture that has to be extracted, not to mention the waste of valuable bio resources. Later, the use of an Al(III) catalyst has proven to incorporate both isomers (with preference for *trans*-LO) into the polymer chain, but molar masses were still less than 11 kDa and monomer conversion was limited to <75%.[24] The present work provides high molar mass (>100 kDa) PLimC in almost quantitative monomer conversion (>90%) for the first time, using a bdi-zinc catalyst with very attractive material properties that might challenge the predominance of BPA-PC by offering a bio-based, non-food, high-T_g alternative. The use of LO with a very high content (>95%) of *trans*-isomer and the absence of impurities with hydroxyl functionality in the monomer were critical points for obtaining high molar mass and almost quantitative conversion of monomer during polymerisation. Both the monomer and polymer synthesis were readily scaled-up to ~1.2 kg per batch. An in-depth study on the kinetics of polymerisation was performed to elucidate the mechanism of the alternating insertion of LO and CO_2.

3.2 Results and discussion

Synthesis of limonene oxide

Coates *et al.*[18] found in 2004 that the copolymerisation of LO and CO_2 with [(bdi)Zn(OAc)] is highly stereoselective with only the *trans* isomer being incorporated into the polymer. It would be desirable to start with LO containing high amounts of *trans* isomer for the reaction with CO_2 to create an efficient reaction in terms of yield. Moreover, the commercial monomer contains large amounts of impurities, including hydroxyl functionalised molecules with high boiling points (170 – 200 °C), as identified by GC-MS (Fig. 3-1a). The hydroxyl acts as a chain transfer agent (CTA),[25] even in very small amounts in the metal catalysed polymerisation of CO_2 and LO, and provides only low molar mass polymers of around 25 kg/mol.[18] In order to overcome these two major problems during copolymerisation, the monomer with a majority of *trans* isomer was synthesised and

hydroxyl groups of impurities are masked in the present work. A slightly modified procedure developed by Gurudutt *et al.* was used for the synthesis of LO to give about 83% of the *trans* isomer (Scheme 3-1).[26] The monomer contained only 7% *cis* isomer and 10% other impurities coming from starting material and side reactions during the formation of bromohydrin (*exo*-double bond was also or exclusively brominated, respectively), as proved by GC (Fig. 3-1c).
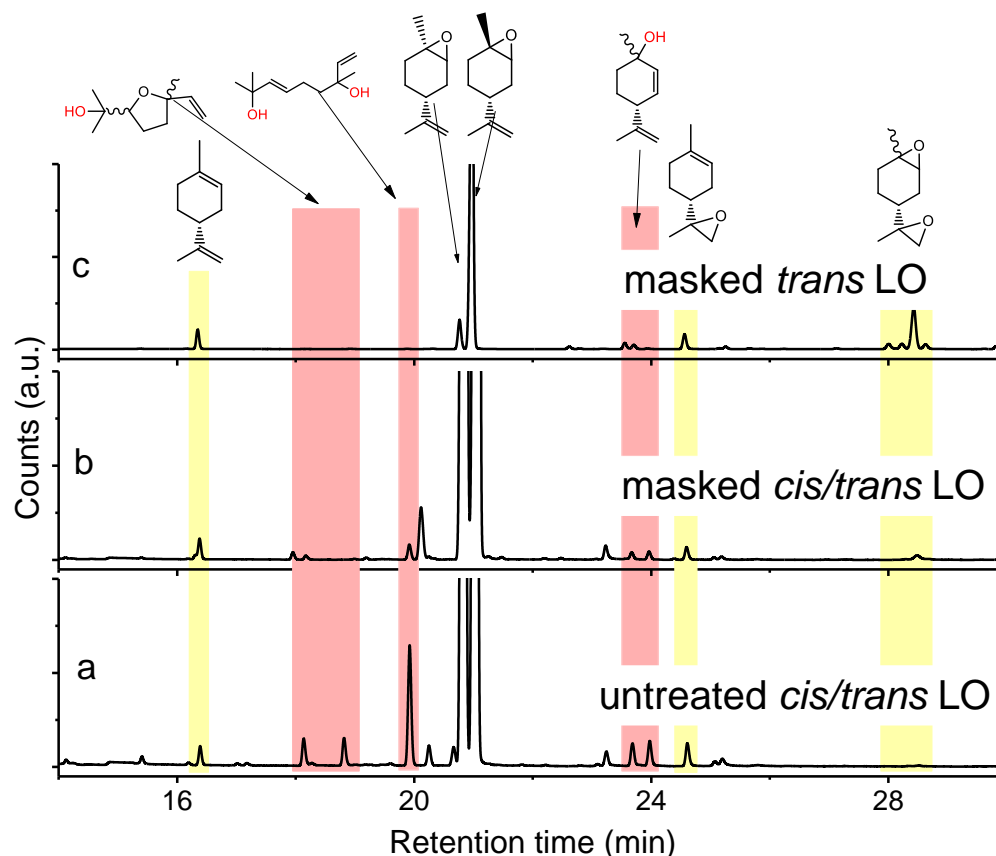
Figure 3-1: Gas chromatograms of a commercial mixture of *cis*- and *trans*-LO (**a**), the same mixture after masking of the hydroxy impurities (**b**) and the masked product from stereoselective synthesis of *trans*-LO (**c**) with structures of identified hydroxyl impurities (by GC-MS).

The synthetic route involves the *endo*-cyclic bromohydrin (regio- and stereoselective for limonene) in aqueous acetone with *N*-bromosuccinimide (NBS) as the bromine source. This bromohydrin is readily converted to the corresponding epoxide in the presence of aqueous sodium hydroxide. The monomer synthesis was successfully scaled up to 1.3 kg of LO per batch by transferring the reaction into a 10 L double-walled glass reactor with stirrer and thermostat to control the reaction temperature between 0–60 °C (Scheme 3-1). All organic solvents employed in the process were recovered by vacuum distillation containing almost no limonene by-products (high boiling liquids). Thus, the solvents can be easily

recycled in the process without prior purification which gives this synthesis a sustainable character. Both the commercial mixture and the stereoselective synthesized LO in this work contain impurities with hydroxyl groups. Although the latter produces fewer of these CTAs, they are still observable in the gas chromatograms (Fig. 3-1a and c). The impurities were not removable by simple distillation and chromatographic methods in an efficient way. Therefore, all hydroxyls were masked by *O*-methylation. Here the WILLIAMSON ether synthesis has proven to be the most efficient reaction by using sodium hydride (NaH) as a deprotonating agent and methyl iodide (MeI) as an *O*-methylating moiety (Scheme 3-2). A gas chromatogram of the commercial LO mixture after such a treatment is shown in Fig 3-1b, where the signals assigned to the hydroxyl impurities have disappeared completely after the masking reaction (or partially depending on reaction time and steric demand of the molecule) Other masking reactions, such as silylation with trimethylsilyl chloride and catalytic amounts of Mg, gave some side reactions with the oxirane, while the use of benzyl bromide instead of MeI slowed down the ether synthesis significantly, i.e. seems to be too hindered to react with the bulky molecules carrying hydroxy groups shown in Fig. 3-1.
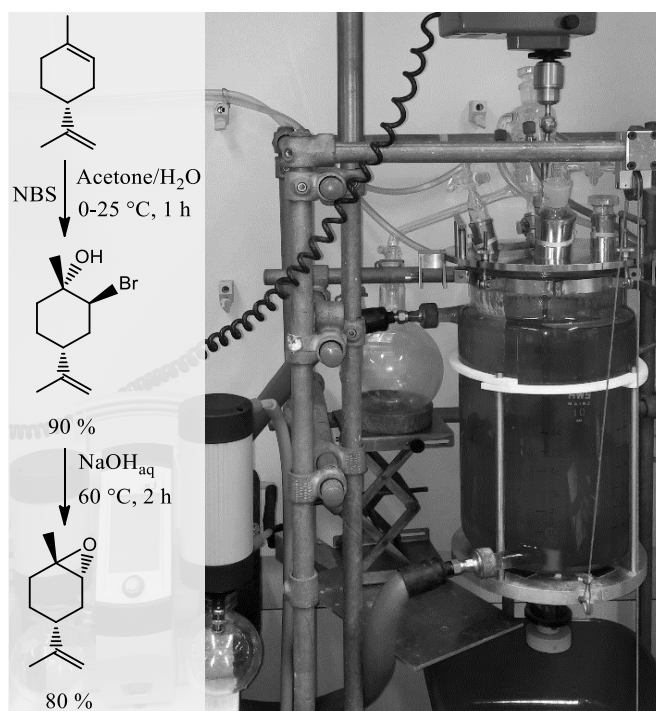
Scheme 3-1: Stereoselective synthesis of *trans*-LO via the corresponding *trans*-bromohydrin that is subsequently ring-closed by the addition of a base at elevated temperature (left) and 10 L reactor employed for monomer synthesis (right).

Another great advantage of this epoxy non-destructive reaction is the simultaneous use of NaH as a drying agent for the monomer. The methylated mixture was then fractionally distilled to give an LO monomer with approximately 85% *trans* isomer and mainly *cis*-LO as a side product. This treatment might also be applicable to other epoxides (or other aprotic monomers) where hydroxyl impurities are disturbing the polymerization.

Synthesis of poly(limonene carbonate)

An inherent problem during the copolymerisation of LO and CO_2 (see Scheme 3-3, Supplementary Figs 3-1 and 3-2 for NMR spectra) to produce PLimC was the limited molecular weight obtained even with very low catalyst concentrations, dried epoxide (Table 3-1, entries 1 – 3) and high conversions (> 90%). We expected longer chains at lower catalyst concentrations for this supposedly living catalytic system,[27] but only slight changes in the molecular weight could be observed when the ratio monomer/catalyst was increased (see Fig. 3-2, red squares). The highest M_n received with a dried sample (over CaH_2 or NaH) of *trans*-LO was 17.1 kDa (entry 1), while $Đ$ was kept between 1.12 – 1.16 (Fig. 3-2, red circles). The low molecular weight obtained was supposedly due to the presence of impurities with hydroxyl groups in the monomer. After the treatment of the dried epoxide with iodomethane (masking agent, Scheme 3-2), the final copolymer had the expected high molecular weight corresponding to the amount of added catalyst (Table 3-1, entries 4 – 8 and Fig. 3-2, blue squares). In this way, we were able to produce PLimC with molar masses up to 109 kDa, which is, to the best of our knowledge, the highest reported M_n for PLimC while keeping Đ low (1.10 – 1.19, Fig. 3-2, blue circles).
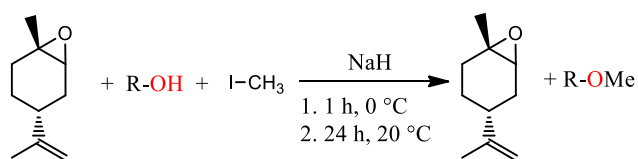
Scheme 3-2: *O*-Methylation of OH-impurities with sodium hydride and methyl iodide by first stirring it for 1 h at 0 °C followed by 24 h at 20 °C.

The linear increase of the molecular weight with a growing LO/catalyst ratio is now in very good agreement with the data calculated (Fig. 3-2, black squares). It is self-explanatory that the molecular weight for almost any application should be as high as possible to maintain a certain mechanical strength. By masking the hydroxyl impurities in the monomer mixture, we are now able to adjust the molecular weight to the value desired, hence, opening the door to a new world of applications for this completely bio-based material (for full

structural characterisation by ^{1}H and ^{13}C NMR, see Supplementary Figs 3-1 and 3-2, respectively, which match well with literature).[18] After gaining full control over the copolymerisation, i.e. the molecular weight of the polymer and stereoselective synthesis of the monomer, the next challenge was to upscale the polymerisation reaction.
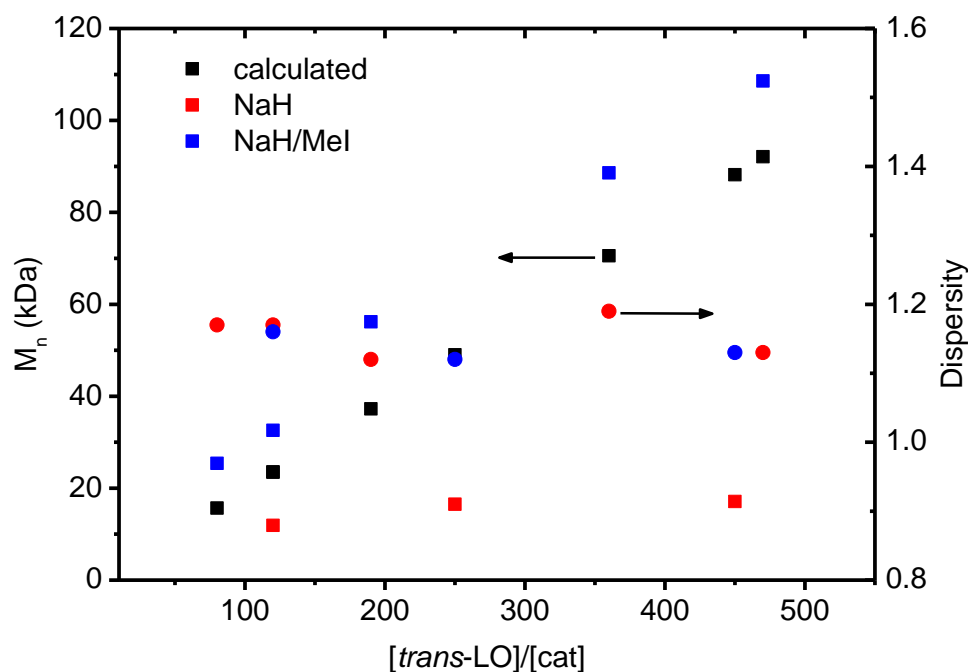
Figure 3-2: Dependency of the molecular weight (determined by CHCl$_3$-GPC) on the amount of catalyst loading after NaH (red squares) and after NaH/MeI- (blue squares) treatment, in comparison with the theoretical values (black squares) for an expected immortal catalytic system. The dispersity of the experimental values are represented by the circles, whereas red corresponds to NaH treatment and blue to the NaH/MeI treatment.

Table 3-1: Copolymerisation of *trans*-LO and CO$_2$ after different treatments of the epoxide with corresponding gel permeation chromatography (GPC) data.

entry	treatment	[*trans*-LO]/[cat]	conversion[a] (%)	$M_{n,calc}$ (kDa)	$M_{n,GPC}$ [b] (kDa)	$Đ$ [b]
1	NaH	450	98	88.2	17.1	1.13
2	NaH	250	98	49.0	16.5	1.12
3	NaH	120	95	23.5	11.9	1.16
4	NaH/MeI	470	85	92.2	108.6	1.13
5	NaH/MeI	360	98	70.6	88.6	1.19
6	NaH/MeI	190	93	37.2	56.2	1.13
7	NaH/MeI	120	93	23.5	32.6	1.15
8	NaH/MeI	80	98	15.7	25.4	1.17

[a] Conversion relative to *trans*-LO in mixture. [b] molecular weights and dispersities were determined by CHCl$_3$ GPC calibrated with polystyrene standards

For this, a monomer/catalyst solution was transferred into an evacuated high-pressure 10 L stainless steel reactor (Scheme 3-3) via cannula, where it is diluted to a 33 vol% solution with toluene via steel tubing connected to a toluene still. After pressurizing the reactor with CO_2, the mixture is stirred for 72 h to produce up to 1.2 kg PLimC, which can be used for further processing.
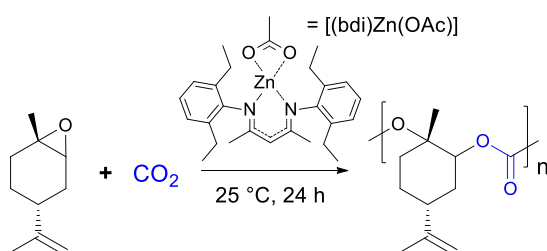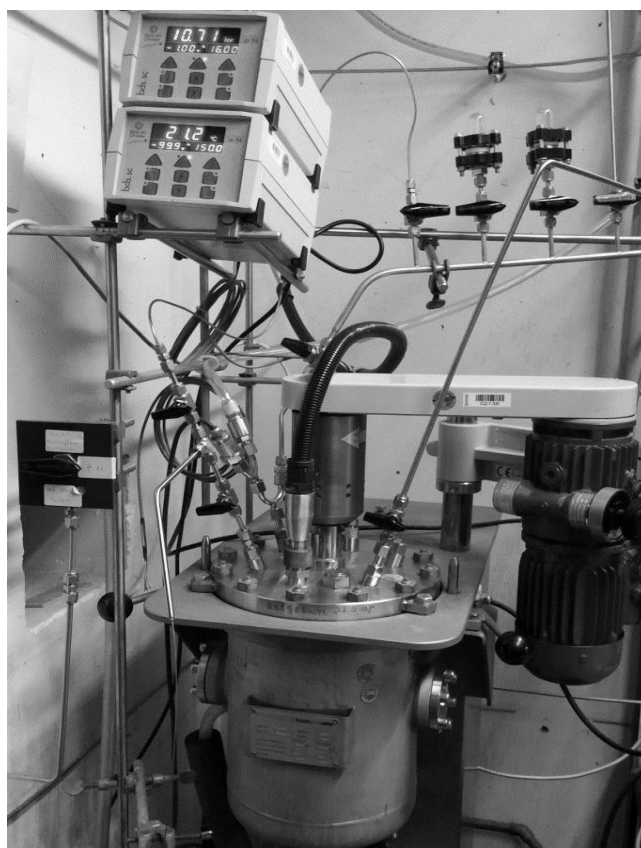
Scheme 3-3: Copolymerisation of *cis/trans*-LO and CO_2 in the presence of a β-diiminate zinc complex and the corresponding 10 L high-pressure reactor used for the production of PLimC on the kilogram scale.

Catalyst removal with immobilised EDTA

The scale up of PLimC raises the question how the amount of organic solvents can be avoided or at least minimised. The work-up of crude PLimC is usually conducted by repeated precipitation of the polymer (dissolved in chloroform or toluene) in methanol to remove residual catalyst. On the kilogram scale, this technique proves very cumbersome

and all but eco-friendly. Therefore, an efficient method of inactivating the Zn(II) metal towards PLimC was developed. One of the most common chelating ligands was used for the improvement of the thermal stability of the product: ethylenediaminetetraacetic acid (EDTA). The decomposition temperature was increased dramatically simply by adding the fully protonated (H_4EDTA) form of the ligand to a crude polymer solution.
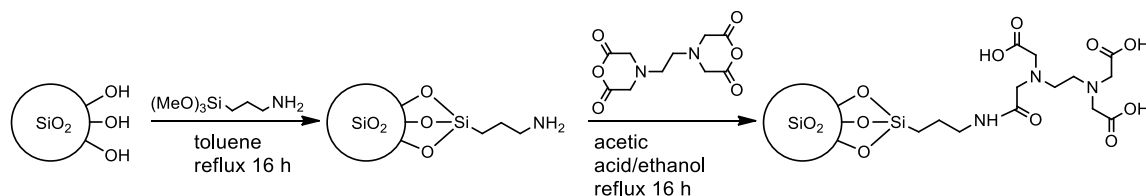
Scheme 3-4: Synthesis of EDTA silica by primary amine functionalisation of silica with 3-aminopropyl-trimethoxysilane and subsequent condensation with EDTA anhydride.

The only drawback of this method comes from the bad solubility of EDTA in $CHCl_3$ or toluene, hence, giving a suspension that is difficult to separate by filtration (the EDTA particles are too small). In order to not only inactivate the metal, but also to separate the inactivated complex (and excess EDTA) from the mixture, the use of immobilised EDTA was a probable solution that also supports the upscaling process, where a packed bed for catalyst removal is mandatory. A method to immobilise EDTA on silica was chosen because of its simplicity and because no swelling is necessary to enter the pores.[28] Firstly, the silica is functionalised with 10% primary amine and a propyl spacer then this amine reacts readily with EDTA anhydride to give an amide-coupled EDTA on silica to give EDTA silica (Scheme 3-4). The reaction was followed by infrared spectroscopy and thermogravimetric analysis (TGA) (see Supplementary Figs 3-4 and 3-5). A very efficient procedure was developed to thermally stabilise PLimC without even precipitating the polymer once. To do this, a freshly prepared reaction mixture in toluene was further diluted with toluene and an end-capping agent acetic anhydride (20 wt% with respect to polymer). Then the solution was subdivided into three vessels for treatment with either no, 1 or 10 wt% EDTA silica, respectively. The mixtures were stirred for 2 h, filtered to remove silica particles and eventually cast into petri dishes to yield films of approximately 200 μm thickness. These films were dried *in vacuo* at 145 °C for 30 min to remove high boiling volatiles above the polymers T_g and then analysed by TGA (Fig. 3-3). The effect of EDTA silica is well illustrated in these thermograms, since obviously without any catalyst removal, the 5% decomposition temperature lies only at 205 °C (end-capping conditions were the same for all three samples).
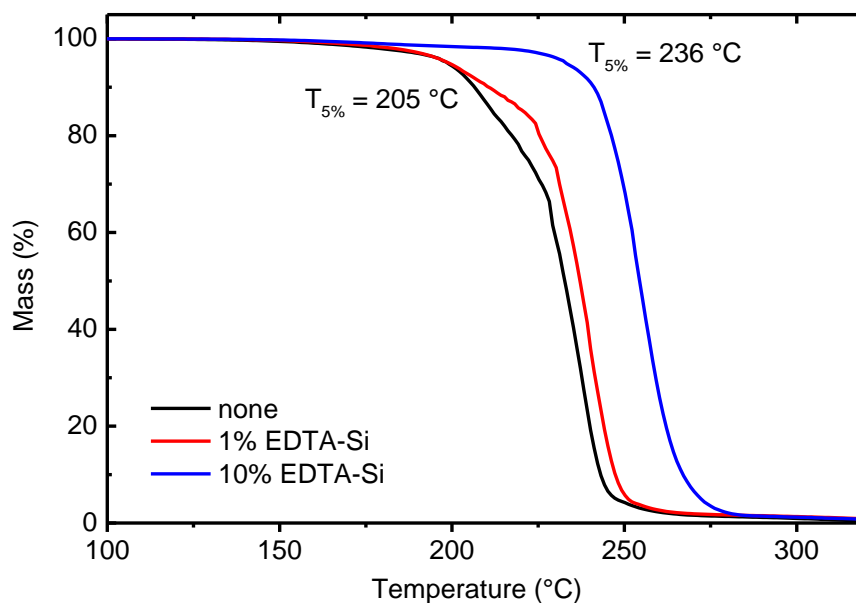
Figure 3-3: TGA of cast films of a crude PLimC solution (in toluene) treated with 20 wt% acetic anhydride and no (black), 1% (red) or 10% (blue) EDTA silica.

There is a slight increase of $T_{5\%}$ with 1% EDTA silica, but still well below 210 °C, whereas with 10% of the immobilised chelating ligand, the thermal stability has risen to 236 °C (close to the all-time maximum for PLimC of 241 °C). Hence, with 10% of that silica, no precipitation of the polymer is needed at all. The reason why 1 wt% is not enough arises simply from the fact that only 10% (or rather less, because immobilisation is hardly quantitative) of the 1% EDTA silica bears EDTA groups, i.e. there is less than 0.2 mol% EDTA in the mixture, which translates to twice as many moles of Zn(II) compared to EDTA in that sample (having used 0.35 mol% of catalyst).

Kinetic studies and mechanistic investigations of the copolymerisation of LO and CO₂

Upscaling the polymer production eventually leads to a re-evaluation of the catalytic system involved. A homogeneous catalyst might be most convenient for gram synthesis, but catalyst removal in up-scaled processes becomes tedious (see section above) and solvent intensive. Therefore, a heterogeneous catalyst is desirable that can remain in the polymer and that, most ideally, works in an aqueous environment to create a completely sustainable synthesis of polycarbonate. For the design of the latter, a deeper understanding of the mechanism of insertion of LO and CO_2 into the Zn-O bond is essential and the kinetic studies presented here can help to elucidate the details of transition states and active species. In order to establish the rate law for the copolymerisation of *trans*-LO and CO_2, the reaction

order in monomer, CO_2 and catalyst were determined. Utilizing *in situ* attenuated total reflectance infrared (ATR IR) spectrometry, the reaction progress was observed by monitoring the increase of the carbonyl vibration stretching-mode of PLimC at 1749 cm^{-1}. All experiments were performed at 20 °C.[18] The kinetic equation can be described by – $d[LO]/dt = k \cdot [CO_2]^a \cdot [LO]^b \cdot [Zn]^c$, where k is the apparent rate constant and $[LO]$, $[CO_2]$ and $[Zn]$ are the concentrations of LO, CO_2 and the catalyst, respectively. Finally, a, b and c are the orders of $[LO]$, $[CO_2]$ and $[Zn]$, respectively. To ascertain the catalyst order, the concentration of $[(bdi)Zn(OAc)]$ was varied from 12.3 – 32.9 mM at otherwise constant reaction conditions at room temperature and 10 bar CO_2 pressure. The reaction rates k_{obs} were determined from the initial slopes. It has to be mentioned that an induction period of about 10 – 20 min was observed for all copolymerisation experiments. The double logarithmic plot of k_{obs} against $[Zn]$ showed that the copolymerisation reaction of LO was nearly first order in catalyst (Supplementary Fig. 3-6). The reaction order in CO_2 was determined to be zero by varying the CO_2 pressure from 5 – 20 bar with an otherwise constant composition of the reaction mixture (Supplementary Fig. 3-7). In order to assign the reaction order in LO, the concentration of LO is normally varied utilizing an additional solvent, such as toluene.[29–31] An experiment of 2.5 mL toluene and 2.5 mL LO at a catalyst loading of 0.4 mol% at 10 bar CO_2 pressure showed an induction period of nearly 1 h. By changing the volume of toluene to 3.0 mL, the induction period was increased to about 2 h. Therefore, rate calculation does not start before the carbonyl band of the polymer begins to rise (Supplementary Fig. 3-8) Experiments with limonene concentrations of 2.44 – 6.10 M were conducted, whereby plotting of $\ln k_{obs}$ against $\ln[LO]$ resulted in an order of two in LO. As the induction process might still have some influence on the linear section of the reaction curve, an additional method for determination of the reaction order for the epoxide was established. Accordingly, an experiment with a catalyst loading of 0.4 mol%, 11 bar CO_2 and 2.5 mL toluene (total volume 5.0 mL) was performed (Supplementary Fig. 3-11a). The concentration of the catalyst and the CO_2 pressure during the entire copolymerisation reaction remained practically unchanged, whereas the concentrations of LO and PLimC were varied. The reaction rate k_{obs} can now be calculated for different epoxide concentrations out of the derivation of the curve measured at different conversions (Supplementary Fig. 3-10, Supplementary Eq. 3-2). The intensity of the carbonyl band of the polymer was correlated to the concentration of the polymer in the mixture by an independent multipoint calibration and, as a consequence, to the concentration of LO, as

shown in Supplementary Table 3-1. Deriving the polynomial copolymerisation curve, the slope of the tangents, directly related to the reaction rate, at 20, 30, 40, 60 and 80% conversion can be calculated. After double logarithmic plotting of the LO concentration against the corresponding reaction rates, the order in epoxide was again determined to be two (Supplementary Fig. 3-11b). Hence, the second method to establish the order in monomer confirms the first result, wherefore the overall rate equation can be written as – $d[LO]/dt = k \cdot [CO_2]^0 \cdot [LO]^2 \cdot [Zn]^1$. The group of Coates *et al.* investigated the reaction order for the copolymerisation of cyclohexene oxide and CO_2 with the same [(bdi)Zn(OAc)] catalyst in 2003.[29] They found an overall rate equation of $-d[CHO]/dt = k \cdot [CO_2]^0 \cdot [CHO]^1 \cdot [Zn]^1$, whereby the reaction order of one in cyclohexene oxide deviates from the reaction order of two in LO. Comparing cyclohexene oxide and LO, the steric demand of the latter attracts attention. The following pathway is proposed bearing all the reaction orders measured in mind (Fig. 3-4). In a first step, the dimeric catalyst coordinates one LO. ^{1}H NMR measurements showed that the catalyst exists preferentially in its dimeric state,[27,29] even in strong coordinating and polar solvents such as tetrahydrofurane (Supplementary Figs 3-12 and 3-13). Due to the steric demand of the monomer, the acetate group of the other zinc centre probably cannot attack the epoxide.
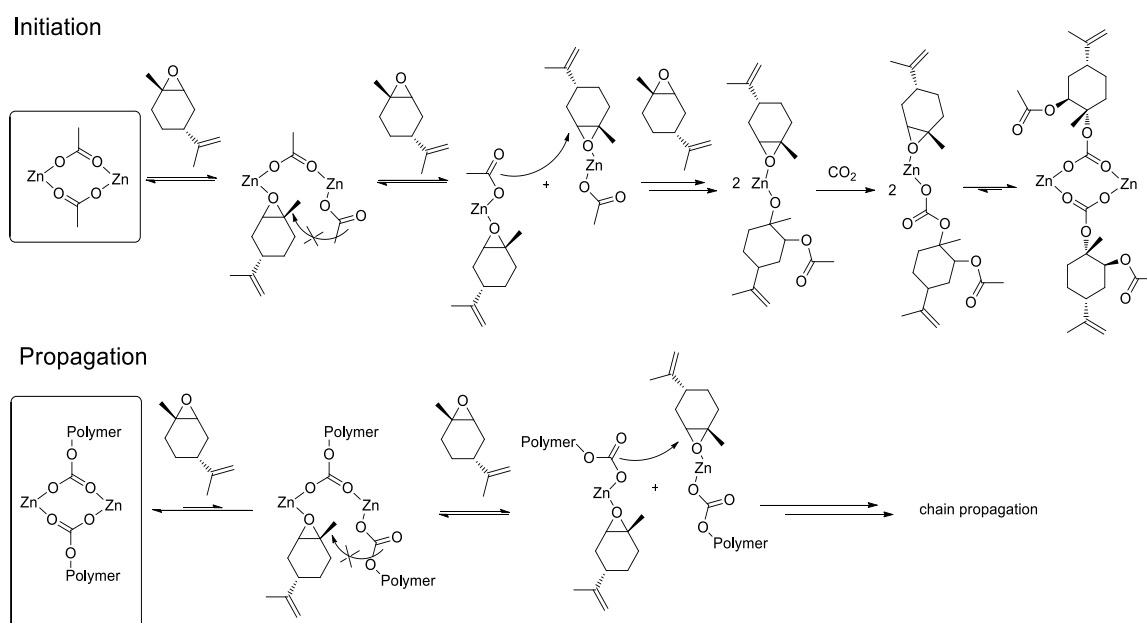
Figure 3-4: Postulated mechanism for copolymerisation of CO_2 and LO with catalyst [(bdi)Zn(OAc)].

After a second LO is coordinated to the second zinc centre the monomeric catalyst can rearrange to enable the nucleophilic attack of the initiating group. Carbon dioxide is inserted and a dimeric state is formed again, as the equilibrium lies on the dimeric side. In order to enable chain propagation, again two LO molecules have to be coordinated to the catalyst in order to separate the two zinc centres.

End-capping of PLimC with anhydrides and silicates

High molecular weight PLimC has a glass transition temperature of 130 °C (for DSC trace see Supplementary Fig. 3-3). This is, to the best of our knowledge, the highest T_g reported for an aliphatic PC and comes relatively close to commercial BPA-PC that has a T_g of 145 °C. On the other hand, the thermal stability of aliphatic polycarbonates is possibly the greatest obstacle when it comes to commercialisation of this polymer class for a broad range of applications.[32,33] Poly(propylene carbonate) has a T_g at around 40 °C and a decomposition temperature of 200 °C seems acceptable.[32] However, this leaves a very narrow processing window for PLimC with its glass transition at 130 °C. To overcome this limitation of a 5% decomposition temperature ($T_{5\%}$) for a catalyst-free polymer at 225 °C (Table 3-2 entry 1, Fig. 3-5), an attempt was made to end-cap the polymer that is presumably terminated by OH groups when precipitated in methanol. Four different anhydrides: acetic anhydride, maleic anhydride, trifluoroacetic anhydride, heptafluoro-butyric anhydride and tetraethyl orthosilicate were chosen as end capping agents.
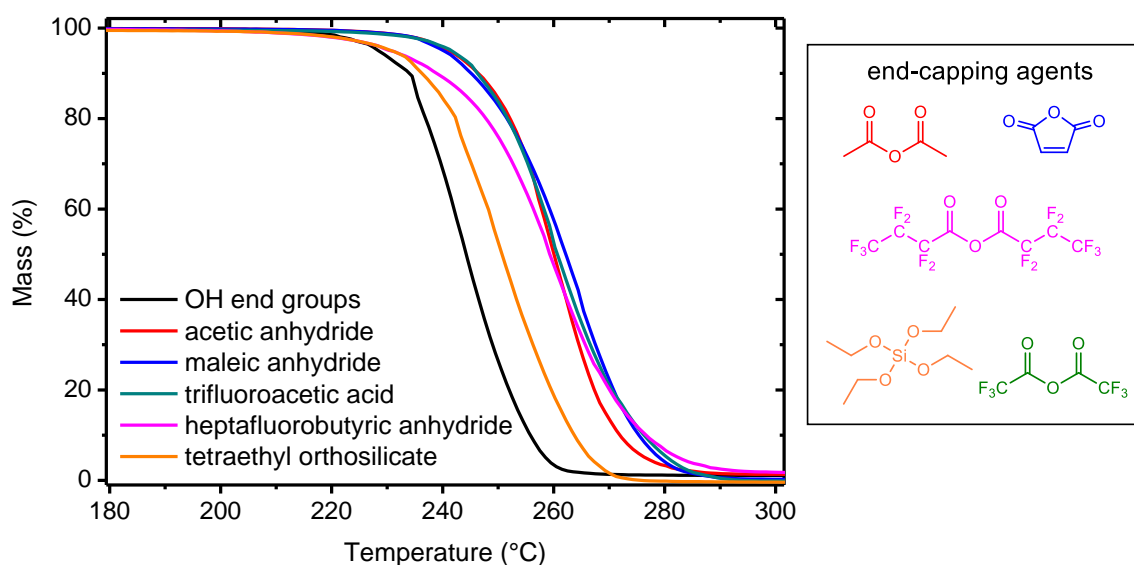
Figure 3-5: TGA of PLimC treated with various end-capping agents compared to an untreated sample (black curve).

With acetic, maleic and trifluoroacetic anhydride, an increase of 15 °C in $T_{5\%}$ and of 16 – 20 °C for the maximum decomposition temperature (highest decomposition rate, T_{max}) could be observed (Table 3-2, entries 2 – 4). Capping the polymer with fluorinated butyric anhydride and silicate only slightly increased the onset of decomposition of PLimC (Table 3-2, entries 5 and 6), while the first at least increased T_{max} significantly.

Table 3-2: Thermal degradation properties of pure and end-capped PLimC.

entry	end-capper	$T_{5\%}$ (°C)	T_{max} (°C)
1	-	225	244
2	acetic anhydride	241	260
3	maleic anhydride	240	265
4	trifluoroacetic anhydride	242	260
5	heptafluorobutyric anhydride	231	261
6	tetraethyl orthosilicate	231	252

This is a hint of only partial end-capping that can result from bad solubility of the end-capping agent (fluorinated butyric anhydride) or low reactivity under the conditions chosen (orthosilicate). End-capping can only slightly improve the thermal stability of PLimC, therefore, the thermal degradation was studied in more detail to find a possible alternative technique of stabilizing the polymer at elevated temperatures.
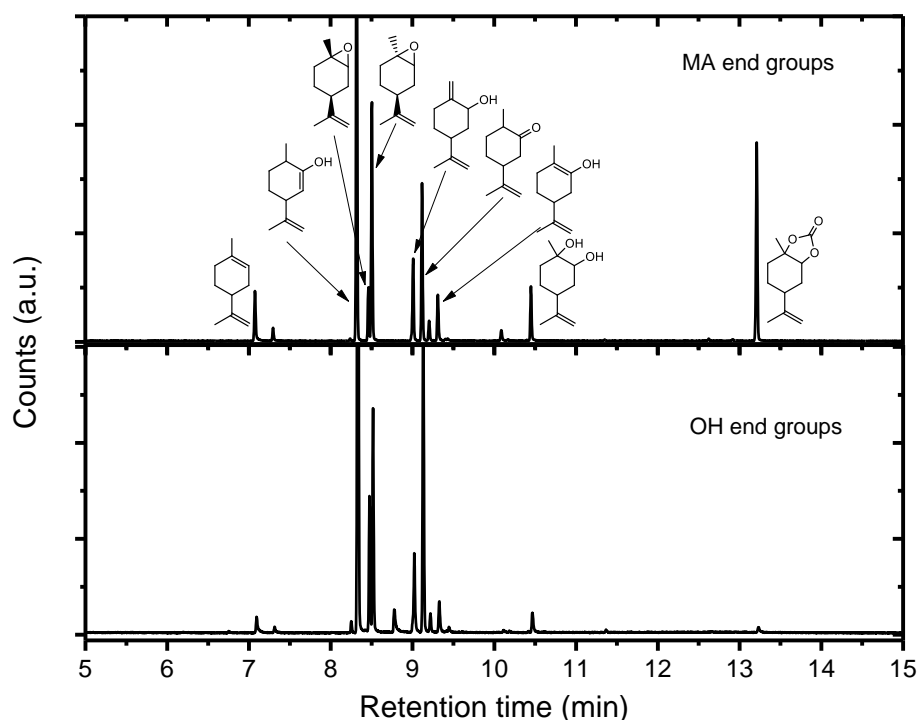
Figure 3-6: Gas chromatogram of the products evolved by heating samples of pure (bottom) and end-capped (top) PLimC for 20 min at 230 °C. The assignment of signals in the top spectrum results from mass spectroscopy analysis.

To understand the mechanisms involved in the degradation of the PC, GC-MS coupled with a thermal desorption unit was employed. Here, the sample is heated to the temperature desired, while its decomposition products are condensed in another chamber for a defined time, where they are eventually injected onto the column. The spectra and therewith potentially identified products from a decomposition of PLimC for 20 °C min at 230 °C are presented in Fig. 3-6. The spectra of PLimC with and without end-capping look very similar and suggest decomposition via abstraction of CO_2, probably by nucleophilic attack at an acidic hydrogen and a subsequent chain reaction. Though interestingly, only the spectrum of maleic anhydride end-capped PLimC shows a signal at 13.2 min, which is tentatively assigned to limonene carbonate which seems to be produced in significant amounts when the polymer is capped with maleic acid. The great variety of decomposition products is also illustrated in Scheme 3-5, where the 'most labile', i.e. acidic protons, are indicated by dashed lines. Those protons might be prone to nucleophilic attack (any nucleophile that is basic enough) and subsequent unzipping reactions then produce the products identified via abstraction of CO_2. The diol might evolve by a different mechanism where no CO_2, but rather CO abstraction is involved. The limonene carbonate mentioned above was possibly the backbiting product of maleic anhydride that activates a new pathway of decomposition to form the cyclic carbonate. This seems unreasonable for an end-capped product that should increase the thermal stability of the polymer, but at least the labile proton of a hydroxyl end group is protected against abstraction and TGA has proven the concept to be successful.
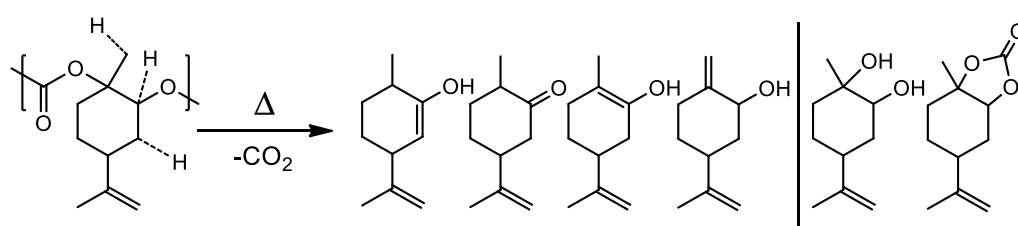
Scheme 3-5: Thermal decomposition products of PLimC proposed by GC MS studies. The dashed lines on **PLimC indicate 'labile' protons and right**-hand side on the product side are decomposition products where no simple CO_2 abstraction mechanism has taken place.

Table 3-3: Collection of general, mechanical, thermal and optical properties of PLimC.

	property	value	unit	method
general	density	1.08	g/cm^3	balance (Archimedes)
	carbonate content	99+	%	^{1}H-NMR
	contact angle to water	93	°	drop shape analyser
	M_n	53.4	kDa	GPC (CHCl$_3$)
	$Đ$	1.10	-	GPC (CHCl$_3$)
mechanical	E-modulus	0.95	GPa	tensile tester
	tensile strength	55	MPa	tensile tester
	elongation at break	15	%	tensile tester
	pencil hardness	B		pencil hardness tester[c]
thermal[a]	T_g	130	°C	DSC
	T_m	-	°C	DSC
	$T_{5\%}$	240	°C	TGA
	T_{max}	265	°C	TGA
optical[b]	transmission	94	%	hazemeter
	haze	0.75	%	hazemeter
	clarity	99.8	%	hazemeter

[a] measured at 10 K min^{-1}, [b] thickness of sample 0.24 mm, [c] test conducted according to ISO 15184 with BYK Pencil Hardness Tester and Derwent Graphic pencils.

The material PLimC possesses a variety of very interesting properties that make it so worthwhile to work with. They are summarised in Table 3-3 with the method of determination in the right hand column. The carbonate content in the backbone is greater than 99% for a polymer with 52.4 kDa and a dispersity of 1.10. Such an alicyclic PC has a density as low as 1.08 g/cm³, which resembles that of PP or PE.
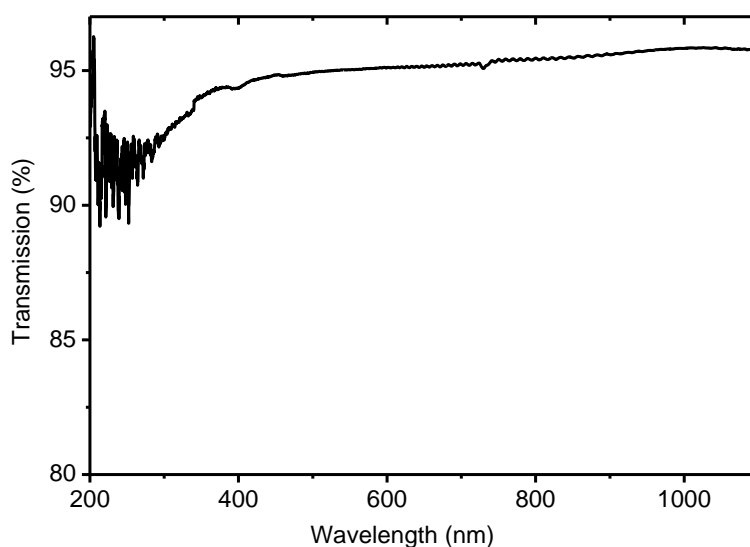
Figure 3-7: UV/Vis spectrum of a 240 μm thick film of PLimC produced by solvent casting.

The tensile properties were tested on a dog-bone shaped specimen produced by hot-pressing and suggest a mechanical behaviour ranging between PS and BPA-PC (Supplementary Fig. 3-14). Though it should be noted that injection moulded samples might improve upon tensile testing. The hardness and scratch resistance was evaluated with respect to pencil hardness, whereby a pencil of hardness B left no scratch behind on the surface of a PLimC film. This is already a significant improvement compared to BPA-PC (Makrolon 2800® Bayer; test with same set-up) that could only resist 8B or softer. Acrylics (ZK50 Plexiglas® Evonik), on the other hand, are resistant to pencils as hard as 5H, but suffer from a very high brittleness. Thermally, this polymer is also surprising with (to the best of our knowledge) the highest reported T_g for an aliphatic PC of 130 °C. This thermal resistance makes it an interesting choice wherever contact with boiling water is likely. The amorphous polymer with its alicyclic structure suggests very attractive optical properties and, indeed, a film produced by solvent casting tested on a hazemeter gave values for transmission, haze and clarity of 94%, 0.75% and 99.8%, respectively. These results were independent of film thickness (tested films of 50–400 μm thickness) and we would ascribe the missing 6% of transmission to 3% reflection on each of the interfaces (air/polymer–polymer/air). Upon reversion, this observation highlights the very low small and wide angle scattering, i.e. the high optical purity of PLimC. An ultraviolet visible (UV/Vis) spectrum of such a film (with a thickness of 240 μm) is also shown in Fig. 3-7. There is almost no absorbance of light in the visible region, thus, making it a perfect choice for applications where high transparency is necessary, e.g. packaging material or optical lenses.

3.3 Conclusions

In conclusion, we would like to present a 100% bio-based high molecular weight PLimC (>100 kDa) where we can tune the molecular weight over a wide range. Very important was the successful conversion of LO to PC by stereoselective high-yield epoxidation of limonene, which is nearly quantitative. The production of LO and PLimC was scaled up to kilograms per batch, while reducing the amount of organic solvents employed by a factor of 10 compared to standard precipitation methods. Kinetic studies suggested a second order dependence on LO concentration and indicates an alternating insertion of CO_2 and LO. PLimC has a range of very attractive properties, e.g. a T_g as high as 130 °C, which is close to technical BPA-based PC. The excellent transparency of PLimC in combination with good

hardness, both better than BPA-PC, makes it a highly promising green coating material, which will be the topic of upcoming work.

3.4 Experimental

Materials

(R)-Limonene (97%), acetyl acetone (99%), 2,4-diethylaniline (99%), *N*-bromosuccinimide (97%), sodium hydride (60% dispersion in mineral oil), iodomethane (99%, stabilised with silver), ethylenediaminetetraacetic acid (EDTA, 98.5%), acetic acid (99%) and acetic anhydride (99%) were used as received. *(R)*-LO (97%) was dried over NaH and distilled. Carbon dioxide (5.0, Linde Gase) was dried by passing through a column packed with a molecular sieve of 3 Å. The catalyst [(bdi)Zn(μ-OAc)][34] and EDTA-silica[28] were synthesised according to literature procedures.

Methods

NMR spectra were recorded on a Bruker AMX-300 operating at 300 MHz. Chemical shifts δ are indicated in parts per million (ppm) with respect to residual solvent signals. Thermogravimetric analysis (TGA) was performed on a Netzsch TG 209 F1 Libra and differential scanning calorimetry (DSC) on a Mettler Toledo DSC 821c, both at a heating rate of 10 K min^{-1} under N$_2$ atmosphere. *In situ* IR measurements were carried out under an argon atmosphere using an ATR IR Mettler Toledo system. IR spectra of solids were obtained with a Digilab Excalibur FTS-3000 equipped with an ATR unit. Gas chromatography spectra were recorded on a Shimadzu QP-5050 with N$_2$ as the carrier gas. GC-MS chromatograms were recorded on an Agilent 5977A MSD with He as the carrier gas. Relative molecular weights and dispersities were determined by GPC on an Agilent 1200 system with chloroform as the eluent and polystyrene as the calibration standard. A Hazemeter BykGardner Haze-Gard Plus and a UV/Vis spectrometer V- 670 (JASCO) were employed for the testing of optical properties of solvent cast PLimC films having a thickness between 100 and 400 μm. A Zwick/Roell Z0.5 with testXpert II software and 5 mm min^{-1} test speed were used for tensile testing of heat pressed PLimC specimen having a thickness of 300 μm. A BYK Pencil Hardness Tester and Derwent Graphic pencils were used to determine pencil hardness.

Synthetic procedures

Synthesis of *trans*-LO. A modified procedure from Gurudutt *et al.*[26] was used. A volume of 1.2 L (8.8 mol) limonene, 1 L water and 4.5 L acetone were filled into a 10 L temperature-controlled reactor. The mixture was cooled down to 0 °C and 9.2 mol *N*-bromosuccinimide was added within 30 min. The solvent was evaporated at 50 °C and the resulting organic phase was diluted with 3 L diethyl ether. After removing the aqueous phase, the organic phase was washed with water once before the ether was removed at 50 °C. The crude bromohydrin was converted directly to the epoxide with 2 L of a 6 M NaOH solution at 60 °C for 1.5 h. The alkaline solution was removed and the crude product diluted with 3 L diethyl ether before it was washed with 1.5 L of a saturated sodium bicarbonate solution and, subsequently, 1.5 L of water. After evaporating the solvent, 1.4 L of the crude product was obtained as a yellow viscous liquid. Gas chromatography analysis revealed a *trans*-LO content of 60%, which was isolated by fractional distillation at 80 °C and dynamic vacuum. The final product consisted of 5% limonene, 9% cis-LO and 85% *trans*-LO and 1% by-products (determined by GC analysis).

Masking of hydroxyl impurities in limonene oxide. All manipulations were carried out under inert atmosphere. The crude oxirane was treated with 0.16 eq. of NaH (60% dispersion in mineral oil) at 0 °C. After stirring for 60 min, 0.08 eq. of iodomethane was added and the mixture was kept at 0 °C for another hour. The process of the reaction was monitored via GC and after 24 h, no more hydroxyl impurities could be detected and the mixture was fractionally distilled at 80 °C in a dynamic vacuum. The main fraction was collected at 5 mbar (~66%, containing 85% *trans*-limonene oxide).

Synthesis of poly(limonene carbonate). An *in vacuo* pre-dried 120 mL autoclave at 90 °C was charged in a glove box with 30 mmol of epoxide, 3 mL toluene and 0.4 mmol catalyst. The closed reactor was stirred for 15 min to dissolve the catalyst before it was evacuated and, subsequently, pressurised with 10 bar CO_2. The reactor was opened after an adequate time and the viscous mixture diluted with toluene before 20 wt% (relative to LO) of acetic anhydride was added. After 1 h, the solution was precipitated in methanol and the product dried *in vacuo*. The product was characterised by ^{1}H and ^{13}C NMR spectroscopy (Supplementary Figs 3-1 and 3-2).

Purification of PLimC with on silica immobilised EDTA (EDTA-Si). An amount of 20 wt% acetic anhydride and 10 wt% EDTA-Si were added to a 0.2 g/mL solution of crude PLimC in toluene and stirred for 3 h at room temperature. The suspension was filtered through a G3 glass frit to remove silica particles. The viscous polymer solution was cast on a glass plate after concentration and dried *in vacuo* at 50 – 120 °C for 12 h.

Acknowledgements

3.5 References

1.   LeGrand, D. G. & Bendler, J. T. *Handbook of Polycarbonate Science and Technology.* (Marcel Dekker, Inc., 2000).

2.   *Bisphenol A (BPA): use in food contact application, U.S. Food and Drug Administration.* (2014).

3.   Yokoe, M., Aoi, K. & Okada, M. Biodegradable polymers based on renewable resources. IX. Synthesis and degradation behavior of polycarbonates based on 1,4:3,6-dianhydrohexitols and tartaric acid Derivatives with pendant functional groups. *J. Polym. Sci. Part A Polym. Chem.* **43,** 3909–3919 (2005).

4.   Chatti, S., Kricheldorf, H. R. & Schwarz, G. Copolycarbonates of isosorbide and various diols. *J. Polym. Sci. Part A Polym. Chem.* **44,** 3616–3628 (2006).

5.   Xia, H., Suo, Z. Y., Qiang, G. J. & Chang, C. J. Synthesis, characterization, and degradation of a novel L-tyrosine-derived polycarbonate for potential biomaterial applications. *J. Appl. Polym. Sci.* **110,** 2168–2178 (2008).

6.   Xin, Y. & Uyama, H. Synthesis of new bio-based polycarbonates derived from terpene. *J. Polym. Res.* **19,** 1-15 (2012).

7.   Klaus, S., Lehenmeier, M. W., Anderson, C. E. & Rieger, B. Recent advances in CO_2/epoxide copolymerization—New strategies and cooperative mechanisms. *Coord. Chem. Rev.* **255,** 1460–1479 (2011).

8.   Bhanage, B. M. & Arai, M. *Transformation and utilization of carbon dioxide.* (Springer Berlin Heidelberg, 2014). doi:10.1007/978-3-642-44988-8

9.   Inoue, S., Koinuma, H. & Tsuruta, T. Copolymerization of carbon dioxide and epoxide with organometallic compounds. *Die Makromol. Chemie* **130,** 210–220 (1969).

10.   Inoue, S., Koinuma, H. & Tsuruta, T. Copolymerization of carbon dioxide and epoxide. *Polym. Lett.* **7,** 287–292 (1969).

11.   Takeda, N. & Inoue, S. Polymerization of 1,2-epoxypropane and copolymerization with carbon dioxide catalyzed by metalloporphyrins. *Die Makromol. Chemie* **179,** 1377–1381 (1978).

12.   Wang, S. J., Du, L. C., Zhao, X. S., Meng, Y. Z. & Tjong, S. C. Synthesis and characterization of alternating copolymer from carbon dioxide and propylene oxide. *J. Appl. Polym. Sci.* **85,** 2327–2334 (2002).

13.   Luinstra, G. A. & Borchardt, E. in *Synth. Biodegrad. Polym.* 29–48 (Springer Berlin / Heidelberg, 2012). doi:10.1007/12_2011_126

14.   Koning, C. *et al.* Synthesis and physical characterization of poly(cyclohexane carbonate), synthesized from CO_2 and cyclohexene oxide. *Polymer* **42,** 3995–4004 (2001).

15. Zhang, Y. *et al.* Synthesis of fully alternating polycarbonate with low T_g from carbon dioxide and bio-based fatty acid. *RSC Adv.* **4,** 36183–36188 (2014).

16. Darensbourg, D. J., Chung, W., Arp, C. J., Tsai, F. & Kyran, S. J. Copolymerization and cycloaddition products derived from coupling reactions of 1,2-epoxy-4-cyclohexene and carbon dioxide. Postpolymerization functionalization via thiol–ene click reactions. *Macromolecules* **47,** 7347–7353 (2014).

17. Winkler, M., Romain, C., Meier, M. A. R. & Williams, C. K. Renewable polycarbonates and polyesters from 1,4-cyclohexadiene. *Green Chem.* **17,** 300–306 (2015).

18. Byrne, C. M., Allen, S. D., Lobkovsky, E. B. & Coates, G. W. Alternating copolymerization of limonene oxide and carbon dioxide. *J. Am. Chem. Soc.* **126,** 11404–11405 (2004).

19. *Citrus Fruit Fresh and Processed, Food and Agriculture Organization of the United Nations.* (2012).

20. Ciriminna, R., Lomeli-Rodriguez, M., Demma Carà, P., Lopez-Sanchez, J. A. & Pagliaro, M. Limonene: a versatile chemical of the bioeconomy. *Chem. Commun.* **50,** 15288–15296 (2014).

21. Park, H. J., Ryu, C. Y. & Crivello, J. V. Photoinitiated cationic polymerization of limonene 1,2-oxide and α-pinene oxide. *J. Polym. Sci. Part A Polym. Chem.* **51,** 109–117 (2013).

22. Bähr, M., Bitto, A. & Mülhaupt, R. Cyclic limonene dicarbonate as a new monomer for non-isocyanate oligo- and polyurethanes (NIPU) based upon terpenes. *Green Chem.* **14,** 1447 (2012).

23. Auriemma, F. *et al.* Stereocomplexed poly(limonene carbonate): a unique example of the cocrystallization of amorphous enantiomeric polymers. *Angew. Chemie Int. Ed.* **54,** 1215–1218 (2015).

24. Peña Carrodeguas, L., González-Fabra, J., Castro-Gómez, F., Bo, C. & Kleij, A. W. Al III-catalysed formation of poly(limonene)carbonate: DFT analysis of the origin of stereoregularity. *Chem. - A Eur. J.* **21,** 6115–6122 (2015).

25. Helou, M., Miserque, O., Brusson, J.-M., Carpentier, J.-F. & Guillaume, S. M. Ultraproductive, zinc-mediated, immortal ring-opening polymerization of trimethylene carbonate. *Chem. - A Eur. J.* **14,** 8772–8775 (2008).

26. Gurudutt, K. N., Rao, S. & Srinivas, P. Stereospecific synthesis of *trans-β*-terpineol. *Flavour Fragr. J.* **7,** 343–345 (1992).

27. Cheng, M. *et al.* Single-site beta-diiminate zinc catalysts for the alternating copolymerization of CO_2 and epoxides: catalyst synthesis and unprecedented polymerization activity. *J. Am. Chem. Soc.* **123,** 8738–8749 (2001).

28. Kumar, R., Barakat, M. A., Daza, Y. A., Woodcock, H. L. & Kuhn, J. N. EDTA functionalized silica for removal of Cu(II), Zn(II) and Ni(II) from aqueous solution. *J. Colloid Interface Sci.* **408,** 200–205 (2013).

29. Moore, D. R., Cheng, M., Lobkovsky, E. B. & Coates, G. W. Mechanism of the alternating copolymerization of epoxides and CO_2 using β-diiminate zinc catalysts: evidence for a bimetallic epoxide enchainment. *J. Am. Chem. Soc.* **125,** 11911–11924 (2003).

30. Jutz, F., Buchard, A., Kember, M. R., Fredriksen, S. B. & Williams, C. K. Mechanistic investigation and reaction kinetics of the low-pressure copolymerization of cyclohexene oxide and carbon dioxide catalyzed by a dizinc complex. *J. Am. Chem. Soc.* **133,** 17395–17405 (2011).

31. Lehenmeier, M. W. *et al.* Flexibly tethered dinuclear zinc complexes: a solution to the entropy problem in CO_2/epoxide copolymerization catalysis? *Angew. Chemie - Int. Ed.* **52,** 9821–9826 (2013).

32. Luinstra, G. A. Poly(propylene carbonate), old copolymers of propylene oxide and carbon dioxide with new interests: catalysis and material properties. *Polym. Rev.* **48,** 192–219 (2008).

33. Thorat, S. D., Phillips, P. J., Semenov, V. & Gakh, A. Physical properties of aliphatic polycarbonates made from CO_2 and epoxides. *J. Appl. Polym. Sci.* **89,** 1163–1176 (2003).

34.   Allen, S. D., Moore, D. R., Lobkovsky, E. B. & Coates, G. W. Structure and reactivity of mono- and dinuclear diiminate zinc alkyl complexes. *J. Organomet. Chem.* **683,** 137–148 (2003).

3.6 Supplementary information

NMR Analysis of PLimC from copolymerisation of *trans*-LO and CO_2 with [(bdi)Zn(OAc)].
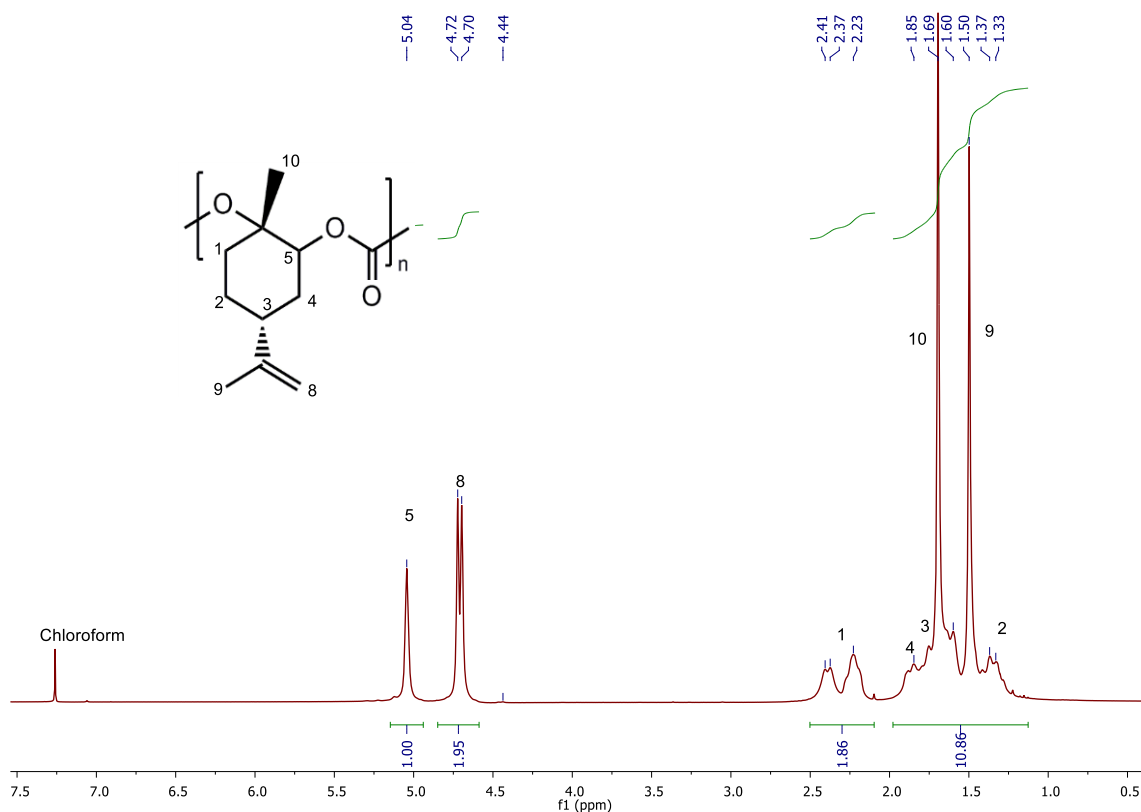
Supplementary Figure 3-1: ^{1}H NMR spectrum of PLimC (entry 5, Table 3-1) recorded at 300 MHz in $CDCl_3$.

Peak assignment:

^{1}H NMR (300 MHz, $CDCl_3$): δ 5.04 (1H, s, C(5)H), 4.71 (2H, m, C(8)H_2), 2.42-2.20 (2H, m, C(1)H_2), 1.85 (2H, m, C(4)H_2), 1.71 (1H, m, C(3)H), 1.69 (3H, s, C(10)H_3), 1.50 (3H, s, C(9)H_3), 1.33 (2H, m, C(2)H_2) ppm
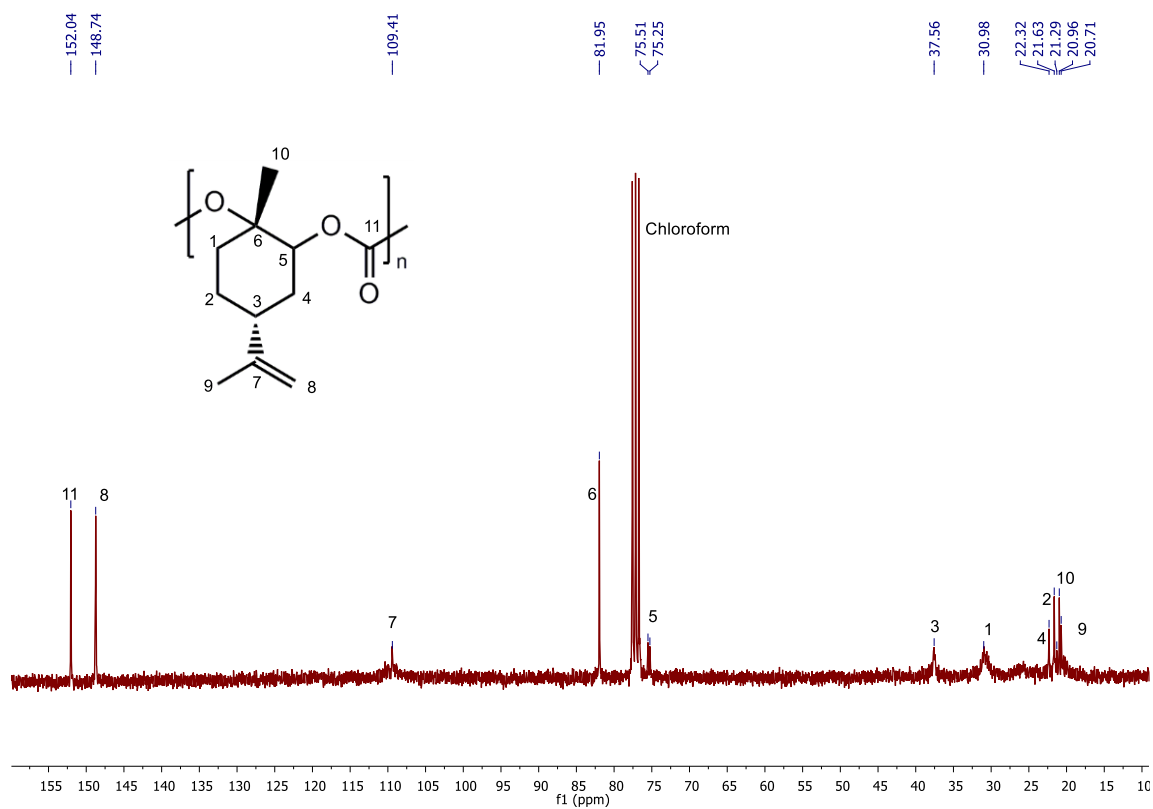
Supplementary Figure 3-2: ^{13}C NMR spectrum of PLimC (entry 5, Table 3-1) recorded at 300 MHz in CDCl$_3$.

Peak assignment:

^{13}C NMR (300 MHz, CDCl$_3$): δ 152.0 (C11), 148.7 (C8), 109.4 (C7), 82.0 (C6), 75.4 (C5), 37.6 (C3), 31.0 (C1), 22.3 (C4), 21.6 (C2), 21.0 (C10), 20.7 (C9) ppm

Thermal analysis of PLimC
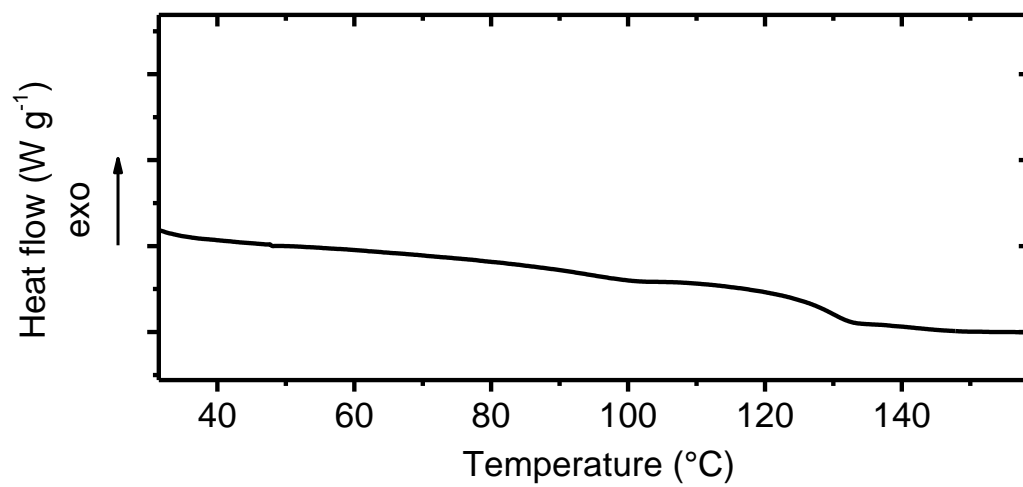
Supplementary Figure 3-3: DSC thermogram of PLimC (entry 5, Table 3-1) with second heating curve measured at 10 K min^{-1}.

Characterisation of EDTA immobilised on silica
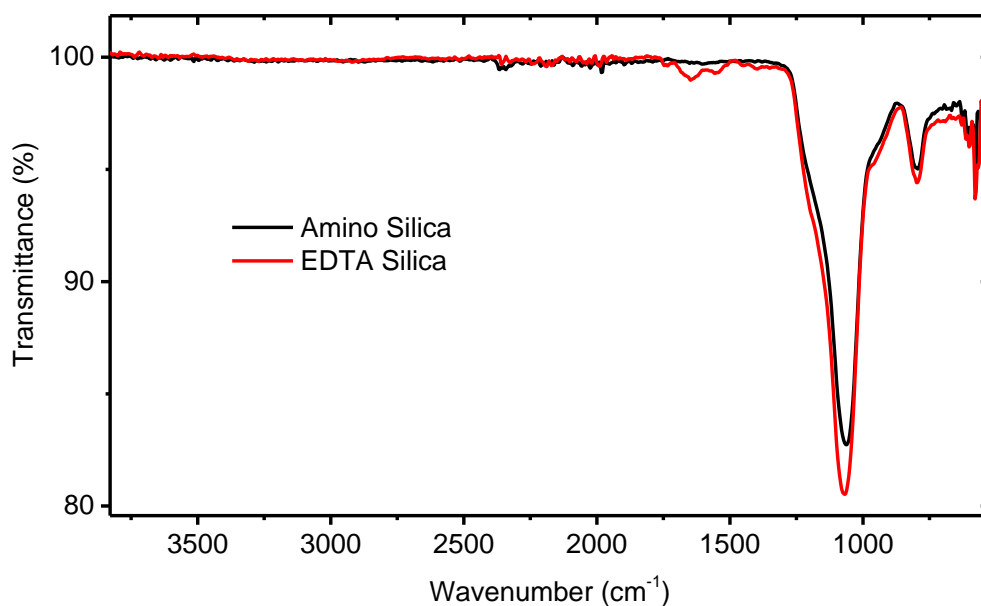
Supplementary Figure 3-4: ATR-FTIR spectra of amino-functionalised silica and EDTA functionalized silica.

The resonances of functionalisation on silica particles are rather low (Supplementary Figure 3-4), i.e. amine vibrations are not observable at all and EDTA carbonyl vibrations are weak. Hence thermogravimetric analysis was employed to quantify the degree of functionalisation (Supplementary Figure 3-5).
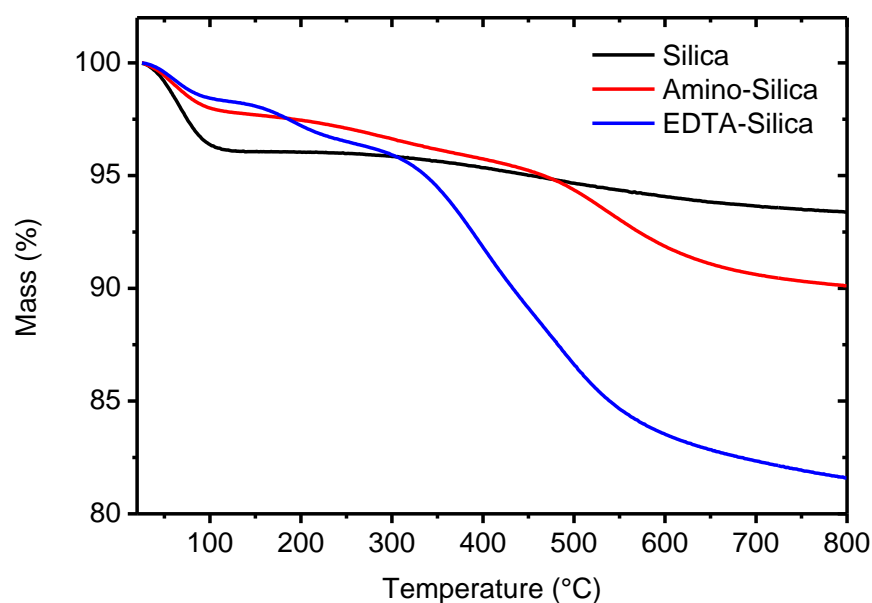
Supplementary Figure 3-5: Thermogravimetric analysis of Silica, amino-functionalised silica and EDTA-functionalized silica.

Kinetic investigation of copolymerisation of LO and CO$_2$
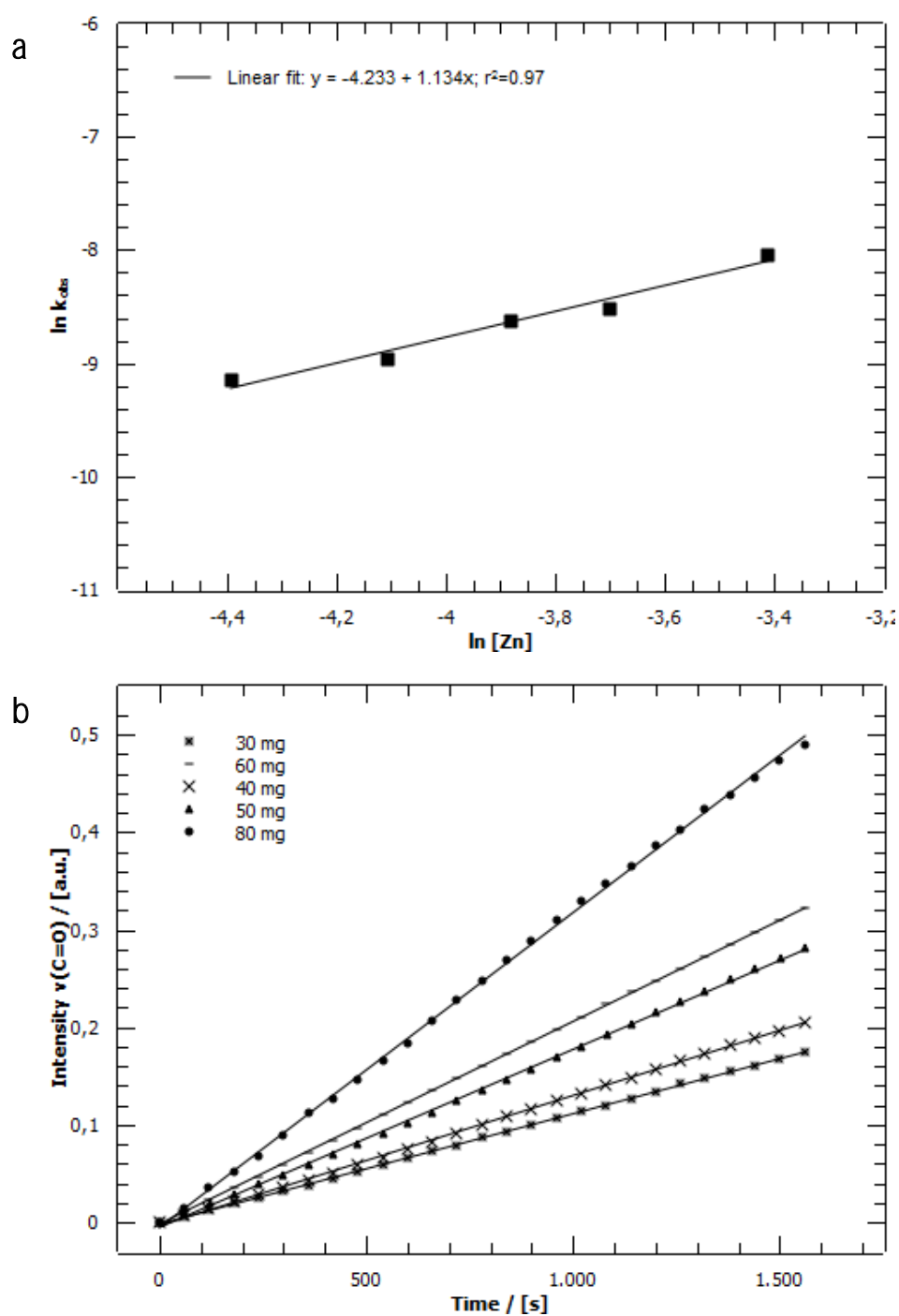
Supplementary Figure 3-6: (**a**): Determination of the order of the catalyst in the copolymerization of CO$_2$ and LO. (**b**) Determination of the copolymerisation rate k$_{obs}$ as a change of absorbance at 1749 cm^{-1} with time at different loadings of [(bdi)Zn(OAc)] (reaction conditions: 5 mL LO, 11 bar CO$_2$, room temperature, catalyst concentration: 12.3 - 32.9 mM, without solvent).
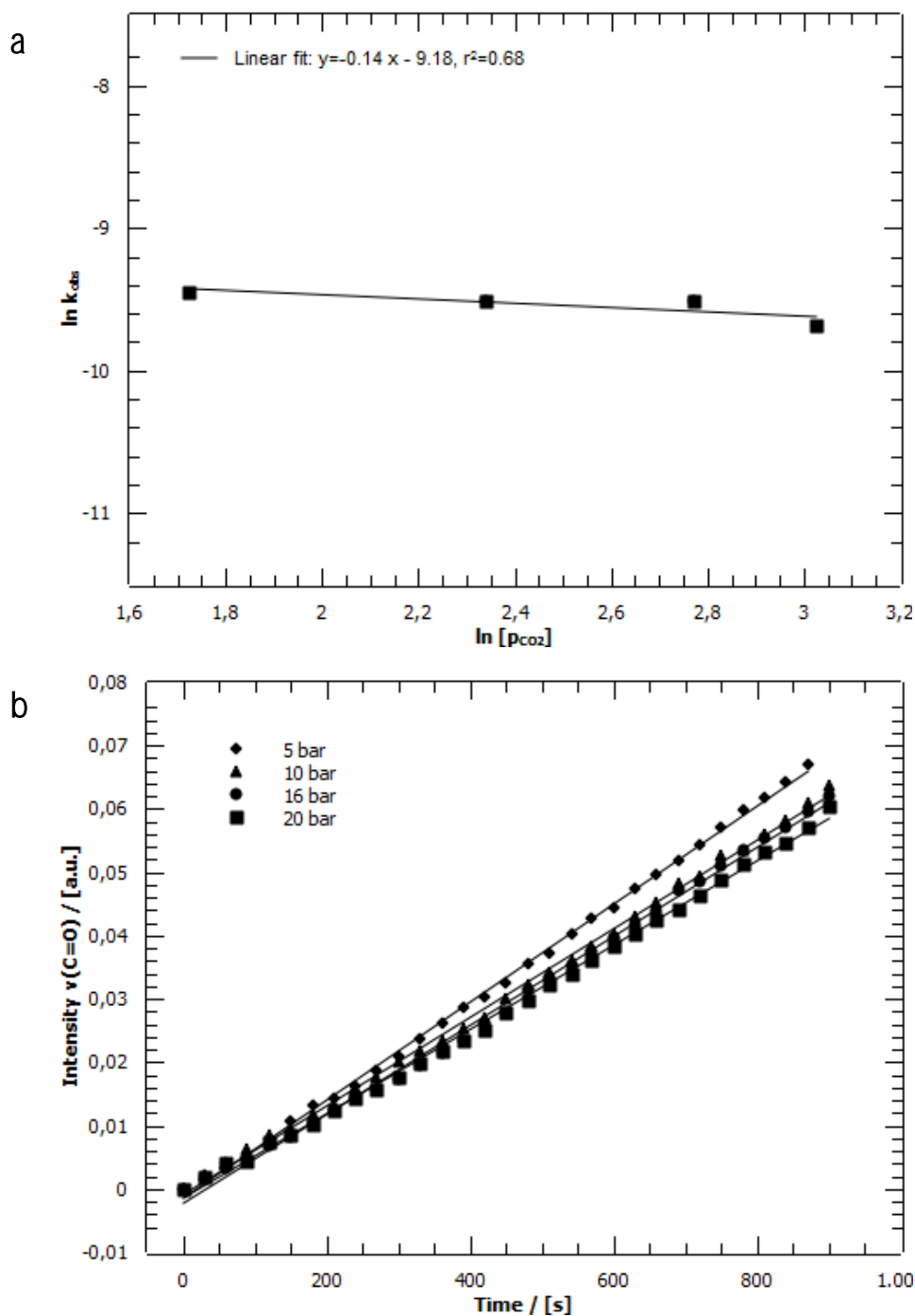
Supplementary Figure 3-7: (a) Determination of the order of CO_2 in the copolymerization of CO_2 and LO. **(b)** Determination of the copolymerisation rate k_{obs} as a change of absorbance at 1749 cm^{-1} with time at different CO_2 pressures (reaction conditions: 5 mL LO, catalyst loading 0.4%, room temperature, CO_2 pressure 5-20 bar).

a

b
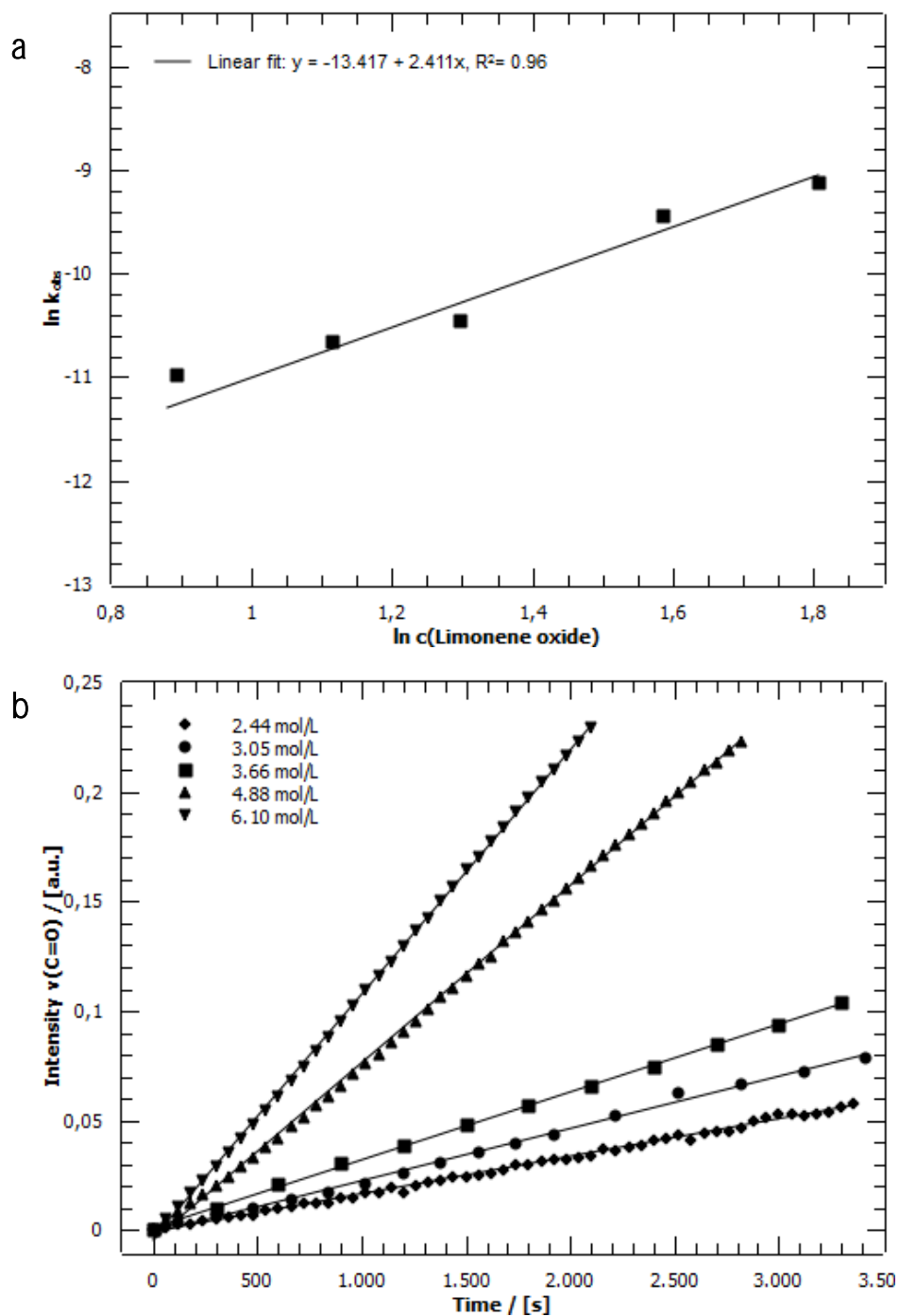
Supplementary Figure 3-8: (a) Determination of the order of LO in the copolymerization of CO_2 and LO. (b) Determination of the copolymerisation rate k_{obs} as a change of absorbance at 1749 cm^{-1} with time at different LO concentrations (reaction conditions: 5 mL LO, catalyst loading 0.4%, room temperature, 11 bar CO_2, concentration LO: 2.4 - 6.1 mol/L).
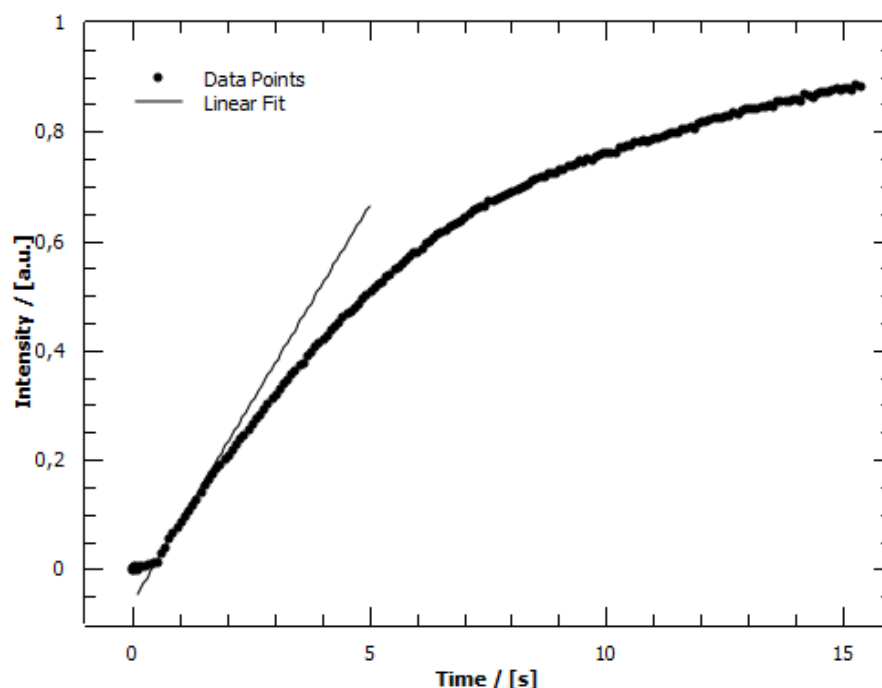
Supplementary Figure 3-9: Intensity of the carbonyl stretching bond of PLimC against time with an induction period of about one hour (reaction conditions: concentration LO: 3.66 mol/L, 11 bar CO_2, room temperature, catalyst concentration: 0.4%, volume (toluene): 2.0 mL).

Supplementary Table 3-1: Determination of the calibration curve by varying concentrations of PLimC and LO.

m of PLimC	V of toluene	V of LO	[LO]	conversion	Intensity of v(C=O)
(g)	(mL)	(mL)	(mol L^{-1})	(a.u.)	(a.u.)
0.00	2.50	2.50	3.05	0	0
0.10	2.50	2.40	2.93	0.04	0.072
0.20	2.50	2.30	2.81	0.08	0.121
0.30	2.50	2.20	2.68	0.12	0.209
0.40	2.50	2.10	2.56	0.16	0.271
0.50	2.50	2.00	2.44	0.20	0.316
0.75	2.50	1.75	2.13	0.30	0.431
1.00	2.50	1.50	1.83	0.40	0.598
1.50	2.50	1.00	1.22	0.60	0.800
2.00	2.50	0.50	0.61	0.80	1.000

Determination of the calibration curve. A defined amount of PLimC, toluene and LO were transferred into the IR-autoclave. After pressurizing the autoclave with 11 bar CO_2 at room temperature the system needs about two hours to completely solve the polymer to get a stable value for the intensity of the carbonyl stretching bond.
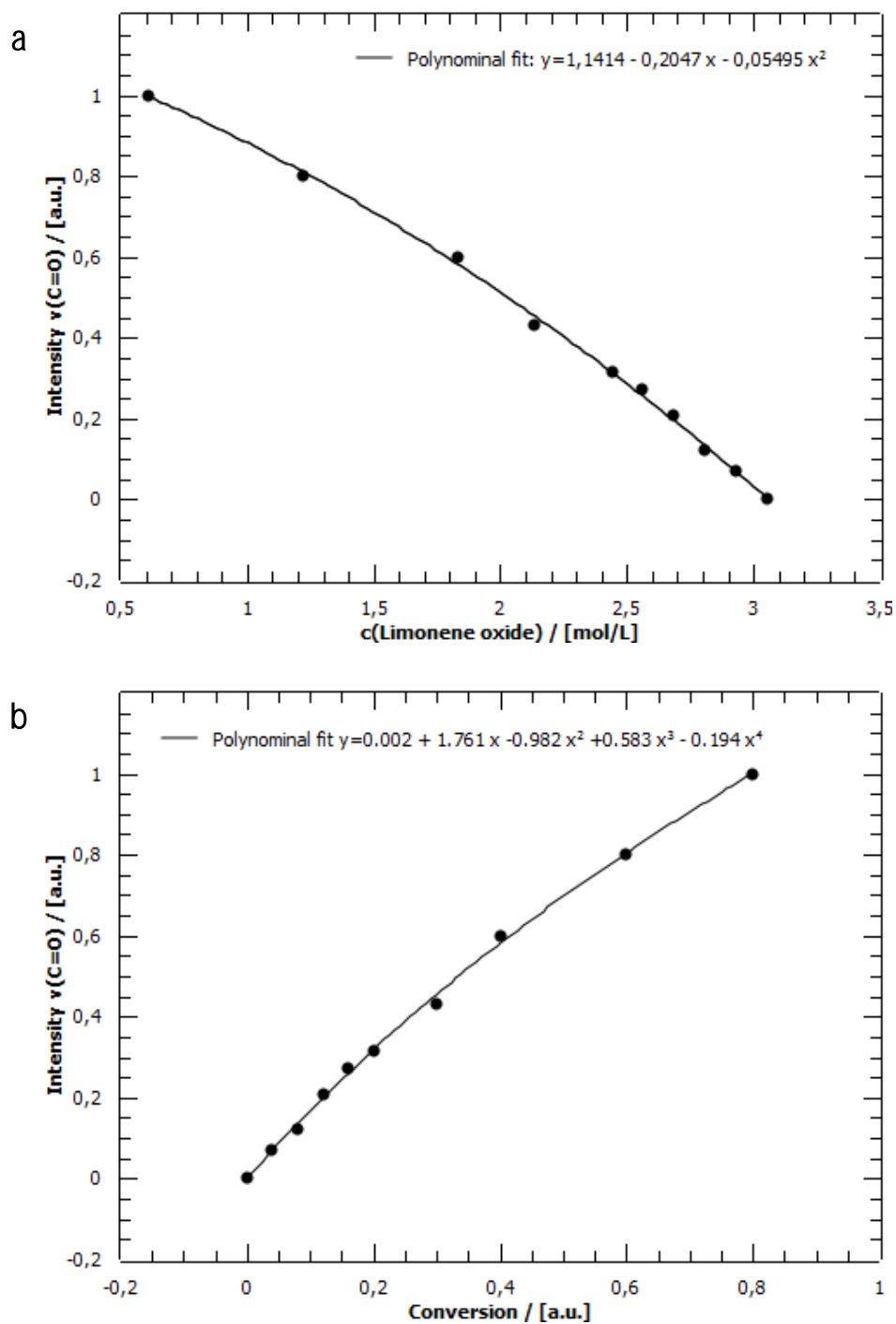
Supplementary Figure 3-10: (**a**) Intensity of the carbonyl stretching bond of PLimC against the concentration of LO measured in the in situ ATR IR. (**b**) Intensity of the carbonyl stretching bond of PLimC against conversion.
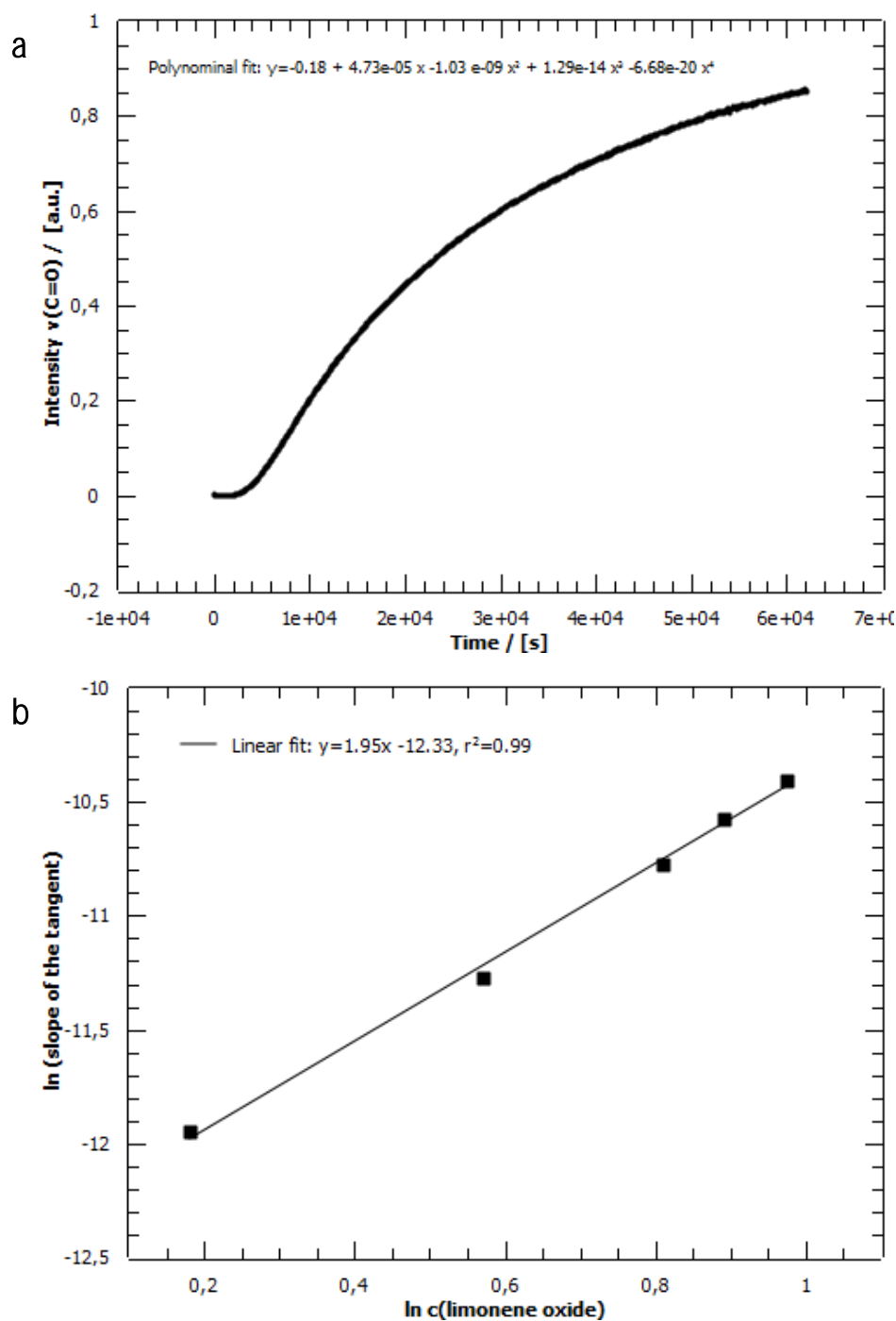
Supplementary Figure 3-11: (a) Intensity of the carbonyl stretching bond of PLimC against time (reaction conditions 2.5 mL LO, 2.5 mL toluene, 11 bar CO_2, room temperature, catalyst loading 0.4%). (b) Determination of the order in LO by double logarithmic plot of the slope of the tangent against the concentration of LO.

Derivation of the polynomial fit:

$$f(x) = -0.18 + 4.73e\text{-}05\ x - 1.03\ e\text{-}09\ x^2 + 1.29e\text{-}14\ x^3 - 6.68e\text{-}20\ x^4 \qquad (3\text{-}1)$$

$$f'(x) = 4.73e\text{-}05 - 2.06e\text{-}09\ x + 3.87e\text{-}14\ x^2 - 2{,}67e\text{-}19\ x^3 \qquad (3\text{-}2)$$

Supplementary Table 3-2: Overview of the correlation of the conversion and the corresponding concentration of LO with the intensity of the carbonyl stretching bond and the slope of the tangent (reaction conditions: 2.5 mL toluene, 2.5 mL limonene oxide, catalyst loading 0.4%, 11 bar CO_2, room temperature).

conversion (a.u.)	intensity ν(C=O) (a.u.)	slope of tangents (f´(x))	ln f´(x)	[LO] (mol L^{-1})	ln[LO]
0.2	0.316	3.01e-05	-10.41	2.44	0.97
0.3	0.431	2.56e-05	-10.57	2.13	0.89
0.4	0.598	2.10e-05	-10.77	1.83	0.81
0.6	0.800	1.27e-05	-11.27	1.22	0.57
0.8	1.000	6.47e-06	-11.95	0.61	0.18
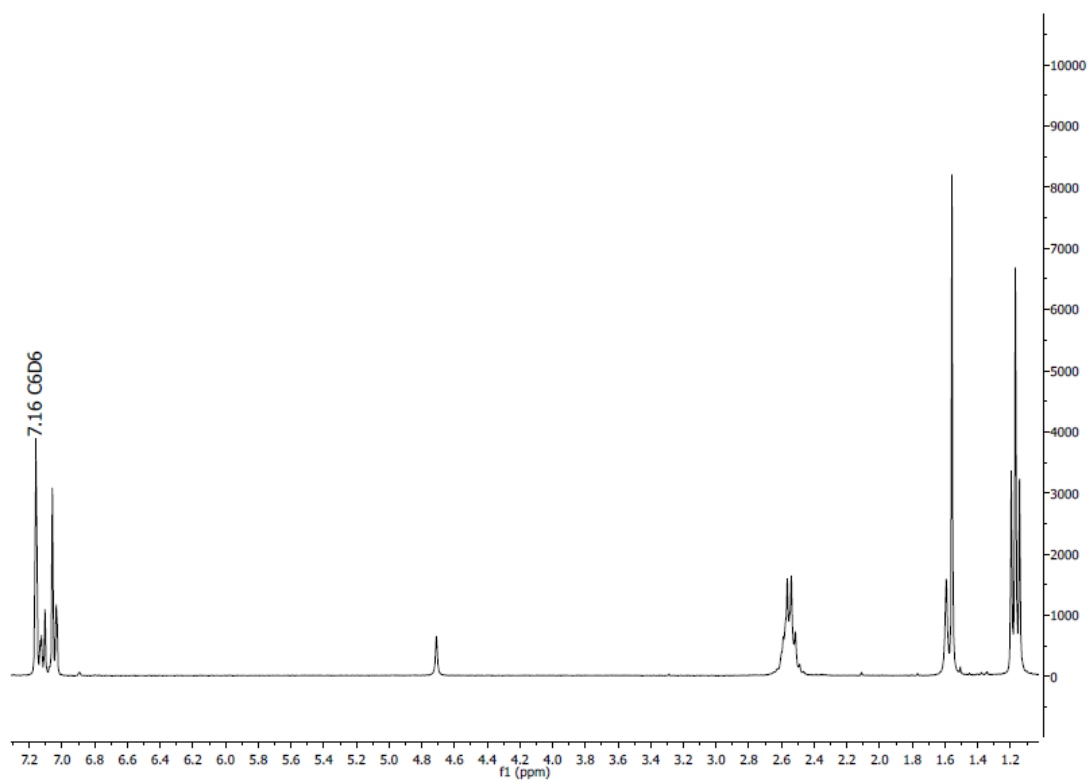
Supplementary Figure 3-12: ^{1}H NMR spectrum of the catalyst [(bdi)Zn(OAc)] recorded in C_6D_6.
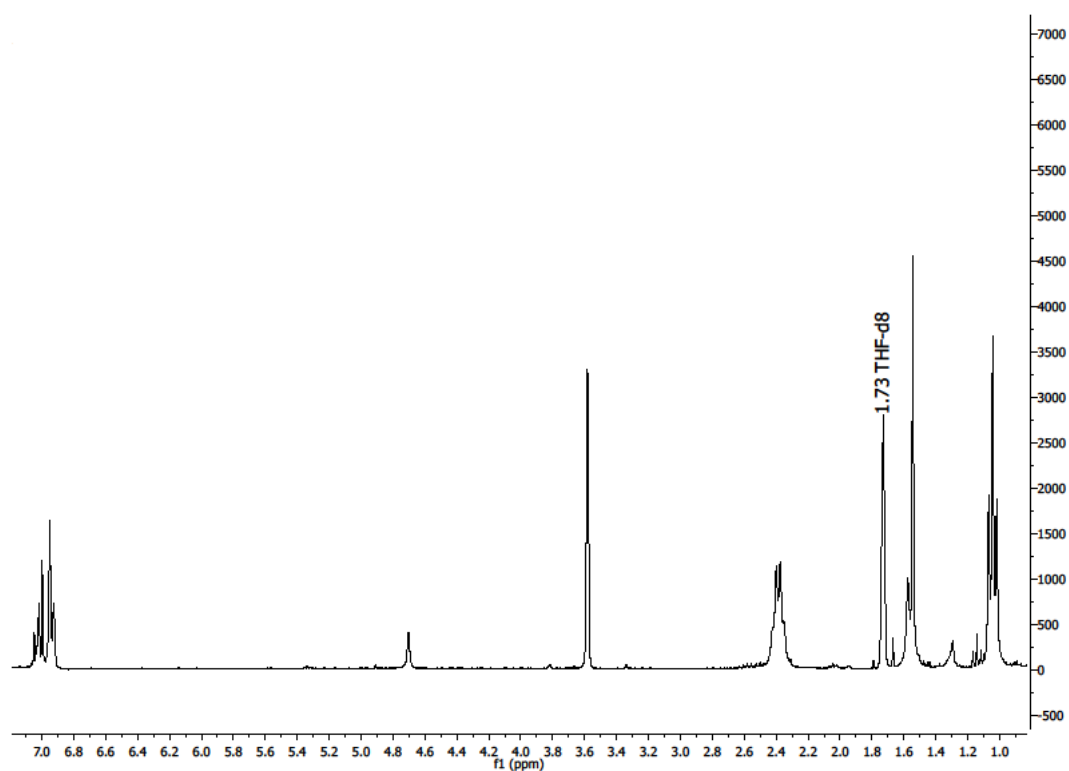
Supplementary Figure 3-13: ^{1}H NMR spectrum of catalyst [(bdi)Zn(OAc)] recorded in THF-d_8.

Stress-strain curves of PLimC
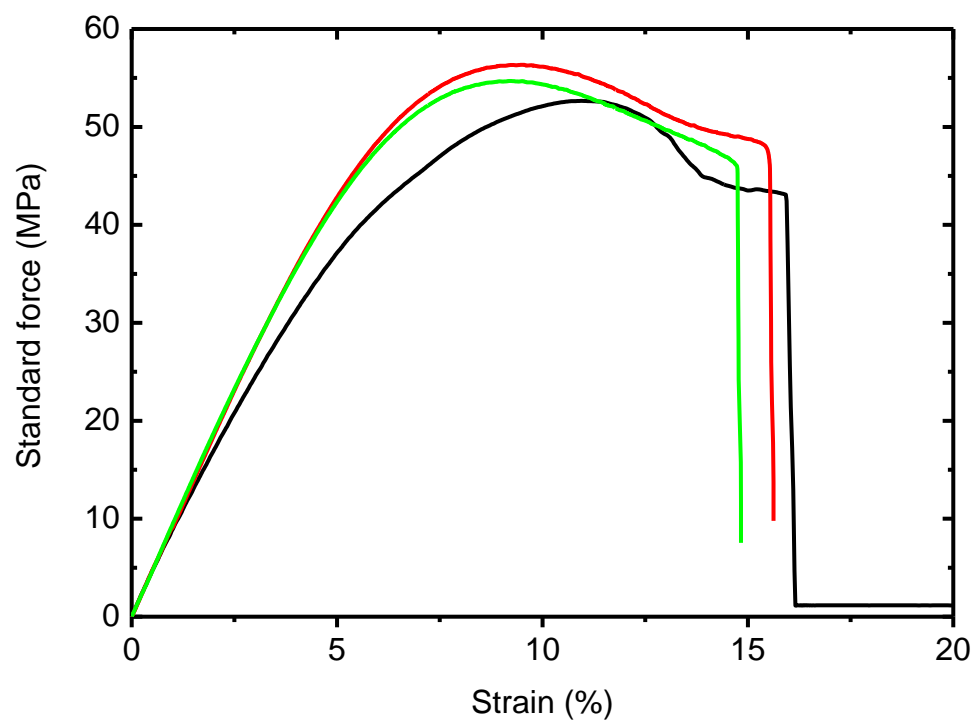
Supplementary Figure 3-14: Stress-strain curves of PLimC with M_n = 54 kDa, measured at a strain rate of 5 mm min^{-1}.

4

Applications of PLimC

Intended to be submitted under the title:

Membranes & breathing glass from bio-based polycarbonate

Oliver Hauenstein,[a] Mushfequr Rahman (HZG),[b] Mohamed Elsayed,[c] Reinhard Krause-Rehberg,[c] Volker Abetz[b] and Andreas Greiner[a]

[a] Macromolecular Chemistry II, University of Bayreuth, Universitätsstr. 30, 95440 Bayreuth, Germany.

[b] GKSS Research Centre Geesthacht GmbH, Institute of Polymer Research, Max-Planck-Str. 1, 21502 Geesthacht, Germany

[c] Physics, Martin-Luther-University of Halle-Wittenberg, 06099 Halle (Saale), Germany

PLimC – a breathing glass
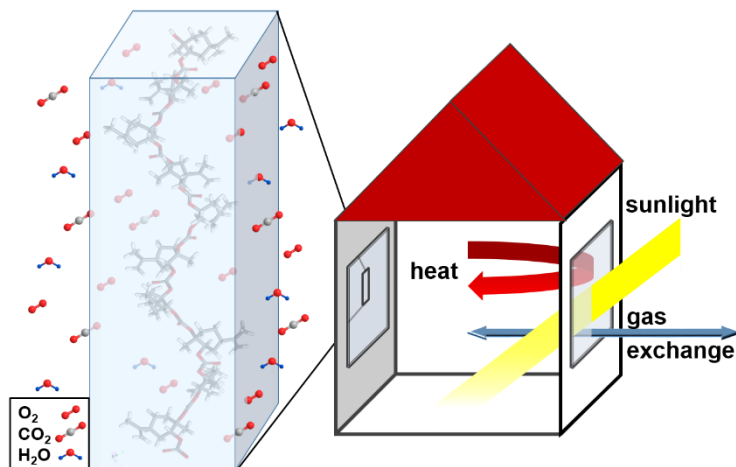
(to be submitted)

Abstract

The separation of CO_2 from fuel or flue gases, often described as carbon capture, is industrially most relevant, as the technique can provide a significant reduction of greenhouse gas emissions. The captured gas can be utilized in industrial processes such as the production of plastics by copolymerization with epoxides. These processes of separation and conversion of CO_2 are unified in the term 'carbon capture and utilization' and we found that the bio-based poly(limonene carbonate) (PLimC) – the copolymer of the orange peel-based limonene oxide (LO) and CO_2 – is a material that unifies both processes in one material. Due to its high CO_2-permeability of 68 barrer combined with a significant selectivity for the gas over N_2, the application of PLimC as a membrane material for carbon capture processes is discussed. However, the bio-based thermoplastic PLimC exhibits not only an exceptionally high permeability but also excellent optical, mechanical and thermal performance. This unique combination of properties renders PLimC the ideal choice for applications as breathing glass. Here, we discuss potential applications of such a breathable glass in well-insulated constructions (passive houses, closed greenhouses) where this material could save substantial amounts of energy by avoidance of any active ventilation.

4.1 Introduction

The anthropogenic emission of CO_2 accumulates to 32 Gt each year, which is mainly caused by incineration of carbon matter. CO_2 is a greenhouse gas that contributes significantly to the warming of the earth's atmosphere[1,2]. Global warming increases chances of catastrophic weather phenomena and a rising sea level and thus impacts our everyday life dramatically. In the last decades, measures have been taken to reduce the emission and to contain the rise of CO_2 levels in the atmosphere. Part of these measures can be described with the concepts of carbon capture and storage/utilization (CCS/CCU)[3-6]. CCU deals with the separation and transformation of CO_2 from process gases (combustion gases in power plants, natural gas etc.) to prevent emission of the greenhouse gas into the atmosphere. The separation step is achieved either by the use of chemical/physical absorbents or by organic/inorganic membrane materials[4,7]. The class of absorbents is nowadays dominated by alkanol amine solutions, e.g. monoethanolamine and diethanolamine, that require high temperatures for regeneration of the solvent[8,9]. Hence, these 'wet-scrubbing' processes are connected to a considerable energy penalty that adds to the total emission of CO_2[10,11]. The more sophisticated – though less developed – technology relies on the use of membrane materials that separate CO_2 from other process gases by size-exclusion (mostly hybrid metal-organic frameworks)[12-14] or solubility/diffusivity mechanisms (polymeric membranes), respectively[15-18]. The latter comprise a group of polymeric materials that exhibit permeabilities P (rate of transport through the matrix) and selectivities α (preference of one gas over the other, in this article the 'ideal selectivity' is calculated as the ratio of two permeabilities) extending over several orders of magnitude[19]. However, those materials frequently suffer from low long-term stability, known as aging, which prevented industrial application so far[20]. The large volumes of CO_2 captured in the industrial processes are either stored in gas tight (often natural) basins (CCS)[5,21] or transformed into high-value chemicals via various chemical routes (CCU). Some of those routes are based on transformations into bulk chemicals (urea, inorganic carbonates via SOLVAY process, methanol etc.)[22,23] while others make use of the catalytic coupling of CO_2 and epoxides to produce cyclic carbonates and polycarbonates (PCs)[24-26]. Coates *et al.* were the first to employ this route for the production of PLimC, the completely bio-based copolymer of the terpene derivative limonene oxide (LO) and CO_2[27-29]. In recent publications we could demonstrate the excellent thermal, optical and mechanical properties of poly(limonene carbonate) (PLimC)

and show the tremendous modification potential of the unsaturated PC by simple manipulations on the double bond[30,31]. Still, unmodified PLimC possesses a set of very interesting properties that were identified during the assessment of the polymer as a barrier material. The analysis revealed a very high permeability for small molecules like H_2 and CO_2. Hence, the material was assessed in terms of membrane applications as it exhibits not only a high permeability but a very good selectivity for CO_2, too. In fact, it is the first material that unifies both carbon capture (separate CO_2 with PLimC membrane) and utilization (copolymerize CO_2 and LO to give PLimC) in one material.. Since PLimC is also very permeable to light and a barrier to heat (insulator) the unique profile of properties renders it a **novel type of material that we define as** 'breathing glass'. Hence, we elaborate on completely new applications of such a breathing window in the construction sector in order to reduce energy consumption.

4.2 Results

Permeation properties of PLimC

In a first step, we wanted to assess the material PLimC (structure depicted Fig. 4-1a) with regard to its permeation properties. Here, we focus on the permeation, thermal and optical properties of PLimC compared with common amorphous thermoplastics and prominent polymeric membrane materials. The first are represented by polyimide (PI), polystyrene (PS), poly(phenylene ether) (PPE), cellulose acetate (CAc), poly(methyl methacrylate) (PMMA) and bisphenol-A polycarbonate (BPA-PC), whereas the latter comprise the polymer with intrinsic microporosity 1 (PIM-1)[32] or poly(1-trimethylsilyl-1-propyne) (PTMSP)[33] (structures of PMMA, BPA-PC, PIM-1 and PTMSP also shown in Fig. 4-1a). Semicrystalline polymers have not been considered, since they usually lack in transparency and gas permeability due to crystallites in the matrix[34–36]. By plotting the O_2- against the CO_2-permeability of those polymers (Fig. 4-1b), the special role of PLimC is illustrated. Compared with engineering thermoplastics like BPA-PC and PMMA, PLimC ($P(CO_2)$ = 68 barrer, 1 barrer = 10^{-10} cm^3 cm cm^{-2} s^{-1} $cmHg^{-1}$) is more permeable by one or two orders of magnitude, respectively, but up to three orders of magnitude less than state-of-the-art membrane polymers like PIM-1 or PTMSP. Thus, this aliphatic PC is located at the interface of common thermoplastics and highly gas permeably polymers. The dependence of the CO_2-permeability on the T_g is shown in Fig. 4-1c. The plot was chosen

to illustrate the rather low softening temperature of PLimC combined with its high permeability, which is atypical with respect to the other shown amorphous polymers. The lower T_g of the material enables the thermal processing of PLimC at much lower temperatures than it is possible for example for PPE or CAc – the latter being the only other bio-based polymer that could be relevant.
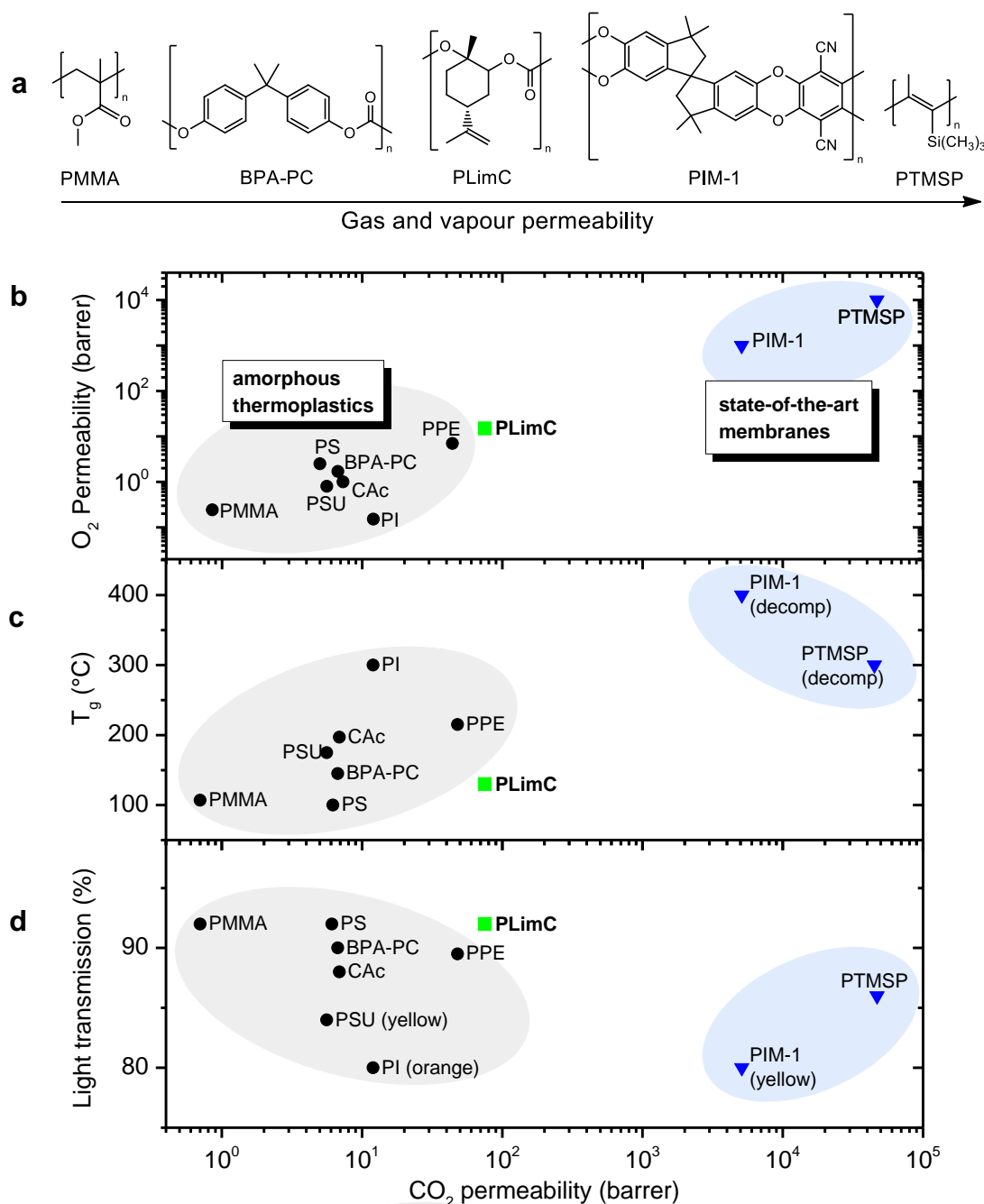
Figure 4-1 | Gas permeability of selected polymers with respect to thermal and optical properties. (a) The molecular structures of PMMA, BPA-PC, PLimC, PIM-1 and PTMSP in order of increasing permeability. (b) O_2 vs. CO_2 permeation of common amorphous thermoplastics (BPA-PC, CAc, PI, PMMA, PPE, PS)[18] in comparison to PLimC. The CO_2 permeabilities of the same polymers are plotted (c) vs. their T_g and (d) vs. their light transmission (specimen of 2 mm thickness).

At lower processing temperatures, the decomposition of the rather labile polymeric materials can be reduced significantly. The highly permeable polymers PIM-1 and PTMSP are not melt-processable at all, as they decompose before the T_g is reached. Another key feature of amorphous polymers is a high transmission of visible light. In Fig. 4-1d, the link between light and molecular (gas) transmission is drawn, where the optical performance is plotted against the CO_2-permeability of the amorphous polymers. PLimC exhibits a very high transparency that is comparable to optical grades of PMMA and PS and superior to the aromatic polymers BPA-PC, PPE and the polyacetylene PTMSP. PI, PSU and PIM-1 are coloured and thus cannot compete in optical applications. This unique combination of permeation, thermal and optical properties, renders PLimC a highly interesting material for membrane processes but also in applications where breathability and optical clarity are required. Both cases are discussed here, starting with the evaluation of the aliphatic polycarbonate in CCU processes.

PLimC – a membrane in CCU processes

Polymeric membrane materials are mainly utilized for the separation of small molecules due to the preferential solubility and/or diffusivity of one or the other in the polymer matrix[18]. PLimC was analysed in regard of the permeabilities of H_2, N_2, O_2, CH_4 and CO_2, which are gases relevant to the chemical and energy industry, e.g. the isolation of oxygen from air (O_2/N_2), the separation of hydrogen from ammonia purge gas (H_2/N_2), the sweetening of natural gas (CO_2/CH_4) or the carbon capture from fuel and flue gases (CO_2/N_2)[18,20]. The measurement of the temperature-dependent transport of such molecules through a film of PLimC (Fig. 4-2d and Supplementary Fig. 4-1) revealed a –for aliphatic PCs unprecedented – high permeability especially for CO_2 ($P(CO_2)$ = 68 barrer at 30 °C). The preferred permeation of CO_2 in the PLimC membrane results in a very good selectivity for carbon capture in fuel or flue gas applications, that is, for the gas pair CO_2/N_2 (Fig. 4-2e and Supplementary Fig. 4-2). In order to elucidate the underlying mechanism of such preferential transport, we employed the time-lag method (see Methods section) to separate the shares of solubility and diffusivity in the term permeability (permeability can be expressed as the product of both). The diffusivity is mainly governed by the kinetics of the gas and the free volume elements in the polymer matrix, whereas the solubility is based on the physico-chemical gas-matrix interactions[18]. Considering the kinetic radii of the investigated gases (see Fig. 4-2f), it is remarkable to see that the very small H_2 (kinetic radius

of 1.44 Å) – with a 49 times higher diffusivity – permeates slower through the dense polymer matrix than the 15% larger CO_2 (1.65 Å). This phenomenon cannot exclusively explained by the higher condensability of CO_2 but rather by the very high affinity of the gas to the PLimC matrix, resulting in an even 52 times higher solubility compared with H_2.
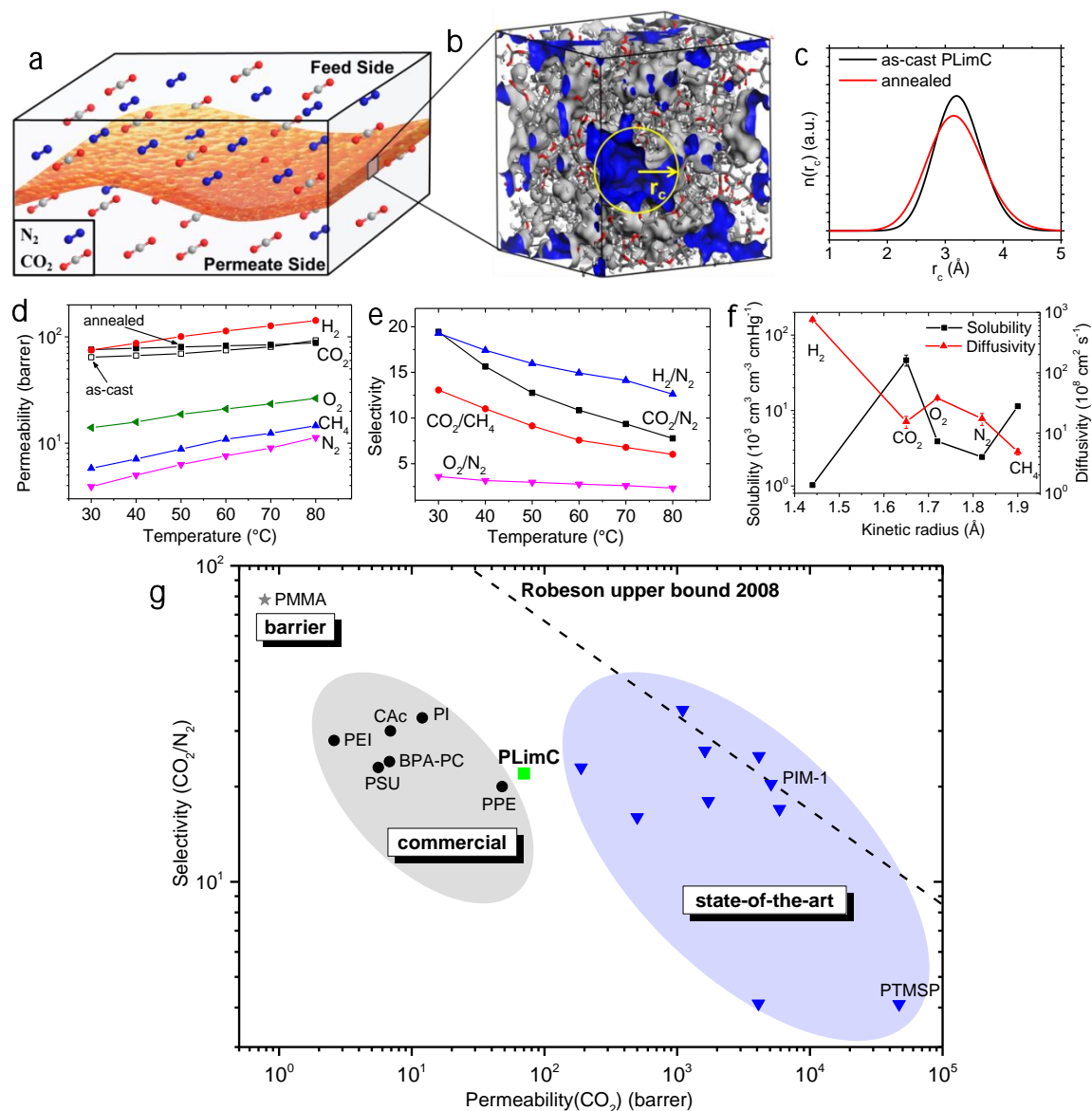
Figure 4-2 | Membrane properties of PLimC. (a) Illustration of PLimC as orange peel-based membrane for a CO_2/N_2 separation process. **(b)** A simulation of an amorphous unit cell of PLimC with eight chains each of ten repeating units and the Connolly surface (blue) to illustrate the loose packing of polymer chains, resulting in big voids in the bulk. **(c)** The cavity size (r_c) distributions of an as-cast film and an annealed film of PLimC determined by PALS measurements. **(d)** Temperature-dependent permeabilities of PLimC for H_2, CO_2, O_2, CH_4 and N_2. For CO_2 the curve of the as-cast film is also shown, since it deviates significantly from the annealed sample. **(e)** Temperature-dependent selectivities of PLimC for the gas pairs H_2/N_2, CO_2/N_2, CO_2/CH_4, and H_2/N_2. **(f)** The solubility and diffusivity of the tested gases in PLimC at 30 °C plotted versus the gases' kinetic radii. **(g)** Robeson plot for the gas pair CO_2/N_2 with PLimC compared to commercial and state-of-the-art polymeric membrane materials. Commercial polymers include: cellulose acetate (CAc), polyimide (PI), polyetherimide (PEI), polysulfone (PSU) and poly(phenylene ether) (PPE) with data from ref 18, state-of-the-art polymers with data from ref 19.

We can only speculate on the role of the functional groups, but the double bond and carbonate groups in the repeating unit are supposedly the key to the high affinity of CO_2 to the polymer. At elevated temperatures, the typical increase of permeability is observed for all gases except for CO_2 that remains at nearly the same level even at 80 °C (Fig. 4-2d). This behaviour results in decreasing selectivities for carbon capture applications as illustrated for the gas pairs CO_2/N_2 and CO_2/CH_4 in Fig. 4-2e and thus higher process temperatures should be avoided. Since the other gas pairs H_2/N_2 and O_2/N_2 are giving selectivities that are surpassed by many other materials and the H_2 and O_2 permeabilities are not as significant[18], this paragraph focuses on the preferential transport of CO_2 and a comparison to established and state-of-the-art polymeric materials for the CO_2/N_2 separation (carbon capture in fuel and flue gas) is drawn here. The CO_2 permeability of PLimC is about one order of magnitude higher than that of standard BPA-PC and even 100 times more permeable than PMMA (Table 4-3)[37,38]. Compared to state-of-the-art membrane materials like the PIM-1 or PTMSP, though, PLimC performs lower by two or even three orders of magnitude, respectively. The lower permeability is probably connected to the smaller cavities in the aliphatic PC that were determined by positron annihilation lifetime spectroscopy (PALS). For PLimC we found a monomodal cavity radius (r_c) distribution with a maximum at 3.3 Å (see Fig. 4-2c, Supplementary Fig. 4-3a and Supplementary Table 4-1), while PIM-1 and PTMSP exhibit a bimodal r_c distribution with small cavities ($r_c < 3$ Å) and a set of large cavities ($r_c > 5$ Å)[39]. These large interconnected cavities are most likely responsible for the very high permeabilities of PIM-1 and PTMSP. However, they tend to collapse upon utilization of the materials as membranes, which eventually leads to deteriorating performance, i.e. aging, a major challenge in polymeric membrane technology. The collapse of cavities can be attributed to the relaxation of polymer chains into a thermodynamically favoured packing, as the production of the membranes from those high-T_g polymers (both PIM-1 and PTMSP decompose before softening)[32,33] is based on solution casting (volatile solvents can increase cavity sizes and interconnectivity of cavities of the resulting polymer film)[39]. PLimC is solution/heat-processable and shows a similar cavity size in both cases (see Supplementary Fig. 4-3b). Thus, for this PC a long-term stability of gas transport properties is anticipated, which is subject of further studies on the material. The significantly larger cavities of PLimC compared to BPA-PC ($r_c = 2.9$ Å) can be assigned to the rather contorted backbone of the alicyclic structure being bridged via the carbonate group in the *1,2*-position of the ring rather than the *1,4*-position (*para-*

position in bisphenol A, see Fig. 4-1d). Furthermore, the bulky *iso*-propylene moiety of PLimC might have a significant impact on the packing density.

To elucidate the structure-properties relationship, a simulation of PLimC chains in an amorphous unit cell is shown in Fig. 4-2b. Ten chains with eight limonene carbonate repeating units each have been allowed to pack in the cell that was subsequently overlaid with a calculation of the CONNOLLY surface (blue). These blue voids represent the free volume (cavities) in the polymer matrix that can also be quantified in a semi-empirical approach by BONDI's group contribution theory[40,41]. In this approach the repeating unit of the polymer is disassembled into fragments (groups) of known volumetric properties and after addition of each fragment's contribution, correlated to the bulk density of the polymer. The resulting value gives an estimate of the so-called fractional free volume (FFV) in a polymer, thus the volume that is not occupied by any molecules. PLimC has a FFV of 0.24 (see Supplementary Table 4-2), similar to the microporous PIM-1 (0.26)[32,39,42] and significantly higher than standard thermoplastics like BPA-PC (0.16)[17,43] though much lower than the high free-volume polymer PTMSP (0.29)[37,44] as shown in Table 4-1. Together with the PALS data a consistent picture for the high permeability of PLimC is drawn. In fact, the data is even suggesting a long-term stability of the cavity size due to hindered packing of the bulky and contorted polymer chains.

The most common technique for the visualization of the benchmarking of new membrane materials is a plot of the selectivity for a given gas pair versus the permeability of the gas in the numerator on a double logarithmic scale[45]. Such a so-called ROBESON-plot for the gas pair CO_2/N_2 is shown in Fig. 4-2g with a selection of commercial and state-of-the-art polymeric membrane materials compared with PLimC[18,19,46,47]. The dashed line illustrates the ROBESON upper bound that was found empirically by Robeson in 2008, indicating the inherent trade-off between permeability and selectivity[48]. Obviously, materials with an appreciable permeability (>10 barrer) that are close to or even beyond this upper bound are of great industrial interest, as they push the boundaries towards a more economical situation, where the overall gas transport through the membrane is improved without substantial sacrifices of the selectivity or vice versa. PLimC cannot surpass the upper bound and numerous polymers have been developed in the laboratory, which perform better in regard of separation properties (for a more comprehensive discussion of state-of-the-art polymeric membranes we would like to refer to reviews by Du *et al.* and Bernardo *et al.*)[19,20].

However, the here presented material is superior to most commercial polymers in this CO_2/N_2 diagram and application as membrane for carbon capture processes is anticipated if long-term stability of the material and the performance for mixed gases are verified. This long-term stability is a major and unfortunately frequent problem of polymeric membranes as the rearrangement, that is, relaxation of polymer chains into a closer packing results in a deteriorating separation performance[20]. The relaxation pathways can be accessible by plasticization effects induced by polar gases like CO_2 or accelerated thermal motion into a thermodynamically more favoured state.

Table 4-1 | Volumetric and transport properties of selected barrier and membrane materials.

polymer	ρ	FFV[a]	r_c[b]	\multicolumn{5}{c}{P}	α	ref
				CO_2	CH_4	N_2	O_2	H_2	CO_2/N_2	
	(g cm^{-3})		(Å)	(barrer)		
PMMA	1.20	0.12	2.4	0.78	0.006	0.01	0.23	4.5	78	38,45
BPA-PC	1.20	0.16	2.9	6.8	0.27	0.33	1.6	13	21	37,43
PLimC	1.08	0.24	3.3	68	5.8	3.5	13	75	22	-
PIM-1	1.08	0.26	2.9; 5.3[c]	6500	430	340	1300	3600	19	42
PTMSP	0.76	0.29	2.6; 6.2[c]	47000	29900	11500	14800	24800	4.1	39

[a]calculated using BONDI's group contribution theory, [b]determined by PALS experiments, [c]PIM-1 and PTMSP exhibit a bimodal cavity size distribution, i.e. two values are given here

In contrast to this aging, PLimC shows an interesting behaviour when exposed to permeation test with different gases and increasing temperature (see Supplementary Figs 4-1 and 4-2). In fact, the permeability and selectivity for CO_2 are improved upon such an annealing at elevated temperature. Consequently, the material can be considered to exhibit an anti-aging behaviour that differs from that of thermally rearranged polymers, which show increased permeability upon rearrangement of the backbone (covalent bonds are destroyed and rebuild)[46]. For PLimC no chemical changes were observed after the annealing and rather a recovery of the original permeability was found upon storing the sample for a week at ambient conditions. Hence, the effect is rather ascribed to a heat-induced increased interconnectivity of cavities in the polymer matrix due to polymer chain rearrangements. This explanation is supported by PALS measurements, where the annealing of PLimC at 85 °C for 6 h lead to a broader size distribution of the cavities, that is, an increased dispersion of τ_3 (see Fig. 4-2c and Supplementary Fig. 4-3). Furthermore,

the 'anti-aging' effect if much more pronounced for the permeabilities of the small molecules H_2 and CO_2. This observation suggests a bottle-neck shaped interconnectivity, resulting in an improved selectivity for those gases with a small kinetic radius (see Fig. 4-2f). Future studies will focus on the exploitation of this effect to improve membrane characteristics of PLimC even further.

PLimC – a breathing glass

The concept of breathable materials that repel liquids or dirt is known from fabrics like Gore-Tex™ etc. Here we would like to expand the concept of breathability to dense and highly transparent polymer sheets, as we found that PLimC is ten times more permeable to gases than BPA-PC[37] and even two orders of magnitude more permeable than PMMA[38] (not to mention the prevalent glass for window panes, bottles etc., the inorganic soda-lime glass, which is virtually a barrier to gases, see Table 4-2). The special profile of properties of PLimC, considering its high permeability to gases and light combined with good mechanical and thermal resistance, suggest applications as 'breathing glass'. The thermoplastic is an optically pure and mechanically robust material and thus state-of-the-art membrane materials have not been considered for this assessment, as they are – to the best of our knowledge – either coloured or even opaque, not melt-processable, expensive and/or do not possess sufficient mechanical strength[33,49–51]. We envision PLimC[30] as breathing glass for window panes in well-insulated houses (so-called passive houses)[52] or greenhouses (so-called closed greenhouses)[53,54] to avoid excessive ventilation and the accompanied heat or water loss, respectively. Due to the inherent breathability of a glass made of PLimC, the gas concentrations of the interior and the exterior are moving towards equilibrium as one of the gases is consumed or produced. A schematic of such an application as glazing in both a passive house and a closed greenhouse is shown in Fig. 4-3. The underlying concept in both cases is a very thoroughly heat-insulated cladding (roofing, walling, doors and windows) that limits overall heat-loss and thus saves substantial amounts of energy. In order to supply resident/plants with fresh air (residents exhale CO_2 that has to be removed, plants need CO_2 for photosynthesis that the leafs have to be provided with) in such closed/passive constructions, there is a constant requirement for active ventilation to realize complete exchange of air within hours (passive houses)[55] or even within minutes (closed greenhouses)[54].
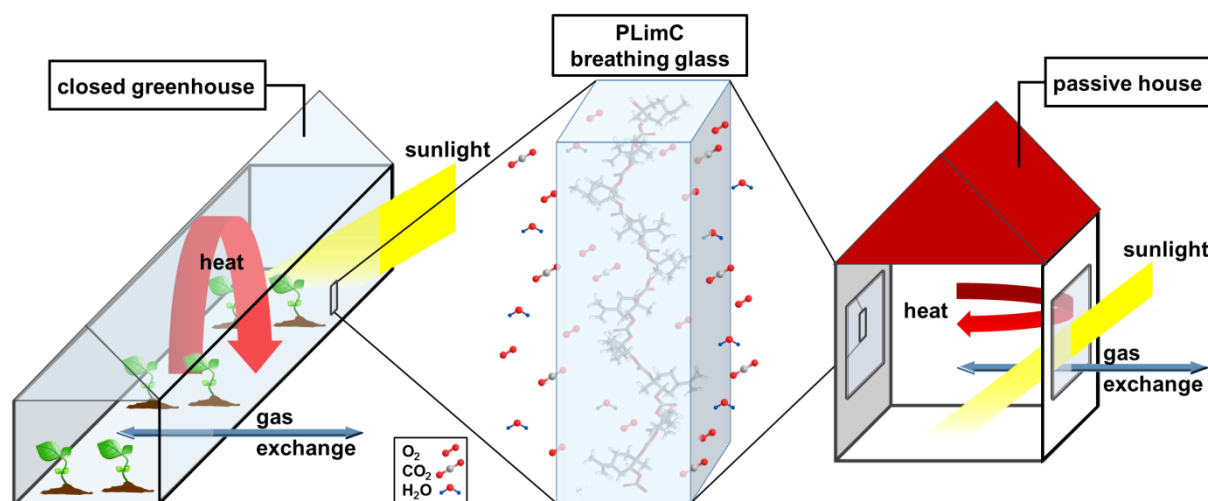
Figure 4-3 | PLimC as breathing glass. A schematic of the highly permeable glazing material is shown that can be used for window panes in passive houses to reduce energy consumption or as glazing sheets for greenhouses to reduce water losses due to continuous ventilation. An estimation of the CO_2-respiration rate of plants and humans in greenhouses or passive houses, respectively, is compared to the permeance of the corresponding glazing area is given in Table 4-2.

Obviously, during colder days – and there exist many in northern Europe – with outside temperatures below 20 °C the exchange of hot air from inside with cold air from outside is accompanied by an enormous loss of heat and thus energy. Hence, the mandatory ventilation systems are equipped with heat recovery devices to reduce energy losses that would otherwise contradict the whole concept of those well-insulated buildings.

Table 4-2 | Comparison of PLimC with typical glazing materials.

property	PLimC	BPA-PC	PMMA	soda-lime glass
permeability				
$\quad CO_2$ (barrer)[c]	68	6.8	0.85	-
$\quad O_2$ (barrer)[c]	12	1.6	0.24	-
$\quad H_2O$ vapour (g mm atm^{-1} m^{-2} d^{-1})	11[d]	4.4	0.005	-
T_g (°C)	130	150	105	573
transmittance (%)	92	90	92	90
refractive index (589 nm, 25 °C)	1.501	1.587	1.491	1.518
specific gravity (g cm^{-3})	1.08	1.20	1.19	2.52
impact resistance[a] (J)	2.00	3.33	0.55	0.33
hardness[b]	B	8B	4H	10H
thermal conductivity (W K^{-1} m^{-1})	0.15	0.20	0.19	1.05

[a]tested in a ball drop experiment on specimen with 2.0 mm thickness and an area of 100 x 100 mm² [b]tested with pencil hardness tester (ranging from 10B being the softest and 10H being the hardest grade on the scale) [c]tested at 30 °C and 100 kPa pressure difference, 1 barrer = 10^{-10} cm³ cm cm^{-2} s^{-1} cmHg^{-1} [d]measured at 50% relative humidity and 22 °C in a constant-pressure setup.

Now, what if there was a way to avoid of such expensive, energy- and maintenance-intensive equipment by rendering the passive house really passive? With a gas permeable glazing like PLimC, the supply with fresh air can occur through this material with – ideally – no need of an active ventilation system. A rough estimate for the counterbalancing of CO_2 levels in passive houses and greenhouses, respectively, each with a PLimC glazing is given in Table 4-3 (and Supplementary Tables 4-3 and 4-4). Not O_2 but only CO_2 and was considered for the calculation as it is the limiting factor in both applications:

- The concentration of CO_2 in the atmosphere of 400 ppm (equals to a partial pressure of 0.04 kPa) is rather low compared to O_2 with about 21% (equals to a partial pressure of 21 kPa) and the permeation through a membrane is directly proportional to the partial pressure difference.

- CO_2 has the higher toxicity at relatively low concentrations, that is, the 5% that we have employed as concentration in the calculation for the passive house can already cause headaches and it should be regarded as upper limit.

The parameters that the estimation is based on are the area and thickness of the glazing, the partial pressure difference between interior and exterior due to respiration, the respiration type (exhaling of CO_2 by residents in a passive house; uptake of CO_2 by plants), the respiration rate[56] and the permeance (P multiplied by the thickness of the membrane; depends on the area and thickness of the glazing and the partial pressure difference of CO_2) of the corresponding PLimC glazing. The numbers were chosen in order to draw a realistic picture of the requirements for each application and the last two values, that is, the respiration rate of the residents/plants and permeance of the glazing are the decisive parameters. The resident in the passive house has a respiration rate of 41 g[CO_2] h^{-1} while the 20 m^2 PLimC glazing could compensate for 1.0 g[CO_2] h^{-1} or 2.5%. In the case of the closed greenhouse, a 500 m^2 large and 0.1 mm thick PLimC cover can account for 0.4 g[CO_2] h^{-1}, whereas the cultivation are of 200 m^2 has a demand of 400 g[CO_2] h^{-1} or, in other words, the demand outweighs the supply by a factor of 1000.

Table 4-3 | Estimation of CO_2 counterbalancing in PLimC-glazed passive and greenhouses.

	passive house	closed greenhouse
area of glazing (m^2)	20	500
thickness of glazing (mm)	1.0	0.1
partial pressure difference CO_2 (kPa)	5.0[a]	0.02
respiration type	exhalation of resident	uptake by plants (200 m^2)
respiration rate[b] (g[CO_2] h^{-1})	41	400
permeance of PLimC glazing[c] (g[CO_2] h^{-1})	1.0	0.4

[a]the partial pressure of 5.0 kPa corresponds to 5% CO_2 in the atmosphere, which is already a value where a headache can occur when exposed to for a longer time [b]values taken from reference [56], [c]calculated from $P(CO_2)$ of PLimC of 68 barrer.

For the greenhouse there is a great obstacle to this natural breathing of the glass due to the inherently low partial pressure difference upon consumption of the gas, e.g. a difference of only 0.02 kPa upon bisection of the atmospheric CO_2 concentration of 400 ppm to 200 ppm (actually most plants prefer higher CO_2 level than 400 ppm). Consequently, the application of PLimC glass in greenhouses is techno-economically less realistic than application of this material in passive houses. Although this first assessment of PLimC as breathable glazing displays only 2.5% compensation of the CO_2 exhaled by the resident of the passive house, **the concept's feasibility is proven. We do not claim to have found ideal parameters for such** an application and therefore we still see a great potential of improvement from both the material scientist's and the engineer's point of view. To be more specific, a material with enhanced gas permeability and a larger and thinner glazing are highly desirable as they contribute proportionally to an increased permeance. Nevertheless, PLimC in its original form is already a very promising candidate, as breathability (ten times more permeable to CO_2, O_2 and H_2O than BPA-PC) and thermal insulation are given and the overall performance as glazing material is outstanding.

After introducing the concept of breathing glasses, we would like to comment on the feasibility of applying PLimC as a window pane by comparing it with the typical glazing materials PMMA, BPA-PC and soda-lime glass. The performance of those materials in (glazing-) relevant physical, mechanical and transport properties was assessed and visualized in the radar chart in Fig. 4-4 (on a scale of 0 to 10, for the worst to the best performance, respectively, with 0 being the centre of the chart; assessment is based on values given in Table 4-2, except for processability, which is based on stability of the melts and the temperatures involved during processing, that is, a correlation with T_g is present). Without commenting on every detail of the plot, it becomes obvious that PLimC covers the

largest area of this chart due to its very balanced profile of properties and the extraordinary permeability of CO_2 (68.0 barrer). In contrast to this transparent membrane, soda-lime glass (no detectable permeability) and PMMA (0.85 barrer) are rather barriers for gases, while BPA-PC (6.8 barrer) is still one order of magnitude less permeable than PLimC. For consideration as a window pane, another important parameter is the mechanical robustness, as a hit on the surface should not shatter the glass immediately. The four materials have been exposed to a ball drop experiment (see methods section and Supplementary Fig. 4-4), with a steel ball of 250 g being released from different heights onto a 1.5 mm thick sheet of the material. The experiment gives valuable information regarding the impact resistance of a material and – as expected – soda-lime glass shatters at very low energies of impact (0.3 J). Among the plastics, PMMA (0.5 J) is known to be rather brittle, while BPA-PC (3.3 J) is one of the most impact resistant polymers on the market. Surprisingly, its aliphatic counterpart PLimC (2.0 J) is only 40% less resistant to the ball impact and four times stronger than PMMA and of course much stronger than soda-lime glass. This property together with a superior hardness to BPA-PC (Table 4-2) would justify an application of PLimC as glazing material. In combination with the high permeability the application as a breathing glass becomes obvious if not compulsory. In order to meet requirements of a passive house, the insulating performance of the windows is another important factor to be considered.
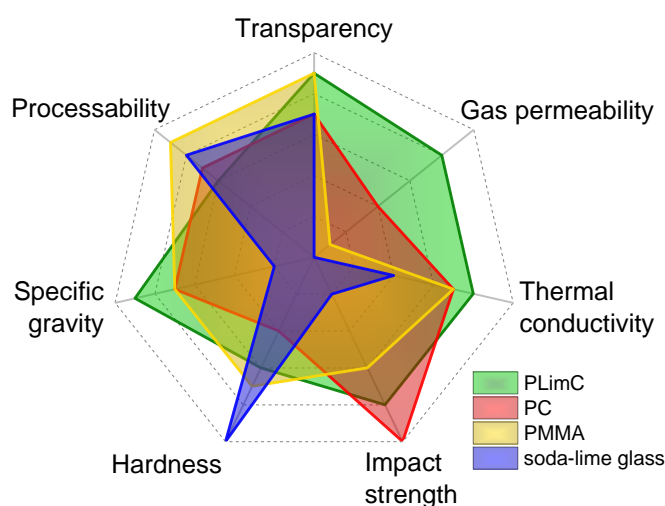
Figure 4-4 | Performance of typical glazing materials. The radar chart illustrates the relative performance of PLimC to the popular glazing materials BPA-PC, PMMA and soda-lime glass in various properties that are relevant for the application as glazing materials (assessment is based on values given in Table 4-2; the processability was assessed with respect to the stability of the melt during processing and is not directly correlated to the T_g of the materials).

Here, PLimC can benefit from the inherently low thermal conductivity of plastics, as it exhibits a seven times lower thermal conductivity (0.15 W K^{-1} m^{-1}) than soda-lime glass (1.05 W K^{-1} m^{-1}). As a consequence, the need for highly sophisticated constructions such as triple-glazing is reduced. The material and manufacturing costs have been omitted on purpose, since for PLimC no industrial process has been developed yet. The great availability of the bio-based raw material limonene (500 kt a^{-1} from orange peel)[57] and CO_2 (32 Gt a^{-1}, anthropogenic emission)[2] should eventually result in a competitive pricing of PLimC on the market. Minor drawbacks of the aliphatic PC are the low degree of hardness and the poor processability (was assessed with respect to the stability of the melt during processing). The first could be tackled by using a highly permeable hard coating, while the latter is still to be solved in a concerted chemistry/engineering approach. However, by reminding the reader of the concept of breathability of the glazing, we anticipate for PLimC that the additional value outweighs the efforts to overcome the obstacles towards the final product by far.

4.3 Outlook

The high CO_2 permeability of PLimC together with a significant selectivity for the gas suggest applications as a membrane material for carbon capture in fuel and flue gases. Compared to commercial membrane materials, PLimC is superior. The anti-aging effect, leading to an increased CO_2 permeability upon prolonged exposure to higher temperatures, might still be advantageous to the high-permeability materials that usually suffer from deterioration performance upon prolonged usage. Future work will focus on the chemical modification of PLimC – as we could show the great versatility before – to improve membrane characteristics even further. In addition to the application as a membrane, the unique profile of properties of PLimC with its excellent mechanical, optical and thermal performance renders it a breathing glass. The application of this new concept to well-insulated constructions such as passive houses, leads to a substantial reduction of heat consumption, as ventilation occurs passively through the windows made of PLimC and there is no need for sophisticated and expensive ventilation system with heat recovery units. The presented calculations suggest that the breathing glass can compensate for a part of the consumed (CO_2-enriched) air and breathability could be improved even further by optimizations of the material and its processing. We are convinced that the concept of

breathing glass is not limited to the here-discussed applications and we are very excited to find new areas of utilization of PLimC.

4.4 Methods

Materials and instrumentation

BPA-PC (Makrolon™ 2800) and PMMA (Plexiglas™ 8H) were used as received. PLimC[30], PMenC and PLimC-ME[31] were synthesized according to literature procedures. The thermal conductivity was measured with a Lasercom FOX 40 (software: WinTherm 50) on specimen with 1.5 mm thickness and polystyrene as reference material. The upper and lower plate temperatures were set to 30 and 20 °C, respectively. The mechanical strength of PLimC was tested in a ball drop experiment with 38 mm steel ball that was dropped onto 2 x 100 x 100 mm³ sheets from various heights through a transparent pipe. The polymer sheets had been hot pressed at adequate temperature (140 °C of pre-shaped by solvent casting and pre-dried specimen of PLimC, 190 °C for PMMA and 240 °C for pre-dried BPA-PC) and fixed in a wooden frame (see Supplementary Fig. 4-4). In the frame, the sheets were supported by rubber on both sides to avoid tension/influences by direct contact between wood and specimen. The stability was compared to PMMA (Plexiglas® 8H, Evonik), PC (Makrolon® 2800, Covestro) and standard soda-lime glass.

Permeability tests

Single gas permeability of N_2, O_2, CH_4, H_2 and CO_2 through the prepared membranes were determined via the constant volume, variable pressure ("time lag") method. The feed pressure was 100 kPa for all the gases. Each measurement was repeated three times and for each sample. Permeability (P), diffusivity (D) and solubility (S) were determined in the temperature range of 30–80 °C from the obtained pressure increase curves using the following equations:

$$P = D \times S = \frac{V_p l}{ART\Delta t} ln \frac{p_f - p_{p1}}{p_f - p_{p2}} \tag{4-1}$$

$$D = \frac{l^2}{6\theta} \tag{4-2}$$

where V_p is the permeate volume, l is the membrane thickness, A is the membrane area, R is the gas constant, p_f is the feed pressure (considered constant) in the time range Δt, p_{p1}

and p_{p2} are permeate pressures at two given times in the region of linear increase, Δt is the time difference between two points on the time-pressure-curve and θ is the time lag.

The ideal selectivity of the membranes is determined according to the following equation.

$$\alpha(A/B) = \frac{P_A}{P_B} \qquad (4\text{-}3)$$

where α(A/B) is the ideal selectivity, and P_A and P_B are single gas permeabilities of the two gases A and B, respectively.

Simulation of an amorphous cell of PLimC

A simulation of an amorphous unit cell of PLimC was carried out with the software Materials Studio (BIOVIA) using molecular dynamics. The cell was filled with eight chains each of ten repeating units and the Connolly surface (blue) was calculated. The parameters for the simulation are the density of PLimC of 1.08 g cm^{-3}, a Connolly radius of 1.0 Å and a grid interval of 0.4 Å.

PALS experiments

PALS measurements were performed using a digital lifetime spectrometer system with a time resolution of 169 ps and the data were analysed using LT9[58]. PALS spectra are composed of three lifetimes that can be extracted by a nonlinear least-squares fit of a weighted sum of exponentials:

$$N(t) = \sum_{i=1}^{k+1} \frac{I_i}{\tau_i} exp\left(-\frac{t}{\tau_i}\right) \qquad (4\text{-}4)$$

where τ_i denotes the mean lifetime of the positron state i and I_i is the relative intensity of the lifetime component. A component with lifetime longer than 2 ns is absolutely attributed to ortho-positronium (o-P$_s$). The o-P$_s$ wave function has a penetration depth of ΔR into the material surrounding the potential well and is equal to the thickness of the electron layer, which is approximately 1.656 Å. If the radius of the well is R, using quantum mechanics the o-P$_s$ pick-off lifetime can be related to the radius of the cavity. Eq. 4-5 provides the relationship between R and τ_3.

$$\tau_3 = \frac{1}{2}\left[1 - \frac{R}{R+\Delta R} + \frac{1}{2\pi} sin\left(\frac{2\pi R}{R+\Delta R}\right)\right]^{-1} \qquad (4\text{-}5)$$

Calculation of the fractional free volume of PLimC

The fractional free volume of an amorphous polymer can be calculated using Eq. 4-6:

$$FFV = \frac{V_f}{V_s} = \frac{(V_{sp} - 1.3 V_{W,s})}{V_{sp}} \qquad (4\text{-}6)$$

The free volume V_f can be expressed mathematically as the difference of the specific volume V_{sp} and the specific van der Waals volume $V_{W,s}$ (has to be multiplied by 1.3 beforehand, to compensate for the molecular steric demand of the polymer chains). $V_{W,s}$ is deduced from the sum of the van der Waals volumes of the individual fragments $V_{W,i}$ shown in Supplementary Table 4-2 divided by their fragmental molar mass M_i. The fragmentation was performed in accordance with BONDI's group contribution theory.[40,41]

Acknowledgements

4.5 References

1. Forster, P., Ramaswamy, V. & Artaxo, P. *Fourth assessment report of the intergovernmental panel on climate change; Chapter 2: changes in atmospheric constituents and in radiative forcing.* (2007).

2. Kaspar, F., Meinshausen, M. & Schulz, M. *Fifth assessment report of the intergovernmental panel on climate change; Chapter I: the physical science basis.* (2013).

3. Haszeldine, R. S. Carbon capture and storage: how green can black be? *Science* **325,** 1647–1652 (2009).

4. **D'Alessandro, D. M., Smit, B. & Long,** J. R. Carbon dioxide capture: prospects for new materials. *Angew. Chemie Int. Ed.* **49,** 6058–6082 (2010).

5. Markewitz, P. *et al.* Worldwide innovations in the development of carbon capture technologies and the utilization of CO_2. *Energy Environ. Sci.* **5,** 7281–7305 (2012).

6. Boot-Handford, M. E. *et al.* Carbon capture and storage update. *Energy Environ. Sci.* **7,** 130–189 (2014).

7. Li, J.-R. *et al.* Carbon dioxide capture-related gas adsorption and separation in metal-organic frameworks. *Coord. Chem. Rev.* **255,** 1791–1823 (2011).

8. Rochelle, G. T. Amine Scrubbing for CO_2 Capture. *Science* **325,** 1652–1654 (2009).

9. Zevenhoven, R. & Fagerlund, J. *Developments and innovation in carbon dioxide (CO_2) capture and storage technology.* (Woodhead Publishing Series in Energy Vol. 2, 2010).

10. Vaidya, P. D. & Kenig, E. Y. CO_2-alkanolamine reaction kinetics: a review of recent studies. *Chem. Eng. Technol.* **30,** 1467–1474 (2007).

11. Yu, T. *et al.* Improving thermal stability of biodegradable aliphatic polycarbonate by metal ion coordination. *Polym. Degrad. Stab.* **94,** 253–258 (2009).

12. Guo, H., Zhu, G., Hewitt, I. J. & Qiu, S. 'Twin copper source' growth of metal–organic framework membrane: $Cu_3(BTC)_2$ with high permeability and selectivity for recycling H_2. *J. Am. Chem. Soc.* **131,** 1646–1647 (2009).

13. Li, J.-R., Kuppler, R. J. & Zhou, H.-C. Selective gas adsorption and separation in metal–organic frameworks. *Chem. Soc. Rev.* **38,** 1477–1504 (2009).

14. McDonald, T. M. *et al.* Cooperative insertion of CO_2 in diamine-appended metal-organic frameworks. *Nature* **519,** 303–308 (2015).

15. Abetz, V. *et al.* Developments in membrane research: From material via process design to industrial application. *Adv. Eng. Mater.* **8,** 328–358 (2006).

16. Ebner, A. D. & Ritter, J. A. State-of-the-art adsorption and membrane separation processes for carbon dioxide production from carbon dioxide emitting industries. *Sep. Sci. Technol.* **44,** 1273–1421 (2009).

17. Yampolskii, Y. Polymeric gas separation membranes. *Macromolecules* **45,** 3298–3311 (2012).

18. Ismail, A. F., Chandra Khulbe, K. & Matsuura, T. *Gas Separation Membranes.* (Springer International Publishing, 2015). doi:10.1007/978-3-319-01095-3

19. Du, N., Park, H. B., Dal-Cin, M. M. & Guiver, M. D. Advances in high permeability polymeric membrane materials for CO_2 separations. *Energy Environ. Sci.* **5,** 7306–7322 (2012).

20. Bernardo, P., Drioli, E. & Golemme, G. Membrane gas separation: a review/state-of-the-art. *Ind. Eng. Chem. Res.* **48,** 4638–4663 (2009).

21. May, F. CO_2 storage in geological rock formations. *VGB PowerTech* **85,** 32–37 (2005).

22. Peters, M. *et al.* Chemical technologies for exploiting and recycling carbon dioxide into the value chain. *ChemSusChem* **4,** 1216–1240 (2011).

23. Quadrelli, E. A., Centi, G., Duplan, J.-L. & Perathoner, S. Carbon dioxide recycling: emerging large-scale technologies with industrial potential. *ChemSusChem* **4,** 1194–1215 (2011).

24. Inoue, S., Koinuma, H. & Tsuruta, T. Copolymerization of carbon dioxide and epoxide with organometallic compounds. *Die Makromol. Chemie* **130,** 210–220 (1969).

25. Coates, G. W. & Moore, D. R. Discrete metal-based catalysts for the copolymerization of CO_2 and epoxides: discovery, reactivity, optimization, and mechanism. *Angew. Chemie Int. Ed.* **43,** 6618–6639 (2004).

26. Lu, X.-B. & Darensbourg, D. J. Cobalt catalysts for the coupling of CO_2 and epoxides to provide polycarbonates and cyclic carbonates. *Chem. Soc. Rev.* **41,** 1462–1484 (2012).

27. Byrne, C. M., Allen, S. D., Lobkovsky, E. B. & Coates, G. W. Alternating copolymerization of limonene oxide and carbon dioxide. *J. Am. Chem. Soc.* **126,** 11404–11405 (2004).

28. Peña Carrodeguas, L., González-Fabra, J., Castro-Gómez, F., Bo, C. & Kleij, A. W. Al III-catalysed formation of poly(limonene)carbonate: DFT analysis of the origin of stereoregularity. *Chem. - A Eur. J.* **21,** 6115–6122 (2015).

29. Li, C., Sablong, R. J. & Koning, C. E. Synthesis and characterization of fully bio-based α,ω-dihydroxyl poly(limonene carbonate)s and their initial evaluation in coating applications. *Eur. Polym. J.* **67,** 449–458 (2015).

30. Hauenstein, O., Reiter, M., Agarwal, S., Rieger, B. & Greiner, A. Bio-based polycarbonate from limonene oxide and CO_2 with high molecular weight, excellent thermal resistance, hardness and transparency. *Green Chem.* **18,** 760–770 (2016).

31. Hauenstein, O., Agarwal, S. & Greiner, A. Bio-based polycarbonate as synthetic toolbox. *Nat.*

Commun. **7,** (2016). doi:10.1038/ncomms11862

32. Budd, P. M. *et al.* Solution-processed, organophilic membrane derived from a polymer of intrinsic microporosity. *Adv. Mater.* **16,** 456–459 (2004).

33. Ichiraku, Y., Stern, S. A. & Nakagawa, T. An investigation of the high gas permeability of poly(1-trimethylsilyl-1-propyne). *J. Memb. Sci.* **34,** 5–18 (1987).

34. McKeen, L. W. & McKeen, L. *Permeability properties of plastics and elastomers.* (Elsevier, 2012). doi:10.1016/B978-1-4377-3469-0.10018-9

35. Allen, S. M., Fujii, M., Stannett, V., Hopfenberg, H. B. & Williams, J. L. The barrier properties of polyacrylonitrile. *J. Memb. Sci.* **2,** 153–163 (1977).

36. Wijmans, J. G. & Baker, R. W. The solution-diffusion model: a review. *J. Memb. Sci.* **107,** 1–21 (1995).

37. Hellums, M. W., Koros, W. J. & Schmidhauser, J. C. Gas separation properties of spirobiindane polycarbonate. *J. Memb. Sci.* **67,** 75–81 (1992).

38. Akai, Y. N., Oshimizu, H. Y. & Sujita, Y. T. Enhancement of gas permeability in HPC , CTA and PMMA under microwave irradiation. *Polym. J.* **38,** 376–380 (2006).

39. Staiger, C. L., Pas, S. J., Hill, A. J. & Cornelius, C. J. Gas separation, free volume distribution, and physical aging of a highly microporous spirobisindane polymer. *Chem. Mater.* **20,** 2606–2608 (2008).

40. Bondi, A. Van der Waals volumes and radii. *J. Phys. Chem.* **68,** 441–451 (1964).

41. Van Krevelen, D. W. & Te Nijenhuis, K. *Properties of Polymers - Their Correlation with Chemical Structure; Their Numerical Estimation and Prediction from Additive Group Contributions.* (Elsevier, 2009). doi:10.1016/B978-0-08-054819-7.00043-1

42. Thomas, S., Pinnau, I., Du, N. & Guiver, M. D. Pure- and mixed-gas permeation properties of a microporous spirobisindane-based ladder polymer (PIM-1). *J. Memb. Sci.* **333,** 125–131 (2009).

43. Dlubek, G. *et al.* The free volume in two untreated, pressure-densified, and CO_2 gas exposed polymers from positron lifetime and pressure-volume-temperature experiments. *e-Polymers* **108,** 1–20 (2007).

44. Nagai, K., Masuda, T., Nakagawa, T., Freeman, B. D. & Pinnau, I. Poly[1-(trimethylsilyl)-1-propyne] and related polymers: synthesis, properties and functions. *Prog. Polym. Sci.* **26,** 721–798 (2001).

45. Robeson, L. M. Correlation of separation factor versus permeability for polymeric membranes. *J. Memb. Sci.* **62,** 165–185 (1991).

46. Park, H. B. *et al.* Polymers with cavities tuned for fast selective transport of small molecules and ions. *Science* **318,** 254–258 (2007).

47. Li, F. Y., Xiao, Y., Chung, T.-S. & Kawi, S. High-performance thermally self-cross-linked polymer of intrinsic microporosity (PIM-1) membranes for energy development. *Macromolecules* **45,** 1427–1437 (2012).

48. Robeson, L. M. The upper bound revisited. *J. Memb. Sci.* **320,** 390–400 (2008).

49. Konnertz, N. *et al.* Molecular Mobility of the High Performance Membrane Polymer PIM-1 as Investigated by Dielectric Spectroscopy. *ACS Macro Lett.* **5,** 528–532 (2016).

50. Bachman, J. E., Smith, Z. P., Li, T., Xu, T. & Long, J. R. Enhanced ethylene separation and plasticization resistance in polymer membranes incorporating metal–organic framework nanocrystals. *Nat. Mater.* 1–7 (2016). doi:10.1038/nmat4621

51. Rahman, M. *et al.* Influence of poly(ethylene glycol) segment length on CO_2 permeation and stability of PolyActive membranes and their nanocomposites with PEG POSS. *ACS Appl. Mater. Interfaces* **7,** 12289–12298 (2015).

52. Feist, W., Schnieders, J., Dorer, V. & Haas, A. Re-inventing air heating: Convenient and comfortable within the frame of the passive house concept. *Energy Build.* **37,** 1186–1203 (2005).

53. Bot, G. *et al.* The solar greenhouse: state-of-the-art in energy saving and sustainable energy supply. *Acta Hortic.* **691,** 501–508 (2005).

54. Heuvelink, E., Bakker, M., Marcelis, L. F. M. & Raaphorst, M. Climate and yield in a closed greenhouse. *Acta Hortic.* **801,** 1083–1092 (2008).

55. Sartori, I. & Hestnes, A. G. Energy use in the life cycle of conventional and low-energy buildings: a review article. *Energy Build.* **39,** 249–257 (2007).

56. Nof, S. Y. *Springer Handbook of Automation.* (Springer, 2009).

57. Ciriminna, R., Lomeli-Rodriguez, M., Demma Carà, P., Lopez-Sanchez, J. A. & Pagliaro, M. Limonene: a versatile chemical of the bioeconomy. *Chem. Commun.* **50,** 15288–15296 (2014).

58. Kansy, J. Microcomputer program for analysis of positron annihilation lifetime spectra. *Nucl. Instruments Methods Phys. Res. Sect. A* **374,** 235–244 (1996).

4.6 Supplementary information

Permeability of PLimC
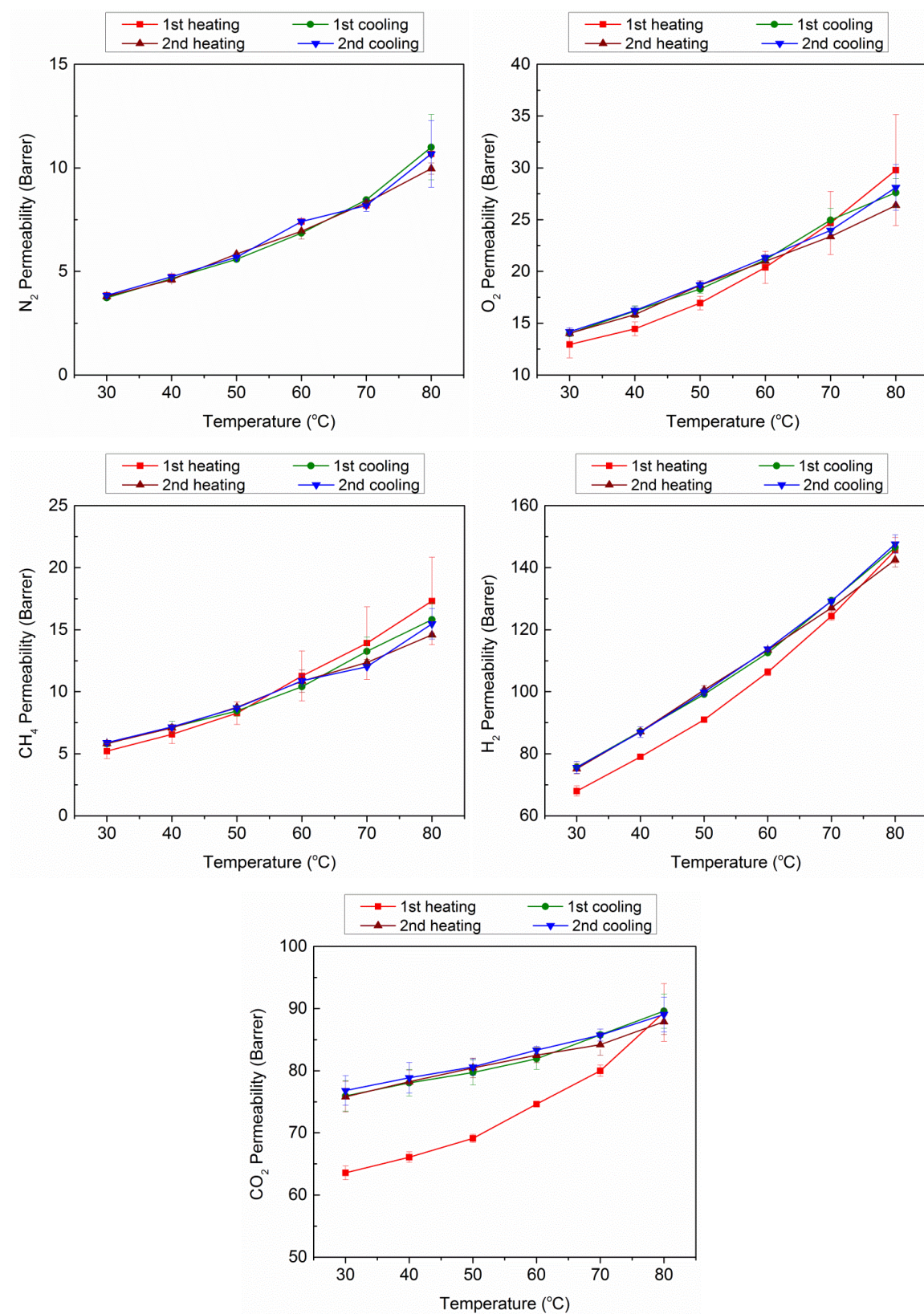
Supplementary Figure 4-1: Temperature-dependent permeability tests of PLimC with the sequence of gases: N_2, O_2, CH_4, H_2, CO_2 and N_2 (the whole measurement was repeated twice to account for reproducibility). For each temperature the sequence of gases was measured in a row before the sample was heated/cooled to the next temperature in the range from 30 to 80 °C.
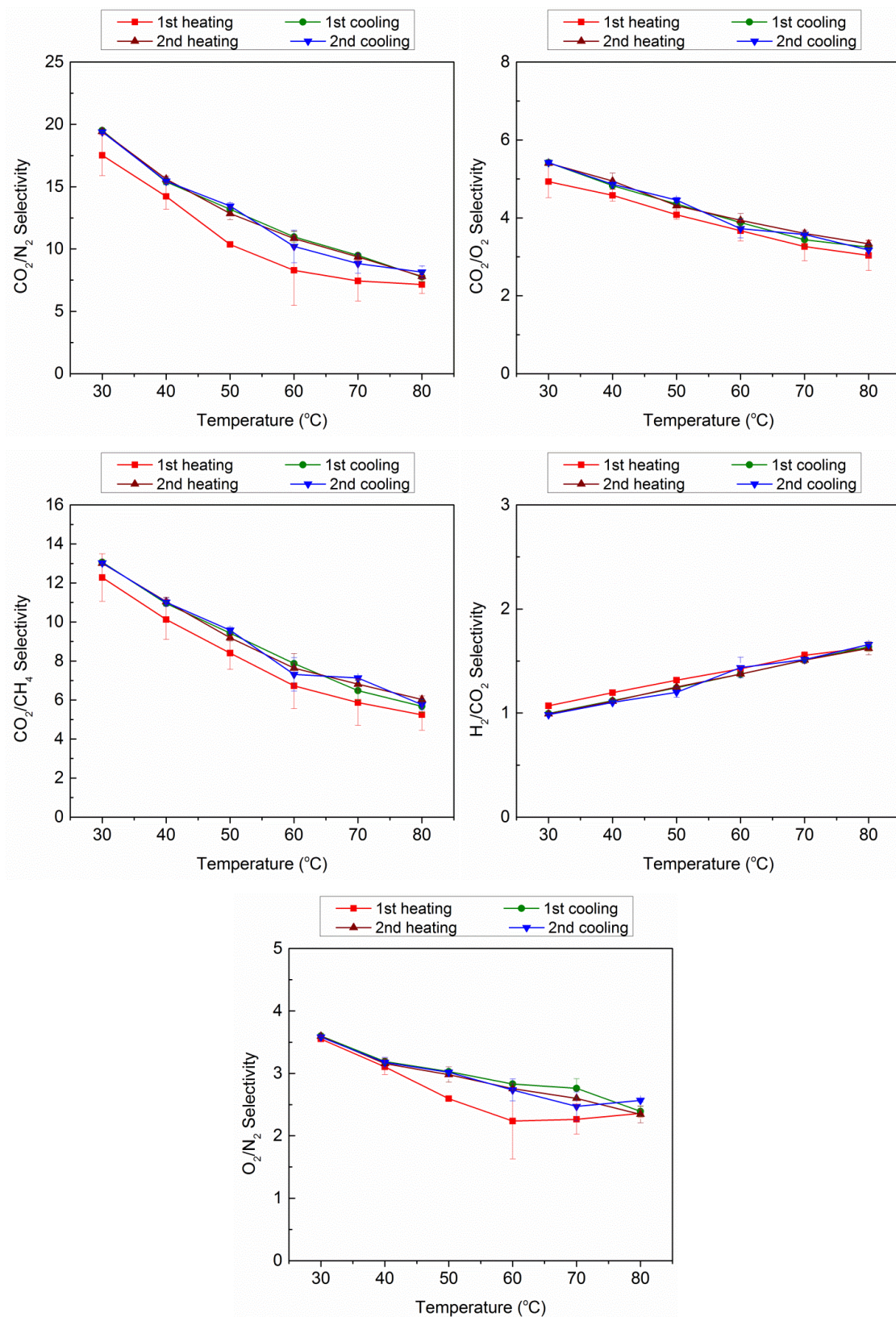
Supplementary Figure 4-2: Temperature-dependent ideal selectivity of PLimC for the gas pairs: CO_2/N_2, CO_2/O_2, CO_2/CH_4, H_2/CO_2 and O_2/N_2, calculated from the single gas permeabilities shown in Supplementary Fig. 4-1.

Positron annihilation lifetime spectroscopy (PALS)

Supplementary Table 4-1 | PALS data of PLimC films prepared by solvent casting or heat pressing.

entry	processing	τ_3 (ns)	I_3 (%)	r_c (Å)
1	solvent	2.56	33	3.32
2	solvent	2.53	32	3.30
3	heat	2.53	34	3.30
4	heat	2.56	37	3.33
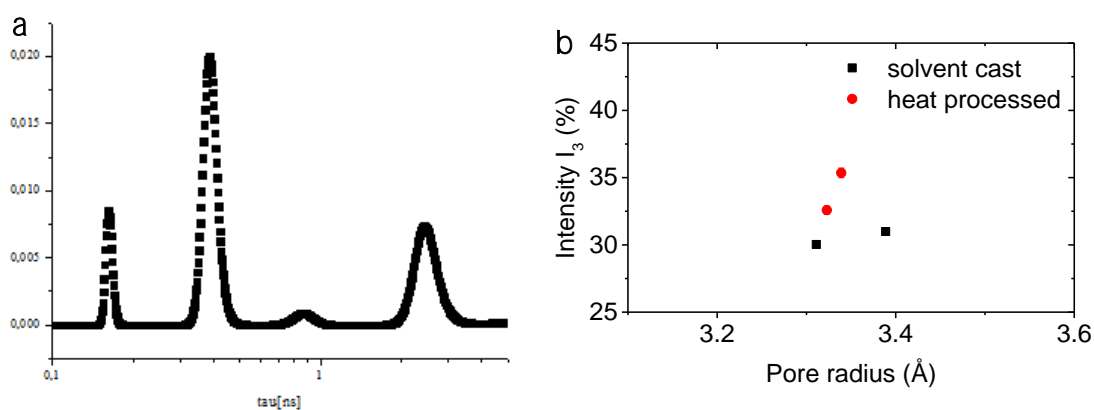
Supplementary Figure 4-3: PALS measurement with the lifetimes of P_s in a PLimC sample prepared by solvent casting (entry 1 from Supplementary Table 4-1). (b) Cavity radius in PLimC films calculated from τ_3 with the corresponding intensity I_3 of the signal. The samples were produced either by solvent casting or by heat pressing.

Calculation of the fractional free volume of PLimC

Supplementary Table 4-2 | The FFV of PLimC and reference materials.

fragment of PLimC	M_I (g/mol)	$V_{W,I}$ (cm³/mol)
	60.01	18.90
CH₃	15.03	13.67
	80.14	46.42
	41.09	27.22
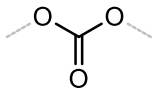
polymer	M (g/mol)	V_W (cm³/mol)	$V_{W,s}$ (cm³/g)	V_{sp} (cm³/g)	FFV (%)	ref.
PLimC	196.27	106.21	0.54	0.93	24	
PTMSP	142.23			1.33	29	[1]
PIM-1	520.62			0.93	24 - 26	[1]
BPA-PC	254.28			0.83	16	[2]

Calculation of the fractional free volume of PLimC using the Bondi's group contribution method. In the upper part the contributing fragments with their van der Waals volumes ($V_{W,i}$) are listed while the lower part shows the corresponding van der Waals volume of the repeating unit (V_W), the specific van der Waals volume ($V_{W,s}$) and the specific volume (V_s) of the polymer are shown.

Ball drop impact resistance
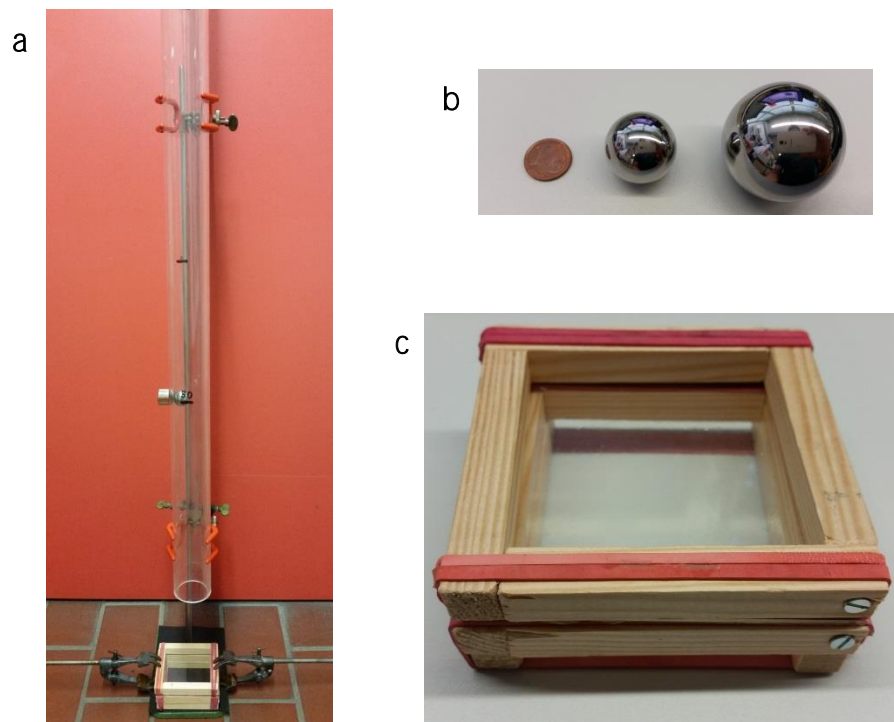
Supplementary Figure 4-4: Ball drop test with (**a**) the whole setup of 2 m transparent pipe with height marks, the steel ball hold by a magnet and the polymer specimen fixed inside a wooden frame. (**b**) The two steel balls used for testing either with 23 or 38 mm diameter. (**c**) A magnification of the 100x100 mm² wooden frame with a polymer sheet inside.

Calculation of respiration rate for glazing applications

Passive house. For the calculation of evolution and removal of CO_2 in a passive house the respiration rate (exhalation of CO_2) of an adult was assumed to be 29 g (CO_2) h^{-1}. The value is obtained for an respiration rate of 6 L min^{-1} and a CO_2 concentration of the exhaled air of 4%.[3] For the calculations shown in Supplementary Table 4-3, a glazing area of the house of 20 m^2 and a glazing thickness of 1.0 mm for a mechanically robust glass and of 0.1 mm for thin-walled glazing, were chosen. The partial pressure difference between inside and outside of the house was set for various air conditions, ranging from lethal ($\Delta p(CO_2)$=10 kPa, that is, 100 000 ppm) to domestically allowed ($\Delta p(CO_2)$=0.5 kPa, that is, 5 000 ppm) CO_2 concentrations.[4]

Supplementary Table 4-3 | PLimC as glazing material in passive houses.

air condition	$\Delta p(CO_2)$ (kPa)	thickness (mm)	permeance of glazing (g[CO_2] (20 m^{-2}) h^{-1})	permeance/respiration (%)
lethal	10	1.0	0.81	2.8
headache	5.0	1.0	0.41	1.4
headache (thin-walled)	5.0	0.1	4.1	14.1
critical	1.5	1.0	0.12	0.4
allowed	0.5	1.0	0.04	0.1

Parameters used for the calculations are $P(CO_2)$ = 68 barrer, thickness of glazing = 1.0 mm, the rate of respiration of one resident is 29 g (CO_2) h^{-1}, $\rho(CO_2)$ = 2.0 mg cm^{-3}, passive house with 20 m^2 glazing and one inhabitant.

Closed greenhouse. For the calculation of supply and demand of CO_2 in a closed greenhouse the respiration rate (uptake of CO_2 for photosynthesis) of the plants was assumed to be $2\,g\,(CO_2)\,m^{-2}\,h^{-1}$ with a total area of $200\,m^2$ of cultivation.[5] For the calculations shown in Supplementary Table 4-4, a glazing area of the house of $500\,m^2$ and a glazing thickness of 0.1 mm for a mechanically robust film and of 0.01 mm for thin-walled glazing, were chosen. The partial pressure difference between inside and outside of the house was set for various air conditions, ranging from high ($\Delta p(CO_2)$=0.01 kPa, that is, an interior CO_2-level of 300 ppm) to low ($\Delta p(CO_2)$=0.04 kPa, that is, an interior CO_2-level of 0 ppm) CO_2 concentrations.

Supplementary Table 4-4 | PLimC as glazing material in closed greenhouses.

CO$_2$ level	$\Delta p(CO_2)$ (kPa)	thickness (mm)	permeance of glazing (g[CO$_2$] (500 m^{-2}) h^{-1})	permeance/respiration (%)
high	0.01	0.1	0.20	0.05
medium	0.02	0.1	0.41	0.1
medium (thin-walled)	0.02	0.01	4.06	1.0
low	0.04	0.1	0.81	0.2

Parameters used for the calculations: $P(CO_2)$ = 68 barrer, the rate of respiration of an area of cultivation of 200 m^2 is 400 g (CO_2) h^{-1}, $\rho(CO_2)$ = 2.0 mg cm^{-3}, greenhouse with 200 m^2 cultivation and 500 m^2 glazing area.

References

1. Thomas, S., Pinnau, I., Du, N. & Guiver, M. D. Pure- and mixed-gas permeation properties of a microporous spirobisindane-based ladder polymer (PIM-1). *J. Memb. Sci.* **333,** 125–131 (2009).
2. Hellums, M. W., Koros, W. J. & Schmidhauser, J. C. Gas separation properties of spirobiindane polycarbonate. *J. Memb. Sci.* **67,** 75–81 (1992).
3. Schmidt, R. F. & Thews, G. *Human Physiology.* (Springer Berlin Heidelberg, 1989).
4. Edwards, R. *Handbook of Domestic Ventilation.* (Taylor and Francis, 2011).
5. Nof, S. Y. *Springer Handbook of Automation.* (Springer, 2009).

5

Modifications of PLimC

Published under the title:

Bio-based polycarbonate as synthetic toolbox

Oliver Hauenstein, Seema Agarwal, Andreas Greiner

Macromolecular Chemistry II, University of Bayreuth and Center of Colloid Science, Universitätsstr. 30, 95440 Bayreuth, Germany
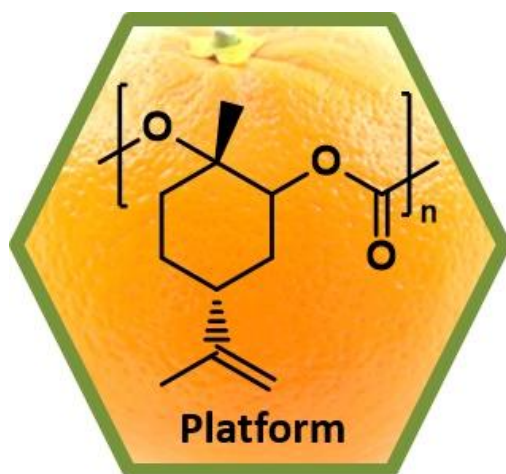
Abstract

Completely bio-based poly(limonene carbonate) is a thermoplastic polymer, which can be synthesized by copolymerization of limonene oxide (derived from limonene, which is found in orange peel) and CO_2. Poly(limonene carbonate) has one double bond per repeating unit that can be exploited for further chemical modifications. These chemical modifications allow the tuning of the properties of the aliphatic polycarbonate in nearly any direction. Here we show synthetic routes to demonstrate that poly(limonene carbonate) is the perfect green platform polymer, from which many functional materials can be derived. The relevant examples presented in this article are the transformation from an engineering thermoplastic into a rubber, the addition of permanent antibacterial activity, the hydrophilization and even pH-dependent water solubility of the polycarbonate. Finally, we show a synthetic route to yield the completely saturated counterpart that exhibits improved heat processability due to lower reactivity.

5.1 Introduction

The petroleum-based plastics industry is facing two major challenges. On the one hand, there is the urgent environmental problem of pollution of the ocean with about 5 million tonnes of plastic waste per year.[1,2] On the other hand, there is a natural limitation of petroleum resources, that eventually leads to a running out of oil and natural gas within this century.[3] In order to overcome these limitations, efforts are directed towards the development of degradable polymers[4,5] and the use of bio-based monomers[6–8], respectively. Sometimes, both classes are combined, i.e. the polymer is bio-based and biodegradable, e.g. poly(lactic acid) (PLA) or polyhydroxyalkanoates (PHA).[9–11] In other instances the polymer can be assigned either to the class of bio-based non-degradable plastics, such as bio-polyethylene (bio-PE) or bio-poly(ethylene terephthalate) (bio-PET), or to the class of biodegradable petro-based plastics, e.g. poly(ε-caprolactone) (PCL) or poly(butylene adipate-*co*-terephthalate) (PBAT).[8,12] However, even for a material which is assigned to both classes – as for PLA – the origin of the bio-based monomers is questionable, as lactic acid is derived from glucose, which is again derived from corn starch. The latter is also an important food resource and as such in competition with the use as precursor for the conversion into plastics. In contrast, limonene – a doubly unsaturated terpene – is a bio-based non-food resource which is mainly derived from the peel of citrus fruits.[13–15] As the major component of orange oil (>90%), it is an abundantly available side-product of the orange industry, produced in amounts of roughly 500 kt per year.[16] Its versatility as a monomer is reflected by the great variety of polymers that are derived from limonene.[13,17–19] In 2004, Coates and colleagues[20] reported the elegant metal-catalyzed conversion of its oxidation product limonene oxide (LO) with CO_2, to give a low molecular weight poly(limonene carbonate) (PLimC) (Fig. 5-1). An Al(III)-based catalyst was recently found to incorporate not only the *trans-* but also the *cis-*isomer of LO, which is an important step towards higher conversions.[21]
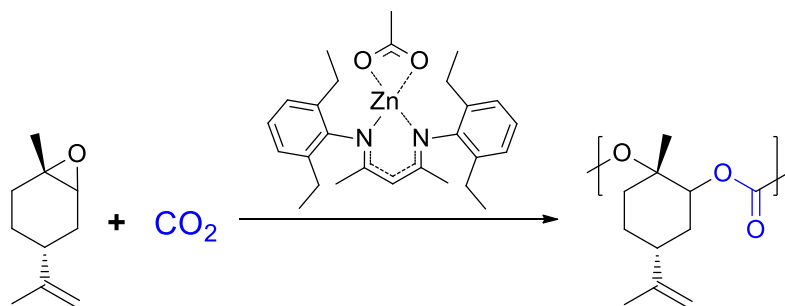
Figure 5-1 | Synthetic route towards PLimC. The copolymerization of limonene oxide and CO_2 in the presence of a β-diiminate zinc catalyst was discovered by Coates *et al.* and optimized in our group to yield high-molecular-weight PLimC.

Inspired by the work of Coates *et al.*,[20] we modified the copolymerization to yield high-molecular weight (> 100 kDa) PLimC in kg quantities[22] with a glass transition temperature of 130 °C, higher transparency than bisphenol-A polycarbonate (BPA-PC; 94% vs. 89%) and improved mechanical properties compared to the petro-based counterpart poly(cyclohexene carbonate) (PCHC, strain at break of 2% vs. 15% for PLimC).[23] The amorphous thermoplastic still possesses one double bond per repeating unit. This suggests a broad range of modifications to tune the properties in almost any direction. Thus, we consider PLimC a platform, from which countless functional materials can be derived. In order to support this statement, we give here relevant examples of straight forward addition reactions, i.e. thiol-ene click chemistry,[24] acid-catalyzed electrophilic addition and metal-catalyzed hydrogenation. The first two are conducted as polymer-analogous reactions, while the latter involves modification of the pre-monomer limonene. The manipulations lead to dramatic changes in the property profile of the engineering thermoplastic PLimC, including a transformation into a rubbery material, antibacterial activity, increased hydrophilicity or even water solubility and last but not least improved melt processability.

5.2 Results

Modification of unsaturated PLimC

The valorization of the platform polymer PLimC is illustrated in Fig. 5-2. When butyl-3-mercaptopropionate (B3MP) is used, an enormous change in mechanical properties is achieved. This leads to a transformation of the high-T_g thermoplastic into rubbery PLimC-B3MP with a nearly three orders of magnitude decreased YOUNG's modulus. Furthermore, this chemistry is also applied to transform PLimC into an antibacterial material, by covalently attaching a tertiary amine to the backbone (PLimC-N) and subsequent

quaternization with an aromatic moiety (PLimC-NQ). The antibacterial activity of PLimC-NQ was successfully tested against *Escherichia coli* (*E. coli*) bacteria. Another aspect is the hypothetical biodegradability of PLimC, which would be expected for an aliphatic polycarbonate, as it was shown for others.[25–27] Initial composting studies on PLimC revealed no degradation after prolonged exposure at elevated temperatures. This rather shows the high bio-stability of the material which is also desirable for many applications. Here, we present two major synthetic routes in order to tune the degradation behaviour of the rigid and hydrophobic polymer, i.e. either an acid-catalyzed electrophilic addition of poly(ethylene glycol)monomethyl ether (PEG-3-OH) resulting in PLimC-PEG or thiol-ene chemistry with mercaptoethanol (ME) to give PLimC-ME or mercaptoacetic acid (MAc) to yield PLimC-MAc, respectively. For the latter, this eventually even leads to pH-dependent water solubility, i.e. the material dissolves readily in basic environment.
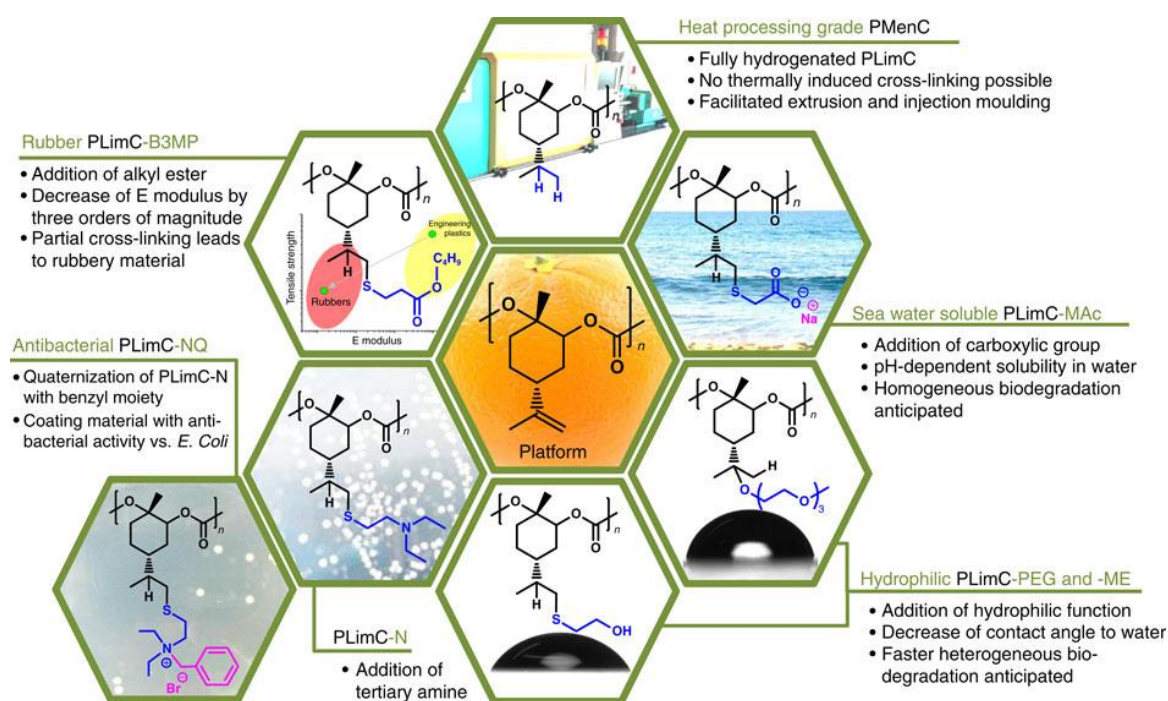
Figure 5-2 | The valorization of PLimC. The versatility of the platform polymer PLimC is illustrated in this hexagon cluster. The double bond is utilized for addition reactions, to induce dramatic changes of the properties of PLimC. The addition of an alkyl ester (PLimC-B3MP) leads to a drop of T_g by 120 °C and of its Young's Modulus by three orders of magnitude to give a PLimC rubber. The addition of a carboxylic group (PLimC-MAc) yields a pH-dependent solubility in water, whereas the functionalization with hydroxyl (PLimC-ME) or polyethylene glycol (PLimC-PEG) groups results in a higher hydrophilicity. The attachment of a tertiary amine (PLimC-N) and subsequent quaternization with an aromatic moiety (PLimC-NQ) leads to antibacterial activity against *E. coli*. Another possibility is the complete hydrogenation of the double bond to give PMenC, a superior material for heat processing.

Apart from the above-mentioned addition reactions, the synthetic route to the fully hydrogenated polycarbonate poly(menthene carbonate) (PMenC) is also reported for the first time. The saturated polycarbonate might be a viable choice for replacing PLimC in thermal processing, as no cross-linking can occur. Thus, starting from the bio-based platform polymer PLimC, we could introduce antibacterial activity (ideal as coating material),[28,29] elastomeric behaviour, hydrophilization, water solubility (both should accelerate biodegradation) and in fact inertness by hydrogenation to improve processing.

The transformation into elastic PLimC

The enormous versatility of PLimC is reflected in an experiment, where the thiol-functionalized ester B3MP – the pure ester is found in many fruits[30] – is clicked to the double bond in nearly quantitative yield (schematic in Fig. 5-3, Supplementary Figs 5-1 – 5-3). The T_g of PLimC lies at 130 °C, rendering it a typical engineering thermoplastic like polyamide, poly(ethylene terephthalate), BPA-PC etc. (yellow region in ASHBY plot of Fig. 5-3, Supplementary Table 5-1).[31] The covalently attached butyl ester B3MP changes the thermal and hence the mechanical properties dramatically, i.e. the T_g drops to 5 °C (Table 5-1, Supplementary Table 5-2, Supplementary Fig. 5-4). Tensile testing of the new material revealed its high maximum elongation ε combined with a low YOUNG's modulus and tensile strength σ_s, respectively. PLimC-B3MP with 0 – 2% residual double bonds in the backbone was prepared by variation of the reaction time (Supplementary Fig. 5-5). Curing the unsaturated polymers at 100 °C for 5 h renders the cross-linked samples insoluble while the mechanical properties can be adjusted (Supplementary Fig. 5-6, for a detailed discussion on the curing process see Supplementary Discussion). These observations combined with the elasticity (Supplementary Fig. 5-7) suggest a transition from the engineering thermoplastics region to the rubber region, i.e. the thermoplastic PLimC has become a PLimC rubber (PLimC-B3MP, red region in Fig. 5-3).[32] This transition enables the application of the bio-based material in completely new areas, where elasticity and softness are required. Furthermore, we introduced a short alkyl chain ester into the repeating unit of PLimC. Addition of longer alkyl chains potentially leads to T_g values well below 0 °C, which is another very important parameter to tune the performance of the resulting rubber.

Table 5-1: Thermal and tensile properties of PLimC,[22] PLimC rubber, PC and silicone rubber.

polymer	T_g (°C)	YOUNG's modulus (MPa)	σ_s (MPa)	ε (%)
PLimC	130	950	55	15
PLimC rubber	5	1.0	6.8	228
BPA-PC	145	2500	65	125
silicone rubber	-125	1.0	4.8 – 7.0	100 - 400

Data for PLimC rubber is taken from a cured sample of PLimC-B3MP with initially 2% unsaturation; for a more comprehensive table of polymers see Supplementary Table 5-1.

This is an example of the transformation of PLimC into a completely new material by simple polymer analogous click chemistry, while keeping the material based on natural resources. Further studies will focus on the reduction of T_g and the control of mechanical properties to expand the coverage of the ASHBY plot.
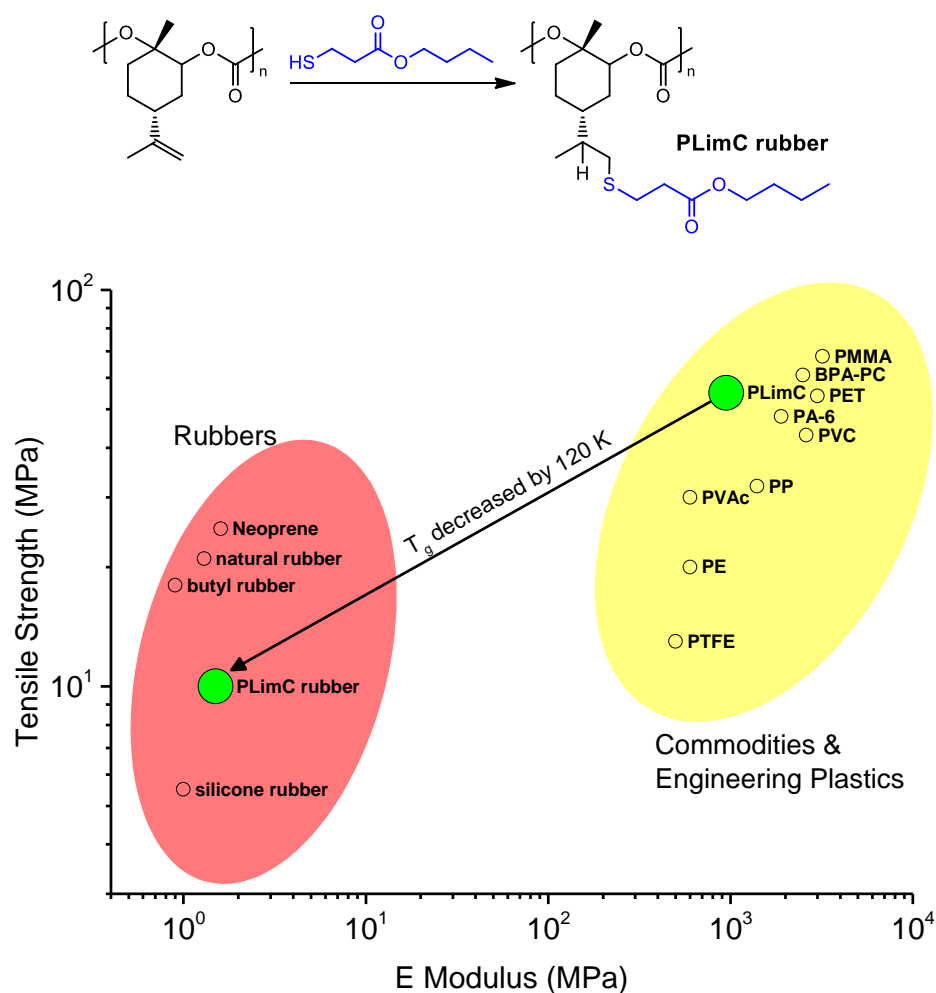
Figure 5-3 | The transformation into elastic PLimC. The schematic illustrates the functionalization of PLimC with B3MP to give PLimC-B3MP, i.e. a PLimC rubber. The YOUNG's moduli of various engineering plastics, commodities (both yellow region) and rubbers (red region) are plotted against their tensile strength. The materials PLimC and PLimC rubber are highlighted as green circles, showing the dramatic change of mechanical properties upon functionalization of pure PLimC with B3MP.

The transformation into antibacterial PLimC

In a recent publication we stated the thermal properties of PLimC, i.e. a T_g of 130 °C and a 5% decomposition temperature ($T_{5\%}$) of 240 °C, resulting in a rather narrow window for processing.[22] As an alternative to thermal processing, i.e. extrusion or injection moulding, the employment of a PLimC solution for the application as a coating is self-evident. The high transparency and good scratch resistance are very promising properties that should yield high-value materials in combination with an extra functionality. We picked one out of many possible functionalizations, to show how PLimC can be transformed into an antibacterial material by rather simple means. The strategy involves the addition of a tertiary amine to PLimC via thiol-ene click chemistry (PLimC-N) and the subsequent quaternization of the amine with an aryl halide (PLimC-NQ) (Supplementary Figs 5-8 - 5-14, Supplementary Tables 5-3 and 5-4). The functionalization was performed with different degrees of functionalization (DFs), though keeping it below 70% to keep the material insoluble in water. Resistance to water is of major importance, to make the material applicable as coatings in everyday life, where contact with water is inevitable. On the other hand, antibacterial activity rises exponentially, if the polymer – or part of it – is water-soluble, since interaction of the charged amine with the bacteria's membrane is facilitated.[33] Therefore, a sample with 20% quaternized amine (PLimC-NQ20) was investigated, which does not disintegrate in contact with water and still shows antibacterial activity by inhibiting bacterial growth. For the evaluation of the antibacterial properties of the coating, films were placed in *E. coli* suspensions and the concentration of the Gram-negative bacteria was assessed after 0, 6, 12, 24 and 48 h (Supplementary Tables 5-5 – 5-7). Compared to pure PLimC, PlimC-NQ20 exhibited a strong inhibitory effect on bacteria growth after 24 h. The ratio of killed bacteria relative to PLimC samples is illustrated in Fig. 5-4. The inhibitory effect for the positive reference material polyhexamethylene guanidine hydrochloride (PHMG) is detected already after 6 h, when all bacteria were killed. The charged PLimC samples are less active. This is not surprising, as they are in condensed state and not dissolved like PHMG. Still, the antibacterial activity could be observed after 12 h of contact with the bacteria suspension, indicating a successful valorization of PLimC into antibacterial PLimC.
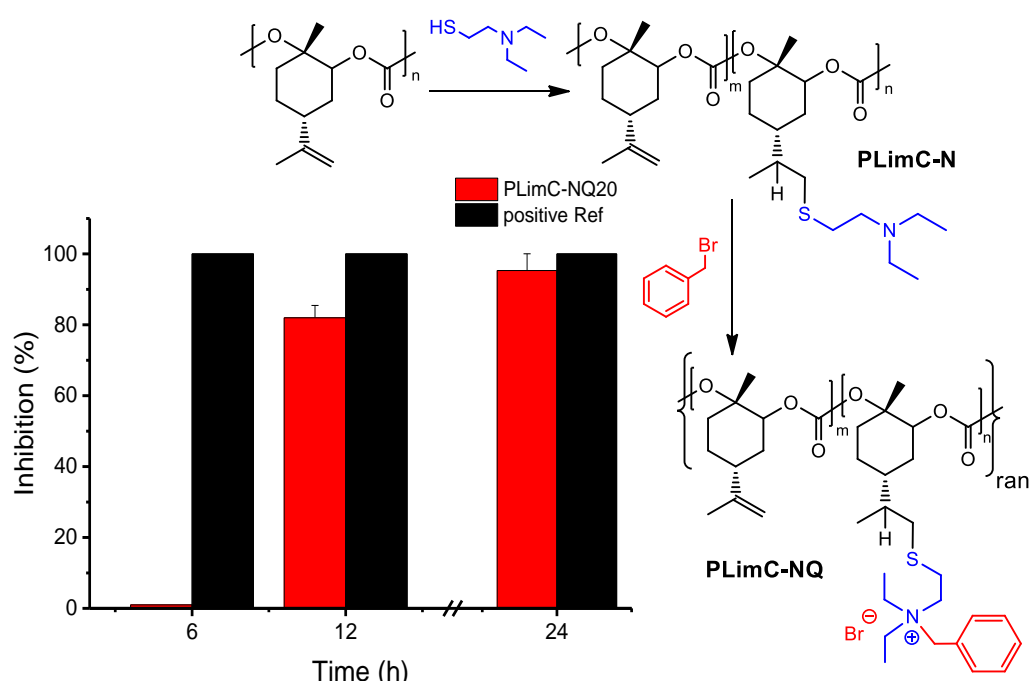
Figure 5-4 | The transformation into antibacterial PLimC. Schematic of the functionalization of PLimC with a tertiary amine (PLimC-N) and the subsequent quaternization with a benzyl moiety (PLimC-NQ). In the column diagram the bacterial inhibition performances of PLimC-NQ20 and a positive reference material (PHMG) relative to pure PLimC in a shaking flask experiment; tested on *E. coli* bacteria in buffer solution with polymer films (20 mg mL^{-1}) at 20 °C, are illustrated. The inhibition was calculated by determination of the cfu of 10-fold diluted dispersions spread on agar plates (Supplementary Table 5-7).

Here, as proof of principle, we can demonstrate that PLimC is readily transformable into a material with antibacterial activity by rather simple and cost-effective means. We would assume though that lots of parameters are still to be optimized, i.e. DF, length of spacer between thiol and amine, nature of the alkyl or aryl moiety on the amine and random distribution of quaternized amine along the backbone of the polymer vs. block copolymer structure. Furthermore, the types of bacteria have to be selected in respect of the targeted application.

The transformation into hydrophilic/water-soluble PLimC

The idea to render PLimC more hydrophilic was born, when studies on the degradation behaviour of pure PLimC in highly active compost at 60 °C (positive reference poly(L-lactic acid) disintegrated within one week) had been stopped after 60 days because no change, neither in the outer appearance nor in molecular weight, had been observed. The rather substantial bio-stability of this aliphatic polycarbonate is most likely explained by the three facts about PLimC. First of all, it has a very rigid backbone, resulting in a high T_g of 130 °C, which is about 100 °C higher than that of the readily biodegradable poly(propylene

carbonate).[34,35] The rigidity of the backbone prevents the polymer chain segments from moving and therefore no exposure of the carbonate groups to enzymes/bacteria is possible. Second, the polymer carries a very bulky 'side group', consisting of the cyclohexane ring connected to an isopropylene group and another methyl moiety vicinal to the carbonate. Thus, even if there are some exposed chains on the surface of such a film, the carbonate group is shielded against any attacking species. Eventually, PLimC is very hydrophobic which is represented by its contact angle to water (CA_W) of 94°. This prevents not only enzymes from penetrating the polymer but also water. Hence, acid or basic hydrolysis – usually the major breakdown mechanism for long polymer chains – is inhibited, so nearly no fragmentation of PLimC for further degradation takes place. In consideration of the underlying circumstances, the hydrophilization of PLimC was assumed to be a likely enabler for biodegradation. Three different strategies were employed to achieve hydrophilic PLimC: two of them involve the well-known thiol-ene chemistry with mercaptoethanol (ME) (Supplementary Fig. 5-15, Supplementary Table 5-8) or mercaptoacetic acid (MAc) as thiols, respectively (Supplementary Fig. 5-16).[36–40] The other strategy is – an even simpler – acid-catalyzed electrophilic addition of PEG-3-OH to the double bond (Supplementary Fig. 5-17, Supplementary Table 5-9). The latter can also be acknowledged as a green reaction, hence keeping the bio-based character of PLimC, while grafting polar functionality. Indeed, the higher the DF, the smaller CA_W becomes. Up to 18% conversion of the double bond was achieved by this electrophilic addition, but since it is acid-catalyzed, hydrolysis of the carbonate is an immanent side reaction, that eventually breaks down the polymer chains (Supplementary Fig. 5-18). So reaction times were kept short and a great excess of PEG-3-OH was maintained. The contact angle could be decreased below 80° with this technique. An even stronger decrease of the CA_W could be achieved by radically adding ME to PLimC. Compared to the acid-catalyzed addition, the advantage of thiol-ene chemistry is the absence of hydrolytic side-reactions. Therefore, higher DFs are easily accessible. Here a DF of 70% resulted in a CA_W of 70°. In order to hydrophilize the polymer even further, PLimC was functionalized with MAc, whereas 100% attachment of the acid yields a polymer with a CA_W of 60°. A side effect of all above-mentioned modifications is the decrease of T_g with increasing DF (Fig. 5-5, stars, Supplementary Figs 5-19 – 5-21). In terms of degradability, this should further promote the breakdown of the polymer. The PEG and ME modified PLimCs were assessed regarding their degradation behaviour in acidic (pH 4), basic (pH 9) and enzymatic environment (esterase) at elevated temperatures

(37 °C). Within the timespan of four weeks no degradation characteristics, i.e. loss of mass, drop in molecular weight or surface alterations, could be observed (Supplementary Fig. 5-22, Supplementary Table 5-10). These observations suggest that neither a bulk nor a surface erosion process is taking place for the samples in those environments on the time scale measured. Keeping in mind that hydrophilicity and the chain flexibility were augmented, but steric shielding of the carbonate group was unchanged (or even higher due to addition reactions), we noticed that the overall stability versus hydrolysis and/or enzymatic attack is still too high. However, on longer time scales, the backbone of PLimC is anticipated to be much more labile than that of a polyolefin and degradation should take place eventually. This makes it an interesting choice, wherever good stability against hydrolysis during application is required, but eventual disintegration on a reasonable timescale is desired.
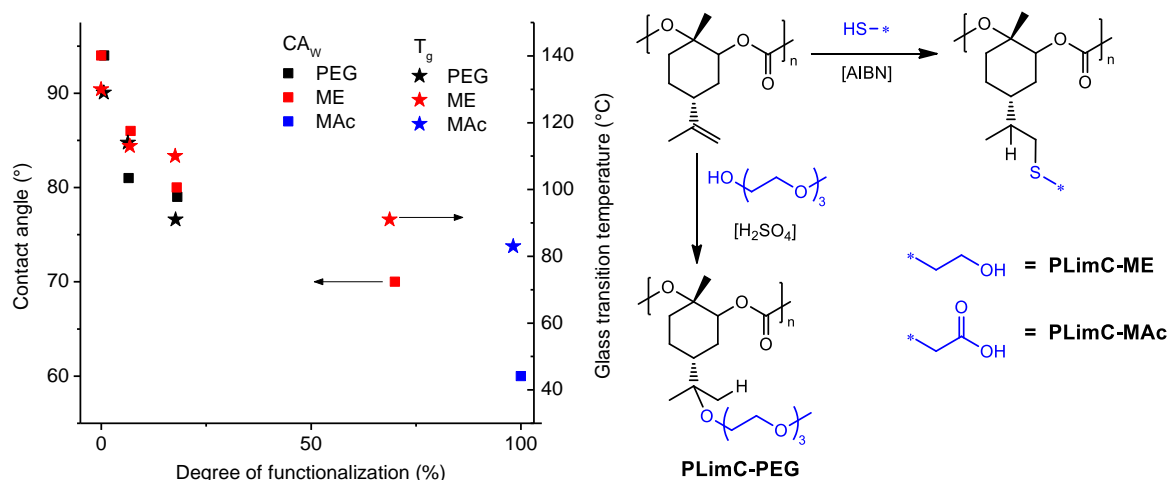
Figure 5-5 | The transformation into hydrophilic/water-soluble PLimC. Dependency of contact angle to water (squares) and T_g (stars) of a PLimC film on the degree of functionalization with PEG-3-OH (black), mercaptoethanol (red) or mercaptoacetic acid (blue), respectively. The schematic of the functionalization is shown for the thiol-ene addition of ME and MAc to give PLimC-ME and PLimC-MAc, respectively, and the electrophilic addition of PEG-3-OH to give PLimC-PEG.

The functionalization of PLimC with acid functionality renders the material not only hydrophilic (CA_W = 60°) but also pH responsive. A film of PLimC-MAc (DF = 100%) placed into a pH > 8 buffer solution will dissolve within minutes. In the dissolved state hydrolysis is of course highly accelerated compared to the condensed state. Therefore, the material would quickly disintegrate in seawater, which is usually slightly basic, and chain scission could readily occur. The exact degradation mechanism is yet to be studied, but this polymer could contribute in reducing the waste accumulation in the oceans.[1]

The saturation of PLimC

Apart from the functionalization of PLimC, of course, it is also possible to hydrogenate the double bond, to render it unreactive, when it is heat processed or stored for a prolonged period of time. In contrast to the aforementioned modifications, this is not a polymer-analogous reaction, but the manipulation is performed on the pre-monomer (R)-limonene. Indeed, this hydrogenation is very regioselective, when a heterogeneous catalyst like Pt on charcoal is used. Hence, a quantitative conversion to menth-1-ene (Men) can be achieved in reasonable time, while separation from the catalyst/carrier material is easy. We used the *N*-bromosuccinimide-(NBS)-route for epoxidation (see Fig. 5-6) of Men to menthene oxide (MenO), as it is an established reaction for the stereo- and regio-selective epoxidation of limonene.[22] The route involves the formation of the bromohydrin MenBrOH and the subsequent ring-closure in a basic medium to yield MenO. The conversion of the monomer MenO and pre-monomers menth-1-ene and MenBrOH, respectively, were monitored by GC analysis (Supplementary Figs 5-23 – 5-25).
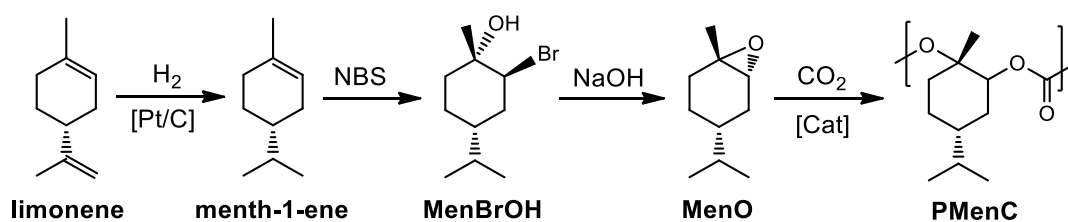
Figure 5-6 | The saturation of PLimC. The synthetic route to PMenC starts from the metal-catalyzed hydrogenation of limonene, followed by the stereoselective epoxidation of menth-1-ene via its bromohydrin (MenBrOH) to *trans*-MenO and the subsequent copolymerization with CO_2 to give the saturated polycarbonate PMenC.

As the catalyst for the production of PMenC by copolymerization with CO_2 is also selective towards the *trans*-isomer of MenO (Supplementary Figs 5-26 – 5-28), we still recommend taking the detour via the bromohydrin, but plan to look into new reactions to perform a more economical oxidation of menthene. The properties of PMenC are very similar to PLimC, as both are high-T_g amorphous polycarbonates (Supplementary Fig. 5-29). The only, and of course anticipated, difference is the inability of the polymer to cross-link or to perform any undesired oxidation reactions at elevated temperatures. For PLimC the addition of antioxidants, i.e. butylated hydroxytoluene derivatives, helps to reduce those side reactions, but for PMenC no additives are needed. Indeed, a better processability, i.e. extrusion and injection moulding, and a prolonged ultraviolet stability are anticipated. Both give extra value to this polymer. A combination of both MenO and LO for

copolymerization with CO_2 is also possible, resulting in a defined number of available double bonds for post-modification reactions as shown above.

5.3 Discussion

In summary, we could show the huge versatility of the green platform polymer PLimC. The valorization was achieved either by polymer analogous thiol-ene chemistry and acid-catalyzed electrophilic addition, or by metal-catalyzed hydrogenation of the pre-monomer. Thiol-ene chemistry proved to be the most versatile technique, adding not only hydrophilicity or pH-dependent solubility, but also antibacterial activity by functionalization with quaternary amines. Even a transformation of the high-T_g thermoplastic PLimC into a rubbery material could be achieved by addition of a thiol. Not as adaptable is the acid-catalyzed electrophilic addition of alcohols, though it proves to be more economical, since no costly functional thiols (employed in great excess) but only PEG and sulphuric acid are needed. Keeping the lability of the backbone of the aliphatic polycarbonate in mind, we note that this method is limited to short reaction times and hence only partial functionalization can be achieved. A quantitative conversion is possible for the regioselective hydrogenation of limonene, resulting in fully saturated PMenC after a few steps. This polycarbonate is oxidation-resistant and thus exhibits improved processability for extrusion and injection moulding. The valorization of PLimC significantly broadens the range of applications, as PLimC-NQ is a viable antibacterial coating material and PLimC-ME, PLimC-PEG and PLimC-MAc could be employed as packaging materials with tuneable degradation/dissolution mechanism.

5.4 Methods

Instrumentation and characterization

NMR spectra were recorded on a Bruker AMX-300 operating at 300 MHz. Chemical shifts δ are indicated in parts per million (ppm) with respect to residual solvent signals. Thermo-gravimetric analysis was performed on a Netzsch TG 209 F1 Libra and differential scanning calorimetry on a Mettler Toledo DSC 821c, both at a heating rate of 10 K min^{-1} under N_2 atmosphere. Infrared spectra of solids were recorded with an ATR unit of a Digilab Excalibur FTS-3000. Gas chromatography was performed on a Shimadzu QP-5050 with N_2 as the carrier gas (temperature profile for GC studies: start at 40 °C hold for 5 min, heating

to 80 °C with 5 °C min^{-1}, heating to 120 °C with 3 °C min^{-1} and hold for 3 min, heating to 300 °C with 30 °C min^{-1}). Relative molecular weights and dispersities were determined by gel permeation chromatography on an Agilent 1200 system with chloroform as the eluent and polystyrene as the calibration standard. A hazemeter BykGardner Haze-Gard Plus and a UV/Vis spectrometer V-670 (JASCO) were employed for the testing of optical properties of solvent cast PLimC films having a thickness between 100 and 400 μm. A Zwick/Roell Z0.5 test equipment with testXpert II software was employed for the tensile testing. The tests were performed at 21 °C and a relative humidity of 20%. The strain rate was set to 5 mm min^{-1} to test the tensile properties of cast polymer films that were die-cut into specimen (dumb-bell shaped) having a width of 2 mm, a length of 20 mm and a thickness of 100 to 200 μm. A BYK Pencil Hardness Tester and Derwent Graphic pencils were used to determine pencil hardness.

Synthetic Procedures

All synthetic manipulations were carried out under exclusion of air in dry conditions, if not otherwise stated. The acid-catalyzed electrophilic addition and the thiol-ene chemistry were carried out as polymer analogous reactions. The hydrogenation of the exo double bond of limonene was performed on the pre-monomer, which was subsequently epoxidized and copolymerized with CO_2, to give the polycarbonate PMenC. A detailed description of the synthetic procedures is given in the Supplementary Methods.

Degradation tests in composting environment

Composting tests were performed on cast films of PLimC (M_n = 54.0 kDa, Đ = 1.11) of 200 μm thickness fixed in slide mounts. The three month matured compost was supplied by an industrial composting plant (Mistelbach) and directly used for PLimC burial tests. As positive reference material poly(L-lactic acid) (NatureWorks) was used. During the test the temperature was kept at 60 °C and the container was vented every two days (every three days after the first two weeks) and humidified if necessary (humidity was estimated by weighing of the container).

Degradation tests in enzymatic environment

The enzymatic tests were performed on cast films of PLimC, PLimC-ME (100% functionalized with ME) and BPA-PC (reference material) having a thickness of 100 µm, which were cut into 40 mg pieces. As media water, pH 4 buffer, pH 9 buffer and an esterase in pH 9 buffer (Esterase EL-01, triacylglycerol lipase, ASA Spezialenzyme GmbH, 1 part of enzyme suspension mixed with 4 parts of buffer solution, replaced after 10 days) were **selected to test the polymer samples' stability against. At a temperature of 37 °C the samples** were shaken in a mechanical shaker (50 rpm) in 40 mL glass containers, which were filled to 75%. The mass loss (balance) and molecular weight (GPC) change were analyzed after 3, 10 and 21 days in triplicate for each sample.

Antibacterial activity tests

Escherichia coli (*E. coli*, DSM no. 1077, K12 strain 343/113, DSMZ) as a Gram-negative test-organism was used to evaluate the antibacterial activity of the polycarbonates. We have chosen the Gram-negative bacteria *E. coli* for the antibacterial activity tests of PLimC-NQ to evaluate the general activity of the polymer towards a very common bacterium. CASO-Boullion was used as nutrient for the *E. coli* (30 g L^{-1} in distilled water for liquid nutrient; 15 g L^{-1} agar–agar in addition for nutrient agar plates). The strain was preserved on nutrient agar plates and liquid cultures were grown by inoculation of liquid nutrient with a single bacteria colony using an inoculation loop. The inoculated broth was incubated with shaking at 37 °C until the optical density at 578 nm had risen to 0.125, indicating a cell density of 10^7-10^8 cfu mL^{-1}. To obtain the final bacterial suspensions the inoculated broth was diluted with buffer solution (phosphate buffered solution, concentration of phosphate ions = 12 mM, pH = 7.4) to an approximate cell density of 10^5 cfu mL^{-1}. The antibacterial activity was determined by the shaking flask method: polymer films with a mass of 40 mg and a thickness of 100 µm were incubated with 2 mL of bacteria suspension at ambient temperature in microcentrifuge tubes with contact times of 6, 12 and 24 h. After the defined time intervals, 100 µL specimens were drawn and spread on nutrient agar plates. After incubation at 37 °C for 24 h, colonies were counted and the reduction was calculated relative to the unfunctionalized PLimC sample.

Acknowledgements

5.5 References

1. Miller, S. A. Sustainable polymers: opportunities for the next decade. *ACS Macro Lett.* **2,** 550–554 (2013).

2. Tuck, C. O., Perez, E., Horvath, I. T., Sheldon, R. A. & Poliakoff, M. Valorization of biomass: deriving more value from waste. *Science* **337,** 695–699 (2012).

3. Bentley, R. W. Global oil and gas depletion: An overview. *Energy Policy* **30,** 189–205 (2002).

4. Kale, G. *et al.* Compostability of bioplastic packaging materials: an overview. *Macromol. Biosci.* **7,** 255–77 (2007).

5. Mecking, S. Nature or petrochemistry?—Biologically degradable materials. *Angew. Chemie Int. Ed.* **43,** 1078–1085 (2004).

6. Mülhaupt, R. Green polymer chemistry and bio-based plastics: dreams and reality. *Macromol. Chem. Phys.* **214,** 159–174 (2013).

7. Babu, R. P., O'Connor, K. & Seeram, R. Current progress on bio-based polymers and their future trends. *Prog. Biomater.* **2,** 8-25 (2013).

8. Iwata, T. Biodegradable and bio-based polymers: future prospects of eco-friendly plastics. *Angew. Chemie Int. Ed.* **54,** 3210–3215 (2015).

9. Müller, H.-M. & Seebach, D. Poly(hydroxyalkanoates): A fifth class of physiologically important organic biopolymers? *Angew. Chemie Int. Ed. English* **32,** 477–502 (1993).

10. Reichardt, R. & Rieger, B. Poly(3-hydroxybutyrate) from carbon monoxide. *Adv. Polym. Sci.* **245,** 49–90 (2011).

11. Dutta, S., Hung, W.-C., Huang, B.-H. & Lin, C.-C. Recent developments in metal-catalyzed ring-opening polymerization of lactides and glycolides: preparation of polylactides, polyglycolide, and poly(lactide-co-glycolide). *Adv. Polym. Sci.* **245,** 219–283 (2011).

12. Siegenthaler, K. O., Künkel, A., Skupin, G. & Yamamoto, M. Ecoflex® and Ecovio®: biodegradable, performance-enabling plastics. *Adv. Polym. Sci.* **245,** 91–136 (2011).

13. Firdaus, M., Montero De Espinosa, L. & Meier, M. A. R. Terpene-based renewable monomers and polymers via thiol-ene additions. *Macromolecules* **44,** 7253–7262 (2011).

14. Blanch, G. & Nicholson, G. Determination of the enantiomeric composition of limonene and limonene-1,2-epoxide in lemon peel by multidimensional gas chromatography with flame-ionization detection and selected ion monitoring mass spectrometry. *J. Chromat. Sci.* **36,** 19-22 (1998).

15. Zhao, J. & Schlaad, H. Synthesis of terpene-based polymers. *Adv. Polym. Sci.* **253,** 151–190 (2012).

16. Ciriminna, R., Lomeli-Rodriguez, M., Demma Carà, P., Lopez-Sanchez, J. A. & Pagliaro, M. Limonene: a versatile chemical of the bioeconomy. *Chem. Commun.* **50,** 15288–15296 (2014).

17. Wilbon, P. A., Chu, F. & Tang, C. Progress in renewable polymers from natural terpenes, terpenoids, and rosin. *Macromol. Rapid Commun.* **34,** 8–37 (2013).

18. Li, C., Sablong, R. J. & Koning, C. E. Synthesis and characterization of fully-biobased α,ω-dihydroxyl poly(limonene carbonate)s and their initial evaluation in coating applications. *Eur. Polym. J.* **67,** 449–458 (2015).

19. Harvey, B. G. *et al.* Sustainable hydrophobic thermosetting resins and polycarbonates from turpentine. *Green Chem.* **18,** 2416-2423 (2016).

20. Byrne, C. M., Allen, S. D., Lobkovsky, E. B. & Coates, G. W. Alternating copolymerization of limonene oxide and carbon dioxide. *J. Am. Chem. Soc.* **126,** 11404–11405 (2004).

21. Peña Carrodeguas, L., González-Fabra, J., Castro-Gómez, F., Bo, C. & Kleij, A. W. Al[III]-catalysed formation of poly(limonene)carbonate: DFT analysis of the origin of stereoregularity. *Chem. - A Eur. J.* **21,** 6115–6122 (2015).

22.   Hauenstein, O., Reiter, M., Agarwal, S., Rieger, B. & Greiner, A. Bio-based polycarbonate from limonene oxide and CO_2 with high molecular weight, excellent thermal resistance, hardness and transparency. *Green Chem.* **18,** 760–770 (2016).

23.   Koning, C. *et al.* Synthesis and physical characterization of poly(cyclohexane carbonate), synthesized from CO_2 and cyclohexene oxide. *Polymer* **42,** 3995–4004 (2001).

24.   Hoyle, C. E. & Bowman, C. N. Thiol-ene click chemistry. *Angew. Chemie Int. Ed.* **49,** 1540–1573 (2010).

25.   Artham, T. & Doble, M. Biodegradation of aliphatic and aromatic polycarbonates. *Macromol. Biosci.* **8,** 14–24 (2008).

26.   Luinstra, G. A. & Borchardt, E. Material Properties of poly(propylene carbonates) *Adv. Polym. Sci.* **245,** 29-48 (2012).

27.   Wu, K.-J., Wu, C.-S. & Chang, J.-S. Biodegradability and mechanical properties of polycaprolactone composites encapsulating phosphate-solubilizing bacterium Bacillus sp. PG01. *Process Biochem.* **42,** 669–675 (2007).

28.   Fuchs, A. D. & Tiller, J. C. Contact-active antimicrobial coatings derived from aqueous suspensions. *Angew. Chemie Int. Ed.* **45,** 6759–6762 (2006).

29.   Sileika, T. S., Barrett, D. G., Zhang, R., Lau, K. H. A. & Messersmith, P. B. Colorless multifunctional coatings inspired by polyphenols found in tea, chocolate, and wine. *Angew. Chemie - Int. Ed.* **52,** 10766–10770 (2013).

30.   Burdock, G. A. *Encyclopedia of Food and Color Additives, Volume 1.* (CRC Press, 1996).

31.   Fried, J. R. *Polymer Science and Technology, Third Edition.* (Prentice Hall, 2014).

32.   Brandrup, J., Immergut, E. H. & Grulke, E. A. *Polymer Handbook, Fourth Edition.* (Wiley, 1998).

33.   Kenawy, E.-R., Worley, S. D. & Broughton, R. The chemistry and applications of antimicrobial polymers: a state-of-the-art review. *Biomacromolecules* **8,** 1359–1384 (2007).

34.   Luinstra, G. A. Poly(propylene carbonate), old copolymers of propylene oxide and carbon dioxide with new interests: catalysis and material properties. *Polym. Rev.* **48,** 192–219 (2008).

35.   Zhou, M., Takayanagi, M., Yoshida, Y., Ishii, S. & Noguchi, H. Enzyme-catalyzed degradation of aliphatic polycarbonates prepared from epoxides and carbon dioxide. *Polym. Bull.* **42,** 419–424 (1999).

36.   Darensbourg, D. J. & Wang, Y. Terpolymerization of propylene oxide and vinyl oxides with CO_2: copolymer cross-linking and surface modification via thiol–ene click chemistry. *Polym. Chem.* **6,** 1768–1776 (2015).

37.   Darensbourg, D. J., Chung, W., Arp, C. J., Tsai, F. & Kyran, S. J. Copolymerization and cycloaddition products derived from coupling reactions of 1,2-epoxy-4-cyclohexene and carbon dioxide. Postpolymerization functionalization via thiol–ene click reactions. *Macromolecules* **47,** 7347–7353 (2014).

38.   Darensbourg, D. J. & Tsai, F.-T. Postpolymerization functionalization of copolymers produced from carbon dioxide and 2-vinyloxirane: Amphiphilic/water-soluble CO_2-based polycarbonates. *Macromolecules* **47,** 3806–3813 (2014).

39.   Gu, L., Qin, Y., Gao, Y., Wang, X. & Wang, F. Hydrophilic CO_2-based biodegradable polycarbonates: Synthesis and rapid thermo-responsive behavior. *J. Polym. Sci. Part A Polym. Chem.* **51,** 2834–2840 (2013).

40.   Zhou, Q. *et al.* Biodegradable CO_2-based polycarbonates with rapid and reversible thermal response at body temperature. *J. Polym. Sci. Part A Polym. Chem.* **51,** 1893–1898 (2013).

5.6 Supplementary information

169

Supplementary Figures
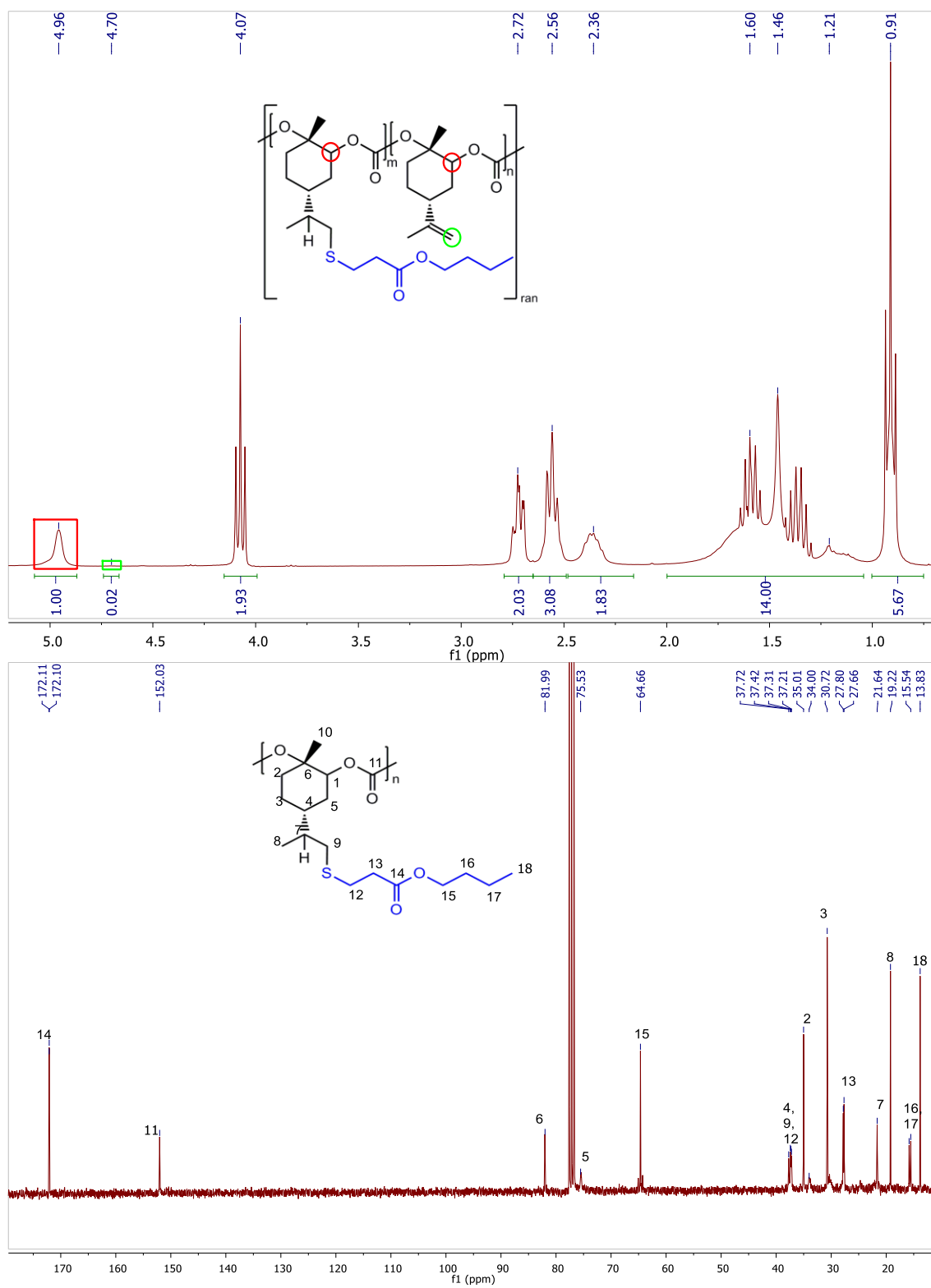
Supplementary Figure 5-1: Representative ^{1}H and ^{13}C NMR spectra (recorded in CDCl$_3$) of PLimC-B3MP$_{1.0}$ after reacting PLimC for 80 min with butyl-3-mercpatopropionate to give 99% conversion. The red rectangle indicates the methine resonance (adjacent to carbonate group) of both the unfunctionalized and the functionalized repeating unit, whereas the green rectangle marks the region where the protons of the (unfunctionalized) double bond are resonating. Since unsaturation is very low in all samples the region 5.2 – 4.6 ppm is magnified for all PLimC-B3MP samples in Supplementary Figure 5-2.
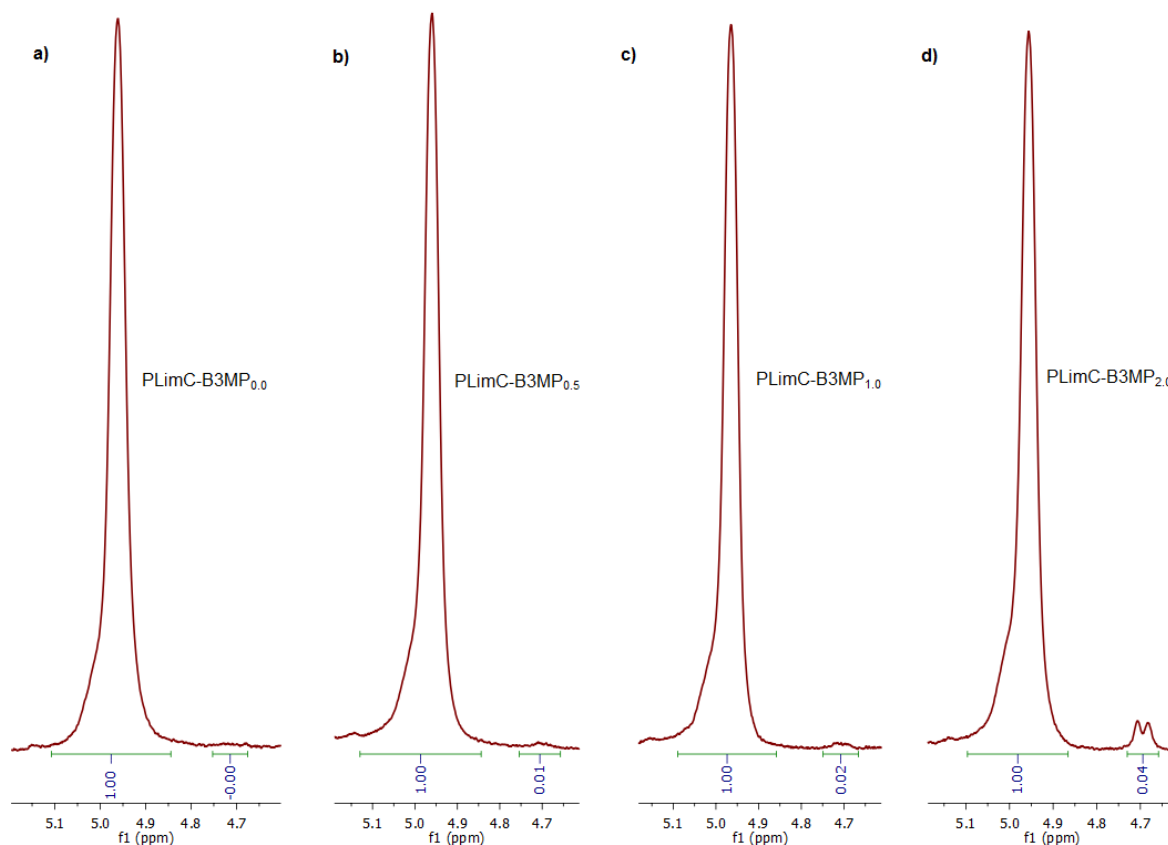
Supplementary Figure 5-2: Magnification of the methine and double bond proton resonances in the ^{1}H NMR spectra of PLimC-B3MP with a) 0%, b) 0.5%, c) 1.0% and d) 2% unsaturation in the backbone. The degree of unsaturation has been determined by integration of the signal at 4.7 ppm with respect to the methine proton at 5.0 ppm.
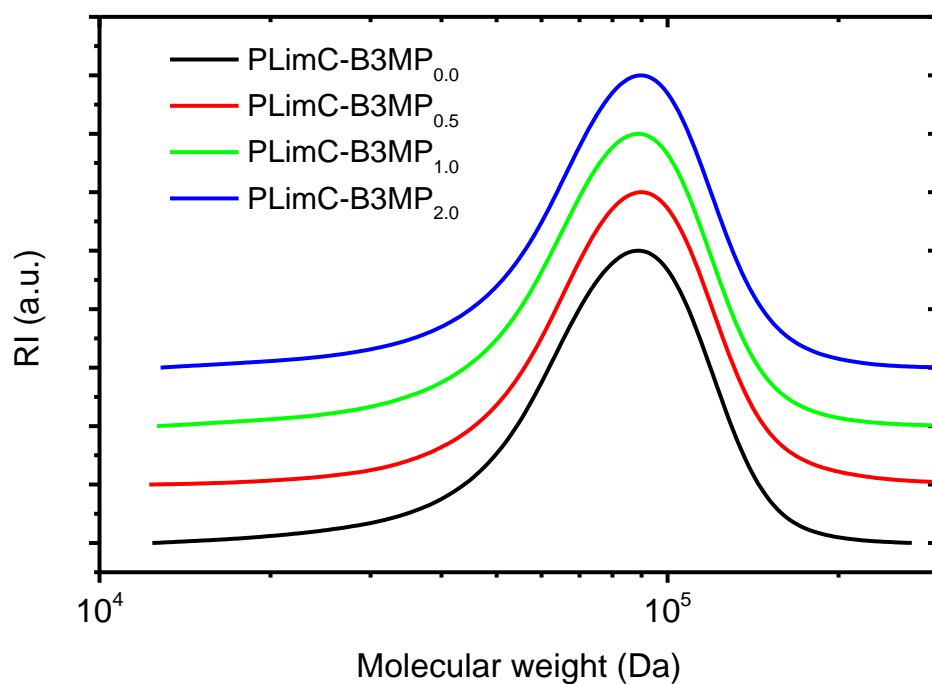
Supplementary Figure 5-3: Molecular weight distribution of the PLimC-B3MP samples with different DFs. Measurements were performed on a GPC with chloroform as eluent.
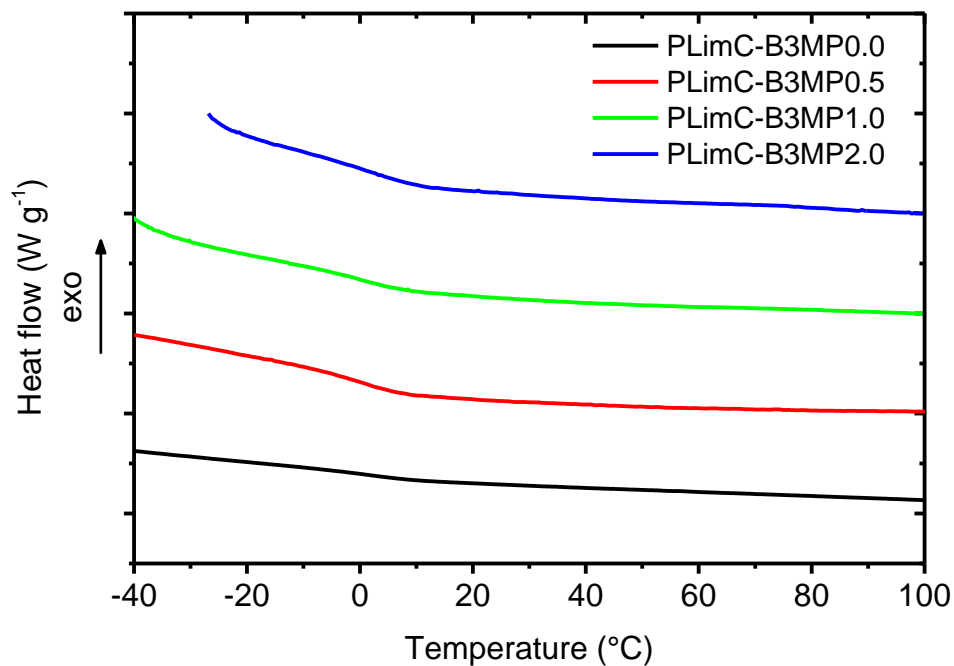
Supplementary Figure 5-4: Second heating cycle in DSC experiment of PLimC B3MP samples with various DFs recorded at 10 K min^{-1} in N$_2$ atmosphere. All samples exhibit a glass transition at about 5 °C, as it was expected, since all samples exhibit a DF close to 100%.
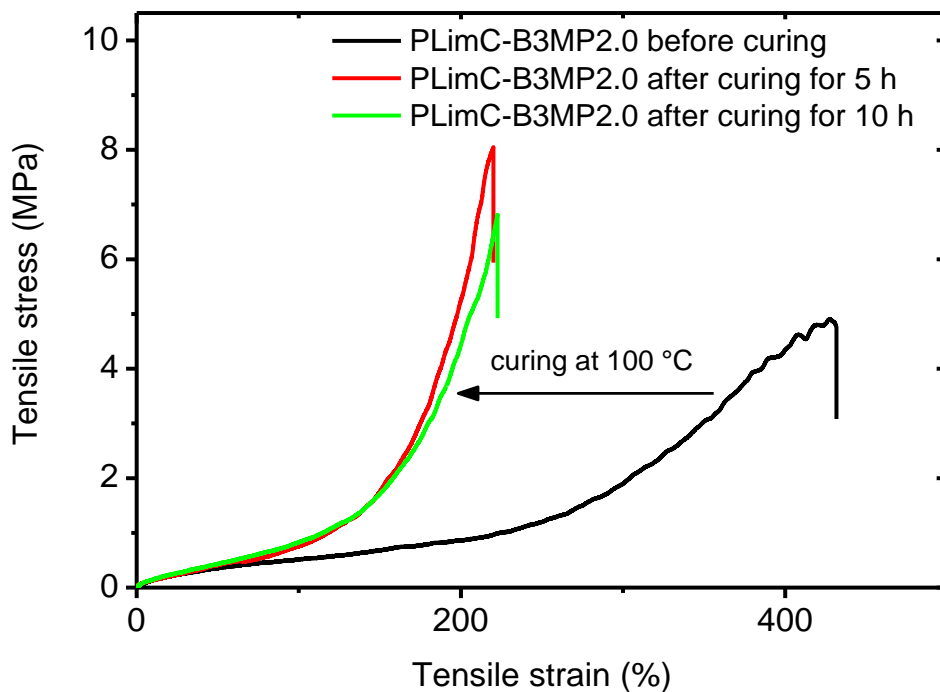
Supplementary Figure 5-5: Effect of curing (time) on the tensile properties of PLimC-B3MP$_{2.0}$. The diagram shows the tensile tests on specimens of PLimC-B3MP$_{2.0}$ performed before curing (black) and after curing in air at 100 °C for 5 h (red) or 10 h (green), respectively. While the curing for 5 h has a dramatic effect on the tensile properties compared to the uncured sample, longer curing time (in total 10 h at 100 °C) does not change the tensile properties any further.

a

b

c

d
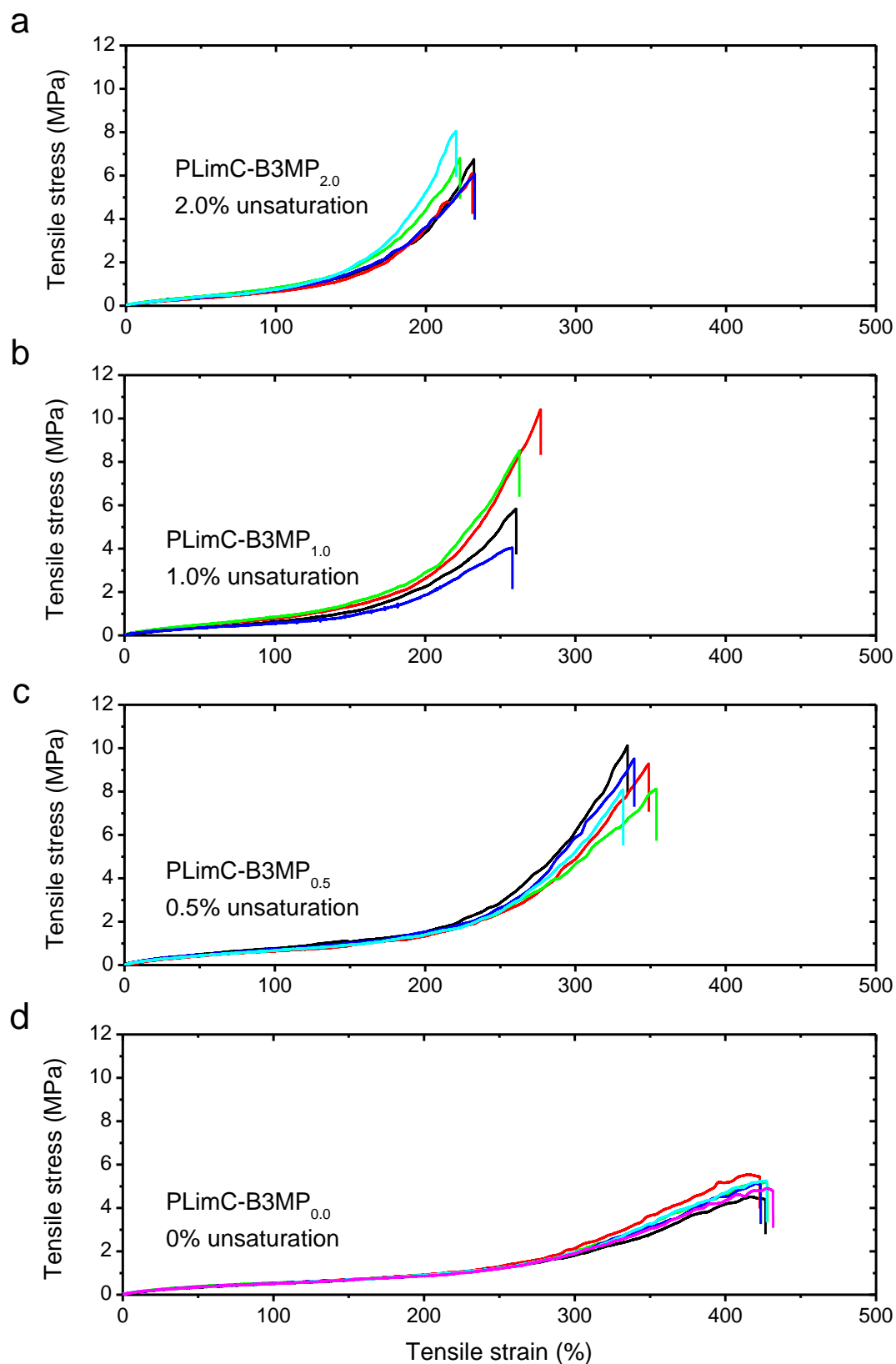
Supplementary Figure 5-6: Stress-strain diagram of tensile testing of cured PLimC-B3MP specimens with (a) 2.0%, (b) 1.0%, (c) 0.5% and (d) 0.0% unsaturation in the (uncured) sample. The measurements were performed at a speed of 5 mm min⁻¹ on specimen with a width of 2 mm, a length of 20 mm and a thickness of 150 µm. The films were cast from a methylene chloride solution, dried *in vacuo* at 20 °C and subsequently cured at 100 °C for 5 h in air.
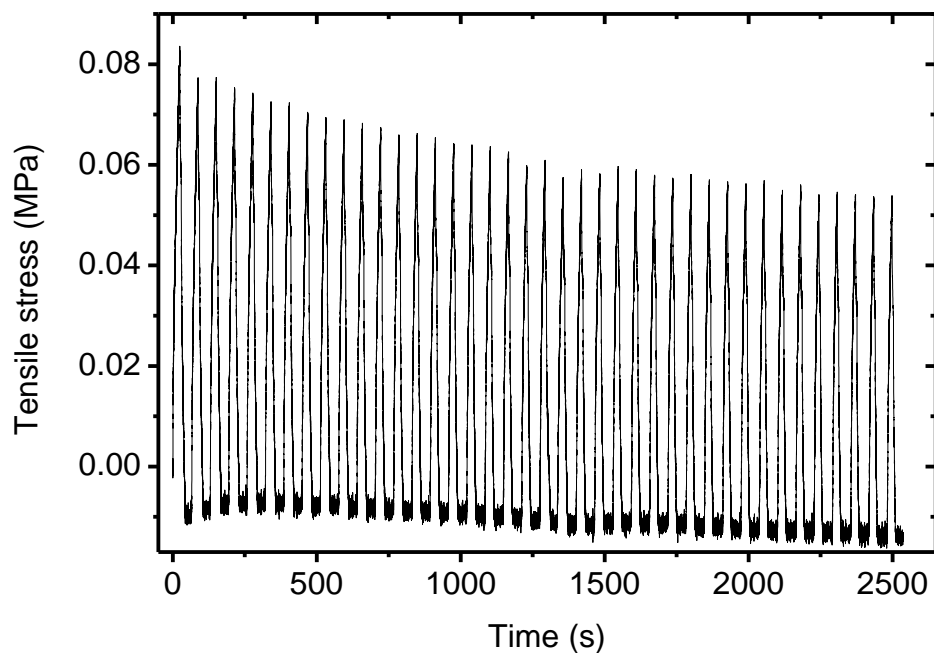
Supplementary Figure 5-7: Evaluation of the elasticity of a cured specimen of PLimC-B3MP$_{2.0}$ by cyclic elongation to 20% strain (40 cycles, 5 s strain, 10 s relaxation, strain rate 10 mm min^{-1}). The strain is not completely reversible (maximum stress drops from 0.08 MPa for each consecutive cycle down to 0.06 MPa for the last cycle), as the T_g (5 °C) of the polymer is very close to the testing temperature of 21 °C, i.e. the slow dynamics can be assigned to the slow segmental motion of the polymer backbone. To improve reversibility in the strain experiment, the modification of PLimC with thiols that lower the T_g well below 0 °C should be used.
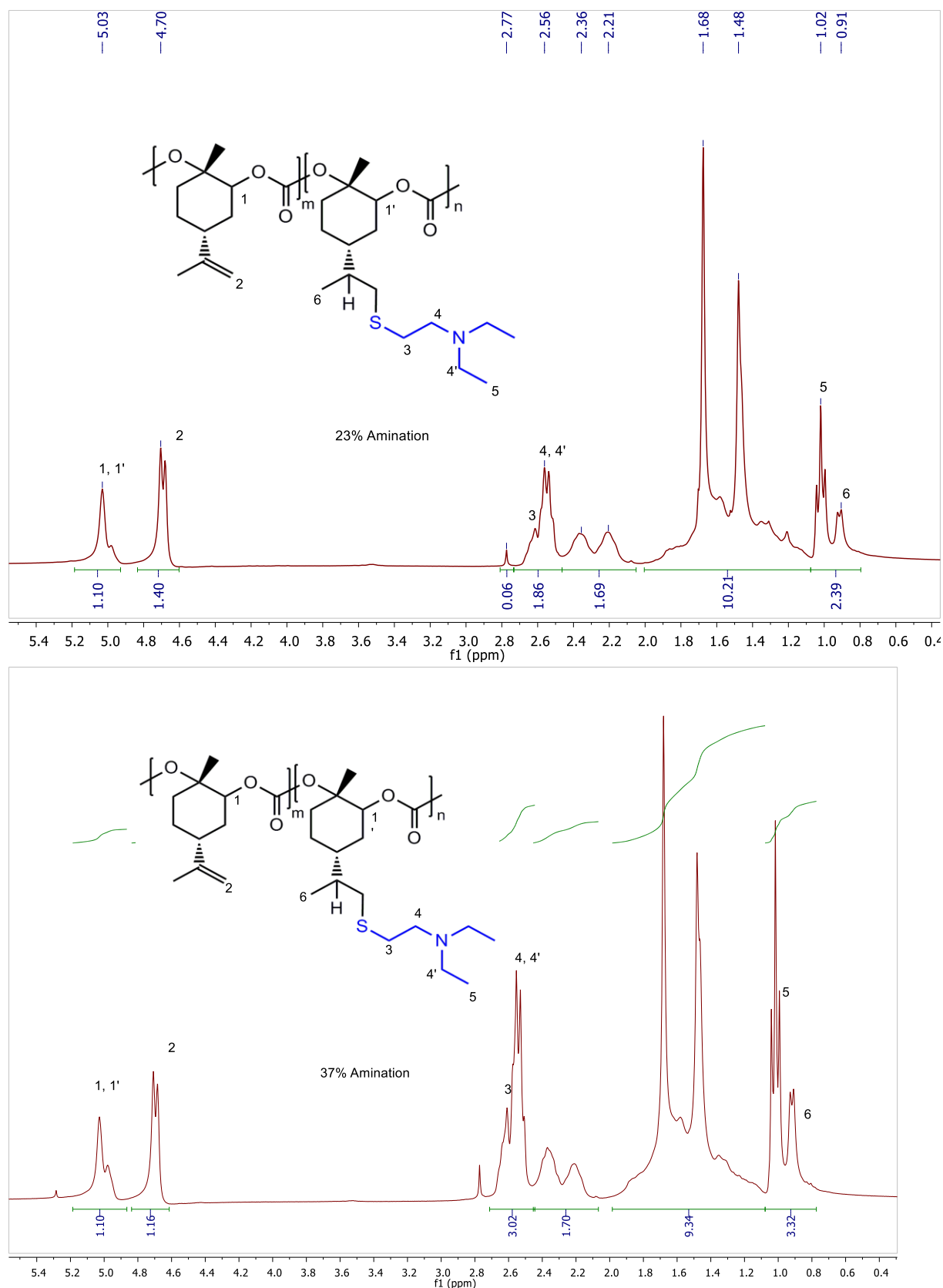
Supplementary Figure 5-8: ^{1}H NMR spectrum (recorded in CDCl$_3$) of PLimC-N23 (57 kDa) after reacting PLimC (treated with antioxidant before) for 3 h with 2-(diethylamino)ethanethiol hydrochloride to give a DF of 23%. ^{1}H NMR spectrum (recorded in CDCl$_3$) of PLimC-N37 (85 kDa) after reacting PLimC for 3 h with 2-(diethylamino)ethanethiol hydrochloride to give a DF of 37%.
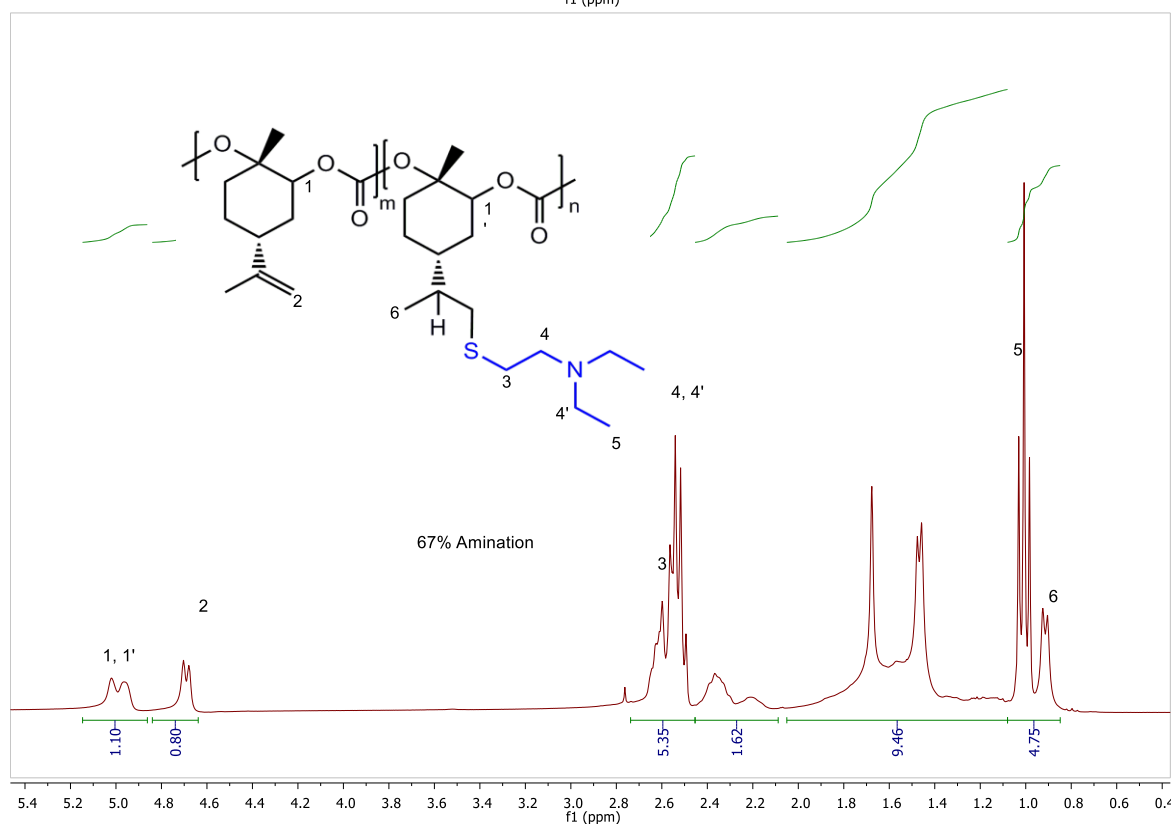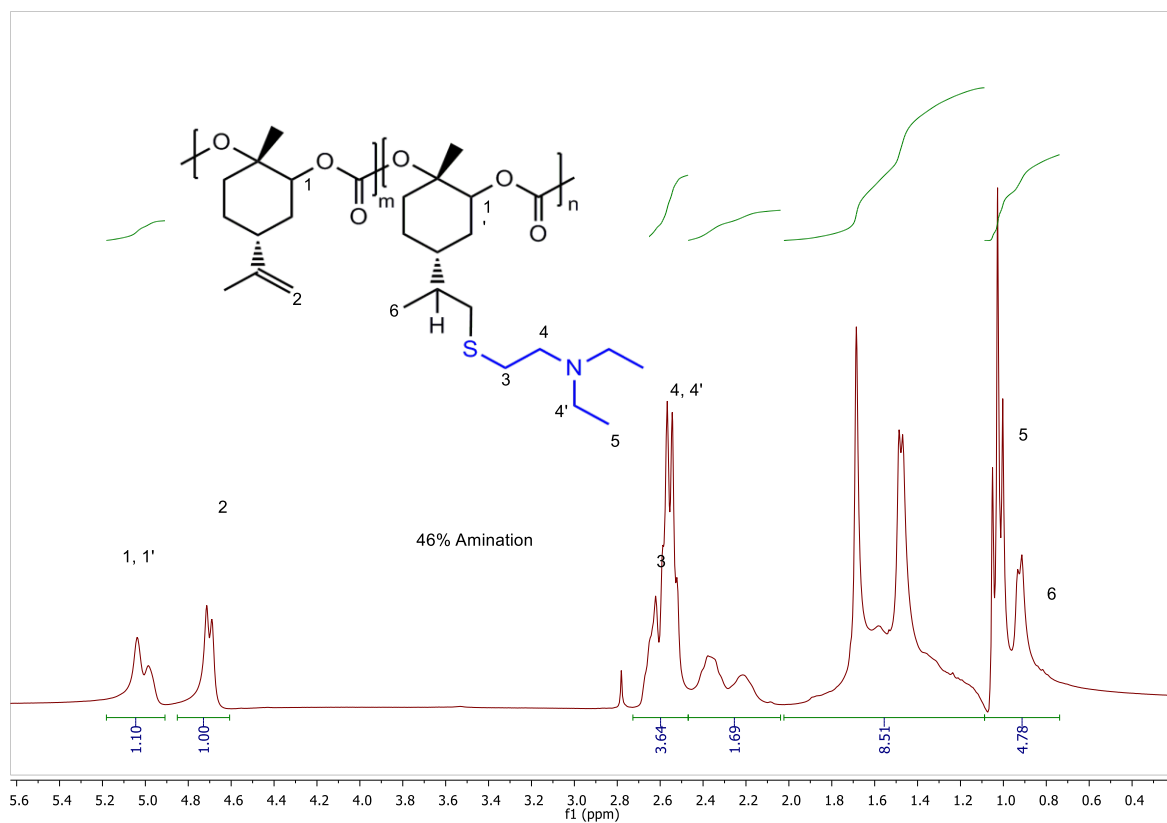
Supplementary Figure 5-9: ^{1}H NMR spectra (recorded in CDCl$_3$) of PLimC-N46 and PLimC-N67 (both 85 kDa) after reacting PLimC for 4 h or 6 h with 2-(diethylamino)ethanethiol hydrochloride to give a DF of 46% and 67%, respectively.
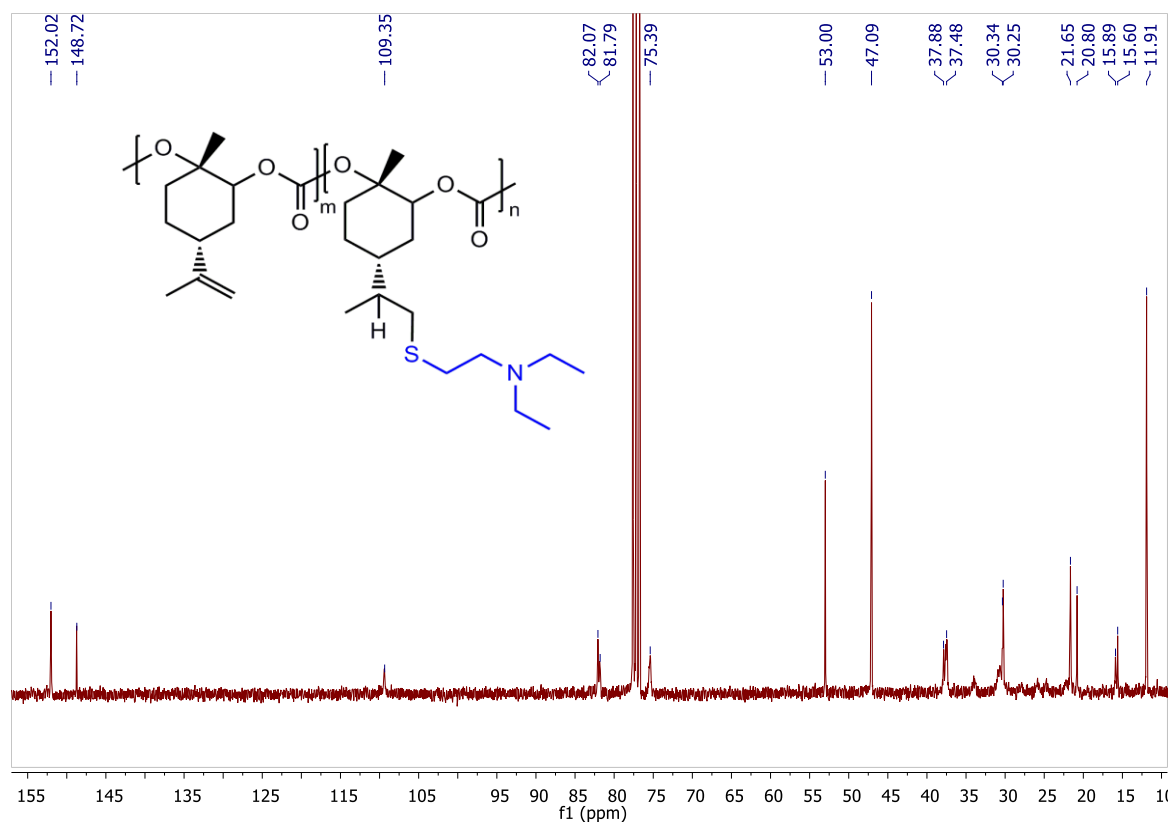
Supplementary Figure 5-10: Representative ^{13}C NMR spectrum (recorded in CDCl$_3$) of PLimC-N67 (85 kDa) after reacting PLimC for 6 h with 2-(diethylamino)ethanethiol hydrochloride to give a DF of 67%.
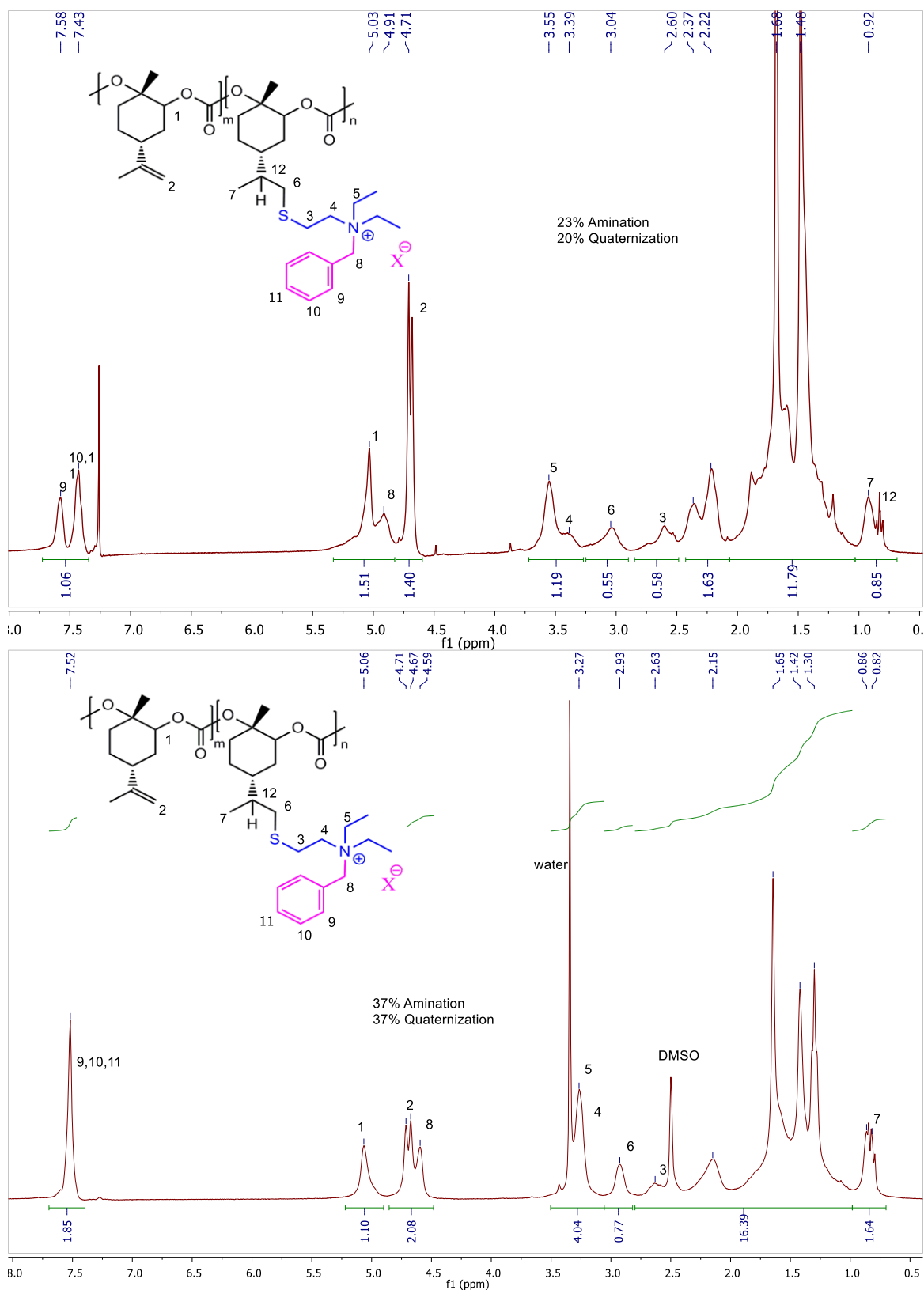
Supplementary Figure 5-11: ^{1}H NMR spectrum (recorded in CDCl$_3$) of PLimC-NQ20 (57 kDa) after reacting PLimC-23N for 24 h with benzyl bromide to give nearly quantitative quaternization of the amine. ^{1}H NMR spectrum (recorded in DMSO-d$_6$) of PLimC-NQ37 (85 kDa) after reacting PLimC-N37 for 24 h with benzyl bromide to give quantitative quaternization of the amine.
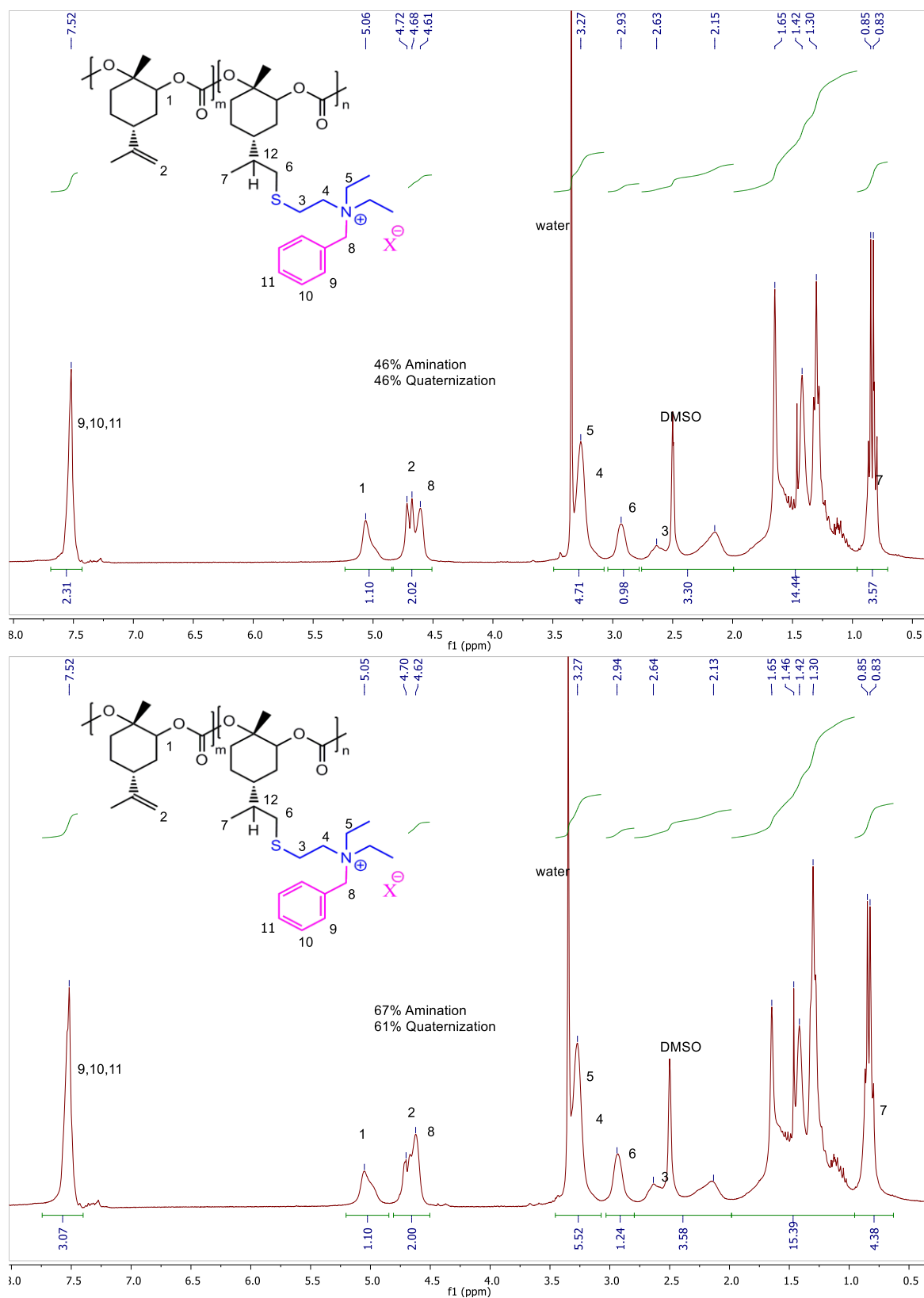
Supplementary Figure 5-12: ¹H NMR spectra (recorded in DMSO-d₆) of PLimC-NQ46 and PLimC-NQ61 (both 85 kDa) after reacting PLimC-N46 and PLimC-N67 for 24 h with benzyl bromide to give quantitative or 90% quaternization, respectively.
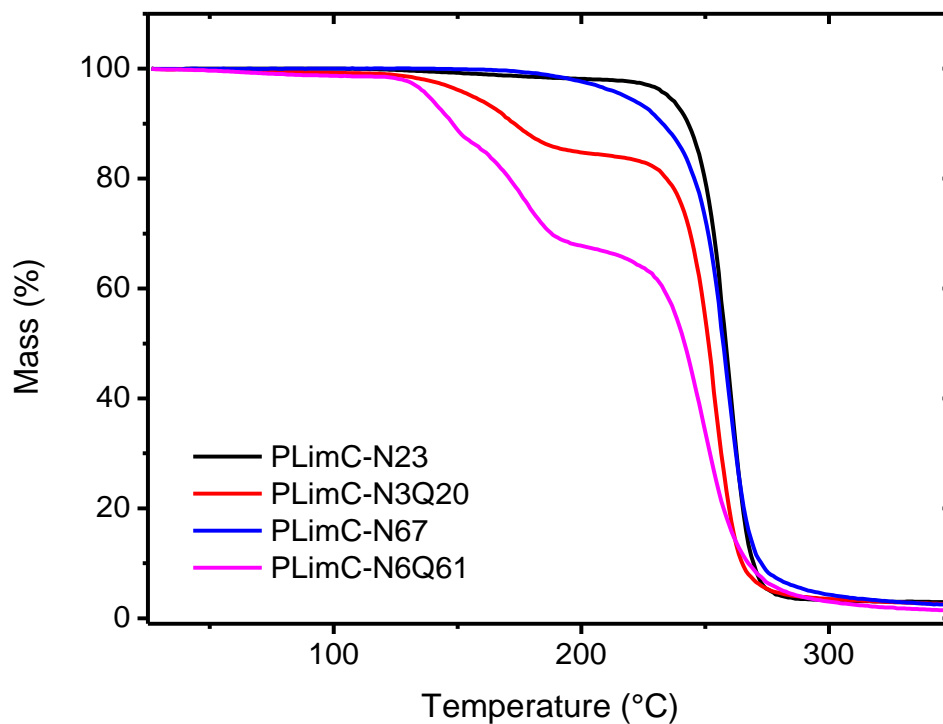
Supplementary Figure 5-13: Thermogravimetric analysis of aminated (PLimC-N) and quaternized (PLimC-NQ) samples of PLimC with different DF, measured at 10 K min^{-1} under N$_2$ atmosphere.
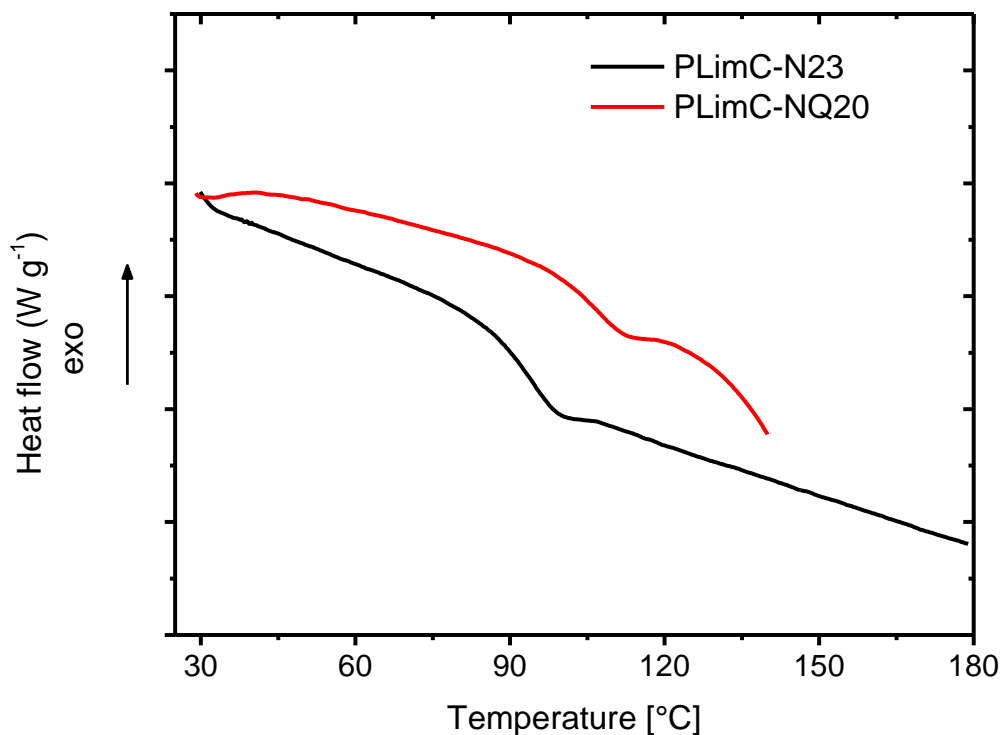
Supplementary Figure 5-14: Second heating runs of DSC experiment of aminated (PLimC-N23) and quaternized (PLimC-NQ20) samples, measured at 10 K min^{-1} in N$_2$ atmosphere. The trace of PLimC-NQ20 is cut off at 140 °C, since decomposition of the sample is already in full progress.
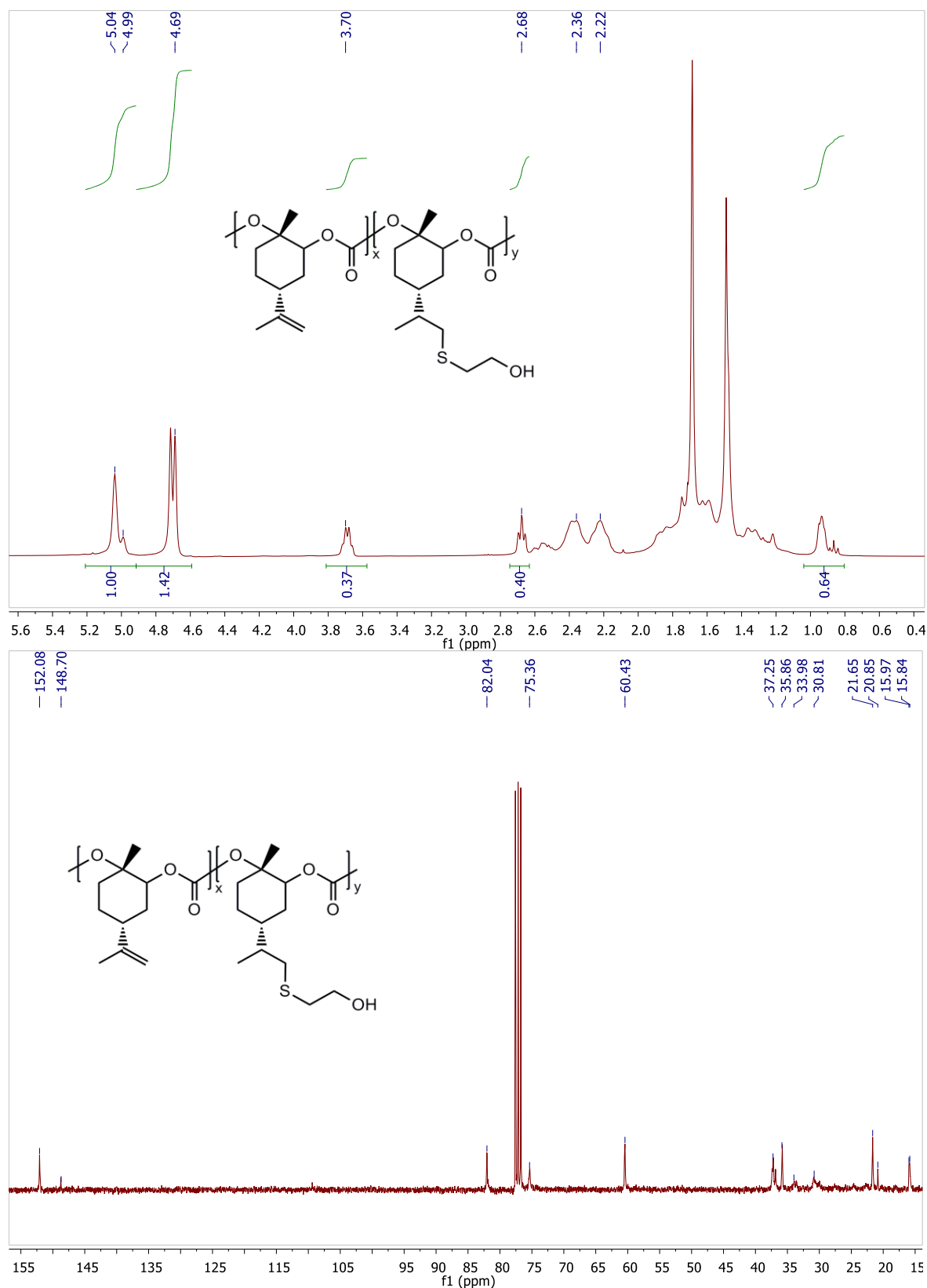
Supplementary Figure 5-15: Representative ^{1}H and ^{13}C NMR spectra (recorded in CDCl$_3$) of PLimC-ME18 after reacting PLimC for 1 h with mercaptoethanol to give 18% conversion.
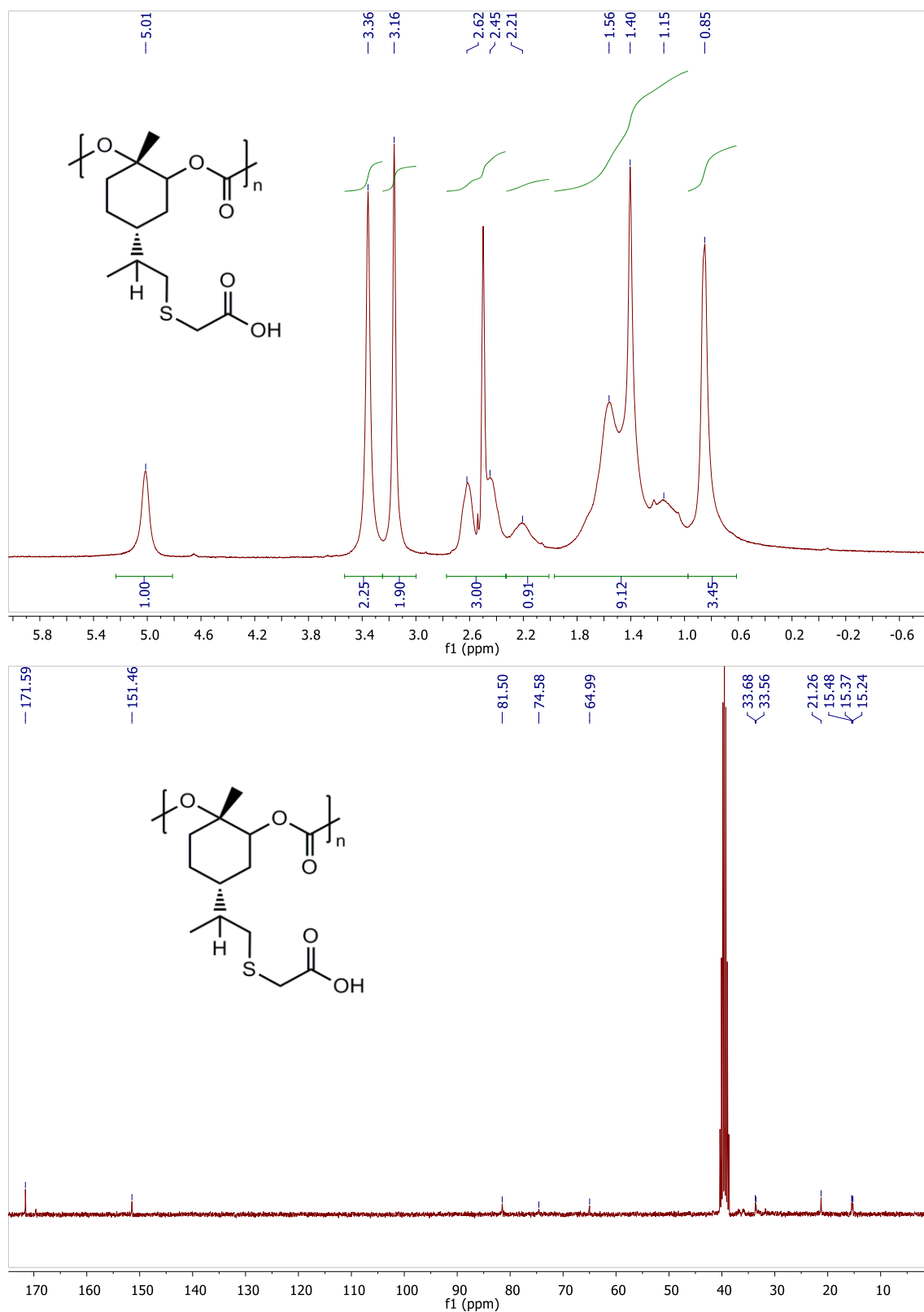
Supplementary Figure 5-16: ^1H and ^{13}C NMR spectra (recorded in DMSO-d^6) of PLimC-MAc after reacting PLimC for 3 h with mercaptoacetic acid to give quantitative conversion.
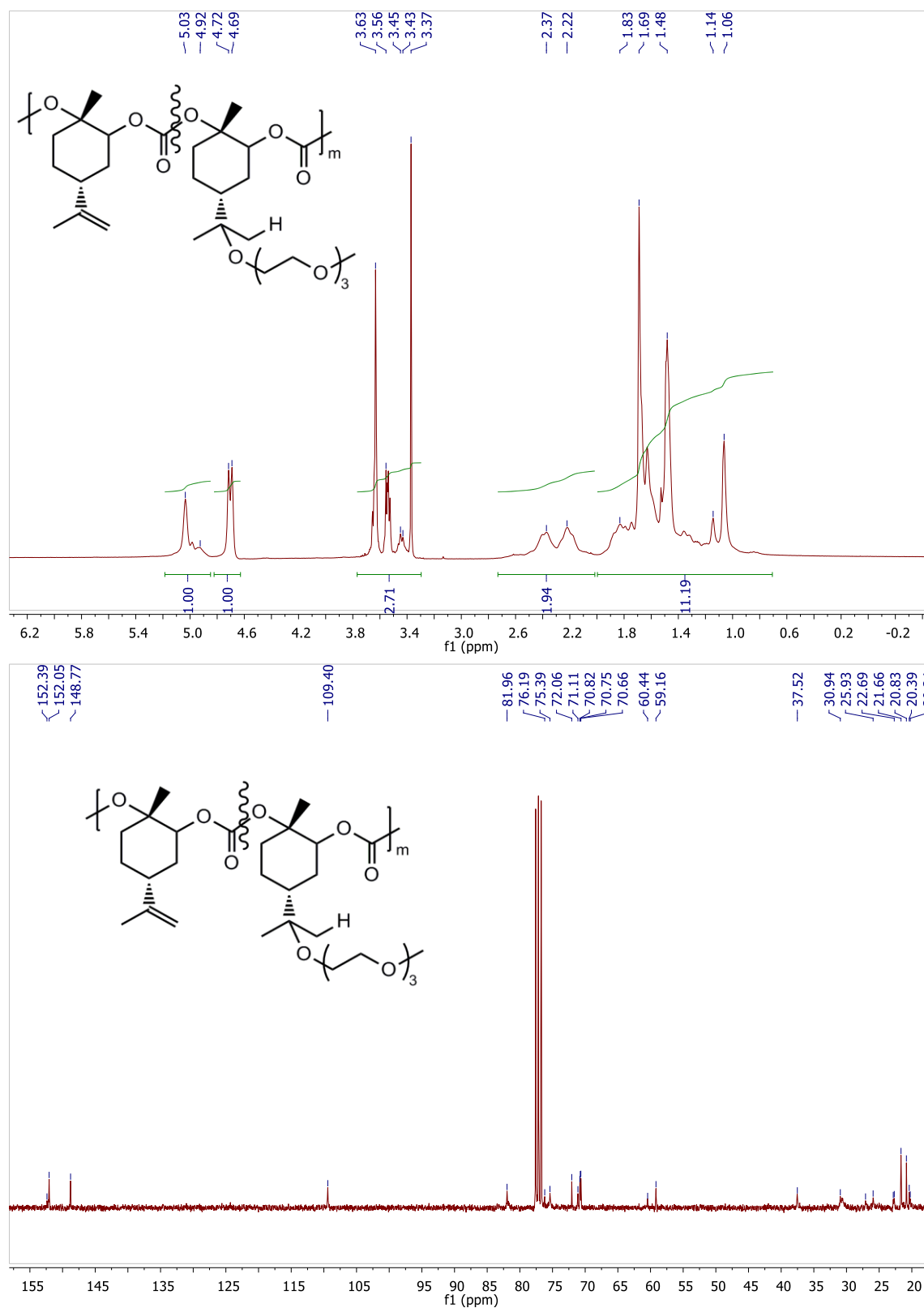
Supplementary Figure 5-17: ^{1}H and ^{13}C NMR spectra (recorded in CDCl$_3$) of PLimC-PEG after reacting PLimC for 68 h with PEG-3-OH to give a degree of functionalization of 18%.
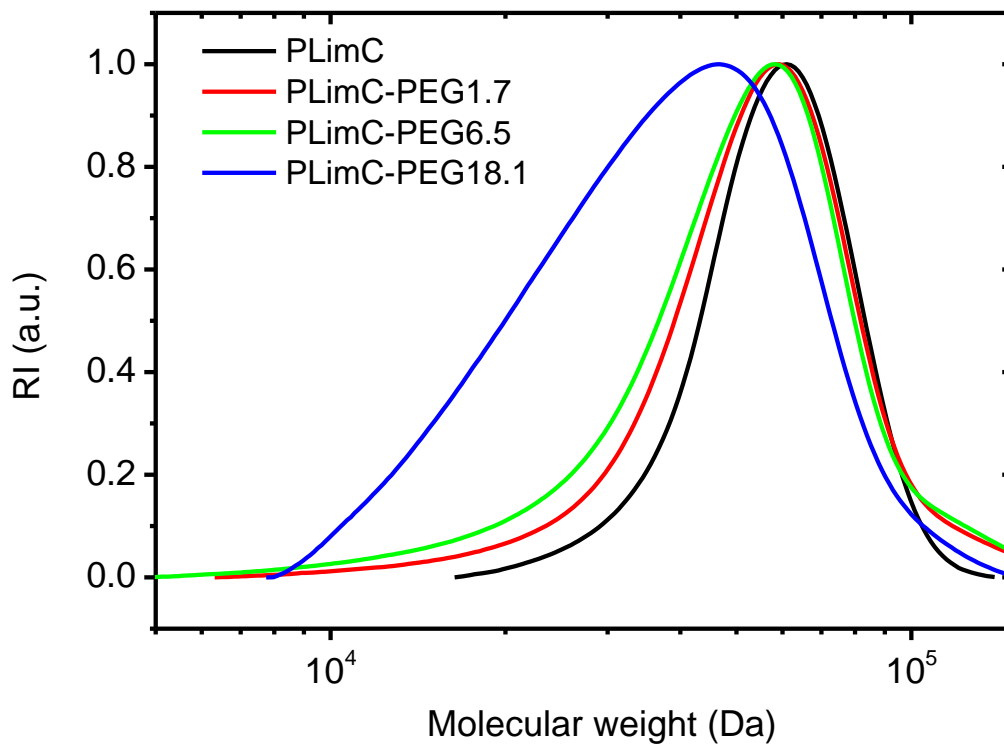
Supplementary Figure 5-18: GPC molar mass distribution (eluent was chloroform, calibration was performed with PS standards) of PLimC and the PEG functionalized samples, showing the effect of the acidic conditions, that degrade PLimC after prolonged exposure.
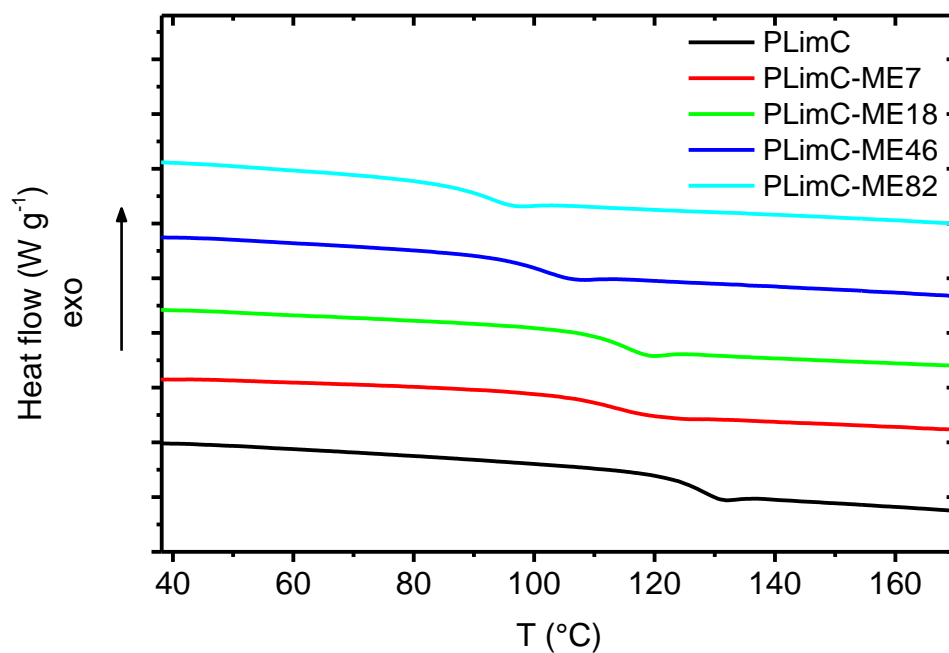
Supplementary Figure 5-19: Development of T_g with increasing functionalization of PLimC with ME. For longer reaction times and higher degree of functionalization the T_g is rising again, because of intermolecular cross-linking between the double bonds.
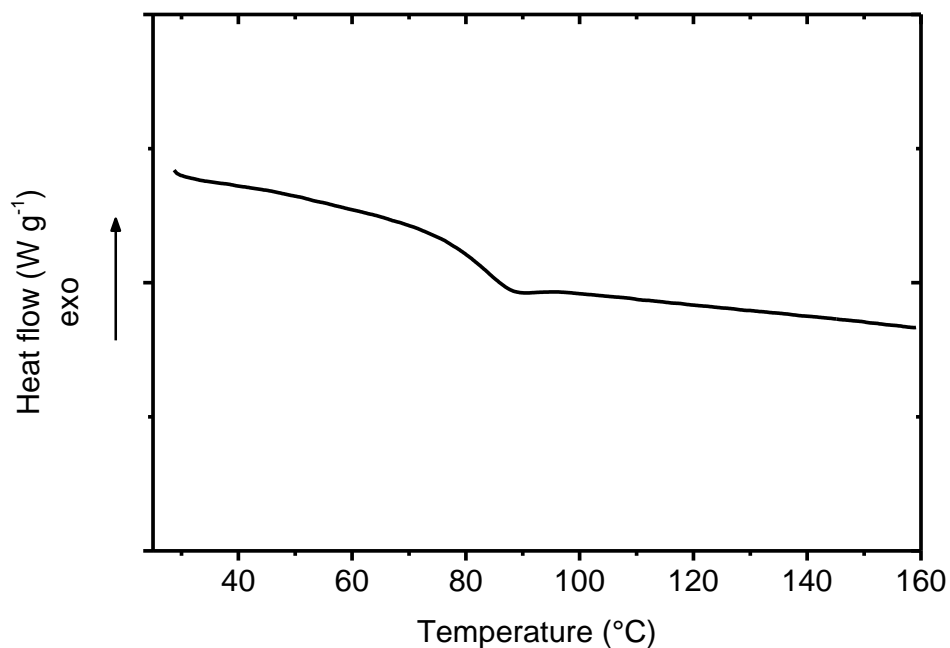
Supplementary Figure 5-20: DSC thermogram of PLimC-MAc measured at 10 K min^{-1} in N$_2$ atmosphere showing a glass transition of the sample at 82 °C.
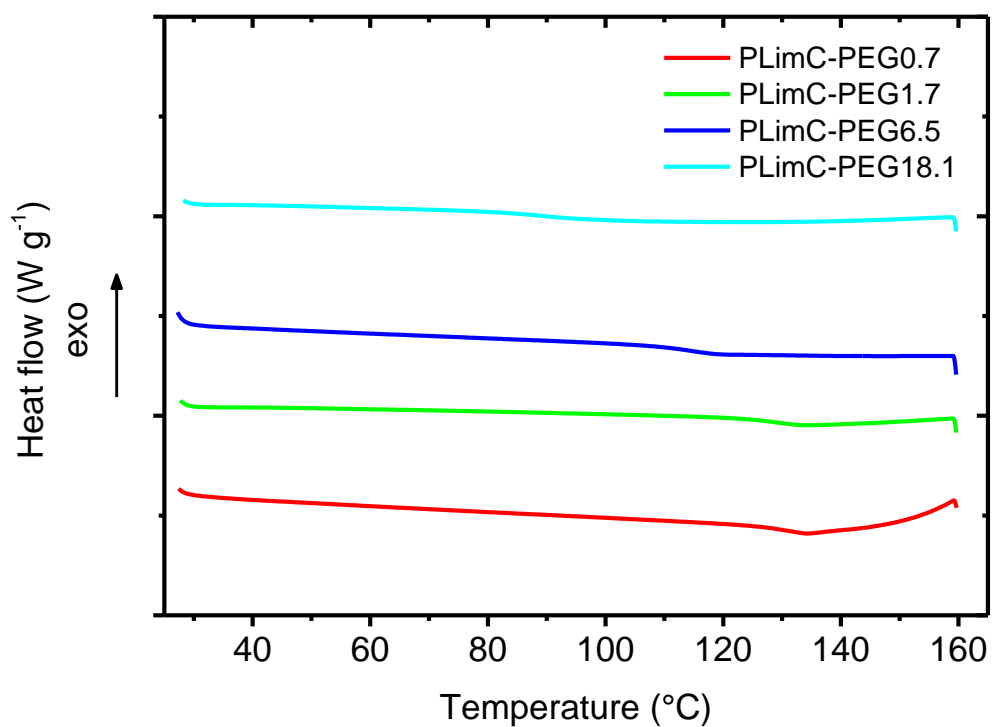
Supplementary Figure 5-21: Second run of DSC experiments of PLimC functionalized with various amounts of PEG-3-OH by acid-catalyzed electrophilic addition of PEG-3-OH.
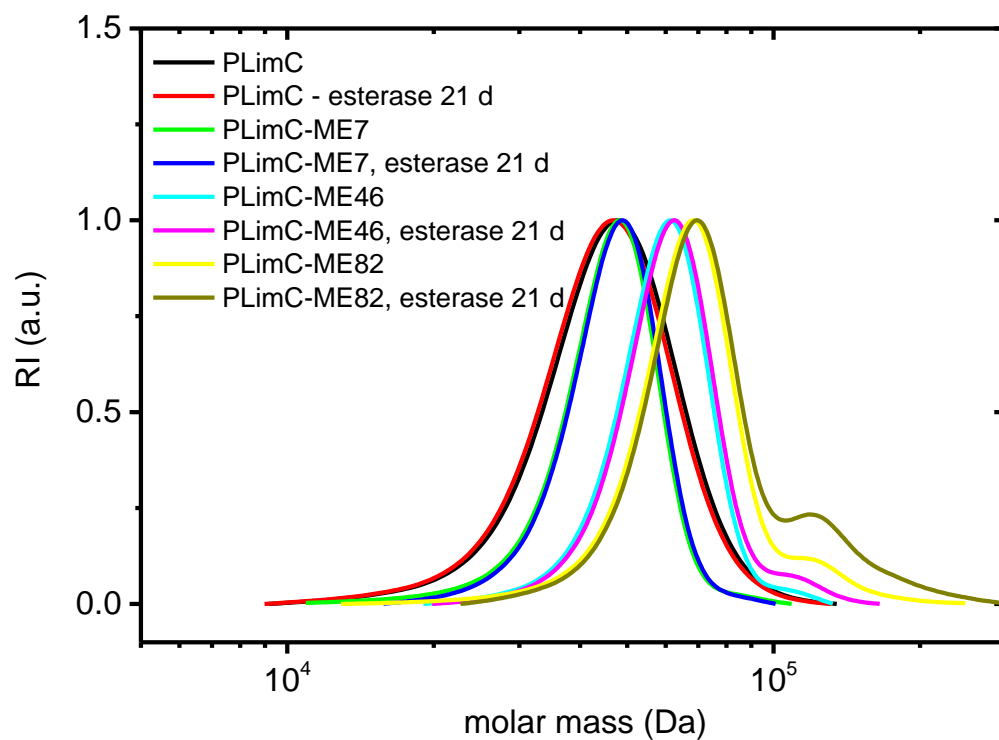
Supplementary Figure 5-22: Molar mass distribution of PLimC, PLimC-ME7/46/82 films before and after immersion for 21 days in an esterase buffer (pH 9) suspension. For all samples no significant change of molar mass distribution is observed, suggesting stability of the samples under these conditions. The eluent for GPC measurements was chloroform.

Chromatogram
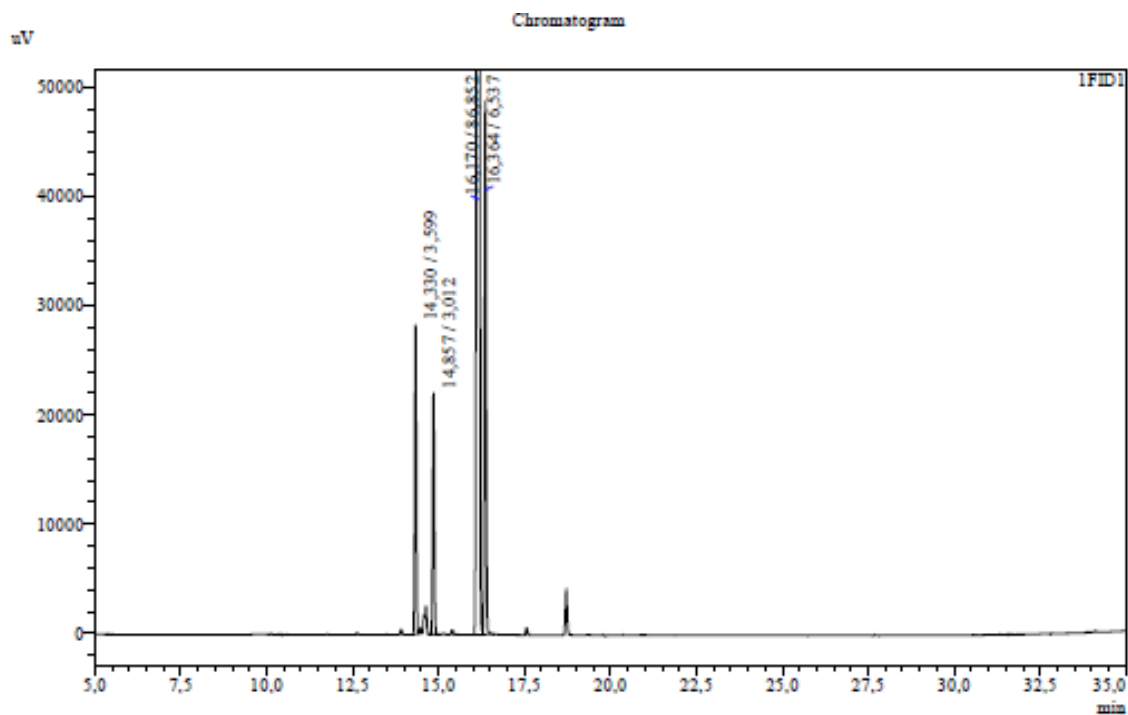
Peak Table

FID1

Peak#	Ret. Time	Area%	Area	Height
1	14.330	3.599	88836	28335
2	14.857	3.012	74344	22143
3	16.170	86.852	2143677	556919
4	16.364	6.537	161346	48906
Total		100.000	2468203	656304

Supplementary Figure 5-23: GC analysis of menth-1-ene with a retention time of 16.4 min, after filtration step to remove the catalyst.

Chromatogram
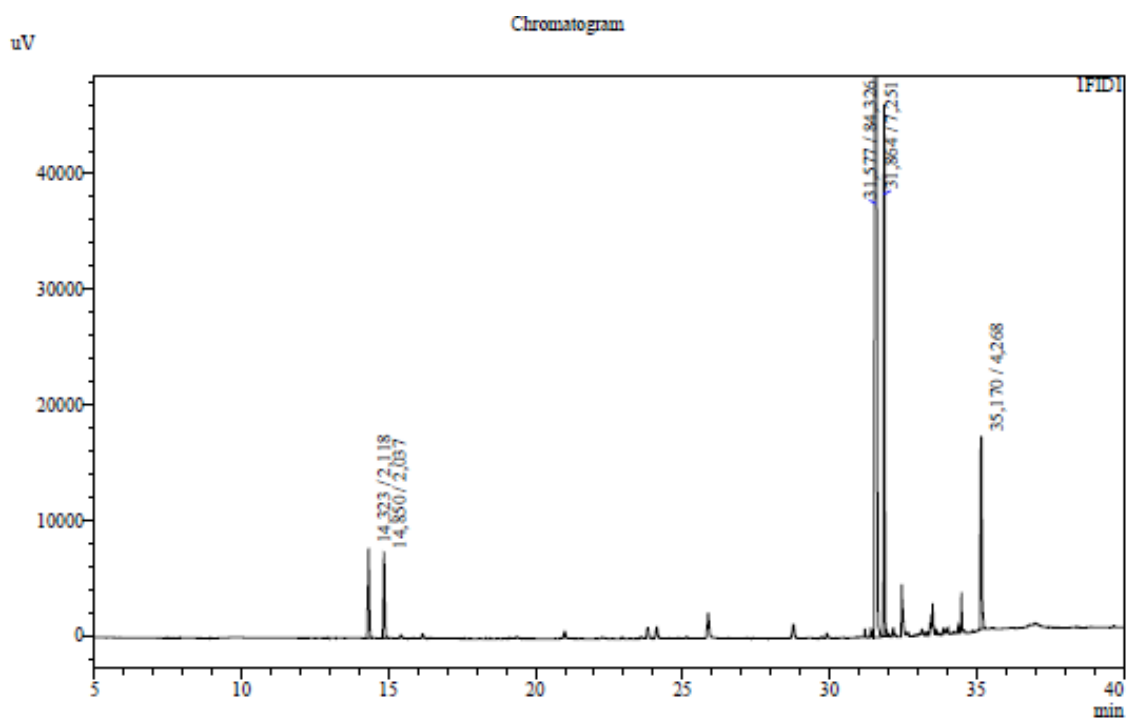
Peak Table

FID1

Peak#	Ret. Time	Area%	Area	Height
1	14.323	2.118	25801	7766
2	14.850	2.037	24812	7379
3	31.577	84.326	1027055	430913
4	31.864	7.251	88309	45974
5	35.170	4.268	51984	16696
Total		100.000	1217961	508727

Supplementary Figure 5-24: GC analysis of the bromohydrin of menth-1-ene (MenBrOH) with retention times of 31.6 min (*cis*) and 31.9 min (*trans*), respectively, which was directly converted into the epoxide without prior purification.

Chromatogram
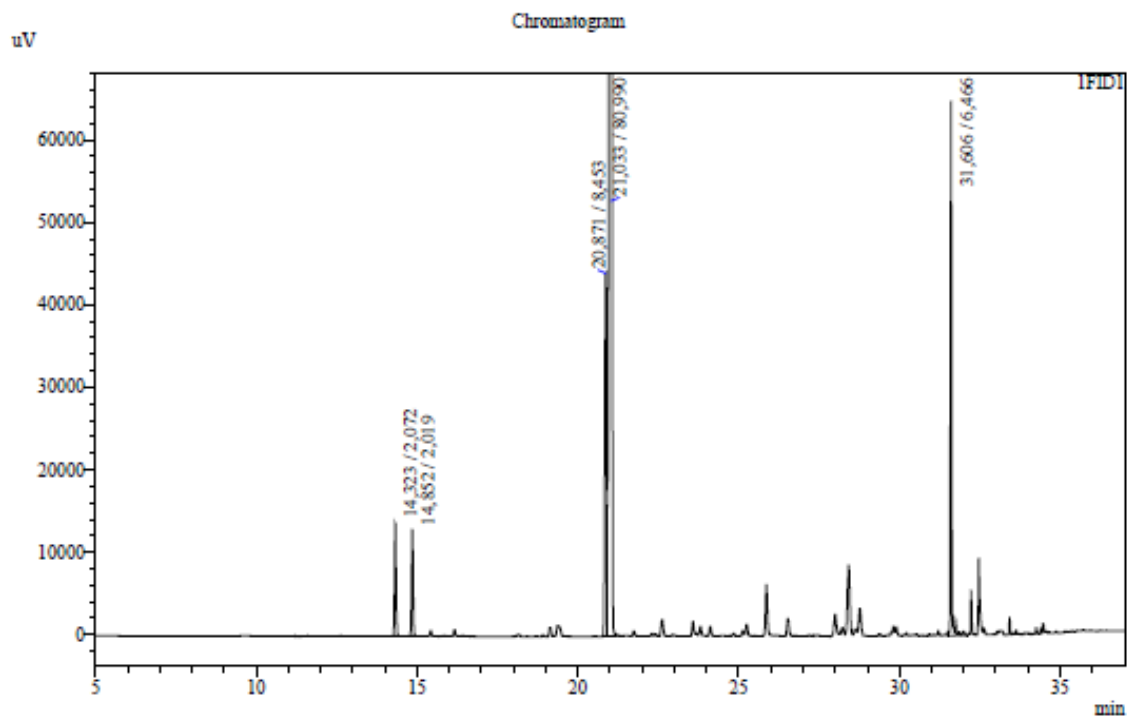
Peak Table

FID1

| Peak#	Ret. Time	Area%	Area	Height
1	14,323	2,072	45127	13779
2	14,852	2,019	43973	12986
3	20,871	8,453	184075	44005
4	21,033	80,990	1763692	415694
5	31,606	6,466	140807	64610
Total		100,000	2177674	551074

Supplementary Figure 5-25: GC analysis of the MenO with retention times of 20.8 (*cis*) and 21.0 (*trans*) min, which was afterwards treated with NaH/ MeI and distilled. In the peak table below, the excess of *trans*-isomer is proven by the relative areas, i.e. 81% for *trans*-MenO.
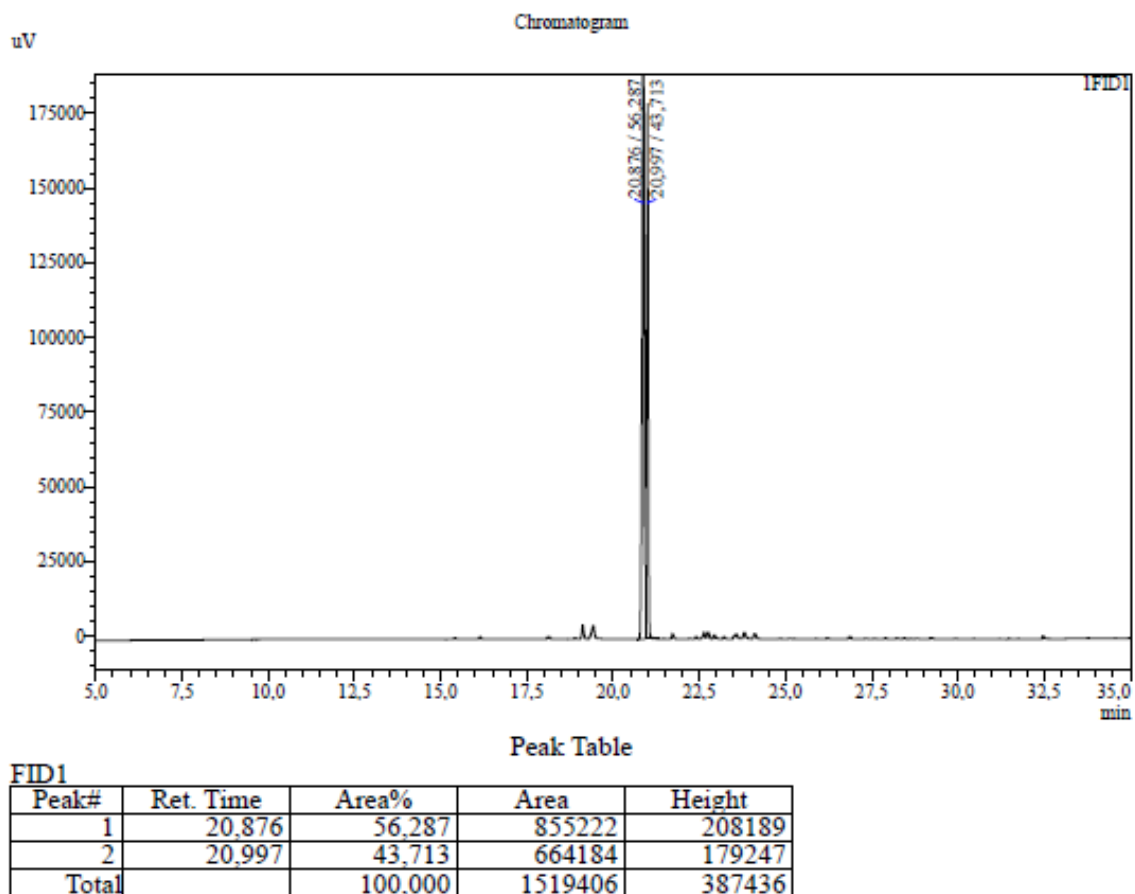
Supplementary Figure 5-26: GC analysis of the precipitation bath of PMenC showing mainly *cis*-MenO (20.9 min) and *trans*-MenO (21.0 min). In the peak table below, the accumulation of *cis*-isomer is proven by the relative areas, i.e. 56% for *cis*-MenO compared to 44% *trans*-MenO, indicating the preferential incorporation of the latter into PMenC.
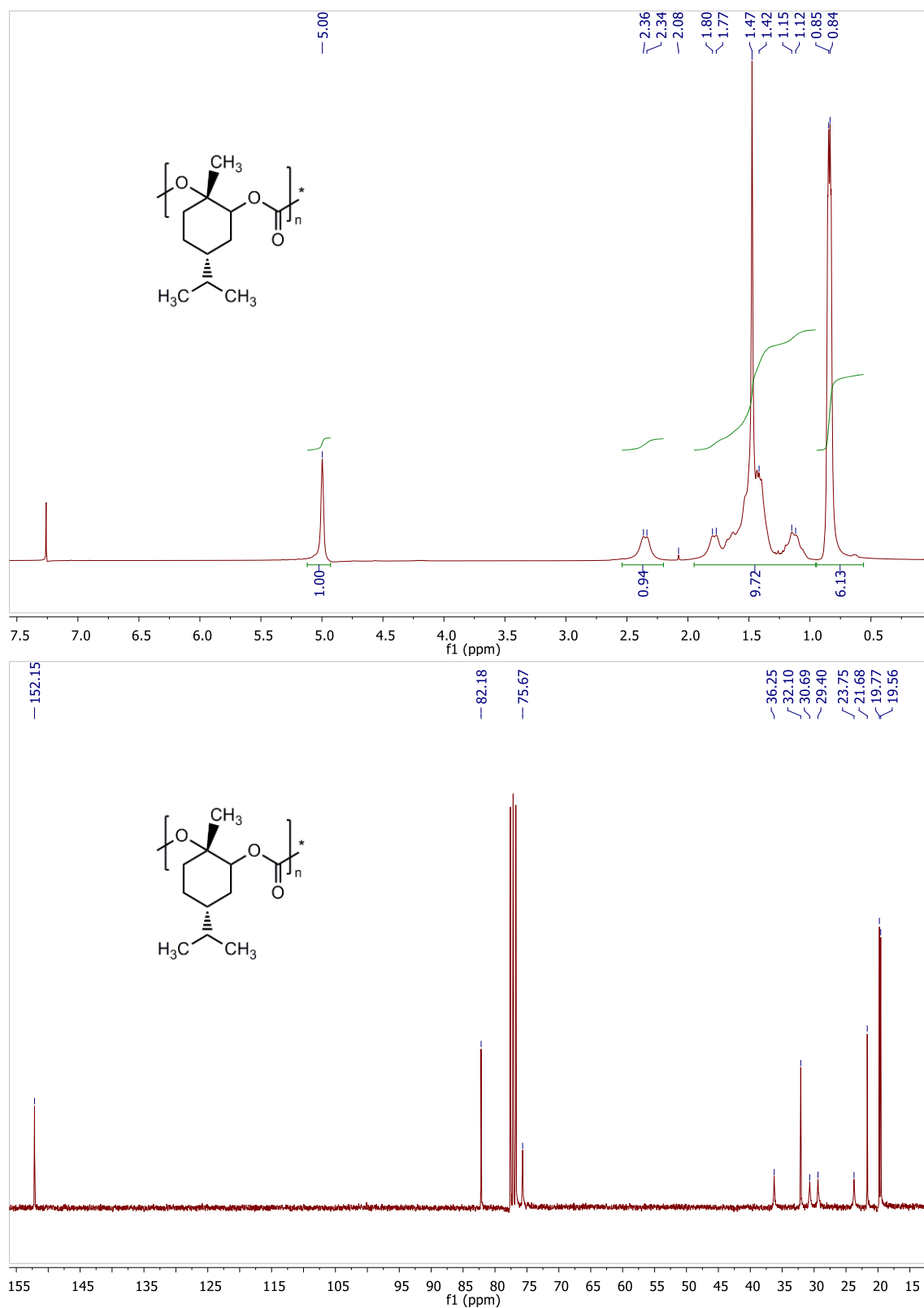
Supplementary Figure 5-27: ^{1}H and ^{13}C NMR spectra (recorded in CDCl$_3$) of PMenC, which was produced by copolymerization of *trans*-menthene oxide with CO$_2$ in the presence of a Zn catalyst. The preferential incorporation is also represented in the NMR spectra of PMenC. The ^{1}H NMR spectrum shows a single peak at 5.00 ppm without any downfield shoulder, which would be an indication of incorporation of the *cis*-isomer into the backbone. This argument is further supported by the ^{13}C NMR spectrum of PMenC, which shows only one carbonyl resonance at 152.2 ppm i.e. no stereo-irregularities are present.
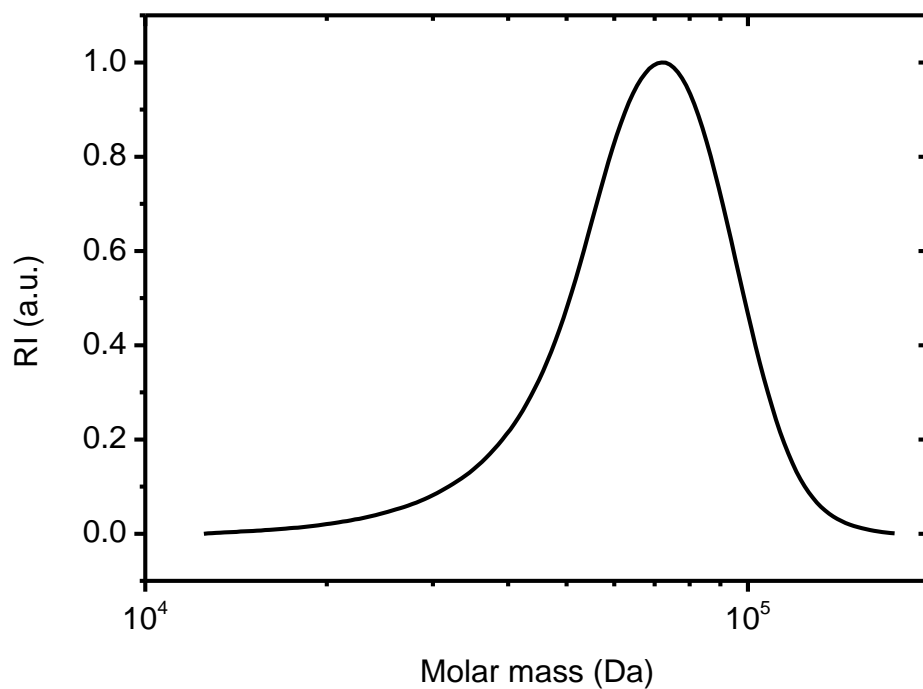
Supplementary Figure 5-28: GPC molar mass distribution (eluent was chloroform, calibration was performed with PS standards) of PMenC. The GPC analysis givs a relative M_n of 61.3 kDa and Đ of 1.14.
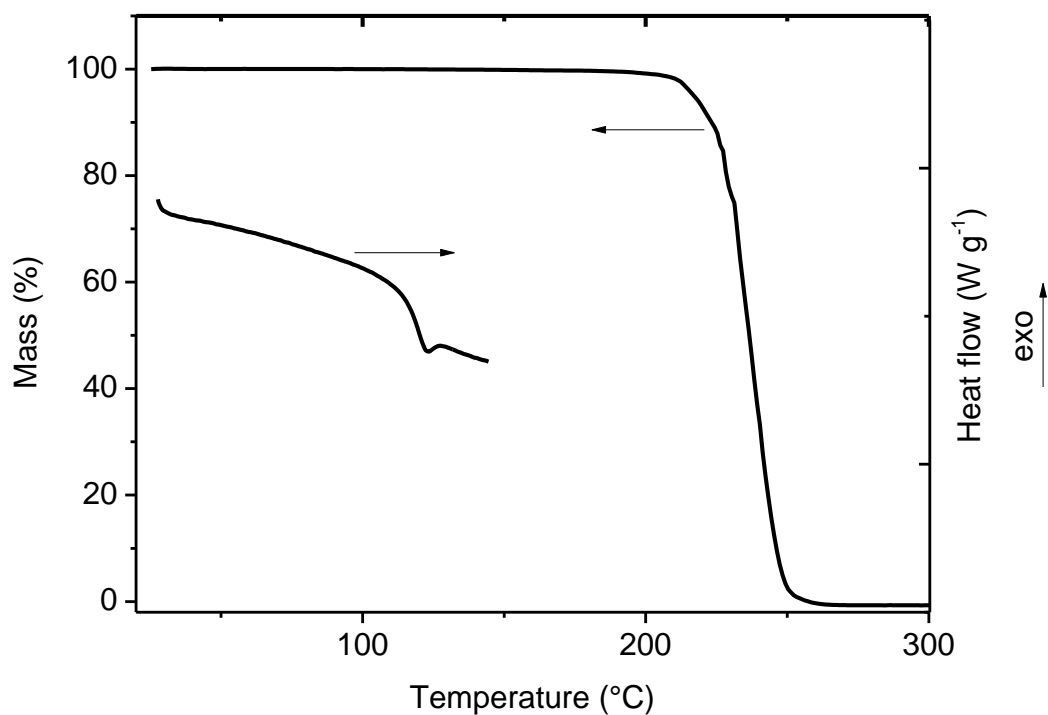
Supplementary Figure 5-29: TGA and DSC (2nd heating cycle) thermograms of PMenC measured at 10 K min^{-1} in N_2 atmosphere. The glass transition temperature is –as for PLimC - found at 130 °C and also the 5% decomposition temperature remains at 240 °C. Hence the hydrogenation has no influence on the thermal properties of this aliphatic polycarbonate.

Supplementary tables

Supplementary Table 5-1: Mechanical properties of selected commodities, engineering plastics and rubbers compared to PLimC and PLimC rubber from selected sources.[1–3]

Polymer	YOUNG's modulus (GPa)	σ_s (MPa)	ε (%)
PLimC	0.95	55	15
PLimC B3MP$_{2.0}$	0.001	6.8	228
PA-6	1.9	50	300
PC	2.5	65	125
PE	0.2 - 1	10 -30.0	600 - 800
PET	3	54	275
PMMA	3.2	65	10
PP	1.4	32	400
PTFE	0.5	13	200
PVAc	0.6	30	10 - 20.0
PVC	2.6	48	30
Silicon rubber	0.001	4.8 - 7.0	100 - 400
natural rubber	0.0013	17-25	750-850
1,4-Polybutadiene	0.0013		
butyl rubber	0.001	18-21	750-950
Neoprene	0.0016	25	800-1000

Supplementary Table 5-2: Functionalization of PLimC with B3MP for various reaction times, resulting in different DFs and therefore different amounts of residual double bonds. The mol% of unsaturation of the uncured sample (100% - DF) is given as subscript in the sample name (i.e. PLimC-B3MP$_{2.0}$ has 2 mol% unsaturated repeating units). The mechanical data was recorded after curing the samples for 5 h at 100 °C in air.

#	sample	t (min)	DF$_{B3MP}$[a) (mol%)	M_n[b) (kDa)	$Đ$[b)	σ_s[c) (MPa)	YOUNG's modulus[c) (MPa)	ε[c) (%)
1	PLimC	0	0	54.3	1.13	950	55	15
2	PLimC-B3MP$_{2.0}$	60	98.0	72.3	1.18	6.8 ± 0.8	1.05 ± 0.12	228 ± 6
3	PLimC-B3MP$_{1.0}$	80	99.0	73.3	1.18	7.2 ± 2.8	0.90 ± 0.15	265 ± 8
4	PLimC-B3MP$_{0.5}$	180	99.5	75.2	1.18	9.0 ± 0.9	0.52 ± 0.05	342 ± 9
5	PLimC-B3MP$_{0.0}$	300	>99.9	76.1	1.17	5.2 ± 0.2	0.32 ± 0.02	426 ± 4

[a)]determined/estimated from analysis of ^{1}H NMR spectra in the region of 4.7 ppm (protons of double bond), [b)]determined by GPC analysis, [c)]determined by tensile tests.

Supplementary Table 5-3: Functionalization of PLimC with 2-(diethylamino)ethanethiol in chloroform at 60 °C for different reaction times and either 6 (entry 1) or 7 (entries 2-4) equivalents of thiol with respect to PLimC double bonds.

#	sample	t (h)	eq. thiol	DF_{amine} (%)	pencil hardness
1	PLimC-N23[a]	3	6	23	7B
2	PLimC-N37	3	7	37	7B
3	PLimC-N46	4	7	46	8B
4	PLimC-N67	6	7	67	8B

[a]molecular weight (M_n) of starting material PLimC was 57.3 kDa

Supplementary Table 5-4: Quaternization of PLimC-N with benzyl bromide for different degrees of amination. Reaction was conducted in neat benzyl bromide (3 eq.) for 24 h without stirring, since the mixture was too viscous. After dilution with THF the polymer solution was repeatedly precipitated in hexane.

#	sample	DF_{amine} (%)	$DF_{quaternized}$ (%)	pencil hardness
1	PLimC-NQ20	3	20	2B
2	PLimC-NQ37	0	37	2B
3	PLimC-NQ46	0	46	3B
4	PLimC-NQ61	6	61	3B

Supplementary Table 5-5: Shaking flask test of PLimC and PLimC-NQ20 (duplicate test) in buffer. In the table the colony forming count (cfu) after the specified time of inoculation is listed, recalculated from the 10-fold diluted sample. Besides the samples also positive reference (water soluble poly(hexamethylene-guanidine) hydrochloride (PHMG) was tested, to compare the antibacterial activity of PLimC-NQ).
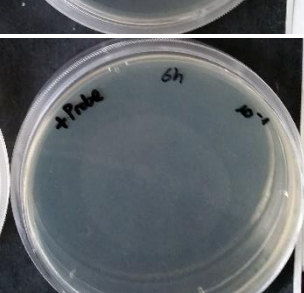
t (h)	N (cfu)	N (cfu)	R (%)	N (cfu)	R (%)	N (cfu)	R (%)
	PLimC	PLimC-NQ20		PLimC-NQ20		PHMG (positive ref.)	
0	170	160	0	180	0	230	0
6	170	160	0	180	0	0	100
12	1870	370	80	260	86	0	100
24[a]	19000	660	97	2000	90	0	100
48[a]	100000	12300	88	10200	90	0	100

[a] estimates are given, as the number of colonies even for the 10-fold dilution was above 300.

Supplementary Table 5-6: Repetition of shaking flask test of PLimC and PLimC-NQ20 (tested in total three times).

| t (h)	N (cfu)	N (cfu)	R (%)	N (cfu)	R (%)
	PLimC	PLimC-NQ20		positive ref. (PHMG)	
6	250	280	0	0	0
12	150	260	0	0	100
24	2000	15	99.3	0	100

Supplementary Table 5-7: Agar plates from spread bacteria suspensions of shaking flask test of PLimC, PLimC-NQ20 and PLimC-NQ37 for 6, 12, 24 and 48 h incubation time. A sample of PLimC-NQ37 was also tested in this run and interestingly, the antibacterial activity was lower compared to the less functionalized samples PLimC-NQ20. We would ascribe this rather unexpected behavior to the higher surface roughness of the cast films of PLimC-NQ37, leading to higher hydrophobicity although more polar groups are grafted to the polymer. Thus interaction with bacteria, i.e. with the cell membrane, is limited, which leads to low antibacterial activity.

time of incubation	6 h	
concentration	10^0	10^{-1}

PLimC-NQ20

PLimC-NQ37

PLimC

Positive reference (PHMG)

Supplementary Table 5-7 continued

time of incubation	12 h	
factor of concentration	10^0	10^{-1}
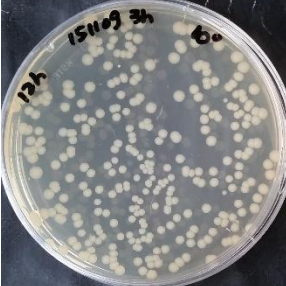
PLimC-NQ20

PLimC-NQ37

PLimC

Supplementary Table 5-7 continued

time of incubation	24 h	
concentration	10^0	10^{-1}
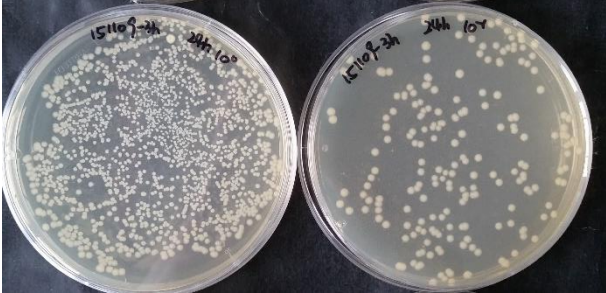
PLimC-NQ20

PLimC-NQ37

PLimC

time of incubation	48 h	
concentration	10^0	10^{-1}
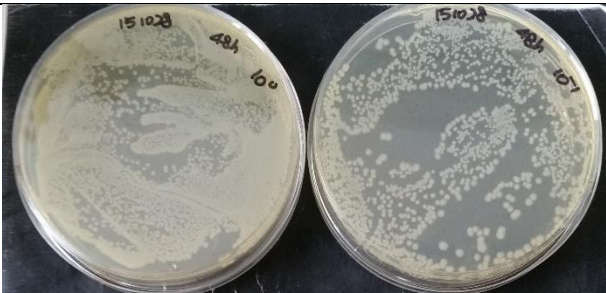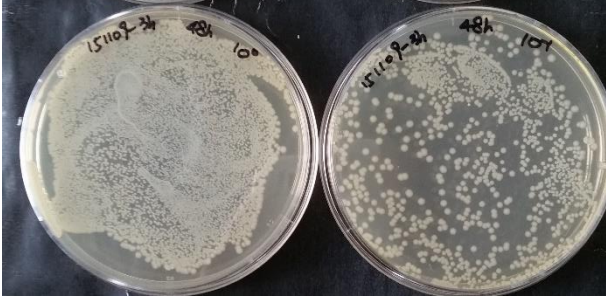
PLimC-NQ20

PLimC-NQ37

Supplementary Table 5-8: Functionalization of PLimC with mercaptoethanol (PLimC-ME) for various reaction times, resulting in different degrees of functionalization and therefore lowered T_g and contact angles to water with respect to pure PLimC. The increasing T_g and CA_W for samples reacted for longer than 6 h, can be explained by cross-linking reactions between the double bonds, as the chain segment mobility is lowered and the cast films show a higher roughness, due to imperfections on the surface.

#	sample	t (h)	DF_{ME} (mol%)	M_n (kDa)	$Đ$	T_g (°C)	CA_W (°)
1	PLimC	0	0	42.1	1.13	130	94
2	PLimC-ME7	1	7	42.9	1.08	113	86
3	PLimC-ME18	2	18	49.2	1.08	110	80
4	PLimC-ME46	3	46	56.5	1.06	100	79
5	PLimC-ME82	6	82	63.4	1.11	91	70
6	PLimC-ME81	16	81	70.5	1.26	95	97[a]

[a]The prolonged reaction times lead to cross-linking, which also influenced surface roughness of cast films and thus the contact angle (higher for increased roughness).

Supplementary Table 5-9: Functionalization of PLimC by sulfuric acid-catalyzed electrophilic addition of PEG-3-OH for different reaction times.

#	sample	DF_{PEG} (%)	t (h)	T (°C)	CA_W (°)	M_n (kDa)	$Đ$	T_g (°C)
1	PLimC	-	-	-	93	54.3	1.10	130
2	PLimC-PEG0.7	0.7	23	20	94	53.2	1.12	
3	PLimC-PEG1.7	1.7	43	30	99	47.2	1.24	129
4	PLimC-PEG6.5	6.5	48	45	81	40.8	1.36	114
5	PLimC-PEG18.1	18.1	68	54	79	31.6	1.32	91

Supplementary Table 5-10: Weight loss studies of PLimC, PLimC-ME7/ME46/ME82 and BPA-PC in various media, i.e. water, esterase, pH and pH 3 buffer for 3, 7 and 21 days. All samples were measured in triplicate and the mean values are given here relative to the original mass in % with standard deviation σ. The change of hydrophilicity and T_g do not promote mass loss of the polymer samples PLimC, PLimC-ME7/46/82 or BPA-PC respectively, for the conditions tested.

medium	t (d)	PLimC m (%)	σ	PLimC-ME7 m (%)	σ	PLimC-ME46 m (%)	σ	PLimC-ME82 m (%)	σ	BPA-PC m (%)	σ
water	3	98.0	0.3	99.0	0.3	98.8	0.3	98.5	0.5	98.5	0.5
	7	97.8	0.2	98.6	0.7	99.0	0.2	98.8	0.6	99.0	0.2
	21	98.6	0.7	98.8	0.1	98.5	0.6	98.5	0.4	99.3	0.1
esterase	3	98.2	0.2	98.8	0.6	97.8	0.5	98.0	0.9	98.5	0.4
	7	99.1	0.0	98.9	0.2	98.3	0.3	99.0	0.5	98.8	0.3
	21	98.0	0.8	99.4	0.3	98.7	0.5	98.8	0.1	97.9	0.8
pH 9	3	98.4	0.5	99.5		98.5	0.5	98.5	0.5	98.8	0.3
	7	99.1	0.4	99.2	0.1	98.3	0.6	97.8	1.0	99.0	0.2
	21	98.9	0.4	98.9	0.6	99.1	0.1	98.6	0.4	98.5	0.6
pH 4	3	99.4	0.3	99.0	0.5	98.5	0.5	98.5	0.3	99.3	0.4
	7	98.6	0.7	98.1	0.7	98.8	0.2	98.8	0.8	98.5	0.8
	21	98.8	0.1	98.3	0.1	97.9	0.6	98.0	0.6	98.9	0.3

Supplementary Discussion

GPC analysis of PLimC-MAc

GPC data of the acid-functionalized PLimC sample (PLimC-MAc) is not given as it is not soluble in $CHCl_3$ and THF (only swells the polymer). The polymer is soluble in DMSO and DMF, though the sample elutes within the exclusion volume of the GPC column set due to the strong interaction with the eluent and weak interaction with the hydrophobic column packing material.

Curing procedure and tensile tests for PLimC rubber

The mechanical properties listed in Supplementary Table 5-2 were measured on samples that had been cured at 100 °C for 5 h in air. The curing procedure was applied in order to induce cross-linking of the residual double bonds in the polymer. After curing, the samples were assessed towards their solubility in chloroform and except for PLimC-B3MP$_{0.0}$ (no cross-linking is possible even when exposed to 100 °C for 24 h) none of them dissolved but only swelling was observed.

To elucidate the mechanism of heat-induced cross-linking, a solution of PLimC-B3MP$_{2.0}$ in chloroform was mixed with 1 wt% butylated hydroxytoluene (BHT, radical inhibitor) and cast into a film. After exposing the dry film to the same curing procedure (100 °C for 5 h) – in contrast to the BHT-free samples – no cross-linking was observable, indicating a free radical cross-linking mechanism between adjacent double bonds of the partially unsaturated samples. The heat-induced cross-linking was proven indirectly by assessing the solubility and the mechanical properties of the cured samples. A direct analysis of residual double bonds by IR spectroscopy is not applicable because the low degree of unsaturation (< 3%) lies beyond the detection limit of the spectrometer. The effect of curing (time) is shown in Supplementary Fig. 5-5 for PLimC-B3MP$_{2.0}$. The curing temperature of 100 °C was chosen due to the trade-off between decomposition of the backbone of the rather labile polycarbonate (as discussed in our previous article on PLimC)[3] and the rate of thermally induced cross-linking (the higher the faster). On the one hand, a curing time of 5 h was found to be sufficient, since longer curing would not change the tensile properties any further. On the other hand, a curing time of 5 h was necessary, since samples heated for only 3 h were still soluble in chloroform. As an initial statement regarding the shelf life of

PLimC-B3MP$_{2.0}$, we can state that a 100 µm film exposed to ambient conditions (21 °C, air with 50% relative humidity, laboratory lighting) for 20 days is still soluble in chloroform.

The mechanical properties of the cured samples of PLimC-B3MP are shown in Supplementary Fig. 5-6. As expected, the introduction of cross-links leads to an increase of YOUNG's modulus and tensile strength while the strain at break is reduced. With increasing cross-linking density, i.e. higher amount of double bonds in the uncured sample, the strain at break is decreasing while the YOUNG's modulus is increasing. The tensile strength σ_s is running through a maximum for low cross-linking density (PLimC-B3MP$_{0.5}$) but remains higher than in the saturated sample (PLimC-B3MP$_{0.0}$). Furthermore, a study of elasticity is shown in Supplementary Fig. 5-7, where a cured PLimC-B3MP$_{2.0}$ sample was strained by 20% in 40 cycles (5 s strain, 10 s relaxation, strain rate 10 mm min^{-1}). The strain is not completely reversible (maximum stress drops from 0.08 MPa for each consecutive cycle down to 0.06 MPa for the last cycle), as the T_g (5 °C) of the polymer is very close to the testing temperature of 21 °C, i.e. the slow dynamics can be assigned to the slow segmental motion of the polymer backbone. To improve reversibility in the strain experiment, the modification of PLimC with thiols that lower the T_g well below 0 °C should be used.

Degradation tests in composting environment

The PLLA samples readily disintegrated within the first two weeks (holes appeared after 8 days), whereas PLimC samples did not show any traces of degradation even after 60 °C days under the conditions mentioned, i.e. no holes, no surface changes overserved by SEM imaging, no change of molecular weight (distribution) measured by GPC. From those observations we concluded, that PLimC possesses a rather good bio-stability against the industrial composting environment.

Degradation tests in enzymatic environment

The enzyme (13 000 units mL^{-1}, substrate: glyceryl tributyrate) was chosen because of its high activity in the cleavage of ester linkages of condensed matter like water-insoluble polyesters that have been synthesized and readily degraded with this enzyme in our group.[4] The change of hydrophilicity and T_g do not promote mass loss of the polymer samples PLimC, PLimC-ME7/46/82 or BPA-PC respectively, for the conditions tested (see Supplementary Table 5-8). Furthermore, for none of the samples a significant change in molar mass was observed (see GPC data in Supplementary Fig. 5-22), from which was

deduced that the investigated polymers are stable under those conditions within 21 days. For further studies either the testing time should be increased or harsher conditions have to be applied. BPA-PC was employed as reference material and so far it can be stated, that PLimC and its modifications exhibit similar stability under those conditions.

The saturation of PLimC

The conversion of the monomer MenO and pre-monomers menth-1-ene and MenBrOH, respectively, were monitored by GC analysis. The chromatograms combined with the peak information are shown in Supplementary Figs 5-23 – 5-25, respectively. The GC analysis of the precipitation bath of PMenC (Supplementary Fig. 5-26) is added to prove the preferential incorporation of *trans*-MenO into the polymer chain. The accumulation of *cis*-MenO after polymerization is obvious, rising from 8% before to 56% after copolymerization with CO_2. The preferential incorporation is also represented in the NMR spectra of PMenC. The ^{1}H-NMR spectrum (Supplementary Fig. 5-27) shows a single peak at 5.00 ppm without any downfield shoulder, which would be an indication of incorporation of the *cis*-isomer into the backbone. This argument is further supported by the ^{13}C-NMR spectrum of PMenC, which shows only one carbonyl resonance at 152.2 ppm i.e. no stereo-irregularities are present. GPC analysis revealed a relative M_n of 61.3 kDa and $Đ$ of 1.14 (Supplementary Fig. 5-28).

Supplementary methods

Materials

(R)-(+)-Limonene (97%, Sigma-Aldrich), hydrogen (5.0, Linde Gase), N-bromosuccinimide (97%, Sigma-Aldrich), sodium hydride (60% dispersion in mineral oil), iodomethane (99%, stabilized with silver), 5% platinum on charcoal (99%), mercaptoethanol (99%, Sigma-Aldrich), mercaptoacetic acid (99%, Sigma-Aldrich), 2-(diethylamino)ethanethiol hydrochloride (95%, Sigma-Aldrich), butyl 3-mercaptopropionate (98%, Sigma-Aldrich), benzyl bromide (99%, Alfa Aesar), poly(ethylene glycol) monomethyl ether (97%, Sigma-Aldrich) were used as received. Azobisisobutyronitrile (AIBN) was recrystallized from methanol. Toluene was dried over sec-butyl lithium and distilled. Tetrahydrofuran was dried over CaH_2 and distilled, further dried over potassium and distilled before use. Chloroform was dried over CaH_2 and distilled. Carbon dioxide (5.0, Linde Gase) was dried by passing it through a column packed with a molecular sieve of 3 Å. The zinc catalyst with β-diiminate (bdi) and acetate ligand [(bdi)Zn(μ-OAc)][5] and PLimC[3] were synthesized according to literature procedures.

Synthetic procedures

All synthetic manipulations were carried out under exclusion of air in dry conditions, if not otherwise stated. The acid-catalyzed electrophilic addition of PEG-3-OH to PLimC and thiol-ene chemistry are polymer analogous reactions. However, the hydrogenation of the *exo* double bond of limonene was performed on the pre-monomer, which was subsequently epoxidized and copolymerized with CO_2, to give the polycarbonate PMenC.
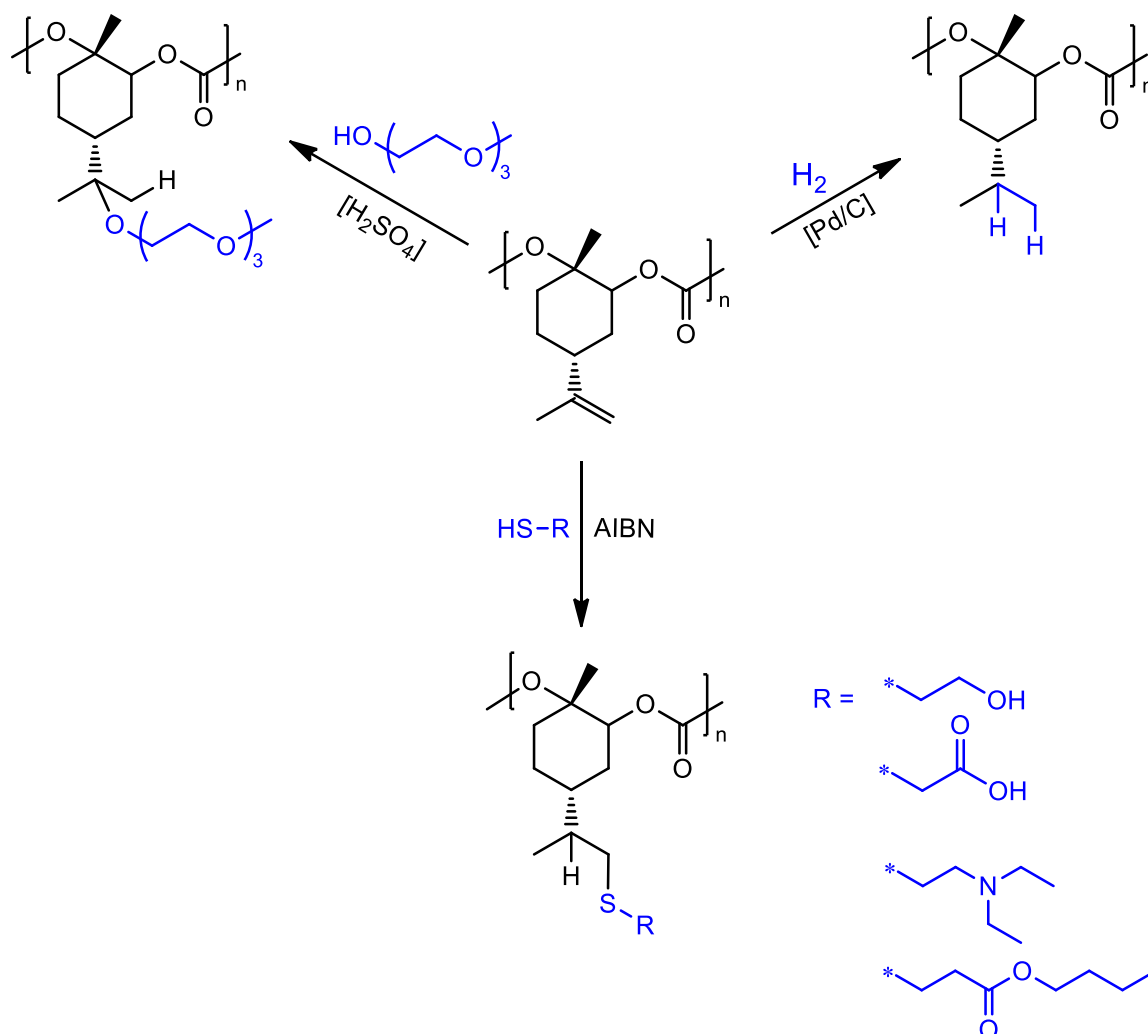
Thiol-ene chemistry on PLimC

PLimC was dissolved in degassed chloroform to produce a 2 wt% solution. After addition of 5 to 40 eq. of the desired thiol, 0.3 eq of AIBN were added. The solution was kept at 60 °C for the desired time, before the solution was concentrated and precipitated in an adequate non-solvent, corresponding to the functionalization, washed and reprecipitated when necessary. The resulting colorless samples were dried at 60 °C in vacuo (except for butyl 3-

mercaptopropionate functionalized PLimC that was dried at 20 °C and 0.02 mbar and stored in argon atmosphere).

PLimC-MAc: Functionalization with mercaptoacetic acid:

The solvent was removed *in vacuo* and the polymer redissolved in acetone before it was precipitated in water several times. The product was functionalized with 100% mercaptoethanol.

^{1}H NMR (300 MHz, DMSO-d[6]): δ 5.01 (1H, s, C*H*O), 3.36 (2H, s, SC*H*₂CH), 3.16 (2H, s, SC*H*₂COOH), 2.62 (1H, m, SCH₂C*H*), 2.36 (1H, m, CHᵃ*H*ᵇCOC=O), 2.22 (1H, m, SCH₂CHC*H*), 1.90 – 0.95 (8H, m, C*H*₃CC*H*ᵃHᵇC*H*₂CHCC*H*₂), 0.85 (3H, s, C*H*₃CHCH) ppm

^{13}C NMR (300 MHz, DMSO-d[6]): δ 171.6 (*C*OOH), 152.0 (*C*O₃), 81.5 (O*C*CH₃), 74.6 (*C*HO), 65.0 (*C*H₂COOH), 33.7, 33.6, 21.3, 15.5, 15.4, 15.2 ppm

PLimC-ME: Functionalization with mercaptoethanol:

The polymer was precipitated in a 1:1 mixture of methanol:water. The product was functionalized with up to 73% mercaptoethanol.

^{1}H NMR (300 MHz, CDCl₃): δ 5.04 (1H, s, C*H*O_unfunctionalized), 4.99 (1H, s, C*H*O_functionalized), 4.71 (2H, d, C=C*H*₂, [2]J=7.4 Hz), 3.70 (2H, m, CH₂C*H*₂OH), 2.68 (2H, m, C*H*₂CH₂OH), 2.55 (1H, m, SCH₂C*H*), 2.36 (1H, m, CHᵃ*H*ᵇCOC=O), 2.21 (1H, m, CH₃CHC*H*), 1.90 – 1.00 (8H, m, C*H*₃CC*H*ᵃHᵇC*H*₂CHCC*H*₂), 0.94 (3H, s, CHCHC*H*₃) ppm

^{13}C NMR (300 MHz, CDCl₃): δ 152.1, 148.7, 82.0, 75.4, 60.4, 37.3, 35.9, 34.0, 33.8, 21.7, 20.9, 16.0, 15.8 ppm

PLimC-B3MP: Functionalization with butyl 3-mercaptopropionate:

The polymer was precipitated in methanol and subsequently dried at 20 °C and 0.02 mbar to avoid cross-linking of residual double bonds. The polymer was stored in Ar atmosphere.

^{1}H NMR (300 MHz, CDCl$_3$): δ 4.96 (1H, s, CHO), 4.07 (2H, m, CH_2OH), 2.72 (2H, m, SCH_2CH$_2$), 2.56 (3H, m, CHCH_2S), 2.36 (2H, m, CH_2COC=O), 2.00 – 1.00 (14H, m, CH_3CCH$_2$CH_2CHCCH_2 / CH_2C(=O)OCH$_2$CH_2CH_2), 0.94 (6H, s, CHCHCH_3 / CH$_2$CH_3) ppm

^{13}C NMR (300 MHz, CDCl$_3$): δ 172.1, 152.0, 82.0, 75.5, 64.7, 37.7, 37.4, 37.3, 37.2, 35.0, 34.0, 30.7, 27.8, 27.7, 21.6, 19.2, 15.5, 13.8 ppm

PLimC-N: Functionalization with 2-(diethylamino)ethanethiol hydrochloride:

The polymer was precipitated in a basic 2:1 mixture of methanol:water (sodium bicarbonate was added, to produce a pH of 8) and washed with slightly basic water.

^{1}H NMR (300 MHz, CDCl$_3$): δ 5.02 (1H, s, CHO$_{unfunctionalized}$), 4.96 (1H, s, CHO$_{functionalized}$), 4.69 (2H, d, C=CH_2, ^{2}J=7.2 Hz), 2.60 (2H, m, SCH_2CH$_2$), 2.54 (2H, m, CH$_2$CH_2N), 2.52 (2H, m, NCH_2CH$_3$), 2.37 (1H, m, CH^aH^bCOC=O), 2.22 (1H, m, CHC=CH$_2$), 2.00 – 1.10 (8H, m, CH_3CCH^aH^{b}CH_2CHCCH_2), 1.01 (2H, t, NCH$_2$CH_3, ^{3}J=7.1 Hz), 0.94 (3H, s, CHCHCH_3, ^{3}J=6.2 Hz) ppm

^{13}C NMR (300 MHz, CDCl$_3$): δ 152.1, 148.7, 109.4, 82.1, 81.8, 75.4, 53.0, 47.1, 37.9, 37.5, 30.4, 30.3, 21.7, 20.8, 15.9, 15.6, 11.9 ppm

PLimC-NQ: Quaternization of PLimC-N with benzyl bromide:

3 eq. benzyl bromide were added to PLimC-N to give a highly viscous mixture. The reaction mixture was kept at 22 °C for 24 h before the polymer was precipitated repeatedly in hexane.

^{1}H NMR (300 MHz, DMSO-d^6): δ 7.52 (5H, m, C$_6$$H_5$), 5.05 (1H, s, C$HO_{unfunctionalized}$), 4.98 (1H, s, C$HO_{functionalized}$), 4.69 (2H, d, C=C$H_2$, ^{2}J=7.2 Hz), 4.62 (2H, m, C$_6$H$_5$CH_2), 3.27 (6H, m, N(CH_2CH$_2$)$_2$CH_2CH$_2$), 2.94 (2H, m, SCH_2CH), 2.64 (2H, m, SCH_2CH$_2$), 2.33 (1H, m, CH^aH^bCOC=O), 2.13 (1H, m, CHC=CH$_2$), 2.00 – 1.00 (14H, m, CH_3CCH^aH^{b}CH_2CH (CHCH_3)CH_2), 0.84 (6H, m, N(CH$_2$CH_3)$_2$) ppm

Acid-catalyzed electrophilic addition of PEG-3 to PLimC

PLimC was dissolved in chloroform (1.3 wt% solution), before 12 eq. of PEG-3-OH and 0.33 eq. of concentrated H_2SO_4 were added. The reaction mixture was stirred for the desired time (24 – 68 h), concentrated *in vacuo* and the polymer precipitated in methanol. The colorless polymers were characterized by NMR/IR spectroscopy and contact angle measurements.

^{1}H NMR (300 MHz, CDCl$_3$): δ 5.04 (1H, s, C*H*O$_{unfunctionalized}$), 4.92 (1H, s, C*H*O$_{functionalized}$), 4.71 (2H, d, C=C*H$_2$*, ^{3}J=7.4 Hz), 3.63 – 3.45 (12H, m, PEG-3), 3.37 (3H, s, PEG-3-C*H$_3$*), 2.42 (1H, m, CH^a*H^b*COC=O), 2.20 (1H, m, C*H*C=CH$_2$), 1.83 (2H, m, CHC*H$_2$*CH), 1.71 – 1.14 (9H, m, C*H$_3$*CC*H^a*H^{b}C*H$_2$*CHCC*H$_3$*), 1.06 (6H, s, CH$_2$OC(C*H$_3$*)$_2$) ppm

^{13}C NMR (300 MHz, CDCl$_3$): δ 152.0 (*C*O$_3$), 148.8 (C=*C*H$_2$), 109.4 (*C*=CH$_2$), 82.0 (O*C*CH$_3$), 76.2 (*C*O*C*H$_2$), 75.4 (*C*HO), 72.0 – 70.7 (PEG-3), 60.4 (PEG-3-*C*H$_3$), 59.2 (CO*C*H$_2$), 37.5 (*C*HC), 30.9 (CH$_2$*C*H$_2$C), 22.3 (CH*C*H$_2$CH), 21.6 (*C*H$_2$CH$_2$C), 21.0 (*C*H$_3$COC), 20.7 (*C*H$_3$C(CH)CH$_2$) ppm

The saturation of PLimC (PMenC)

Synthesis of menth-1-ene.[6] In a 130 mL stainless-steel autoclave 32 mL (*R*)-limonene and 0.05 mol% Pt (5 wt% on C) were added. The autoclave was pressurized with 10 atmospheres of H_2 and the suspension was stirred for 11 h at 25 °C. After filtration through a G4 glass frit the regioselectively hydrogenated terpene was used for stereoselective epoxidation. The reaction was monitored by gas chromatography. The colorless liquid consisted of 3.6% *cis*-menthane, 3.0% *trans*-menthane, 86.9% menth-1-ene and 6.5% (*R*)-limonene (retention times: 14.33 (*cis*-menthane), 14.86 (*trans*-menthane), 16.17 (menth-1-ene), 16.36 min (*(R)*-limonene)).

Synthesis of trans-menth-1-ene oxide. The procedure for the stereoselective epoxy-dation of menth-1-ene is analogue to the stereoselective epoxidation of *(R)*-limonene described elsewere.[3,7] The epoxidation of menth-1-ene has also been subject in patent literature.[8] The final product was analysed by gas chromatography and consisted of 2.0% *cis*-menthane, 2.0% *trans*-menthane, 8.5% *cis*-MenO and 85% *trans*-MenO and 6.5% by-products (retention times: 14.85 (cis-menthane), 20.87 (*cis*-MenO), 21.03 min (*trans*-MenO).

Masking of hydroxyl impurities in menth-1-ene oxide. Hydroxyl-containing impurities were masked according to a procedure previously described.[3] The product was purified by vacuum distillation. The purified product used for polymerization consisted of 0.9% *cis*-menthane, 1.0% *trans*-menthane, 9.0% *cis*-MenO and 88.9% *trans*-MenO.

Synthesis of poly(menthene carbonate). The polymerization was carried out in accordance to the copolymerization of LO and CO_2 that was described elsewhere.[3] The product was characterized by ^{1}H and ^{13}C NMR spectroscopy. The precipitation bath was concentrated in vacuo and the residue analyzed by GC, whereas the chromatogram revealed an accumulation of *cis*-MenO, supporting the expectation that only the *trans*-isomer would be incorporated into the polymer.

^{1}H NMR (300 MHz, $CDCl_3$): δ 5.00 (1H, s, C*H*O), 2.35 (1H, m, CH^a*H*^{b}COC=O), 1.95 – 1.00 (10H, m, C*H₃*CC*H*^{a}H^{b}C*H₂*C*H*(C*H₂*)C*H*), 0.85 (6H, m, CH(C*H₃*)₂) ppm

^{13}C NMR (300 MHz, $CDCl_3$): δ 152.0 (*C*O₃), 82.2 (CO*C*CH₃), 75.7 (O*C*H), 36.3 (*C*HCH(CH₃)₂), 32.1 (CH*C*H(CH₃)₂), 30.7 (CH₂*C*H₂C), 23.8 (CH*C*H₂CH), 21.7 (*C*H₂CH₂C), 19.8 (*C*H₃CCH₃), 19.6 (CH₃C*C*H₃) ppm

References

1. Fried, J. R. *Polymer Science and Technology, Third Edition*. (Prentice Hall, 2014).

2. Brandrup, J., Immergut, E. H. & Grulke, E. A. *Polymer Handbook, Fourth Edition*. (Wiley, 1998).

3. Hauenstein, O., Reiter, M., Agarwal, S., Rieger, B. & Greiner, A. Bio-based polycarbonate from limonene oxide and CO_2 with high molecular weight, excellent thermal resistance, hardness and transparency. *Green Chem.* **18,** 760–770 (2016).

4. Buchholz, V., Agarwal, S. & Greiner, A. Synthesis and enzymatic degradation of soft aliphatic polyesters. *Macromol. Biosci.* **16,** 207–213 (2016).

5. Allen, S. D., Moore, D. R., Lobkovsky, E. B. & Coates, G. W. Structure and reactivity of mono- and dinuclear diiminate zinc alkyl complexes. *J. Organomet. Chem.* **683,** 137–148 (2003).

6. Newhall, W. F. Derivatives of (+)-limonene. I. Esters of *trans*-p-menthane-1,2-diol. *J. Org. Chem.* **23,** 1274–1276 (1958).

7. Gurudutt, K. N., Rao, S. & Srinivas, P. Stereospecific synthesis of *trans*-*β*-terpineol. *Flavour Fragr. J.* **7,** 343–345 (1992).

8. Leffingwell, J. C. & Shackelford, R. E. Verfahren zur Herstellung von 1-Menthenepoxyd. DE 1807324 (1967).

6

Conclusion & future prospects

The material PLimC is a highly versatile thermoplastic that shows high performance with respect to optical, mechanical and permeation properties. The successful production of high-molecular-weight PLimC can be regarded as *the enabler* towards the exploitation of the polymer as an engineering thermoplastic with the mandatory robustness. Only this robustness can give the manufactured fibres, thin films or sheets of PLimC the integrity to be used in any application. It is the basis for utilization of PLimC as a coating, a membrane and especially as a breathing glass that was introduced within this thesis as innovative concept. The concept relies on the high transparency, impact resistance and – most importantly – on the facile transport of small molecules of CO_2 and O_2. I could show in feasibility studies that windows made of the breathing glass PLimC can supply the interior of well-insulated houses with fresh air. Hence the need for active energy-intensive ventilation systems can be reduced.

Since the supply through the polymeric breathing glass cannot yet compensate for the demand of fresh air completely, the gas transport properties of PLimC should be enhanced even further. And here the unsaturated polycarbonate is at its most impressive, as it can be tuned in almost any direction – I have shown some examples in this thesis – executing simple chemistry on the double bond. This aspect of modifications of PLimC should be expanded by adding new functionalities to the platform but also by optimizing the parameters of the already presented materials. The optimization is necessary to identify the configuration of the bio-based material that can compete with established coatings, rubbers, biodegradables etc. A slightly different approach that was only touched upon in this thesis, is the copolymerization of LO, CO_2 with a third monomer, be it another epoxide, a lactone or even an anhydride (less protic catalyst are necessary to incorporate the latter). This approach shows great promise to alter the stability of the backbone, thus leading to different mechanisms of degradation and decomposition.

Coming back to the basis PLimC, there is still some work to be done in order to improve the economics and the processing of the material. Regarding the economics, the choice of catalyst has to be reconsidered, as the copolymerization of both *trans-* and *cis-*LO with CO_2 to give a high-molecular-weight PLimC (>80 kDa) is highly desirable. Furthermore, the catalyst should exhibits a *TOF* that is acceptable for implementation within an industrial process of the production of PLimC. The improvement of the rate of copolymerization is

challenging for the sterically demanding LO – for the employed catalyst we have found a 2nd order dependency on LO – but here the key to an efficient synthesis of PLimC is located.

With respect to the aspect of processing PLimC, there is a huge potential for the solvent-based manufacture of fibres (e.g. from electrospinning) and films but also for the foaming in supercritical CO_2. Nevertheless, the processing of the melt of PLimC is a major problem of the engineering thermoplastic, because the decomposition and softening temperature lie within a 100 K window. Hence, the viscosity of the melt is hardly low enough in the temperature region that would allow for decomposition-free processing of the aliphatic polycarbonate. Either additives, chemical manipulations on the backbone or engineering solutions have to be developed to give PLimC the processability it needs to compete with established materials. This aspect could also turn out to be crucial in the case, where the bio-based polymer is to be blended with commodities or other engineering thermoplastics in order to increase the green character of the petroleum-based plastics.

.

Acknowledgements

Special thanks to Peter und Melissa for many events and to my lab mates Amanda, Judith and Liao who would take care of a very comfortable atmosphere during work. Here, I also have to mention the whole group, which was very open-minded and always willing to help.

I would like to thank Tobias – many thanks for having lunch at 12:15 pm and for giving the thesis its consistency – and Holger, but also Arne and Markus (who did not make it to Bayreuth) for the friendship that started back then in the first semester and has continued ever since to be the steady basis of my academic life. I have always enjoyed our various trips, as I enjoyed the competitive 'kicker matches' against Amir.

Hui, thank you for sharing your life with me. You must have compromised a lot to get along with a German 'Riesennase' and still I think that we have a very rich and exciting life.

Even longer, my parents Bärbel and Michael and my sisters Ina – great thanks for improving the language of this thesis – and Kathi would support me in all of my decisions and I am very grateful for having you.

(Eidesstattliche) Versicherung und Erklärung

(§ 8 S. 2 Nr. 6 PromO)

Hiermit erkläre ich mich damit einverstanden, dass die elektronische Fassung meiner Dissertation unter Wahrung meiner Urheberrechte und des Datenschutzes einer gesonderten Überprüfung hinsichtlich der eigenständigen Anfertigung der Dissertation unterzogen werden kann.

(§ 8 S. 2 Nr. 8 PromO)

Hiermit erkläre ich eidesstattlich, dass ich die Dissertation selbständig verfasst und keine anderen als die von mir angegebenen Quellen und Hilfsmittel benutzt habe.

(§ 8 S. 2 Nr. 9 PromO)

Ich habe die Dissertation nicht bereits zur Erlangung eines akademischen Grades anderweitig eingereicht und habe auch nicht bereits diese oder eine gleichartige Doktorprüfung endgültig nicht bestanden.

(§ 8 S. 2 Nr. 10 PromO)

Hiermit erkläre ich, dass ich keine Hilfe von gewerblichen Promotionsberatern bzw. -vermittlern in Anspruch genommen habe und auch künftig nicht nehmen werde.

. . . .

Ort, Datum, Unterschrift